Efficient Wireless Communication in Healthcare Systems; Design and Performance Evaluation

by

Saeed Rashwand

A thesis submitted to

The Faculty of Graduate Studies of

The University of Manitoba

in partial fulfillment of the requirements

of the degree of

Doctor of Philosophy

Department of Computer Science

The University of Manitoba

Winnipeg, Manitoba, Canada

August 2012

Thesis advisor   Author

Jelena Misic and Rasit Eskicioglu   **Saeed Rashwand**

Efficient Wireless Communication in Healthcare Systems; Design and Performance Evaluation

Abstract

Increasing number of ageing population and people who need continuous health monitoring and rising the costs of health care have triggered the concept of the novel wireless technology-driven human body monitoring. Human body monitoring can be performed using a network of small and intelligent wireless medical sensors which may be attached to the body surface or implanted into the tissues. It enables carers to predict, diagnose, and react to adverse events earlier than ever. The concept of Wireless Body Area Network (WBAN) was introduced to fully exploit the benefits of wireless technologies in telemedicine and m-health.

The main focus of this research is the design and performance evaluation of strategies and architectures that would allow seamless and efficient interconnection of patient's body area network and the stationary (e.g., hospital room or ward) wireless networks. I first introduce the architecture of a healthcare system which bridges WBANs and Wireless Local Area Networks (WLANs). I adopt IEEE 802.15.6 standard for the patient's body network because it is specifically designed for WBANs. Since IEEE 802.15.6 has strict Quality of Service (QoS) and priorities to transfer the medical data to the medical server a QoS-enabled WLAN for the next hop is needed to preserve the end-to-end QoS. IEEE 802.11e

standard is selected for the WLAN in the hospital room or ward because it provides prioritization for the stations in the network. I investigate in detail the requirements posed by different healthcare parameters and to analyze the performance of various alternative interconnection strategies, using the rigorous mathematical apparatus of Queuing Theory and Probabilistic Analysis; these results are independently validated through discrete event simulation models.

This thesis has three main parts; performance evaluation and MAC parameters settings of IEEE 802.11e Enhanced Distributed Channel Access (EDCA), performance evaluation and tuning the MAC parameters of IEEE 802.15.6, and designing a seamless and efficient interconnection strategy which bridges IEEE 802.11e EDCA and IEEE 802.15.6 standards for a healthcare system.

Contents

Chapter 1

Introduction

In this chapter, I first briefly describe Wireless Sensor Networks (WSNs) as the basis of healthcare systems. Wireless Body Area Networks (WBANs) as the main building block of a healthcare system and their healthcare applications are introduced. The currently available projects which aim to provide a human body monitoring system are described. The wireless technologies which the projects employ and their shortcomings are described. I discuss the research presented in this thesis toward an efficient healthcare system. I conclude the chapter with a short summary of the introduction chapter.

1.1 Wireless Sensor Networks

The advances in the semiconductor and microelectronics industry, energy storage technologies, sensor and wireless communication technologies during the past decade have made available a new type of communication networks. The networks are composed of battery-powered integrated wireless sensor devices which are constantly being miniatur-

1

ized. The technology developments have made it possible to create sensors which are very small in size, sensitive in sensing, efficient in power consumption, powerful in processing and affordable to be considered disposable. Wireless Sensor Networks (WSNs) are self-organizing and infrastructure-less wireless networks made of small devices equipped with special sensors and wireless transceivers. Thanks to the technological advances the concept of a truly pervasive WSN is rapidly becoming a reality. The main goal of a WSN is to collect data from the environment and send it to a reporting center where the data is aggregated and analyzed [1; 2].

Smart sensor devices must be capable of supporting wireless communication, computation, storage and sensing. Thus, the smart devices have often the following parts: a microcontroller for computation, flash memories for recording the sensed and the program data, a wireless transceiver, an antenna, an analogue-to-digital converter (ADC), one or more sensors, and a power source. Most WSNs rely on a communication stack that includes physical, *Medium Access Control (MAC)*, network, and transport layers. There are many different protocols for each of the layers. These protocols are specifically designed for WSNs and are different from the ones for wired networks or other wireless networks such as Wi-Fi. In fact, constraints and characteristics of the smart devices, the sensor network and the environment in which they reside raise the need for different solutions [3].

1.2   Wireless Body Area Networks

The novel wireless technology-driven human body monitoring is an unobtrusive, continuous, and ubiquitous body monitoring system to improve the health quality and decrease the healthcare costs. Human body monitoring can be performed using a network of wireless

sensors which are either attached to the body surface or implanted into the tissue. Recent technology developments have produced small and intelligent medical sensors which can be worn or implanted in the human body. The sensors collect and transfer the medical data to the center in which the data is aggregated and analyzed. A wireless network is designed for monitoring the health variables to avoid the physical mobility constraints which a wired network may cause. A wireless network provides better access and enables greater physical mobility. Wireless communications support ubiquitous connectivity, better interoperability and facilitating inexpensive deployment [4].

A wireless network of sensors which monitors the body's health increases the chance to diagnose cardiac arrhythmias earlier in at-risk groups. It also provides continuous checking of the disease progression and patient's response to any treatment initiated (Section 1.2.1). The wireless network could pervasively monitor patients in the hospital wherever they are which is desirable for the healthcare providers and the patient. The monitoring system enables carers to predict, diagnose, and react to adverse events earlier than ever. It may help the patient to leave the hospital sooner (Section 1.2.2). An unobtrusive monitoring sensor network to monitor an elderly person's health is invaluable which provides a high quality of life. The system gives feedback to the person's carers and family members (Section 1.2.3). The concept of ubiquitous human body monitoring system with regards to physical, physiological, and biomedical parameters in any environment and without activity restriction provides invaluable benefits for all people. The system is becoming a reality with the important advances in sensor, miniaturised processor, wireless data transmission technologies, increased battery duration, reduced energy consumption, and power scavenging (Section 1.2.4) [5].

In order to provide a monitoring system the concept of *m-health* was defined as "mobile computing, medical sensor, and communications technologies for health care" [6]. The concept of Wireless Body Area Network (WBAN) was first introduced by Van Dam *et al.* in 2001 to fully exploit the benefits of wireless technologies in telemedicine and m-health [7; 8]. The human body environment is smaller than the usual WSN environment and requires a different type and frequency of monitoring, with presence of different challenges than those faced by WSNs. The different characteristics and requirements have triggered the introduction of WBANs. Many challenges of WBANs are similar to those of WSNs. However, there are some important differences between the two networks which are illustrated in Table 1.1.

Similarities among WBANs, WSNs and MANETs provide the opportunity to understand communications in WBANs by considering the protocols, mechanisms and studies for WSNs and MANETs. However, as Table 1.1 indicates there are fundamental and important differences among the networks' functionalities which make most of the solutions for WSNs and MANETs inappropriate for WBANs. Thus, novel protocols and mechanisms must be designed for WBANs to consider the typical properties of the network. In the following some major differences between WBANs and WSNs are illustrated:

- There are no redundant devices in WBANs contrary to the classical WSN environments. All nodes in the network must be highly robust, reliable, and accurate. The lost information from one node often cannot be recovered by other nodes.

- Due to the special features of the environment in which the WBAN operates (human body) the data loss is more significant. The signals of the sensors, specially the implanted ones, are considerably attenuated because the propagation of the waves

Table 1.1: Different challenges faced by WSN and BSN [5].

Challenges	WSN	BSN
Scale	As large as the environment being monitored (metres/kilometres)	As large as human body parts (millimetres/centimetres)
Node Number	Greater number of nodes required for accurate, wide area coverage	Fewer, more accurate sensors nodes required (limited by space)
Node Function	Multiple sensors, each performs dedicated tasks	Single sensors, each performs multiple tasks
Node Accuracy	Large node number compensates for accuracy and allows result validation	Limited node number with each required to be robust and accurate
Node Size	Small size preferable but not a major limitation in many cases	Pervasive monitoring and need for miniaturisation
Dynamics	Exposed to extremes in weather, noise, and asynchrony	Exposed to more predictable environment but motion artefacts is a challenge
Event Detection	Early adverse event detection desirable; failure often reversible	Early adverse events detection vital; human tissue failure irreversible
Variability	Much more likely to have a fixed or static structure	Biological variation and complexity means a more variable structure
Data Protection	Lower level wireless data transfer security required	High level wireless data transfer security required to protect patient's information
Power Supply	Accessible and likely to be changed more easily and frequently	Inaccessible and difficult to replace in implantable setting
Power Demand	Likely to be greater as power is more easily supplied	Likely to be lower as energy is more difficult to supply
Energy Scavenging	Solar, and wind power are most likely candidates	Motion (vibration) and thermal (body heat) most likely candidates
Access	Sensors more easily replaceable or even disposable	Implantable sensor replacement difficult and requires biodegradability
Biocompatibility	Not a consideration in most applications	A must for implantable and some external sensors. Likely to increase cost
Context Awareness	Not so important with static sensors where environments are well defined	Very important because body physiology is very sensitive to context change
Wireless Technology	Bluetooth, Zigbee, GPRS, and wireless LAN, and RF already offer solutions	Low power wireless required, with signal detection more challenging
Data Transfer	Loss of data during wireless transfer is likely to be compensated by number of sensors used	Loss of data more significant, and may require additional measures to ensure QoS and real-time data interrogation capabilities

takes place in or on a lossy medium. New mechanisms may be required to ensure the QoS and real time data interrogation capabilities. However, in WSNs the data loss may be covered by other sensors and the attenuation level is often lower.

- The sensors which are either implanted into the tissue or attached on the surface of body must be very small in size to support unobtrusive monitoring of the patients. However, in WSNs the sensor size is not the main concern though smaller sensors are preferred. The small size of the WBAN sensors strongly affects the power resources of the devices. The power supply recharge of the devices are often impossible and its replacement is also difficult. Thus, a long lifetime of the sensors is required. Several years is desirable as the lifetime of the sensors, and especially the implanted ones.

- The sensors in a WBAN are located in or on the human body which can be in motion. This challenge for WBAN is more difficult to address than WSNs. Thus the WBAN must be robust against the high probable network topology changes. In addition, biological variation and complexity cause a more variable structure.

- The data obtained by the network contains the medical information which requires high reliability and low delay to pass on to the central server. In fact, early event detection is a vital requirement for the network.

The currently available wireless technologies such as Bluetooth [9], Zigbee [10], GPRS [11] and Wi-Fi [12] are not appropriate for WBANs. The available protocols and standards do not consider the main features of WBANs. Current Wireless Personal Area Networks (WPANs) do not meet the medical (proximity to human tissue) and relevant communication regulations for some application environments. They also do not support the combination

of reliability, QoS, low power, data rate and non-interference required to broadly address the breadth of body area network applications [13]. Due to lack of an appropriate wireless technology which satisfies all the requirements of the WBANs the IEEE 802.15 Working Group formed Task Group 6 (TG6) in November 2007 to develop a communication standard optimized for low power devices and operation on, in or around the human body (but not limited to humans) to serve a variety of applications including medical and personal entertainment [14].

Examples of the applications served by the proposed standard are: *Electroencephalogram (EEG)*, *Electrocardiogram (ECG)*, *Electromyography (EMG)*, vital signals monitoring (temperature (wearable thermometer), respiratory, heart rate, pulse oximeter, blood pressure, oxygen, pH value , glucose, and cardiac arrhythmia), wireless capsule endoscope (gastrointestinal), wireless capsule for drug delivery, deep brain stimulator, cortical stimulator (visual neurostimulator, audio neuro stimulator, Parkinsons disease, etc.), remote control of medical devices such as pacemaker, actuators, insulin pump, hearing aid (wearable and implanted), retina implants, disability assistance, such as muscle tension sensing and stimulation, wearable weighing scale, fall detection, aiding sport training. This will include body-centric solutions for future wearable computers [13].

The IEEE 802.15.6 standard is briefly introduced in Section 3.1. A medical WBAN example is shown in Fig. 1.1. The depicted WBAN includes a few sensors to monitor the vital health information of the body. The sensors are placed on the surface of the body, in cloth, or implanted. They measure EEG, ECG, blood pressure, blood oxygen, blood glucose, temperature of the body, respiration rate, position and motions of the person.
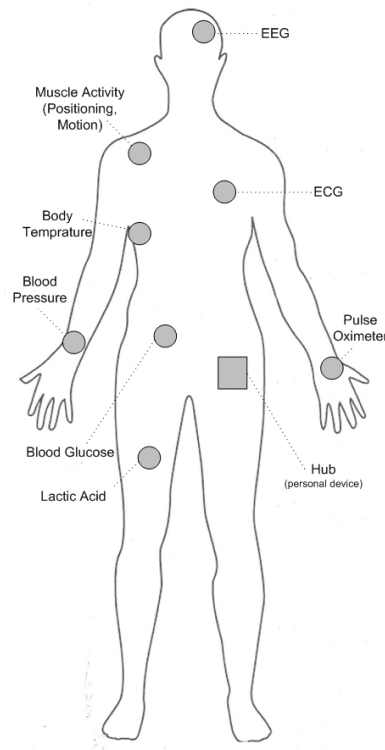
Figure 1.1: A medical WBAN example with a few nodes and a hub monitoring the human body

1.2.1 Monitoring Patients with Chronic Diseases

The Cardio Vascular Disease (CVD) is the main cause of death throughout the world, representing 30% of all global deaths. The World Health Organization (WHO) reported that more than 17 millions people in 2004 died of coronary heart disease or strokes in the world which the number will increase to almost 23.6 millions in 2030. The continuous monitoring and proper health care may prevent the deaths caused by CVD [15]. As another example the heart rhythm abnormalities (arrhythmias) such as *atrial fibrillation* are occurring in as many as 4% of the world population over the age of 60, increasing with age to almost 9% in octogenarians [16]. Discovering the early symptoms of atrial

fibrillation including fatigue and palpitations may help the patient to get earlier medical advice or treatment. Performing continuous ECG increases the chance of early detection of the abnormality. It helps the healthcare providers to start the treatment sooner to prevent the longer-term complications of tachycardia (rapid heart rate), mediated cardiomyopathy (causing heart failure) and stroke. ECG is a recording of the electric potential, generated by the electric activity of the heart, on the surface of the thorax. ECG thus represents the extracellular electric behavior of the cardiac muscle tissue [17]. Apart from early detection of the disease, regular monitoring improves controlling the heart rate, which results in prevention of much of the associated morbidity and morality. WBANs offer the pervasive and continuous monitoring of the heart activity to diagnose cardiac issues earlier than ever. They also monitor the disease progression and patient's response to any treatment.

High blood pressure (hypertension) is a type of cardiovascular disease which affects approximately 75 million people in the united states alone [18]. The WBAN offers an early diagnose of the high blood pressure using serial blood pressure measurements during the patients' normal daily lives. It also monitors the effect of the treatment on the disease. Early diagnose helps to control risk factors such as smoking and high cholesterol.

Diabetes is a well-known chronic progressive illness which occurs as a result of problems with the production and supply of insulin in the body. It is estimated that 285 million people around the world have diabetes. It is expected that the number raises to 485 million by 2030. Diabetes may cause many short-term complications such as low blood sugar, lactic acidosis, and bacterial/fungal infections and long-term complications such as eye disease (retinapathy), kidney disease (nephropathy) and nerve disease (neuropathy). The diagnosis is often made by measuring fasting blood glucose (which is abnormally raised).

The WBAN offers continuous monitoring of the patients which require regular administration of insulin during a day with blood glucose "pinprick" testing. The WBAN may include an glucose injection actuator to improve the quality of healthcare [19; 20].

The mentioned illnesses are just few diseases which justify how continuous monitoring of the human body by WBANs improves the healthcare quality. Numerous other examples of diseases would benefit from continuous or prolonged monitoring [21; 22; 23; 24]. Table 1.2 lists some of the disease processes and the parameters that may be used to monitor them [5].

1.2.2   Monitoring Hospitalized Patients

Patients in hospital currently receive various levels of monitoring intensity which ranges from intermittent (every a few hours in the case of those who suffer with stable conditions), to intensive (every hour), and finally to continuous invasive and non-invasive monitoring such as that seen in the Intensive Care Unit (ICU). The monitoring is normally in the forms of vital signs measurements (ECG, blood pressure, heart rate, respiratory rate, and body temperature), visual appearance (assessing their level of consciousness), and verbal response (asking them how much pain they feel). Employing WBANs for monitoring the patients offers that they will no longer need to stay in bed, but will be able to move around freely [5]. In addition, the data is gathered during a longer time interval much more frequently and with earlier detection of any medical event. The doctors are able to control the disease progression or the effects of the treatment [21]. The next step for any "hospital of the future" would be to adopt a ubiquitous and pervasive in-patient monitoring system enabling carers to predict, diagnose, and react to adverse events earlier than ever before.

Table 1.2: Disease processes and the parameters commonly used to monitor these diseases. Suggested sensor types for measurement of these parameters are listed in brackets.

Disease Process	Physiological Parameter	Biochemical Parameter
Hypertension	Blood pressure (implantable/ wearable mechanoreceptor)	Adrenocorticosteroids (implantable biosensor)
Ischaemic Heart Disease	Electrocardiogram (ECG), cardiac output (implantable/ wearable ECG sensor)	Troponin, creatine kinase (implantable biosensor)
Cardiac Arrhythmias/ Heart Failure	Heart rate, blood pressure, ECG, cardiac output (implantable/ wearable mechanoreceptor and ECG sensor)	Troponin, creatine kinase (implantable biosensor)
Cancer (Breast, Prostate, Lung, Colon)	Weight loss (body fat sensor) (implantable/ wearable mechanoreceptor)	Tumour markers, blood detection (urine, faces, sputum), nutritional albumin (implantable biosensors)
Asthma / COPD	Respiration, peak expiratory flow, oxygen saturation (implantable/ wearable mechanoreceptor)	Oxygen partial pressure (implantable/wearable optical sensor, implantable biosensor)
Parkinsons Disease	Gait, tremor, muscle tone, activity (wearable EEG, accelerometer, gyroscope)	Brain dopamine level (implantable biosensor)
Alzheimers Disease	Activity, memory, orientation, cognition (wearable accelerometer, gyroscope)	Amyloid deposits (brain) (implantable biosensor/EEG)
Stroke	Gait, muscle tone, activity, impaired speech, memory (wearable EEG, accelerometer, gyroscope)	
Diabetes	Visual impairment, sensory disturbance (wearable accelerometer, gyroscope)	Blood glucose, glycated haemoglobin (HbA1c) (implantable biosensor)
Rheumatoid Arthritis	Joint stiffness, reduced function, temperature (wearable accelerometer, gyroscope, thermistor)	Rheumatoid factor, inflammatory and autoimmune markers (implantable biosensor)
Renal Failure	Urine output (implantable bladder pressure/volume sensor)	Urea, creatinine, potassium (implantable biosensor)
Vascular Disease	Peripheral perfusion, blood pressure, aneurism sac pressure. (wearable/implantable sensor)	Haemoglobin level (implantable biosensor)
Infectious Diseases	Body temperature (wearable thermistor)	Inflammatory markers, white cell count, pathogen metabolites (implantable biosensor)
Post-Operative Monitoring	Heart rate, blood pressure, ECG, oxygen saturation, temperature (implantable /wearable and ECG sensor)	Haemoglobin, blood glucose, monitoring the operative site. (implantable biosensor)

1.2.3   Monitoring Elderly Patients

A special group of people being "at high risk" are the elderlies who face enormous medical conditions. WBANs offer an invaluable healthcare regular and non-intrusive monitoring for them. Due to recent progresses in medical science the life expectancy has increased by 25 years making the size of the group to increase along with its potential demand upon healthcare resources [25]. It is shown that at times of the year when the weather conditions are at their extremes (either very cold or very hot), elderly patients are at increased risk of requiring hospital admission. The risk is triggered by not being able to seek medical help early enough for simple and treatable conditions, which eventually may lead to significant morbidity [26].

1.2.4   Pervasive Patient Monitoring

The recent technological advances in sensor miniaturization, implantable sensors, power supplies, wireless technologies, reduced energy consumption and power scavenging have brought the concept of "ubiquitous" and "pervasive" human well-being monitoring. *Micro Electro-Mechanical System* (MEMS) technology is another area which helps the sensors to be smaller in size and more powerful in sensing, processing, storage and communication [27]. Pervasive WBAN will allow access to accurate medical information at any time and place, ultimately improving the quality of the service provided.

Early diagnosis of any illness can be helpful for all people. The pervasive monitoring system results in earlier administration of the appropriate treatment, and the prevention of disease-related morbidity. Maintaining the long time medical data helps the healthcare providers to perform a better treatment in case of any disease diagnosis. At present, much

of the data captured even with the aid of continuous patient monitoring is lost, but in conjunction with an automated pervasive monitoring system all data gathered could be stored for later review and trend analysis [5].

The development of implantable sensors offers WBANs one of its most exciting components. The European Commission project "Healthy Aims" has been focused on specific sensor applications, namely for hearing aids (cochlear implant), vision aids (retinal implant), detecting raised orbital pressure (glaucoma sensor), and intracranial pressure sensing (implantable pressure sensor). Other implantable devices include Medtronic's "Reveal Insertable Loop Recorder", which is a fully implantable cardiac monitor used to record the heart rate and rhythm during instances of unexplained fainting, dizziness, or palpitations. The device provides the clinician with an ECG that can be used to identify or rule out an abnormal heart rhythm as the cause of these symptoms. CardioMEMS is a company that produces an implantable pressure sensor. It can take pressure readings following implantation into an aneurism sac at the time of endovascular repair [5].

1.3 Existing WBAN Projects

In the recent years, a large body of work related to WBANs has appeared in the literature. The attempts are mostly focused on proposing solutions for the issues of the WBANs. Before introducing the IEEE 802.15.6 standard the structure of WBANs and protocols and mechanisms of the physical layer and MAC sublayer of WBANs have been the most important concerns which attracted attention of many researchers. In [5; 8] the authors provide a comprehensive survey on WBANs.

There are currently several research groups throughout the world which have focused on

design and implementation of a WBAN. The researchers have employed different wireless technologies in their projects in the field of wireless short-range connectivity, such as the IEEE 802 familly of WPANs, WLANs, Bluetooth and Zigbee. Due to major drawbacks of other WPAN and WLAN solutions the IEEE 802.15.4 [28]/zigbee system has been the most favoured approach in the existing projects before the IEEE 802.15.6 standard is introduced.

There are few projects which employ Bluetooth for implementing the WBAN [29; 30; 31]. Jovanov and Otto *et al.* developed a prototype WBAN based on a multi-tier architecture to handle the communications within the WBAN and between WBANs using off-the-shelf wireless sensors such as the Tmote Sky from Sentilla [32]. In [33] the authors presented a few applications exploiting natural human detection interface based on their own WBAN solution, called WiMoCA. The sensors were represented by tri-axial integrated MEMS accelerometers to detect postures and gestures of the human body. The WiMoCA is designed in a way to detect both static postures and dynamic every day life actions.

From WBAN perspective the Bluetooth technology has severe drawbacks which make it inappropriate for WBANs. Automatic network formation is not supported in Bluetooth and the network formation is slow. Inquiry phase for other Bluetooth devices discovery disrupts transmission on the frequency band. The power consumption of Bluetooth is not efficient enough for WBANs [5]. A comprehensive discussion about Bluetooth, performance modelling and analysis of Bluetooth networks can be found in [34].

Most of the currently existing projects of WBANs employ IEEE 802.15.4 standard as the wireless communication technology. IEEE 802.15.4 is more power efficient and has a simpler protocol stack compared to Bluetooth. The authors in [35] provide an extensive performance modelling and interconnections of IEEE 802.15.4.

Researchers in Harvard University in CodeBlue and Mercury projects have developed WBANs which employ IEEE 802.15.4. The CodeBlue is a distributed WBAN including a pulse oximeter, two-lead ECG, and a specialized motion-analysis sensor board for sensing and transmitting vital signs and geolocation data using the Tmote Sky platform [36; 37; 38]. Mercury is wearable, wireless sensor platform for monitoring movement and physiological conditions for motion analysis of patients being treated for neuromotor disorders, such as Parkinson's Disease, epilepsy, and stroke [39].

Ayushman is a ZigBee-based real-time sensor network based on a health monitoring infrastructure in which MicaZ and TelosB motes are employed for implementation [40]. The developed system includes a wireless ECG, an oximeter, gait monitoring and environment monitoring using off-the-shelf components.

The Human++ research project by IMEC-NL targets the realization of miniaturized, intelligent and autonomous wireless sensor nodes for WBANs [41]. This project develops an IEEE 802.15.4-based wireless network which comprises a series of miniature sensor/actuator nodes. The target of such a monitoring system is to acquire, process, store, and visualize a number of physiological parameters, including EEG/ECG/EMG biopotential signals, in an unobtrusive and ambulatory way. The system is designed to be highly power efficient inasmuch as the system is able to work for 3 months using two AA batteries in series operating in the 2.4 GHz ISM band. In this project, thermal energy scavenging using Thermoelectric Generators (TEG) is utilized in order to increase the system lifetime.

In the European MobiHealth project a generic WBAN for healthcare and a generic m-health service platform was developed, trialled and evaluated [42]. The MobiHealth Service Platform manages WBANs by deploying Bluetooth and Zigbee for ambulant pa-

tient monitoring and ubiquitous healthcare service.. It handles external communications between the BANs and a remote healthcare server using 2.5/3G public wireless networks (GPRS and UMTS). The project aims at different applications such as large scale disaster and emergency system and provision of remote monitoring services to support work and recreation in extreme environments. The MobiHealth BAN continuously monitor vital signs of a patient who is equipped with medical sensors, such as blood pressure, heart rate, activity and ECG.

In [43] AlarmNet was presented which is an assisted-living and residential monitoring network for pervasive, adaptive healthcare. In this project, an extensible and heterogeneous network middleware was proposed which takes into account the environmental, system, and resident context. MicaZ and Telos Sky motes are employed in the implementation in which the WBAN measures heart rate, pulse oximetry, ECG, and body movement.

The authors in [44] proposed a ZigBee-based WBAN platform for developing physical sensor node in relay-time health monitoring. In this project, ZiGW (ZigBee/Internet Gateway) was used for connecting WBAN and Internet. Using the proposed method an ECG monitoring system was implemented so that the real-time ECG signals can be remotely monitored by physicians and stored in an online ECG database.

There are more studies in the literature which employ IEEE 802.15.4 for design and implementation of a WBAN [45; 46; 47; 48]. They all have came to the conclusion that though IEEE 802.15.4 was the most suitable available wireless technology for WBANs the results of the IEEE 802.15.4-based network is rather poor. In [49] the performance of Bluetooth and IEEE 802.15.4 is compared when they are employed for a WBAN. The results show that neither has significant advantages compared to the another one.

Before introducing the IEEE 802.15.6 standard IEEE 802.15.4 was considered the most suitable physical layer and MAC sublayer protocol for WBANs due to the following reasons; the MAC is designed for low power and short range communications and short message transmissions. The standard provides combination of TDMA on CSMA/CA for MAC and peer to peer-based communications. However, it does not provide priorities for CSMA MAC mechanism.

However, as indicated in the IEEE 802.15.6 standard, none of WPANs including IEEE 802.15.4-based networks meet the medical (proximity to human tissue) and relevant communication regulations for some applications. They do not support the combination of reliability, QoS, low power, data rate and non-interference required to broadly address the breadth of body area network applications. IEEE 802.15.4 supports the data rate of up to 250kb/s which is not sufficient for WBANs. In [50; 51] the authors explore IEEE WPAN technologies for medical implant communications. It shows that WPAN standards are not appropriate for implementing WBANs because WBAN devices are physically located on the surface or inside of a person's body which is a lossy environment for the electromagnetic waves.

In addition to the projects which use the WPAN technologies, there are few studies in the literature which introduce specific MAC protocols for WBANs. In [52] a slave-master architecture was designed for the communication in the WBAN. This protocol was extended in [53] in which the time is divided into frames. Each frame can be accessed by one node based on the Earliest Deadline First Algorithm (EDFA).

A MAC protocol is proposed in [54] for a star-networked WBAN employing TDMA to reduce collision and idle listening. H-MAC protocol [55] is a TDMA-based approach for a

star-topology WBAN in which the nodes are synchronized by the human heartbeat rhythm. Though these protocols are specifically designed for WBANs they do not support QoS, low power and data rate required for WBANs. In [56] a contention-based MAC protocols is designed for WBANs. The proposed protocol provides the opportunity for switching from an inactive period to an active phase without providing a suitable Quality of Service such frame priorities.

In [57] the MAC protocols submitted to IEEE 802.15.6 Task Group by public or private organizations are introduced and analyzed to check if they satisfy the requirements of WBANs. In the study fifteen diverse points are considered for comparing the protocols, such as Quality of Service, reliability, topology, scalability, power efficiency, and performance evaluation.

1.4   Research Presented in This Thesis

Many of the technologies envisaged for use in wireless healthcare systems are available today, in the form of either research prototypes or even commercial solutions. However, little is known about their interplay in a real environment. Issues related to their performance are the subject of much attention from both researchers and practitioners.

The main objective of this thesis research is an in-depth investigation into a number of interrelated issues pertaining to the analysis, design, and performance evaluation of the healthcare networks. This research focuses on the design and performance evaluation of strategies and architectures that allow seamless and efficient interconnection of patient's body area network and the stationary (e.g., hospital room or ward) wireless networks.

WBANs must support the combination of reliability, QoS, low power, high data rate and

non-interference to address the breadth of WBAN applications. I adopt the IEEE 802.15.6 standard for the patient's body network (WBAN) [13].

The medical data collected by the hub in the WBAN might be partly processed, including data aggregation, compression, encryption, etc. The processed data needs to be transmitted to a destination outside the transmission range of the WBAN. The destination could be a medical server to store and maintain all the medical records. The healthcare providers of the person may regularly access the information and inspect the data for any symptoms of any diseases. In addition, the data may be processed further by the server to extract the vital health information. The person's healthcare providers may be immediately informed by the server in case of any physical disorders.

In order to provide an unobtrusive healthcare system for the patients the WBAN hub must communicate with an access point by a wireless connection. It seems reasonable to adopt one of the existing WLAN standards from the ubiquitous IEEE 802.11 family for the stationary network. Since IEEE 802.15.6 has strict QoS and priorities to transfer the medical data to the server a QoS-enabled WLAN for the next hop is needed to preserve the end-to-end QoS. I adopt IEEE 802.11e standard since the IEEE 802.11e EDCA provides QoS which matches the requirements of IEEE 802.15.6 QoS [58].

The WBAN hubs are referred as bridge because they communicate in both WBAN and WLAN. I refer to the devices as bridge since they communicate with the sensors and actuators inside the WBAN and convey the data to the WLAN. In Fig. 5.1 networking structure of a healthcare system including the WBANs, bridges, and the WLAN is depicted.

I investigate in detail the requirements posed by different healthcare parameters and analyze the performance of various alternative interconnection strategies, using the rigorous
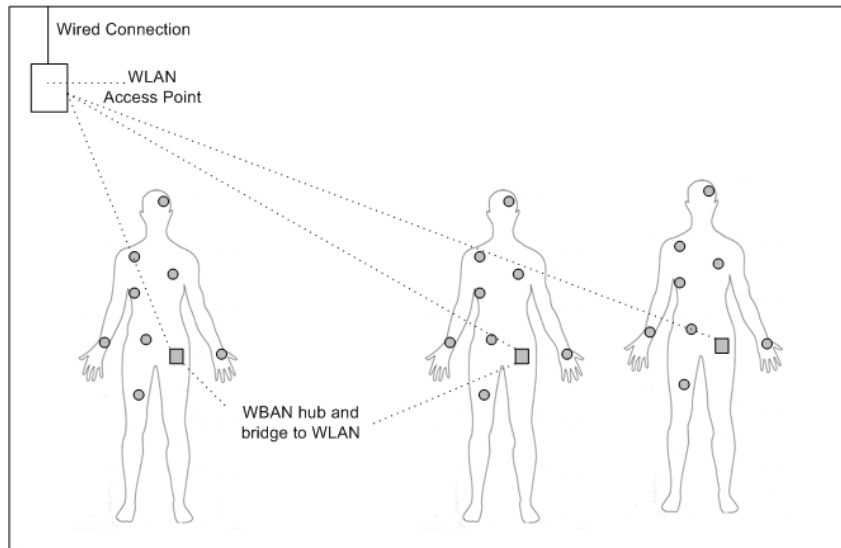
Figure 1.2: Networking structure of a healthcare system

mathematical apparatus of Queuing Theory and Probabilistic Analysis; these results will be independently validated through simulation models.

The work presented in this thesis is divided in three parts; performance evaluation and MAC parameters settings of IEEE 802.11e EDCA, performance evaluation and tuning the MAC parameters of IEEE 802.15.6, and designing a seamless and efficient interconnection strategy which bridges IEEE 802.11e and IEEE 802.15.6 standards for a healthcare system.

In the first part of our study, I evaluate performance of IEEE 802.11e EDCA considering all the four differentiation parameters as described in the standard. The evaluation of the standard is performed to understand the impacts of the differentiation parameters on the performance of an IEEE 802.11e EDCA-based WLAN. I combine the queuing analysis of the node, probabilistic modelling of the activity on the medium and the backoff process, and Markov chain analysis in order to arrive at a model which covers both non-saturation and saturation regimes. I develop simulation models for validating the analytical results. In

this study, I model the impacts of an error-prone channel condition the number of frames served in a TXOP service period. I investigate the effects of bursty frame arrivals on the network performance. I measure the vital network performance descriptors such as mean frame access delay and mean throughput of nodes in the network. I will study how varying TXOP values based on the network parameters can improve the network performance. The effects of the differentiation parameters on the saturation and non-saturation boundaries for all the four access categories are also investigated by the analytical and simulation models. Chapter 2 covers the IEEE 802.11e EDCA-based WLANs performance evaluation.

In the second part of the study, I investigate the performance of the IEEE 802.15.6-based WBANs. I study how the differentiation parameters (minimum and maximum Contention Window values) affect the performance of each User Priority in the network. I examine the impacts of the lengths of different access phases on accesses to the medium by each user priority under both saturation and non-saturation regimes. I analyze how the saturation and non-saturation boundaries change when the lengths of the access phases, node populations, and frame sizes vary. I investigate the performance of the standard under saturation and non-saturation regimes and error-prone channel using both accurate analytical and simulation models. I study the critical network performance descriptors such as mean frame access delay and normalized throughput of all the user priorities in the network throughout the chapter under different conditions. Chapter 3 includes the IEEE 802.15.6-based WBANs performance evaluation.

Since the signal transmission in WBANs takes place around or in the human body, the channel fading significantly affects the networks error performance. In Chapter 4, I investigate the impacts of Bit Error Rate (BER), which is caused by the channel fading,

on MAC level performance of IEEE 802.15.6 CSMA-based WBANs. I evaluate MAC performance descriptors of the networks based on the Signal to Noise Ratio (SNR) values for different UPs. The BER values for different nodes are calculated according to the channel quality, diversity level, and SNR values. The obtained BER values for different UPs are used for calculating the data frame error rates of the UPs in the network. Thereafter, I calculate the data frame response times for all UPs. I also investigate the effects of the diversity level on MAC performance measures of WBANs.

Finally, in the third part, in Chapter 5 I introduce a bridging mechanism between the WLAN and the WBANs considering the results acquired during the first two parts of our study. I investigate how to set the differentiation parameters of both standards, IEEE 802.15.6 and IEEE 802.11e, to achieve the desirable interconnection performance and provide the QoS required by the healthcare system. I develop a prioritized bridging mechanism between the IEEE 802.15.6-based WBANs and the IEEE 802.11e EDCA-based WLAN to convey the medical data to the medical center. Bridging WBANs and WLAN imposes lots of challenges which must be considered for designing efficient and seamless communications in the healthcare networks. Setting the MAC parameters of the IEEE 802.15.6 and IEEE 802.11e EDCA standards affects the network performance. The WBAN differentiation parameters, CW_{min} and CW_{max}, are constant according to IEEE 802.15.6. However, all four differentiation parameters of IEEE 802.11e EDCA (CW_{min}, CW_{max}, AIFS, and TXOP) are configurable. I map the 8 User Priorities in the WBAN into the 4 Access Categories (ACs) in the WLAN to provide the required quality of service and prioritization for the WBAN nodes. I investigate the impacts of a variety of network parameters on performance of interconnection between IEEE 802.15.6 and IEEE 802.11e. I study how the

number of patients in the healthcare network, the number of other devices in the WLAN, channel quality, WBAN and WLAN prioritizing MAC parameters affect the performance of the patient's healthcare network.

1.5 Summary of the Chapter

In this chapter, I stated our research goals toward an efficient and applicable healthcare system. I introduced the applications and the structure of a human body monitoring system. The existing WBAN projects and their shortcomings were discussed to take a closer look at the considered problem in this thesis. I finally outlined our research presented in this thesis including the design and performance evaluation of strategies and architectures that would allow seamless and efficient interconnection of patient's body area network and the stationary wireless network.

Chapter 2

Performance Evaluation of IEEE 802.11e-Based WLANs

In this chapter, I investigate the IEEE 802.11e performance by considering all four differentiation parameters, as specified in the standard. I precisely model the IEEE 802.11e EDCA through analytical and simulation models. I evaluate the impacts of the differentiation parameters on the IEEE 802.11e EDCA-based network performance under saturation and non-saturation regions for all the four Access Categories (ACs) [59; 60; 61]. The analytical models consist of the queuing model of the node, probabilistic model of the activity on the medium, backoff process model and Markov chain analysis. Due to random distribution of time between observation points I model the system as semi Markov process. I investigate the effects of an error-prone channel on the number of served frames during a TXOP period. I study how different network parameters such as number of contending stations from each access category, different arrival rates and different frame sizes affect the performance of the stations in the network [62]. In addition, I investigate the effects of bursty frame arrivals on the network performance [59]. I measure the vital network performance descriptors such as mean frame access delay and mean throughput of the nodes in the network. I study how varying TXOP values based on the network parameters can

24

improve the network performance [59; 62; 63].

This chapter is organized as follows: Section 2.1 briefly describes the contention-based function of IEEE 802.11e EDCA. In Section 2.2 the related work on performance evaluation of IEEE 802.11e EDCA is described. Section 2.3 addresses the contributions of this chapter. Section 2.4 provides a comprehensive description of the analytical model including the backoff, queueing, and Markov chain models. In Section 2.5 the performance descriptors are introduced and computed. Section 2.6 introduces the parameters used in the analytical and simulation models for the network performance evaluation. In Section 2.7 the network performance under bursty traffic, error-prone channel during saturation and non-saturation regimes is investigated through the normalized throughput, frame access delay and success probability of acquiring TXOP period for ACs. The analytical results are validated with the simulation results in this Section as well. In Section 2.8 I study the impacts of different arrival rates on the performance of all the access categories. In Section 2.9 I investigate the affects of frame sizes on the network performance. Section 2.10 examines how the populations of the access categories effect the performance of the system. Finally, Section 2.11 concludes the chapter providing main findings of research presented in this chapter.

2.1 IEEE 802.11e EDCA Standard

IEEE 802.11 is currently the de-facto standard for WLANs, which is implemented in most available commercial products due to its robustness, simplicity and low cost. In order to support QoS in wireless networks, the IEEE 802.11 Working Group proposed a new standard, IEEE 802.11e [58]. The standard includes a contention-based medium access

function, called Enhanced Distributed Channel Access (EDCA), which allows traffic differentiation for the stations in the network.

EDCA delivers traffic based on differentiating 8 User Priorities (UPs) mapped into 4 Access Categories (ACs); Background, Best Effort, Video, and Voice. The differentiation is achieved by varying the following four differentiation parameters; Amount of time a station senses the channel to be idle before backoff countdown or transmission (Arbitrary Inter-Frame Space - AIFS), the length of contention window for backoff (minimum and maximum Contention Windows - CW_{min} and CW_{max}), and the duration a station may transmit after it accesses the channel (Transmission Opportunity - TXOP). Each AC has its own queue and channel access differentiation parameters. A station is referred to AC_k if it has an AC_k queue. The EDCA provides a better QoS to higher priority access categories, in which AC_3 and AC_0 are the highest and the lowest priority ACs, respectively. However, due to the probabilistic nature of channel access, the EDCA cannot provide hard QoS guarantees such as strict delay bound.

An AC_k station wins a TXOP period if the station's Carrier Sense (CS) mechanism (either physical or virtual) determines that the medium is idle at the $AIFS_k$ slot boundary, which will be discussed later in this chapter, and the backoff time for the AC has expired. Every slot has a length of $\omega = 20\mu$sec.

- A station which desire to initiate transferring a data frame performs a backoff procedure. The Backoff count value for an AC_k station is an integer drawn from a uniform distribution over the interval $[0, CW_k]$, where CW_k is an integer within the range of two differentiation parameters of $CW_{k,min} = W_{k,0} - 1$ and $CW_{k,max} = W_{k,max} - 1 = W_{k,m_k} - 1$. A station starts the backoff procedure with the CW set to the $CW_{k,min}$.

Whenever there is an unsuccessful access to the medium CW is set to $2(CW+1)-1$ until reaching the maximum value $CW_{k,max}$. The size of contention window for an AC_k station for the ith backoff stage $i = 0..R$ has the value of

$$
W_{k,i} = \begin{cases} 2^i W_{k,0}, & \text{if } 0 \leq i \leq m_k \\ 2^{m_k} W_{k,0} = W_{k,max}, & \text{if } m_k < i \leq R \end{cases} \tag{2.1}
$$

Every station maintains a retry count taking an initial value of zero. The retry count, the backoff phase, is incremented when there is an unsuccessful medium access.

- A station which desires to initiate transferring a data frame invokes the CS mechanism to determine whether there is any activity during each backoff slot. If no medium activity is detected for the duration of a particular backoff slot, the backoff procedure decrements its backoff counter by one. Otherwise, the backoff procedure is suspended; the backoff timer is not decremented for that slot. If the medium is busy the AC_k station defers until the medium is sensed idle without interruption for a period of time equal to $AIFS_k$ when the last frame detected on the medium was received correctly. However, required uninterrupted idle period length is equal to $EIFS - DIFS + AIFS_k$ when the MAC FCS (Frame Check Sequence) value of the received frame was not correct. The duration of $AIFS_k$ is equal to $SIFS + AIFSN_k\omega$, $k = 0, 1, 2, 3$, where ω is the slot duration, the value of $AIFSN_k$ is greater than or equal to 2, and the duration of $SIFS$ in slots are expressed as $aifs_k$ and $sifs$, respectively. After the uninterrupted idle time, the station generates a random backoff period for an additional deferral time before transmitting, unless the backoff timer already contains a non-zero value.

Transmission begins when the backoff timer reaches zero. In case of successful

acknowledged transmissions, the backoff procedure begins at the end of the received ACK frame. In case of unsuccessful transmissions, it begins at the end of the required time-out interval.

- The fourth differentiation parameter of the IEEE 802.11e EDCA standard is the TXOP_k value, which is the basic unit of allocation of the right to transmit onto the wireless medium. The TXOP_k is defined by a starting time and a defined maximum length. In this chapter, I consider the TXOP_k period as the time required for un-interrupted transmission of one RTS/CTS control frame and M_k data frames. The initiation of the TXOP occurs when the EDCA rules permit access to the medium.

According to the standard, when the TXOP period is successfully accessed or the data frame is dropped, due to exceeding the retry limit, the station has to perform the zero-th backoff phase. It is performed with the minimum contention window size and zero value for retry count regardless of whether there is any data frame in the queue or not. When the backoff counter reaches zero the station checks if there is any pending frame in the queue. If the queue is empty the station enters into the idle state until a data frame (or a burst of data frames if applicable) arrives from the upper layer. Upon arrival of the data frame to the queue the medium must be found idle for AIFS_k so that the station wins the TXOP period. Otherwise, the backoff procedure is continued in the first backoff stage for the station.

The standard is ambiguous regarding the error recovery during TXOP period. It states that the station may recover its uninterrupted access to the medium during the TXOP period in the case that the transmitted data frame is failed because of error on the channel. There can be two different approaches for implementation to either recover the error in the TXOP period or releasing the rest of the TXOP period. I assume that all the stations in the network

recover the error by continuing their transmission during TXOP period if there is sufficient time.

2.2 Related Work

In the recent years, a large body of work has appeared in the literature dealing with analytical or simulation models to investigate the effects of the differentiation parameters on IEEE 802.11e EDCA performance. Due to the large complexity of the IEEE 802.11e standard the currently available models ignore some important specifications of the standard, which make them inaccurate.

The proposed models often extend the Bianchi's two dimensional Markov chain model to take into account different differentiation parameters of IEEE 802.11e EDCA. They are divided into two groups considering saturation and non-saturation conditions. Most of the research in this area has focused on suggesting an analytical model for IEEE 802.11e EDCA given saturation condition [64; 65; 66; 67; 68; 69; 70; 71; 72; 73]. A queue in a station is saturated if there is always a data frame waiting to be served. All the referred models either ignore some differentiation parameters or have inaccuracies related to the backoff procedure. Network saturation regime is close to unstable operation of nodes' queues and is often used just to derive limiting values of throughput and backoff time for traffic classes.

Characterization of the burstiness of network traffic is a key issue in traffic engineering. It has been known for a long time that data streams in Local Area Networks (LANs) are bursty [74]. The authors in [74] proved that traffic in Ethernet LANs has self-similarity and long-range dependence behaviour on multiple time scales. That is, the traffic in the

network is bursty at any scale of observations.

Normal network operation is non-saturated and stable. Contrary to the saturation condition, there are few models which consider unsaturated situation. The models proposed in [75; 76; 77; 78] ignore at least one of the differentiation parameters, mostly TXOP, and assume an ideal channel condition. The proposed model in [79] is a multi-dimensional Markov chain which covers all the parameters under finite load and error prone channel. This model suffers from an inaccuracy related to the AIFS sensing period. Hence, a precise model is still required to include all IEEE 802.11e differentiation parameters under bursty traffic, non-saturation condition and noisy channel.

2.3 Contributions of research presented in this chapter

In this work, I model IEEE 802.11e EDCA single-hop network under bursty arrivals. The contributions of this work can be summarized as follows:

- Due to the necessity of an accurate model for IEEE 802.11e EDCA I have developed an analytical model which includes backoff process, queuing, and Markov chain models. The model considers all four differentiation parameters as described in the standard. The error prone channel and both saturation and non-saturation situations are covered by the model. I validate the analytical results by the developed simulation model which accurately follows the same conditions and assumptions of the analytical model.

- The developed analytical and simulation models accurately address all the differentiation parameters under error prone channel, finite load and bursty traffic. To our best knowledge, this work is the first analytical model for IEEE 802.11e EDCA under

bursty traffic. I model the queuing of the stations based on the arrival of bursts and the contention-based EDCA transmission service provided to the frames. I calculate the idle period length for all ACs which imposes a high complexity to the whole model. Computing an accurate idle period duration is one of the most important shortcomings of the currently available models.

- I investigate the effects of TXOP allocation on network performance when the frames arrive in burst through analytical and simulation models. I demonstrate that TXOP differentiation is more effective under bursty traffic than for Poisson traffic.

- I investigate how TXOP values affect the boundaries between saturation and non-saturation conditions and improve the network performance in case of bursty arrival for the stations.

Our study regarding the effects of differentiation parameters on performance of the IEEE 802.11e EDCA-based network in [63] indicates that increasing TXOP value can improve the total performance of the network. I noticed that under non-bursty traffic increasing the length of TXOP allocation increases backoff countdown duration that may result in starvation for lower priority classes. According to our studies, under non-bursty traffic the lower priority classes have almost no benefit from TXOP allocation while the higher priority classes benefit moderately.

2.4   Analytical Model

I first define the concepts that we use throughout the study following the IEEE 802.11e standard. In this work, I assume that there are all the four ACs of Background, Best Effort,
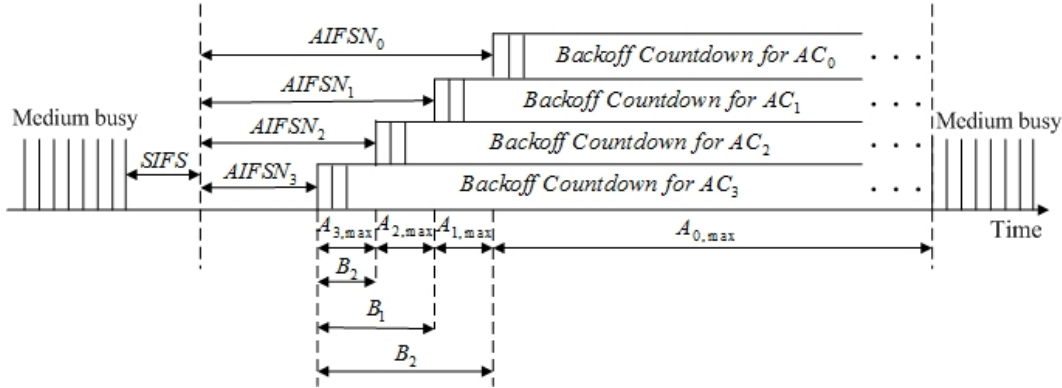
Figure 2.1: Prioritizing EDCA stations using AIFS$_k$ differentiation parameter

Video, and Voice. For focusing on the differentiation parameters and achieving clearer results I assume that each station has only one AC. I consider a single-hop ad-hoc network with n_k nodes which transmit data frames with traffic class k. I assume that all the stations deploy RTS/CTS mechanism for accessing the TXOP service period. The size of the data frames is set to l_d. I assume that the channel is noisy and variable ber represents the value of Bit Error Rate. I define $\delta = (1 - ber)^{rts_b + cts_b}$ as the probability that neither RTS nor CTS is failed due to the noisy channel. Moreover, $\sigma = (1 - ber)^{l_{d,b} + ack_b}$ is defined as the probability that the data frame and its acknowledgement do not experience noise error. The subscript b indicates the values in bits.

The timing diagram which shows access categories priority according to their AIFS values is shown in Fig. 2.1 [73]. I call the counter during AIFS$_k$ freezing counter. The freezing counter is set to B_k whenever there is a transmission on the medium during the backoff procedure, where $B_3 = 0$ and $B_k = AIFSN_k - AIFSN_3, \quad k = 0, 1, 2$. The backoff counter starts counting down when the freezing counter reaches zero. I introduce $A_k, \quad k = 0..3$ as period of time in which only stations of access category k or higher

can decrement their backoff counter or transmit on the medium. Maximum length of A_k is

$A_{k,max}$, $k = 0..3$ in slots, which is computed as follows:

$$A_{k,max} = \begin{cases} AIFSN_{k-1} - AIFSN_k, & \text{if } k = 1, 2, 3 \\ W_{0,max}, & \text{if } k = 0 \end{cases} \tag{2.2}$$

I denote τ_k as the transmission probability by an AC_k station assuming the medium is

idle. Thus, the probability that the medium remains idle in the time period A_k is equal to

$$f_k = \prod_{i=k}^{3} (1 - \tau_i)^{n_i} \tag{2.3}$$

The probability that the channel is idle during the backoff counter decrement transition

of an AC_k station is called g_k and computed as

$$
\begin{aligned}
g_0 &= \frac{f_0}{1 - \tau_0} \\
g_1 &= (1 - f_1^{A_1,max}) \frac{f_1}{1 - \tau_1} + f_1^{A_1,max} \frac{f_0}{1 - \tau_1} \\
g_2 &= (1 - f_2^{A_2,max}) \frac{f_2}{1 - \tau_2} + f_2^{A_2,max} \left[(1 - f_1^{A_1,max}) \frac{f_1}{1 - \tau_2} + f_1^{A_1,max} \frac{f_0}{1 - \tau_2} \right] \\
g_3 &= (1 - f_3^{A_3,max}) \frac{f_3}{1 - \tau_3} + f_3^{A_3,max} \left\{ (1 - f_2^{A_2,max}) \frac{f_2}{1 - \tau_3} + \right. \\
&\quad \left. f_2^{A_2,max} \left[(1 - f_1^{A_1,max}) \frac{f_1}{1 - \tau_3} + f_1^{A_1,max} \frac{f_0}{1 - \tau_3} \right] \right\}
\end{aligned}
\tag{2.4}
$$

I assume burst data frame arrival for all the stations in the network with the arrival rate

of λ_k while the burst mean size is equal to h_k that will be defined later in this chapter. Fi-

nally, I assume that all the nodes' queues have infinite capacity in the case that the station

is under saturation condition.

2.4.1   Backoff Process Model of a Station

In this section, I model the stations' backoff process to access the medium. To compute the performance descriptors I need the PGF of the time which the station spends at every stage of backoff procedure before acquiring the $TXOP$ period. I employ the Markov chain shown in Fig. 4.1 and Fig. 2.3. The PGF of the $TXOP$ transmission period for an AC_k station is equal to $S_k(z) = z^{rts+sifs+cts} \sum_{m=1}^{M_k} \xi_{k,m} z^{m(l_d+3sifs+ack)}$, where $\xi_{k,m}$ indicates the probability that the station transmits m frames during $TXOP_k$. During this time other stations pause their backoff procedure until the medium will be idle again for their own AIFS duration. The PGF $\Xi_k(z) = \sum_{m=1}^{M_k} \xi_{k,m} z^m$ will be derived in the next section. However, if RTS control frame transmitted by a station collides with another transmission or fails due to noisy channel the PGF of transmission failure time is equal to $C(z) = z^{rts+sifs+cts}$.

A building block of the frame service time PGF is the transfer PGF for passing through the freezing counter block which either has loopback to the top when the value of backoff counter is non-zero, or skips loopback when the backoff counter is zero. In the following text, I compute PGF for the time spent in the freezing countdown and backoff countdown for an AC_k station. I develop the PGF for time spent in every backoff stage and generally PGF for time spent during backoff procedure. First, I compute PGF of freezing countdown duration for an AC_k station. Probability of successful TXOP access, $p_{S,l}$, and probability of unsuccessful TXOP access, $p_{C,l}$, by other stations in the network during freezing countdown in the period A_l are computed as follows:

$$p_{S,l} = \delta \sum_{i=l}^{3} \frac{n_i \tau_i \prod_{j=l}^{3} (1 - \tau_j)^{n_j}}{(1 - \tau_i)} \tag{2.5}$$

$$p_{C,l} = 1 - f_l - p_{S,l} \tag{2.6}$$

As a result, I compute the PGF of the freezing countdown pause duration in the period A_l, $l = 1, 2, 3$ because of successful TXOP access of other stations, $S_{A,l}(z)$, and unsuccessful TXOP access of other stations, $C_{A,l}(z)$, as

$$S_{A,l}(z) = \delta \sum_{i=l}^{3} \frac{n_i \tau_i \prod_{j=l}^{3} (1 - \tau_j)^{n_j}}{(1 - \tau_i)} S_i(z) \tag{2.7}$$

$$C_{A,l}(z) = (1 - f_l - p_{S,l}) C(z) \tag{2.8}$$

According to the IEEE 802.11e standard, if the last frame was received with incorrect MAC FCS the medium must be sensed idle for duration of $aifs_k + 1 + ack$ to start the backoff countdown. In this model, the probability that the EIFS event occurs for an AC_k station is equal to $p_{eifs,k} = 1 - g_k \delta \sigma$.

Transfer PGF $\Psi_{F,k}(z)$, $k = 0..3$ for the case that backoff counter is equal to zero is calculated as follows:

$$\Psi_{F,3}(z) = (p_{eifs,3}z + 1 - p_{eifs,3})z^{aifs_3} \tag{2.9}$$

$$\Psi_{F,k}(z) = \frac{(p_{eifs,k}z + 1 - p_{eifs,k})z^{aifs_3} \prod_{i=k+1}^{3} (f_i z)^{A_{i,max}}}{1 - z^{aifs_3} \sum_{i=k+1}^{3} \left((S_{A,i}(z) + C_{A,i}(z)) \sum_{n=0}^{A_{i,max}-1} z(zf_i)^n \prod_{l=i+1}^{3} (f_l z)^{A_{l,max}} \right)}$$

Transfer PGF $\Psi_{NF,k}(z)$, $k = 0..3$ for the case when the backoff counter is non-zero is different from $\Psi_{F,k}(z)$ because of having the loopback to the top of the block. $\Psi_{NF,k}(z)$ for an AC_k station is calculated as follows:

$$\Psi_{NF,3}(z) = \frac{(p_{eifs,3}z + 1 - p_{eifs,3})z^{aifs_3}\frac{f_3}{1-\tau_3}z}{1 - z^{aifs_3}z(S_{A,3}(z) + C_{A,3}(z))}$$

$$\Psi_{NF,k}(z) = \frac{(p_{eifs,k}z + 1 - p_{eifs,k})z^{aifs_3}\prod_{i=k+1}^{3}(f_iz)^{A_{i,max}}\frac{f_k}{1-\tau_k}z}{\Psi_{den,k}} \qquad (2.10)$$

where

$$\Psi_{den,k} = 1 - z^{aifs_3+1}\Big(\sum_{i=k+1}^{3} T_{A_i}(z) \sum_{n=0}^{A_{i,max}-1} (zf_i)^n \prod_{l=i+1}^{3}(f_lz)^{A_{l,max}} + T_k(z)\prod_{i=k+1}^{3}(f_iz)^{A_{i,max}}\Big)$$

$$(2.11)$$

I also define $T_{A,i}(z) = S_{A,i}(z) + C_{A,i}(z)$. $\Psi_{NF,k}(z)$ is the PGF of the time required for decrementing the backoff counter by one for an AC_k station. Note that the decrement occurs in period A_k, where even the same access category station can access the medium. When the station enters the ith backoff stage the freezing and backoff countdowns must be performed until the backoff counter reaches 0. I develop the PGF for the time required to pass through the ith backoff stage. I calculate the probability that a station successfully accesses to medium. I also calculate the probability that the medium is unsuccessfully access by the stations. During the backoff countdown these probabilities are different than the correspondent values that I computed before in period A_l, because I do not know where exactly the interruption occurs for the AC_k station. Thus, probability that the backoff count for traffic class k will be suppressed in the period A_l, $l = 0..k$, due to successful accessing the TXOP period by another station is equal to

$$p_{S,k,l} = \delta\sum_{i=l}^{3}\frac{n_i\tau_i\prod_{j=l}^{3}(1-\tau_j)^{n_j}}{(1-\tau_i)(1-\tau_k)} - \frac{\delta\tau_k}{(1-\tau_k)^2}\prod_{i=l}^{3}(1-\tau_i)^{n_i} \qquad (2.12)$$

However, the probability that the station has to pause the backoff countdown due to failed medium access by another station in the period A_l, $l = 0..k$ is computed as follows:

$$p_{C,k,l} = 1 - \frac{f_l}{1 - \tau_k} - p_{S,k,l} \tag{2.13}$$

Therefore, the PGFs of the times that an AC_k station has to pause due to the transmissions are calculated as follows:

$$S_{P,k,l}(z) = \delta \sum_{i=l}^{3} \frac{n_i \tau_i \prod_{j=l}^{3} (1 - \tau_j)^{n_j}}{(1 - \tau_i)(1 - \tau_k)} S_i(z) - \frac{\delta \tau_k}{(1 - \tau_k)^2} \prod_{i=l}^{3} (1 - \tau_i)^{n_i} S_k(z) \tag{2.14}$$

$$C_{P,k,l}(z) = (1 - \frac{f_l}{1 - \tau_k} - p_{S,k,l})C(z) \tag{2.15}$$

Hence, PGF of duration of medium occupancy in period A_l during the backoff countdown for an AC_k station because of successful TXOP period access by another station is $S_{P,k,l}(z)$. Now, I compute the lateral transfer PGFs which connect the backoff freezing blocks as following

$$\Psi_{C,0}(z) = g_0 z + T_{P,0,0} z B f l_0(z)$$

$$\Psi_{C,1}(z) = g_1 z + \left((1 - f_1^{A_1,max}) T_{P,1,1} + f_1^{A_1,max} T_{P,1,0} \right) z \Psi_{NF,1}(z)$$

$$\Psi_{C,2}(z) = g_2 z + \left((1 - f_2^{A_2,max}) T_{P,2,2} + f_2^{A_2,max} \left[(1 - f_1^{A_1,max}) T_{P,2,1} + f_1^{A_1,max} T_{P,2,0} \right] \right) \cdot$$

$$z \Psi_{NF,2}(z)$$

$$\Psi_{C,3}(z) = g_3 z + \left((1 - f_3^{A_3,max}) T_{P,3,3} + f_3^{A_3,max} \left[(1 - f_2^{A_2,max}) T_{P,3,2} + \right. \right.$$

$$\left. \left. f_2^{A_2,max} [(1 - f_1^{A_1,max}) T_{P,3,1} + f_1^{A_1,max} T_{P,3,0}] \right] \right) z \Psi_{NF,3}(z) \tag{2.16}$$

where $T_{P,k,l} = S_{P,k,l}(z) + C_{P,k,l}(z)$. Now I can write the PGF of the time spent during the ith backoff stage for $i = 0, 1..R$ for an AC_k station as

$$\Psi_{k,i}(z) = \frac{\Psi_{F,k}(z)}{W_{k,i}} + \frac{\Psi_{NF,k}(z)}{W_{k,i}} \sum_{l=1}^{W_{k,i}-1} \Psi_{C,k}(z)^l \qquad (2.17)$$

Therefore, the PGF for the total time spent during backoff procedure for an AC_k station

is computed as follows:

$$
\begin{aligned}
\Psi_{T,k}(z) &= \sum_{i=1}^{m_k+1} (\prod_{j=0}^{i-1} \Psi_{k,j}(z))(1 - \delta g_k)^{i-1} C(z)^{i-1} \delta g_k \\
&+ \sum_{i=m_k+1}^{R} (\prod_{j=0}^{m_k} \Psi_{k,j}(z)) \Psi_{k,m_k}(z)^{(i-m_k)} (1 - \delta g_k)^i C(z)^i \delta g_k \\
&+ (\prod_{j=0}^{m_k} \Psi_{k,j}(z)) \Psi_{k,m_k}(z)^{(R-m_k)} (1 - \delta g_k)^{R+1} C(z)^{R+1} \qquad (2.18)
\end{aligned}
$$

I compute the partial backoff time which includes all the backoff phases except the

zeroth bakoff stage. I call the PGF of the time spent during this part of backoff procedure

as $\Psi_{NT,k}(z)$ for an AC_k station.

$$
\begin{aligned}
\Psi_{NT,k}(z) &= \sum_{i=2}^{m_k+1} (\prod_{j=0}^{i-1} \Psi_{k,j}(z))(1 - \delta g_k)^{i-1} C(z)^{i-1} \delta g_k \\
&+ \sum_{i=m_k+1}^{R} (\prod_{j=0}^{m_k} \Psi_{k,j}(z)) \Psi_{k,m_k}(z)^{(i-m_k)} (1 - \delta g_k)^i C(z)^i \delta g_k \\
&+ (\prod_{j=0}^{m_k} \Psi_{k,j}(z)) \Psi_{k,m_k}(z)^{(R-m_k)} (1 - \delta g_k)^{R+1} C(z)^{R+1} + \delta g_k \quad (2.19)
\end{aligned}
$$

Therefore, the mean total backoff procedure and the mean of the partial backoff proce-

dure for an AC_k station are $\overline{\Psi_{T,k}(z)} = \Psi'_{T,k}(1)$ and $\overline{\Psi_{NT,k}(z)} = \Psi'_{NT,k}(1)$, respectively.
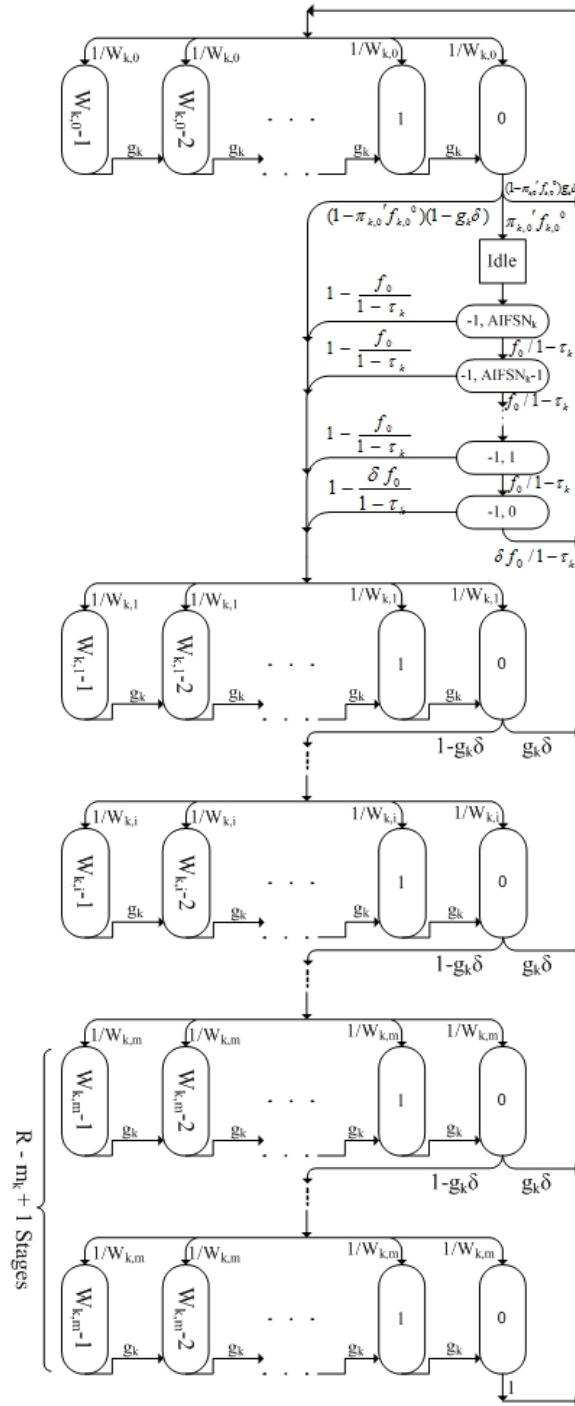
Figure 2.2: Markov chain for AC_k
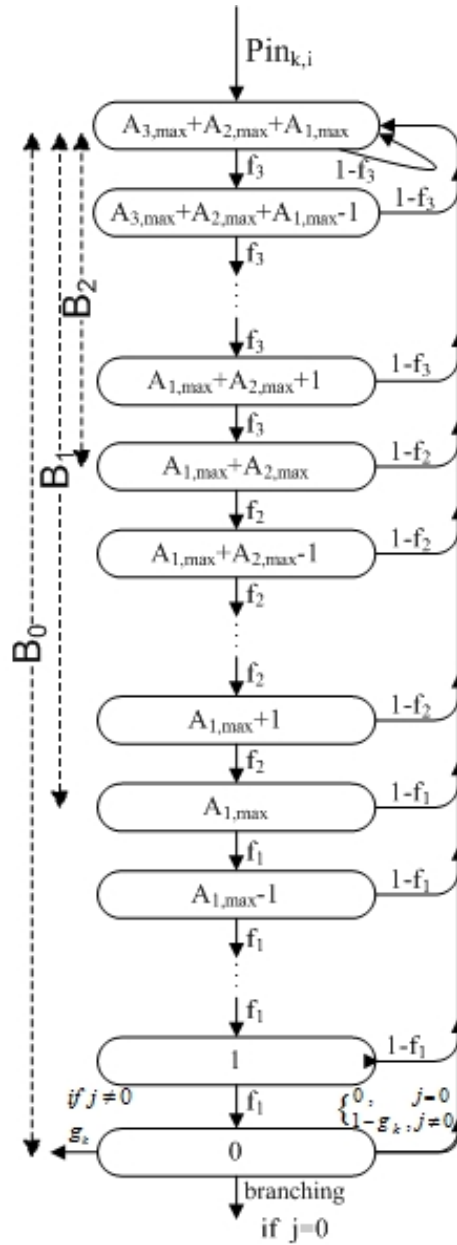
Figure 2.3: Sub-chain for freezing counter for AC_k

2.4.2   Queuing Model of a Station

I model the AC_k queues using an $M^{[x]}/G/1$ system with vacation and burst arrival. The $M^{[x]}/G/1$ queuing system is a single-queue, single server system with Poisson arrivals of

data frames, and a general service time distribution. λ_k indicates the Poisson arrival rate

of bursts. Each arrival for this queue corresponds to the arrival of a burst of messages.

The burst size is generally distributed and multiple bursts are independent and identical

distributed. I assume that $h_{k,r}$ indicates the probability that the burst size H_k for an AC_k

station is equal to r, where $r = 1, 2, ...$ and $k = 0, 1, 2, 3$. $H_k(z)$ and h_k are the probability

generating function (PGF) and the mean value of H_k :

$$
\begin{aligned}
H_k(z) &= \sum_{r=1}^{\infty} h_{k,r} z^r \\
h_k &= E[H_k]
\end{aligned}
\tag{2.20}
$$

The entity in the station which is responsible for data frame transmission is called

server. A data frame in the queue is served when it is successfully transmitted. The time

interval when the server performs the backoff procedure or is idle due to an empty queue

is called a vacation period. A time interval when the station has uninterrupted access to the

medium for data frame transmission is called a busy period. That is, the TXOP period is the

busy period in which the station is allowed to transmit its frames continuously. Otherwise,

it is vacation period. Thus, the server has busy periods and vacation periods alternatively,

and is at all times in one of the two conditions. The system cannot be empty when the

vacation period ends.

I use the following parameters in the system. Let $B_k^*(s)$ and b_k be the Laplace-Stieltjes

transform (LST) of the distribution function (DF) and the mean of the message service time

(i= 2, 3, ...). The traffic intensity or the offered load is given by

$$
\rho_k = \lambda_k b_k h_k
\tag{2.21}
$$

which is shortly called server utilization, that is, the long-run fraction of the time that the server is busy transmitting the data frames. The vacation period includes different probable vacation periods, $V_{k,0}$, $V_{k,1}$, $V_{k,2}$, $V_{k,3}$, and $V_{k,I}$.

$V_{k,0}$ is the duration in which the AC_k station spends for doing the zeroth backoff phase. This phase has to be done regardless of number of data frames waiting in the queue. As computed before, the PGF of the $V_{k,0}$ duration is equal to $\Psi_{k,0}(z)$ with LST of $\Psi_{k,0}^*(s) = \Psi_{k,0}(exp(-s))$. As a result, I are able to compute the PGF for number of arrivals during the zero-th vacation as $\Phi_{k,0}(z) = \sum_{i=0}^{\infty} \phi_{k,i}^0 z^i = \Psi_{k,0}^*(\lambda_k - \lambda_k H_k(z))$.

The remaining phases of the backoff procedure, first phase to R-th phase, form $V_{k,1}$. PGF for duration of the first vacation was calculated as $\Psi_{NT,k}(z)$ and its LST is equal to $\Psi_{NT,k}^*(z) = \Psi_{NT,k}(exp(-s))$. PGF for number of arrivals during this time can be computed as $\Phi_{k,1}(z) = \sum_{i=0}^{\infty} \phi_{k,i}^1 z^i = \Psi_{NT,k}^*(\lambda_k - \lambda_k H_k(z))$. I call the summation of the zero-th and the first vacation as $V_{k,2}$ having PGF of $\Psi_{T,k}(z)$ and LST of $\Psi_{T,k}^*(z) = \Psi_{T,k}(exp(-s))$.

The third vacation, $V_{k,3}$, is the duration of time that the station senses the medium to be idle after exiting from the idle state. If the medium is idle for $AIFS_k$ the station successfully accesses the medium. Otherwise, the station hast to continue the backoff procedure. I assume that the LST for this vacation period is equal to $exp(-s \cdot aifs_k)$. Hence, the PGF for number of arrivals during $V_{k,3}$ is equal to $\Phi_{k,3}(z) = \sum_{i=0}^{\infty} \phi_{k,i}^3 z^i = exp(-\lambda_k(1 - H_k(z)) \cdot aifs_k)$.

Finally, $V_{k,I}$ indicates the duration of time that the AC_k station spends in the idle state waiting for a data frame to arrive from the upper layer. I calculate this period of time in section V. The PGF for number of arrivals during idle state is equal to $\Phi_{k,I}(z) = \sum_{i=0}^{\infty} \phi_{k,i}^I z^i =$

$H_k(z)$. In fact, the first arrival of a burst of frames terminates this period.

The system is examined at a set of embedded Markov points including the vacation termination times and the service completion times. The parameter $\theta_{k,i}$ shows the joint probability that a Markov point is a vacation termination time and that there are i of AC_k data frames in the queue at the time, $i = 1, 2, ...$ In addition, I define $\pi_{k,i}^{(m)}$ as the joint probability that a Markov point is the m-th service completion time in the TXOP period and that there are i AC_k data frames in the queue at that time, $i = 0, 1, 2, ...$ and $m = 1..M_k$.

$$
\begin{aligned}
\theta_{k,i} &= \sum_{m=1}^{M_k} \pi_{k,0}^{(m)} \phi_{k,0}^0 \sum_{t=1}^{i} \phi_{k,t}^I \left(\frac{f_0}{1-\tau_k}\right)^{AIFSN_k} \delta \phi_{k,i-t}^3 \\
&+ \sum_{m=1}^{M_k} \pi_{k,0}^{(m)} \phi_{k,0}^0 \sum_{t=1}^{i} \phi_{k,t}^I \left(1 - \left(\frac{f_0}{1-\tau_k}\right)^{AIFSN_k} \delta\right) \sum_{j=0}^{i-t} \phi_{k,j}^3 \phi_{k,i-t-j}^1 \\
&+ \sum_{m=1}^{M_k} \pi_{k,0}^{(m)} \phi_{k,i}^0 g_k \delta + \sum_{m=1}^{M_k} \pi_{k,0}^{(m)} \sum_{l=1}^{i} \phi_{k,l}^0 (1 - g_k\delta) \phi_{k,i-l}^1 \\
&+ \sum_{j=1}^{i} \pi_{k,j}^{(M_k)} \left(\phi_{k,i-j}^0 g_k \delta + (1 - g_k\delta) \sum_{l=0}^{i-j} \phi_{k,l}^0 \phi_{k,i-l-j}^1\right)
\end{aligned}
\tag{2.22}
$$

The above formula includes four different components. The first component (the first two series) corresponds to the situation when the queue is empty after the zero-th backoff. In this case, the queue was empty before starting the zero-th backoff and during this backoff stage the MAC layer has not received any data frame from the upper layer. Thus, the station must pause until receiving at least one data frame to proceed the backoff procedure. The station remains in the idle state until receiving a data frame. The second component is related to the case that queue is empty before beginning the zero-th backoff, but some data frames arrive during this time period and medium is accessed by the station. The third component indicates the similar situation like the previous one but the TXOP period is not successfully accessed because of transmission failure of RTS or CTS. Thus, the station has

to follow the backoff procedure entering the first backoff stage. Finally, the forth part of the formula shows the case when the queue is not empty before starting the zero-th backoff stage. Hence, the queue will be non-empty before the backoff procedure is completed. The GF for $\{\theta_{k,i}; i = 1, 2, 3, ...\}$ is computed as

$$
\begin{aligned}
\Theta_k(z) \ = \ & \sum_{i=1}^{\infty} \theta_{k,i} z^i = \Phi_{k,I}(z)\Phi_{k,3}(z)((\frac{f_0}{1-\tau_k})^{AIFSN_k}\delta \\
& + (1 - (\frac{f_0}{1-\tau_k})^{AIFSN_k}\delta)\Phi_{k,1}(z)) \sum_{m=1}^{M_k} \pi_{k,0}^{(m)} \\
& + (\Phi_{k,0}(z) - \phi_{k,0}^0)(g_k\delta + \Phi_{k,1}(z)(1 - g_k\delta)) \sum_{m=1}^{M_k} \pi_{k,0}^{(m)} + \\
& \Phi_{k,0}(z)(g_k\delta + \Phi_{k,1}(z)(1 - g_k\delta)) \sum_{j=1}^{\infty} \pi_{k,j}^{(M_k)} z^j
\end{aligned}
\tag{2.23}
$$

In the above formula, $\Phi_{k,I}(z)$ is the PGf for the number of arrivals during the idle state. Note that for a non-bursty traffic $\Phi_{k,I}(z) = z$. However, in a system having burst arrival the PGF for number of data frame arrivals is equal to $\Phi_{k,I}(z) = H_k(z)$.

Considering that the required time for transmitting one single frame including transmission of the data frame and reception of its ACK and three SIFS waiting time is equal to $l_d + 3sifs + ack$, number of frame arrivals during the single frame transmission for a station of AC_k is computed as the following:

$$
A_k(z) = \sum_{i=0}^{\infty} a_{k,i} z^i = \exp\left(\lambda_k(H_k(z) - 1)(l_d + 3sifs + ack)\right)
\tag{2.24}
$$

where I have used $a_{k,i}$ as the probability that i AC_k frames arrive during the frame service time. Then I find the steady-state distribution $\{\pi_{k,i}^{(m)}, i = 0, 1, 2, 3, ...\}$ for the number of frames left behind in the queue after transmission of the m-th frame in the TXOP period for a AC_k station. The GF for $\{\pi_{k,i}^{(m)}\}$ is as follows:

$$\Pi_{k,m}(z) = \sum_{i=0}^{\infty} \pi_{k,i}^{(m)} z^i \qquad m = 1..M_k \qquad (2.25)$$

where I have

$$\pi_{k,i}^{(1)} = \sum_{j=1}^{i+1} \theta_{k,j} \sigma a_{k,i-j+1} + \sum_{j=1}^{i} \theta_{k,j}(1-\sigma)a_{k,i-j} \qquad (2.26)$$

$$\pi_{k,i}^{(m)} = \sum_{j=1}^{i+1} \pi_{k,j}^{(m-1)} \sigma a_{k,i-j+1} + \sum_{j=1}^{i} \pi_{k,j}^{(m-1)}(1-\sigma)a_{k,i-j} \qquad m = 2..M_k \quad (2.27)$$

Therefore, having the above values I are able to compute the generating function $\Pi_{k,1}(z)$ as following

$$\begin{aligned} \Pi_{k,1}(z) &= \sum_{i=0}^{\infty} z^i \sum_{j=1}^{i+1} \theta_{k,j} \sigma a_{k,i-j+1} + \sum_{i=0}^{\infty} z^i \sum_{j=1}^{i} \theta_{k,j}(1-\sigma)a_{k,i-j} \\ &= \Theta_k(z) \frac{A_k(z)(\sigma + (1-\sigma)z)}{z} \end{aligned} \qquad (2.28)$$

If I introduce PGF of $\Omega_k(z) = \frac{A_k(z)(\sigma + (1-\sigma)z)}{z}$ I have simply $\Pi_{k,1}(z) = \Theta_k(z)\Omega_k(z)$. I compute the generating functions for number of frames left behind in the queue for $m = 2..M_k$ as

$$\begin{aligned} \Pi_{k,m}(z) &= \sum_{i=0}^{\infty} \pi_{k,i}^{(m)} z^i = \sum_{i=0}^{\infty} z^i \sum_{j=1}^{i+1} \pi_{k,j}^{(m-1)} \sigma a_{k,i-j+1} + \sum_{i=0}^{\infty} z^i \sum_{j=1}^{i} \pi_{k,j}^{(m-1)}(1-\sigma)a_{k,i-j} \\ &= (\Pi_{k,m-1}(z) - \pi_{k,0}^{(m-1)}) \frac{A_k(z)(\sigma + (1-\sigma)z)}{z} \\ &= (\Pi_{k,m-1}(z) - \pi_{k,0}^{(m-1)})\Omega_k(z) \end{aligned} \qquad (2.29)$$

Based on the above relationships among Θ_k and $\Pi_{k,m}(z)$ I write all the generating functions $\Pi_{k,m}(z), m = 1..M_k$ based on Θ_k as follows:

$$\Pi_{k,m}(z) = \Theta_k(z)\Omega_k^m(z) - \sum_{j=1}^{m-1} \pi_{k,0}^{(j)}\Omega_k^{m-j}(z) \qquad m = 1..M_k \tag{2.30}$$

Substituting (2.30) for $m = M_k$ into (2.23) and solving the resulting equation for $\Theta_k(z)$,

I obtain

$$\begin{aligned}
\Theta_k(z) &= \frac{\sum_{m=1}^{M_k} \pi_{k,0}^{(m)}\left[\Phi_{k,I}(z)\Phi_{k,3}(z)\phi_{k,0}^0\left((\frac{f_0}{1-\tau_k})^{AIFSN_k}\delta + (1 - (\frac{f_0}{1-\tau_k})^{AIFSN_k}\delta)\Phi_{k,1}(z)\right)\right]}{1 - \Omega_k^{M_k}(z)(g_k\delta + \Phi_{k,1}(z)(1 - g_k\delta))\Phi_{k,0}(z)} \\
&+ \frac{\sum_{m=1}^{M_k} \pi_{k,0}^{(m)}\left[(\Phi_{k,0}(z) - \phi_{k,0}^0)(g_k\delta + \Phi_{k,1}(z)(1 - g_k\delta))\right]}{1 - \Omega_k^{M_k}(z)(g_k\delta + \Phi_{k,1}(z)(1 - g_k\delta))\Phi_{k,0}(z)} \\
&- \frac{(\sum_{j=1}^{M_k} \pi_{k,0}^{(j)}\Omega_k^{M_k-j}(z))(g_k\delta + \Phi_{k,1}(z)(1 - g_k\delta))\Phi_{k,0}(z)}{1 - \Omega_k^{M_k}(z)(g_k\delta + \Phi_{k,1}(z)(1 - g_k\delta))\Phi_{k,0}(z)}
\end{aligned} \tag{2.31}$$

Now, I introduce $fd_k(z) = z^{M_k}$ and $gd_k(z) = -A_k(z)^{M_k}(\sigma + (1 - \sigma)z)^{M_k}(g_k\delta +$

$\Phi_{k,1}(z)(1 - g_k\delta))\Phi_{k,0}(z)$. I define $\{gd_{k,r} = Prob[Gd_k = r; r = 0, 1, 2, ...]\}$ for a random

variable Gd_k. For the generating function $Gd_k(z)$ of $\{gd_{k,r}\}$ on $|z| = 1 + \epsilon$ for a small

$\epsilon > 0$, I have

$$\begin{aligned}
|Gd_k(z)| &= |\sum_r gd_{k,r}z^r| \leq \sum_r gd_{k,r}|z|^r = \sum_r gd_{k,r}(1 + \epsilon)^r \\
&= \sum_r gd_{k,r}(1 + r\epsilon) + o(\epsilon) = 1 + \epsilon E[Gd_k] + o(\epsilon) \tag{2.32}
\end{aligned}$$

Using the above bound for $gd_k(z)$, I get

$$\begin{aligned}
|gd_k(z)| &\leq 1 + \Big(M_k(\lambda_k h_k b_k + (1 - \sigma)) + ((1 - g_k\delta)\lambda_k h_k E[V_{k,1}]) + \\
&\quad \lambda_k h_k E[V_{k,0}]\Big)\epsilon + o(\epsilon) \\
&= 1 + \Big(M_k\rho_k' + \lambda_k((1 - g_k\delta)h_k E[V_{k,1}] + h_k E[V_{k,0}])\Big)\epsilon + o(\epsilon) \tag{2.33}
\end{aligned}$$

Where $b_k = l_d + 3sifs + ack$ and $\rho'_k = \rho_k + (1 - \sigma) = \lambda_k h_k b_k + (1 - \sigma)$. In addition, I

have

$$|fd_k(z)| = (1 + \epsilon)^{M_k} = 1 + M_k\epsilon + o(\epsilon) \tag{2.34}$$

Thus, according to (2.33) and (2.34), if

$$\rho'_k + \frac{\lambda_k((1 - g_k\delta)h_k E[V_{k,1}] + h_k E[V_{k,0}])}{M_k} < 1 \tag{2.35}$$

then $|fd_k(z)| > |gd_k(z)|$ on $|z| = 1 + \epsilon$. Therefore, based on Rouché's theorem [80],

$fd_k(z)$ and $fd_k(z) + gd_k(z)$ have the same number of zeros inside $|z| = 1 + \epsilon$. Hence, the

equation $1 - \Omega_k^{M_k}(z)(g_k\delta + \Phi_{k,1}(z)(1 - g_k\delta))\Phi_{k,0}(z)$ which is the denominator of $\Theta_k(z)$

has M_k roots inside $|z| = 1 + \epsilon$. Except $z = 1$, the other $M_k - 1$ roots are computed from

the Lagrange's theorem [80], for $m = 1..M_k - 1$, as following

$$z_{k,m} = \sum_{n=1}^{\infty} \frac{e^{\frac{2\pi mni}{M_k}}}{n!} \frac{d^{n-1}}{dz^{n-1}} \left\{ \left(A_k(z)(\sigma + (1 - \sigma)z) \right)^{M_k} (g_k\delta + \Phi_{k,1}(z)(1 - g_k\delta))\Phi_{k,0}(z) \right\}^{n/M_k} \Big|_{z=0} \tag{2.36}$$

Hence, because $\Theta_k(z)$ is analytic in the area $|z| \leq 1$, the numerator of $\Theta_k(z)$ must have

the same roots of its denominator. Therefore, $z = z_{k,m}, m = 1..M_k - 1$ must be $M_k - 1$

roots of the numerator of (2.31). Subsequently, I obtain $M_k - 1$ equations as follows:

$$0 = \sum_{m=1}^{M_k} \pi_{k,0}^{(m)} \left[\Phi_{k,I}(z_{k,m})\Phi_{k,3}(z_{k,m})\phi_{k,0}^0 \left(\left(\frac{f_0}{1 - \tau_k} \right)^{AIFSN_k} \delta + \left(1 - \left(\frac{f_0}{1 - \tau_k} \right)^{AIFSN_k} \delta \right) \cdot \right. \right.$$
$$\left. \Phi_{k,1}(z_{k,m}) \right) \right] + \sum_{m=1}^{M_k} \pi_{k,0}^{(m)} \left[(\Phi_{k,0}(z_{k,m}) - \phi_{k,0}^0)(g_k\delta + \Phi_{k,1}(z_{k,m})(1 - g_k\delta)) \right] -$$

$$(\sum_{j=1}^{M_k} \pi_{k,0}^{(j)}\Omega_k^{M_k-j}(z_{k,m}))(g_k\delta + \Phi_{k,1}(z_{k,m})(1 - g_k\delta))\Phi_{k,0}(z_{k,m}) \qquad (2.37)$$

However, since $\Theta_k(z)$ contains M_k unknown variables $\{\pi_{k,0}^{(m)}; m = 1..M_k, k = 0, 1, 2, 3\}$, I require another equation to be able to solve the set of equations for the unknowns. The last equation is provided by the normalization equation $\Theta_k(1) + \sum_{m=1}^{M_k} \Pi_{k,m}(1) = 1$. Thus, I introduce summation of all generating functions of the queue length during TXOP period as

$$\begin{aligned} \Pi_k(z) &= \sum_{m=1}^{M_k} \Pi_{k,m}(z) = \Theta_k(z)\Omega_k(z) + \sum_{m=2}^{M_k} \left(\Theta_k(z)\Omega_k^m(z) - \sum_{j=1}^{m-1} \pi_{k,0}^{(j)}\Omega_k^{m-j}(z)\right) \\ &= \frac{\Omega_k(z)[\Theta_k(z)(1 - \Omega_k^{M_k}(z)) - \sum_{j=1}^{M_k-1} \pi_{k,0}^{(j)}(1 - \Omega_k^{M_k-j}(z))]}{1 - \Omega_k(z)} \qquad (2.38) \end{aligned}$$

For calculating the last equation from $\Theta_k(1) + \Pi_k(1) = 1$ I apply $l'H\hat{o}pital's$ rule. After applying the required derivations I obtain

$$\Theta_k(1) = \frac{\Theta_{k,num}{}'(1)}{\Theta_{k,den}{}'(1)} \qquad (2.39)$$

where

$$\begin{aligned} \Theta_{k,num}{}'(1) &= \sum_{m=1}^{M_k} \pi_{k,0}^{(m)}\left[\phi_{k,0}^0(\Phi_{k,I}'(1) + \Phi_{k,3}'(1) + (1 - (\frac{f_0}{1 - \tau_k})^{AIFSN_k}\delta)\Phi_{k,1}'(1)) - \right. \\ &\quad \left. (1 - g_k\delta)\Phi_{k,1}'(1)\right] \\ &\quad + \sum_{m=1}^{M_k} \pi_{k,0}^{(m)}(1 - \phi_{k,0}^0)(1 - g_k\delta)\Phi_{k,1}'(1) - \sum_{j=1}^{M_k-1} (M_k - j)\pi_{k,0}^{(j)}\Omega_k'(1) \\ \Theta_{k,den}{}'(1) &= -M_k\Omega_k'(1) - (1 - g_k\delta)\Phi_{k,1}'(1) - \Phi_{k,0}'(1) \qquad (2.40) \end{aligned}$$

where $\Phi_{k,I}'(1) = h_k$, $\Phi_{k,3}'(1) = \lambda_k h_k AIFSN_k$, and $\Omega_k'(1) = A_k'(1) - \sigma = \lambda_k h_k(l_d +$

$3sifs + ack) - \sigma$. However, for computing $\Pi_k(1)$ I require to apply $l'H\hat{o}pital's$ rule twice. Hence, after doing the required derivations I have

$$
\begin{aligned}
\Pi_k(1) &= \frac{\Pi_{k,num}''(1)}{\Pi_{k,den}''(1)} = (M_k)\frac{\Theta_{k,num}'(1)}{\Theta_{k,den}'(1)} - \sum_{j=1}^{M_k-1} \pi_{k,0}^{(j)}(M_k - j) \\
&= M_k\Theta_k(1) - \sum_{j=1}^{M_k-1} \pi_{k,0}^{(j)}(M_k - j)
\end{aligned}
\tag{2.41}
$$

Therefore, the M_k-th equation is provided from $\Theta_k(1) + \Pi_k(1) = \frac{X_{Num}}{X_{Den}} = 1$ where

$$
\begin{aligned}
X_{Num} &= -(M_k + 1)\sum_{m=1}^{M_k} \pi_{k,0}^{(m)}\Big[\phi_{k,0}^0(\Phi_{k,I}'(1) + \Phi_{k,3}'(1) + (1 - (\frac{f_0}{1 - \tau_k})^{AIFSN_k}\delta)\Phi_{k,1}'(1)) \\
&\quad -(1 - g_k\delta)\Phi_{k,1}'(1) + (1 - \phi_{k,0}^0)(1 - g_k\delta)\Phi_{k,1}'(1)\Big] \\
&\quad -(M_k + 1)\sum_{j=1}^{M_k-1} (M_k - j)\pi_{k,0}^{(j)}\Omega_k'(1) \\
&\quad -[M_k\Omega_k'(1) + (1 - g_k\delta)\Phi_{k,1}'(1) + \Phi_{k,0}'(1)]\sum_{j=1}^{M_k-1} \pi_{k,0}^{(j)}(M_k - j) \\
X_{Den} &= M_k\Omega_k'(1) + (1 - g_k\delta)\Phi_{k,1}'(1) + \Phi_{k,0}'(1)
\end{aligned}
\tag{2.42}
$$

Now, I compute PGF for number of frame transmissions during TXOP period for an AC_k station, $\Xi_k(z)$ as

$$
\Xi_k(z) = \sum_{m=1}^{M_k} \xi_{k,m}z^m = \frac{1}{\Pi_k(1)}\Big(\sum_{m=1}^{M_k-1} \pi_{k,0}^{(m)}z^m + (\Pi_k(1) - \sum_{m=1}^{M_k-1} \pi_{k,0}^{(m)})Z^{M_k}\Big)
\tag{2.43}
$$

The mean number of transmitted frames for an AC_k station is equal to $\overline{\Xi_k(z)} = \Xi_k'(1) = \frac{1}{\Pi_k(1)}\Big(\sum_{m=1}^{M_k-1} m\pi_{k,0}^{(m)} + M_k(\Pi_k(1) - \sum_{m=1}^{M_k-1} \pi_{k,0}^{(m)})\Big)$. Therefore, mean number of successfully transmitted frames for an AC_k station during TXOP is equal to $\Xi_k'(1)\sigma$.

2.4.3   Markov Chain Model of the Station

The entire Markov chain for an AC_k station is shown in Fig. 4.1 and Fig. 2.3. The Markov chain represents a random process with stationary distribution $b_{k,i,j,t}$, where $k = 0, 1, 2, 3$ indicates the traffic class that the station belongs to, $i = 0..m_k..R$ denotes the backoff stage in the backoff procedure invoked by the station, $j = 0..W_{k,i} - 1$ indicates the value of the backoff counter, and $t = 0..B_k$ shows the value of the freezing counter. The Markov chain includes only the time slot that the stations in the network are active listening to the medium for counting down their backoff or freezing counter to acquire TXOP period successfully. The time that any station in the network transmits on the medium is excluded from the chain to achieve a more accurate access probability for stations in the network. The time between two successive Markov points is a random variable which affects the steady state probabilities. Therefore, the process under consideration is a semi Markov process [81]. For evaluating the semi Markov process I need DTMCs and the time distributions between the Markov points.

The most important parameter calculated from the whole system is access probability τ_k which is the probability of accessing the medium when medium is not busy. Access probability is defined as $\tau_k = \sum_{i=0}^{R} b_{k,i,0,0} + b_{k,-1,0}$, where $b_{k,i,0,0}$ is the stationary probability of having backoff counter and freezing counter equal to zero during i-th backoff stage for an AC_k station, and $b_{k,-1,0}$ is the stationary probability that freezing counter reaches zero after arriving any data frame during idle state.

According to the standard, the zero-th backoff must be performed after completing the TXOP period, in case of successful TXOP access, or dropping the data frame, in case of unsuccessful accessing TXOP period at the end of the R-th backoff phase. Therefore, the

station checks the buffer to find a data frame waiting at the end of the zero-th backoff stage, as shown in the Markov chain. In the following, I find the required equation to be added to the set of equations that I have obtained in the previous sections. The set of equations will be solved to find all the unknown parameters in the system.

At first, I define some parameters as follows:

$$Y_k = 1 + \sum_{i=k+1}^{3} \left(\prod_{j=i+1}^{3} f_j^{A_{j,max}} \sum_{t=1}^{A_{i,max}} f_i^t \right) \qquad k = 0..3 \tag{2.44}$$

$$\chi_k = \prod_{i=k+1}^{3} f_i^{A_{i,max}} \tag{2.45}$$

I define $pin_{k,i}$ as the input probability to each block in the i-th backoff stage for $i = 0..R$. Thus, for $k = 0..3$ and $i = 0..R$ I have

$$b_{k,i,j,B_k} = \frac{pin_{k,i}((W_{k,i} - j) - (W_{k,i} - 1 - j)g_k)}{\chi_k g_k} \qquad 0 < j \le W_{k,i} - 1$$

$$b_{k,i,0,B_k} = \frac{pin_{k,i}}{\chi_k}$$

$$b_{k,i,j,0} = \frac{(W_{k,i} - j)pin_{k,i}}{g_k} \qquad 0 < j \le W_{k,i} - 1$$

$$b_{k,i,0,0} = W_{k,i}pin_{k,i} \tag{2.46}$$

Hence, using the above values I obtain the following summations for $k = 0..3$, $i = 0..R$, and $0 < j \le W_{k,i} - 1$

$$\sum_{t=0}^{B_k} b_{k,i,j,t} = pin_{k,i}\left(\frac{Y_k((W_{k,i} - j) - (W_{k,i} - 1 - j)g_k)}{\chi_k g_k} + (W_{k,i} - 1 - j) \right)$$

$$\sum_{t=0}^{B_k} b_{k,i,0,t} = pin_{k,i}\left(\frac{Y_k}{\chi_k} + (W_{k,i} - 1) \right) \qquad 0 \le i \le R \tag{2.47}$$

Therefore, I are able to compute the summation of all the stationary distributions $b_{k,i,j,t}$ at the i-th backoff phase for $i = 0..R$ as follows:

$$
\begin{aligned}
S_{k,i} &= \sum_{j=0}^{W_{k,i}-1} \sum_{t=0}^{B_k} b_{k,i,j,t} \\
&= pin_{k,i}\Big[\frac{(W_{k,i}-1)W_{k,i}}{2} + \frac{Y_k}{\chi_k}\big(1 + \frac{(W_{k,i}-1)W_{k,i}}{2g_k} - \frac{(W_{k,i}-1)(W_{k,i}-2)}{2}\big)\Big]
\end{aligned}
\tag{2.48}
$$

Then, I compute the values of $pin_{k,i}$, $0 \leq i \leq R$ as follows:

$$
b_{k,1,0,0} = W_{k,1}pin_{k,1} = b_{k,0,0,0}\Big[(1-\pi'_{k,0}\phi^0_{k,0})(1-g_k\delta)+\pi'_{k,0}\phi^0_{k,0}(1-\delta(\frac{f_0}{1-\tau_k})^{AIFSN_k+1})\Big]
\tag{2.49}
$$

As a result,

$$
pin_{k,1} = \frac{b_{k,0,0,0}\Big[(1-\pi'_{k,0}\phi^0_{k,0})(1-g_k\delta)+\pi'_{k,0}\phi^0_{k,0}(1-\delta(\frac{f_0}{1-\tau_k})^{AIFSN_k+1})\Big]}{W_{k,1}}
\tag{2.50}
$$

From the Markov chain it is clear that $b_{k,i,0,0} = (1-g_k\delta)^{i-1}b_{k,1,0,0}$, $0 < i \leq R$. Thus, for $i = 1..R$ I have

$$
\begin{aligned}
pin_{k,i} &= \frac{(1-g_k\delta)^{i-1}b_{k,1,0,0}}{W_{k,i}} \\
&= \frac{(1-g_k\delta)^{i-1}b_{k,0,0,0}\Big[(1-\pi'_{k,0}\phi^0_{k,0})(1-g_k\delta)+\pi'_{k,0}\phi^0_{k,0}(1-\delta(\frac{f_0}{1-\tau_k})^{AIFSN_k+1})\Big]}{W_{k,i}}
\end{aligned}
\tag{2.51}
$$

And finally, $pin_{k,0} = \frac{b_{k,0,0,0}}{W_{k,0}}$. In addition, from the Markov chain I obtain

$$
b_{k,-1,t} = \pi'_{k,0}\phi^0_{k,0}\big(\frac{f_0}{1-\tau_k}\big)^{AIFSN_k-t}b_{k,0,0,0}
\tag{2.52}
$$

Therefore, I have

$$
\begin{aligned}
S_{k,-1} &= \sum_{t=0}^{AIFSN_k} b_{k,-1,t} = \pi'_{k,0}\phi^0_{k,0}\Big(\sum_{t=0}^{AIFSN_k} (\frac{f_0}{1-\tau_k})^{AIFSN_k-t}\Big)b_{k,0,0,0} \\
&= \pi'_{k,0}\phi^0_{k,0}b_{k,0,0,0}\Big(\frac{1-(\frac{f_0}{1-\tau_k})^{AIFSN_k+1}}{1-(\frac{f_0}{1-\tau_k})}\Big)
\end{aligned}
\tag{2.53}
$$

At this point, I calculate the access probability τ_k as

$$
\begin{aligned}
\tau_k &= \sum_{i=0}^{R} b_{k,i,0,0} + b_{k,-1,0} \tag{2.54} \\
&= b_{k,0,0,0}\Big[1 + (\frac{f_0}{1-\tau_k})^{AIFSN_k}\pi'_{k,0}\phi^0_{k,0} + [(1-\pi'_{k,0}\phi^0_{k,0})(1-g_k\delta) + (\pi'_{k,0}\phi^0_{k,0}) \\
&\quad *(1-\delta(\frac{f_0}{1-\tau_k})^{AIFSN_k+1})](1+(1-g_k\delta)+(1-g_k\delta)^2+...+(1-g_k\delta)^{R-1})\Big]
\end{aligned}
$$

As a result, I obtain $b_{k,0,0,0} = \frac{\tau_k}{u_k}$, where u_k is equal to

$$
\begin{aligned}
u_k &= 1 + (\frac{f_0}{1-\tau_k})^{AIFSN_k}\pi'_{k,0}\phi^0_{k,0} + [(1-\pi'_{k,0}\phi^0_{k,0})(1-g_k\delta) \\
&\quad +(\pi'_{k,0}\phi^0_{k,0})(1-\delta(\frac{f_0}{1-\tau_k})^{AIFSN_k+1})](\frac{1-(1-g_k\delta)^R}{g_k\delta})
\end{aligned}
\tag{2.55}
$$

The probability that an AC_k station waits in the idle state for a data frame arrival is calculated as $P_{k,idle} = 1 - \frac{\overline{L_{Act,k}}}{\overline{L_{Tot,k}}}$, where $\overline{L_{Act,k}}$ is the mean time that the station is not in the idle state and $\overline{L_{Tot,k}}$ is the average total time between two successive successfully TXOP accesses of the station. First, I compute these distances in the form of LST using the queuing model presented in the previous section:

$$
L^*_{Act,k}(s) = S_k(exp(-s))\Psi_{k,0}(exp(-s))\{\pi'_{k,0}\phi^0_{k,0}exp(-sAIFSN_k)
$$

$$* \left(\left(\frac{f_0}{1-\tau_k} \right)^{AIFSN_k} \delta + \left(1 - \left(\frac{f_0}{1-\tau_k} \right)^{AIFSN_k} \delta \right) \Psi_{NT,k}(exp(-s)) \right)$$

$$+ (1 - \pi'_{k,0} \phi^0_{k,0})(g_k \delta + (1-g_k\delta)\Psi_{NT,k}(exp(-s))) \Big\} \tag{2.56}$$

$$L^*_{Tot,k}(s) = S_k(exp(-s))\Psi_{k,0}(exp(-s))\Big\{ \pi'_{k,0}\phi^0_{k,0} exp(-sAIFSN_k)$$

$$* \frac{\lambda_k}{\lambda_k+s} \left(\left(\frac{f_0}{1-\tau_k} \right)^{AIFSN_k} \delta + \left(1 - \left(\frac{f_0}{1-\tau_k} \right)^{AIFSN_k} \delta \right) \Psi_{NT,k}(exp(-s)) \right)$$

$$+ (1 - \pi'_{k,0}\phi^0_{k,0})(g_k\delta + (1-g_k\delta)\Psi_{NT,k}(exp(-s))) \Big\} \tag{2.57}$$

where $\frac{\lambda_k}{\lambda_k+s}$ is LST of exponentially distributed data frame burst inter-arrival time. Note

that for a station with bursty arrival the idle state ends when a burst of data frames arrives.

Thus, I have $\overline{L_{Act,k}} = - \frac{dL_{Act,k}}{ds}\Big|_{s=0}$ and $\overline{L_{Tot,k}} = - \frac{dL_{Tot,k}}{ds}\Big|_{s=0}$.

Finally, I use the normalization condition of the Markov chain which indicates that

summation of all the probabilities is equal to 1.

$$1 = \sum_{i=-1}^{R} S_{k,i} + P_{k,idle} = \tag{2.58}$$

$$\pi'_{k,0}\phi^0_{k,0}b_{k,0,0,0} \left(\frac{1 - \left(\frac{f_0}{1-\tau_k} \right)^{AIFSN_k+1}}{1 - \left(\frac{f_0}{1-\tau_k} \right)} \right) + P_{k,idle}$$

$$+ \sum_{i=0}^{R} pin_{k,i} \left[\frac{(W_{k,i}-1)W_{k,i}}{2} + \frac{Y_k}{\chi_k} \left(1 + \frac{(W_{k,i}-1)W_{k,i}}{2g_k} - \frac{(W_{k,i}-1)(W_{k,i}-2)}{2} \right) \right]$$

Now, I are able to solve the system of equations to find the required parameters. Hav-

ing all the equalities together I have $4 + M_k$ unknown variables of $\tau_k, k = 0..3$ and

$\pi^{(m)}_{k,0}, m = 1..M_k$.

2.5 Performance Metrics

In this section, I define the performance measures to study the network's behaviour. First, I define normalized throughput as one of the major performance metrics. The normalized throughput for AC_k is defined as the fraction of time in which the channel is used to successfully transmit AC_k frames excluding the headers. The normalized throughput is computed as

$$\tau_{Norm,k} = \frac{E[L]\Xi'_k(1)\sigma}{L_{Tot,k}} \tag{2.59}$$

where $E[L]$ is equal to the required number of slots for transmission of a data frame's payload. In addition, I calculate the mean frame access delay. Frame access delay is defined as the time interval between the instant the frame arrives to the queue and the time when the frame reception is acknowledged by the receiver. Access delay is also called frame response time that is known as the single most important performance measure [80]. The mean access delay of a data frame consists of the waiting time W (the interval from the arrival time to the time when its service is started) and the service time. I assume that $W^*_k(s)$ is the LST of distribution function for W. Therefore, the access delay, $T^*_k(s)$, is computed as

$$T^*_k(s) = W^*_k(s)B^*_k(s) \tag{2.60}$$

where $B^*_k(s)$ is the LST of distribution function of frame service time. For calculating the mean waiting time I employ the property of First Come First Served (FCFS) M/G/1 service that the number of frames left behind by a departing frame is equal to the number of frames that arrived while the frame was in the system. That is,

$$\frac{\Pi_k(z)}{\Pi_k(1)} = W_k^*(\lambda_k - \lambda_k H_k(z)) A_k(z) \tag{2.61}$$

The burst size distribution can be generally selected. Deploying the PGF of the burst size distribution and $s = \lambda_k - \lambda_k H_k(z)$ in the above formula results the LST of waiting time, $W_k^*(s)$. For instance, if I assume that the burst size is geometrically distributed I have $H_k(z) = \frac{z}{z+(1-z)h_k}$. After substituting $s = \lambda_k - \lambda_k H_k(z)$ in the above formula I obtain

$$W_k^*(s) = \frac{\Pi_k\left(\frac{h_k(\lambda_k - s)}{h_k \lambda_k + s(1-h_k)}\right)}{\Pi_k(1) A_k\left(\frac{h_k(\lambda_k - s)}{h_k \lambda_k + s(1-h_k)}\right)} \tag{2.62}$$

Then, I compute the mean service time as $\overline{W_k} = -\frac{d}{ds} W_k^*(0)$. The mean access delay can be calculated from the above formulas.

2.6 Parameters Used in Performance Evaluation

In order to investigate an IEEE 802.11e EDCA-based WLAN performance I have conducted an experiment. I used Maple 13 [82] for solving the system of equations (3.36) - (2.58). I used a PC with 2.4 GHz Core 2 Duo and 4GB of RAM for solving the whole model. In order to decrease the model complexity I have applied an iterative approach. I used OPNET simulator [83] to validate the analytical results.

During the experiment, I consider four ACs as defined in the standard. I assume that each station has exactly one queue with a specific AC. I consider a single-hop ad-hoc network with 5 nodes which transmit AC_k frames. The frames' destination is randomly chosen. The transmission rate is set to 2 Mbps (Mega bit per second). Frames' payload size is set to 100 B. All stations employ RTS/CTS mechanism for transmission of data frames. Therefore, collision could occur just for RTS frames. In the simulation model, I set the

stations' buffer size to 32 KB to investigate the frames' waiting time under the saturation region. Hence, buffer overflow occurs in saturation condition for all the stations and the extra frames are dropped. Because the storage size is large it does not affect the waiting time of the data frames under non-saturation condition. Note that this is the only difference between the simulation and the analytical models.

In our work, I fix three differentiation parameters of $AIFS_k$, CW_{min} and CW_{max}. I adopt $AIFSN_3 = 2$, $AIFSN_2 = 3$, $AIFSN_1 = 5$, $AIFSN_0 = 7$ to clearly distinguish the performance descriptors of different ACs. The values $CW_{min} = 31$ and $CW_{max} = 511$ are selected for all the ACs. Number of backoff phases is controlled with $m_k = 4$, $(k = 0..3)$. In addition, the retry limit, R, is set to 7 for both simulation and the analytical models. ber is set to $2 * 10^{-5}$. I assume that the burst size is a geometrically distributed random variable in which $h_{k,r}$, $H_k(z)$ and h_k are as follows:

$$
\begin{aligned}
h_{k,r} &= (1 - p_k)^{r-1} p_k & r = 1, 2, 3, ... \\
H_k(z) &= \sum_{r=1}^{\infty} h_{k,r} z^r = \frac{z p_k}{1 - z(1 - p_k)} = \frac{z}{z + (1 - z) h_k} & (2.63) \\
h_k &= E[H_k] = \frac{1}{p_k}
\end{aligned}
$$

I set the mean burst size to $h_k = 5$ and the mean burst arrival rate, λ_k, varies from 1 to 20 bursts per second (bps). Then, I vary the $TXOP_k$ to understand its affects on the performance descriptors.

Throughout the study, TXOP duration is set to one MSDU, 4900, 6000, and 11100μ seconds that is the required transmission time for one, four, five, and ten data frames ($M_k = 1, 4, 5, 10$), respectively. In all the plots $solid$, $dotted$, $dashed$, and $dash - dotted$ lines represent the corresponding values for AC$_0$, AC$_1$, AC$_2$, and AC$_3$, respectively.

(a) Normalized throughput   (b) Average period length between   (c) Average access delay
                                              two successive TXOP Accesses
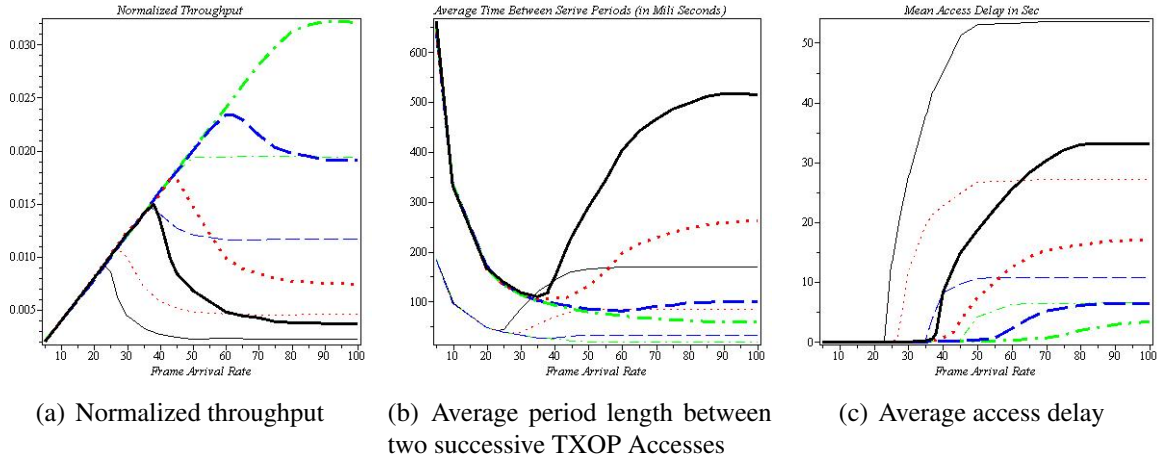
Figure 2.4: Normalized throughput, average service period length and mean access delay - no burst TXOP = 0 & mean burst size = 5 TXOP = 6000 μs

2.7 Impacts of Burst Sizes and TXOP Lengths on an IEEE 802.11e EDCA-based WLAN Performance

Our study indicates that the TXOP differentiation parameter noticeably improves the network performance when the frames arrive in burst. Fig. 2.4 depicts simulation results for the normalized throughput, the average duration between two successive TXOP accesses by a station, and the mean frame access delay for all ACs. The thin lines indicate the values where arrival process is not bursty and TXOP value is set to 0 for all the ACs. The thick lines show the values where the frames arrive to the queue in burst having mean burst size equal to 5. In latter case, TXOP is set to 6000 μsec for all ACs which is the required transmission time for five data frames of 100B payload size.

Fig. 2.4 (a) indicates that the normalized throughput is significantly improved for all the stations when TXOP limit matches the average burst size. In this case the saturation

(a) Normalized throughput for $\text{TXOP}_k = 0$

(b) Normalized throughput for $\text{TXOP}_k = 4900\mu s$

(c) Normalized throughput for $\text{TXOP}_k = 6000\mu s$

(d) Mean access delay for $\text{TXOP}_k = 0$

(e) Mean access delay for $\text{TXOP}_k = 4900\mu s$

(f) Mean access delay for $\text{TXOP}_k = 6000\mu s$
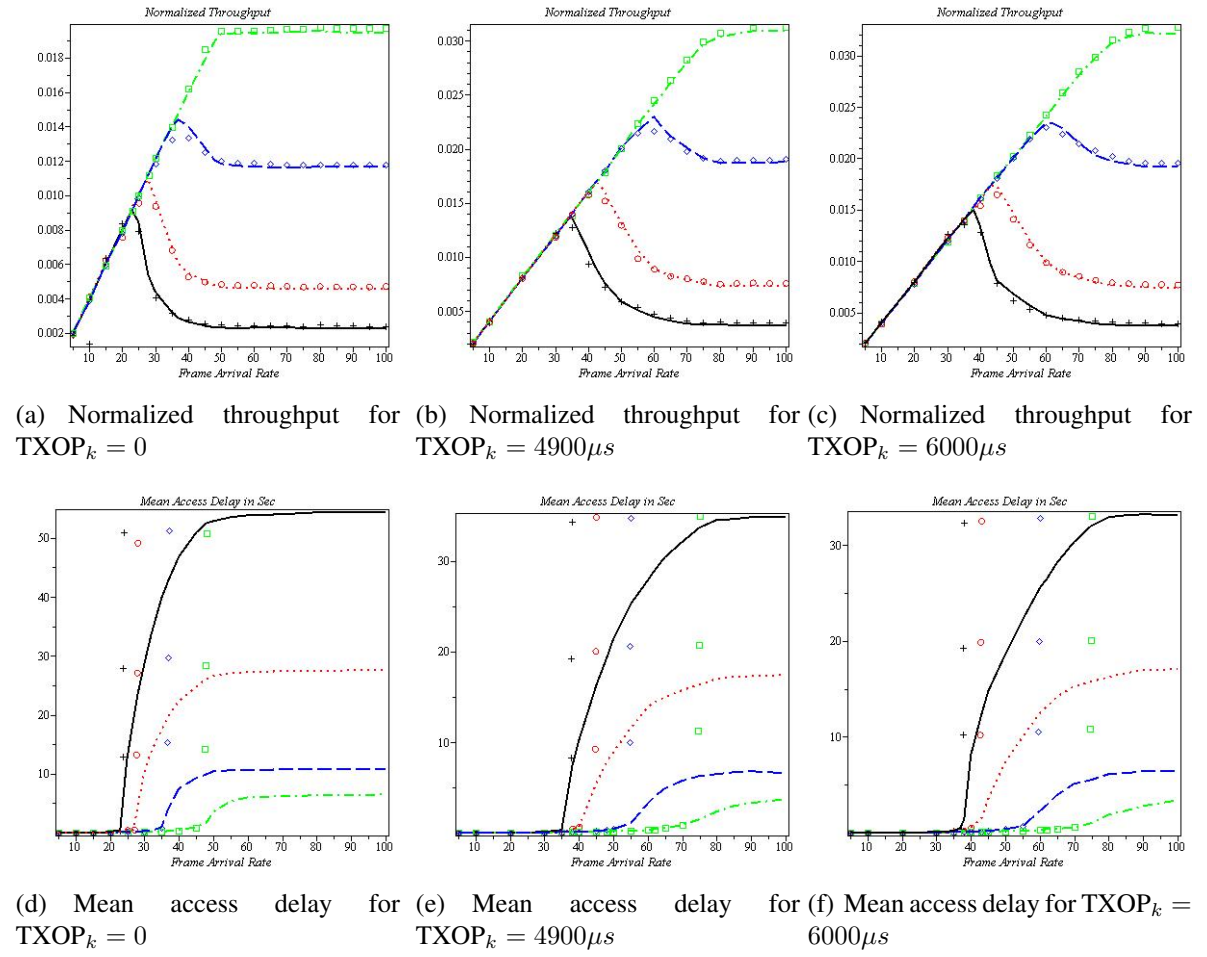
Figure 2.5: Normalized throughput and mean access delay for mean burst size = 5

boundaries are shifted by at least 20 frames per second for all ACs.

Fig. 2.4 (b) indicates that when the frames arrive in burst and TXOP is employed the average time between two successive TXOP accesses for all the ACs during non-saturation region is considerably increased compared to the case when TXOP=0 and arrival process is not bursty. The competition among the stations decreases when a single backoff serves a group of data frames.

Fig. 2.4 (c) depicts the mean frame access delay for the two cases when the buffer

capacity is finite. When every station is allowed to transmit just one data frame during TXOP period the mean access delay is much higher than the case when stations can transmit up to 5 data frames during the access period.

Fig. 2.5 and Fig. 2.6 depict the analytical and simulation results for the network performance metricsunder bursty traffic when TXOP limit increases. In the first row of Fig. 2.5, the analytical results for the normalized throughput are accompanied by the simulation results. The analytical results are shown in point style. Cross, circle, diamond, and box symbols are used for showing the analytical values for normalized throughput for access categories of 0, 1, 2, and 3, respectively. The plots show that the results match acceptably. The normalized throughput plots clearly show non-saturation regions and in fact saturation and non-saturation boundaries for all the ACs. Fig. 2.5 depicts the normalized throughput values for the cases that mean burst size is equal to 5 while TXOP value varies.

I note that as the traffic increases, the network moves through linear (non-saturation) regime, to saturation regime. Figs. 2.5 (a-c) clearly indicate that increasing TXOP value pushes the saturation boundaries and extends the non-saturation region for all the access categories. In addition, the plots in the first row show that having larger values for TXOP improves the normalized throughput of all ACs. In fact, in case of burst arrival and under non-saturation condition, having larger TXOP allows the stations to have higher chance to transmit all the frames in a burst during a TXOP period. Therefore, the stations need smaller number of attempts to compete for the medium. Hence, the access probabilities of higher priority classes decrease which improves total normalized throughput.

The plots in the second row of Fig. 2.5 indicate that if I assume that the buffer sizes are finite the mean access delay of the data frames sharply increases during saturation condition

especially for lower priority classes. However, when the queue size is considered infinite the mean frame access delay tends to infinity under saturation condition. TXOP value growth improves the mean access delay because smaller number of attempts is required for transmitting the same number of data frames.

(a) Service period for $\text{TXOP}_k = 0$

(b) Service period for $\text{TXOP}_k = 4900\mu s$

(c) Service period for $\text{TXOP}_k = 6000\mu s$

(d) Success probability for $\text{TXOP}_k = 0$

(e) Success probability for $\text{TXOP}_k = 4900\mu s$

(f) Success probability for $\text{TXOP}_k = 6000\mu s$

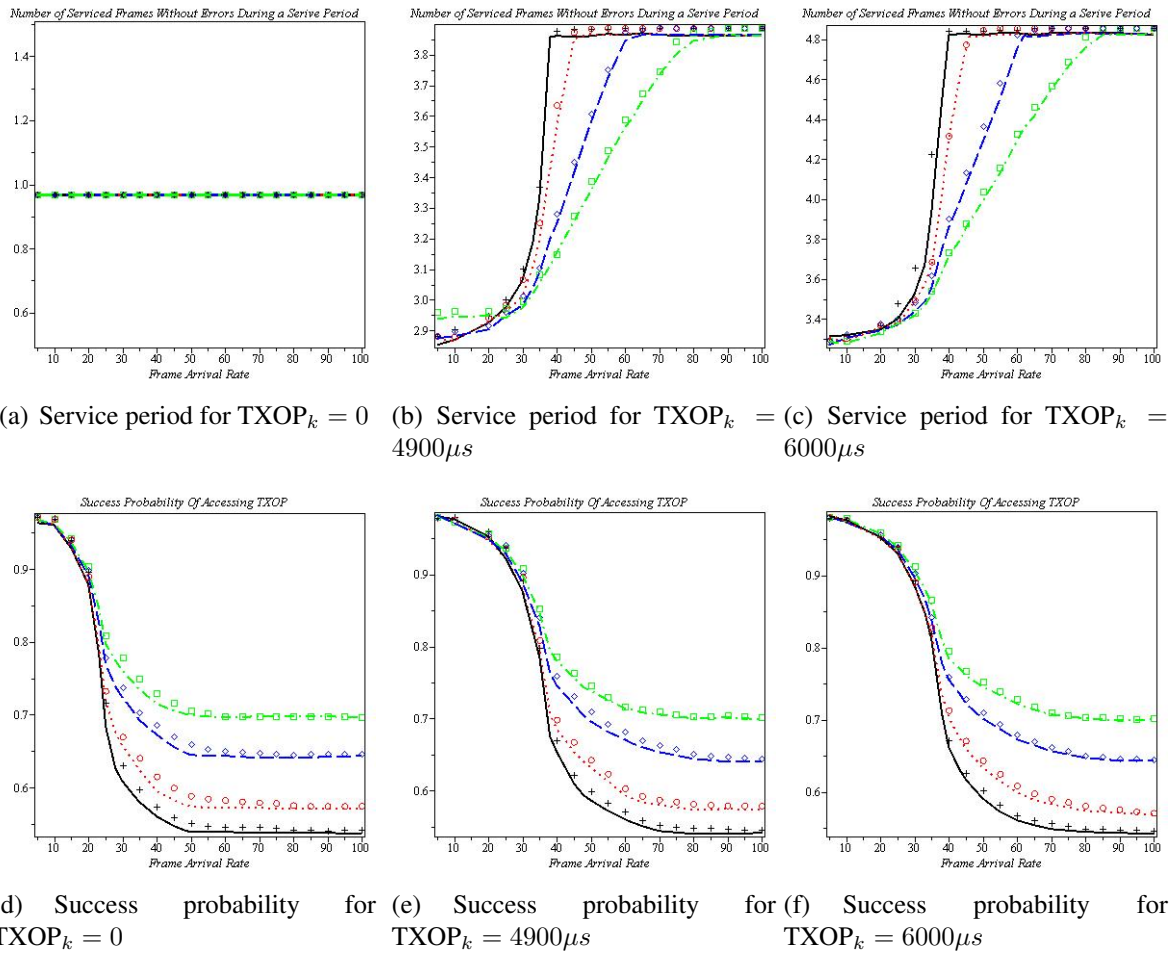Figure 2.6: Mean number of successfully transmitted frames during TXOP period and success probability of acquiring TXOP for mean burst size = 5

The plots in the first row of Fig. 2.6 depict mean number of successfully transmitted frames when the TXOP period increases for all the ACs. The plots clearly show the saturation and non-saturation boundaries for all the ACs. For instance, for the case when

$M_k = 4$ the boundaries occur at approximately 37, 43, 61, and 80 fps, for stations of AC_0, AC_1, AC_2, and AC_3, respectively. However, when M_k is equal to the mean burst size the boundaries happen at 39, 45, 63, and 83, for access categories 0, 1, 2, and 3, respectively. Note that according to the performance descriptors there is a small improvement between the performance for these two cases. The reason is that the burst size is geometrically distributed in which the mean and the standard deviation are equal to 5 and 4.472 approximately. It is expected that if the burst size distribution was deterministic the improvement would be more noticeable.

The second row of Fig. 2.6 represents the success probability of winning the medium and accessing the TXOP period. The plots indicate that the simulation and the analytical results match acceptably. Increase of network traffic decreases success probability of accessing TXOP with high slopes until all the stations in the network operate under saturation condition. Note that how the success probability decreases when the network is unstable where some stations in the network are under saturation condition. The success probability of access to TXOP is as low as 54% for the lowest priority class when all the stations in the network are saturated. It indicates that an IEEE 802.11e EDCA-based WLAN is highly sensitive to traffic. Therefore, admission control is necessary for such a network to aid the stations to avoid starvation.

At the end, I investigate the performance improvement when TXOP is allocated for transmitting a number of frames larger than the mean burst size. In Fig. 2.7 I compare the simulation results for the cases where $M_k = 5$, $k = 0..3$ and $M_k = 10$, $k = 0..3$. The mean burst size is equal to 5 for both cases which corresponds to $p_k = 0.2$, $k = 0..3$ in the equations (2.63). The thin lines indicate the values for the case where $M_k = 5$ while

(a) Normalized throughput

(b) Average period length between two successive TXOP accesses

(c) Mean number of successfully transmitted frames during a service period
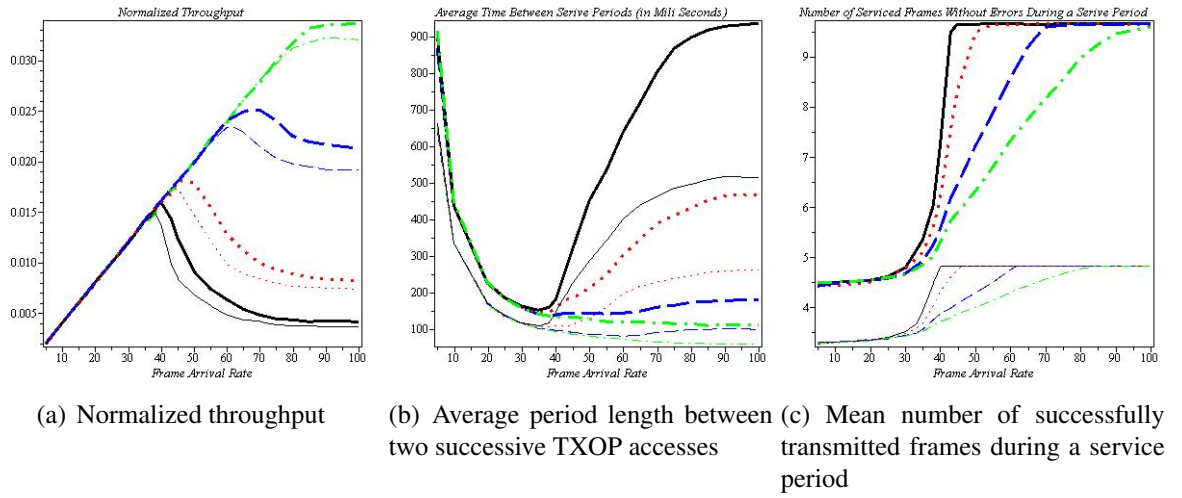
Figure 2.7: Normalized throughput, mean access delay, and mean number of successfully transmitted frames in a service period - mean burst size = 5 TXOP = 6000 μs & TXOP = 11100 μs

the thick lines indicate the values when $M_k = 10$. Because the burst size is geometrically distributed with parameter p_k the probability that size of an arrived burst is larger than M_k is equal to $P_{out} = (1 - p_k)^{M_k}$. The probability that the burst size is too large to be accommodated in one TXOP period is approximately 0.328 where $M_k = 5$. However, when $M_k = 10$ this probability is approximately 0.107. Increasing TXOP limit from $M_k = 5$ data frames to $M_k = 10$ data frames extends slightly the stability region of the network and each station. Allocating TXOP limit corresponding to the average burst size seems sufficient though tail of geometric distribution covers up to 32.8%. During non-saturation region the remaining burst after one service period may be combined with the new burst which helps the stations to utilize the TXOP period well. During saturation region every station uses the whole TXOP period and competes continuously for the medium which may result in starvation for lower priority classes.

Thus, under non-saturation condition, larger TXOP limit decreases the backoff time

causing the wireless medium to be more utilized which pushes the saturation boundaries to some extent. Allocating a TXOP value which is larger than or equal to the mean burst size decreases the requirement of the stations to compete for the medium because the whole burst of data frames is most likely transmitted during a TXOP period. Hence, the total network performance is improved. However, our study indicates that large TXOP allocations do not significantly improve the network performance and may raise unfairness and security concerns since nodes can start sending large bursts which will always use whole TXOP allocation.

2.8 Performance Evaluation of an IEEE 802.11e EDCA WLAN under Different Frame Arrival Rates

In this section, I study how different frame arrival rates for ACs affects the network performance. Given different frame arrival rates for ACs I investigate how differentiation parameters improve the network performance.

Throughout this section, I assume that the frame arrival rates for different access categories have the ratios of 2, 4, 7, and 10 for AC_0, AC_1, AC_2, and AC_3, respectively. For instance, given number of 5 the data frame arrival rates of AC_0, AC_1, AC_2, and AC_3 are equal to 10, 20, 35, and 50 frames per second, respectively. However, for a given number of 10 the data frame arrival rates of AC_0, AC_1, AC_2, and AC_3 are equal to 20, 40, 70, and 100 frames per second, respectively.

I study four different scenarios during this section, as shown in Table 2.1. For the first two scenarios, I apply AIFS prioritization among ACs. I set the AIFS parameter for different ACs to $AIFSN_0 = 7$, $AIFSN_1 = 5$, $AIFSN_2 = 3$, and $AIFSN_3 = 2$, as before. All

ACs have identical TXOP values, in the experiments.

In the first scenario, I set TXOP to 0 for all the ACs. That is, all the stations are allowed to transmit just one data frame upon winning the medium access. For the second scenario, the TXOP value is set to $11100\mu sec$ for all the ACs which is the sufficient transmission time for 10 data frames. In fact, this scenarios help to find out how TXOP value affects the network's non-saturation regions when the frame arrival rates of ACs are not identical.

In the next two scenarios in this section, I prioritize the ACs through TXOP values. I assume that all the stations in the network have the same AIFS value where $\text{AIFSN}_k = 2$, $k = 0..3$. I set the transmission Opportunities for different ACs to $\text{TXOP}_0 = 2750\mu sec$, $\text{TXOP}_1 = 4900\mu sec$, $\text{TXOP}_2 = 8000\mu sec$, and $\text{TXOP}_3 = 11100\mu sec$ which are the sufficient transmission time for 2, 4, 7, and 10 data frames, respectively.

In the third scenario, I assume that the single frame arrival process is Poisson. In the last scenario the data frames arrive in burst where the burst size is constant. The burst size for AC_0, AC_1, AC_2, and AC_3 are set to 2, 4, 7, and 10 frames, respectively. Note that the burst size corresponds to the frame arrival rate ratios for different access categories in the first three scenarios of this section. In the last scenario for a given number of 5 the burst arrival rates for all the ACs are equal to 5 arrivals per second.

Table 2.1: Different Frame Arrival Rate Impacts Experiments

scenario	AIFSN_k	TXOP_k	Burst Size
1	7, 5, 3, 2	0	No Burst
2	7, 5, 3, 2	11100 μsec	No Burst
3	2	2750, 4900, 8000, 11100 μsec	No Burst
4	2	2750, 4900, 8000, 11100 μsec	2, 4, 7, 10

Note that in Fig. 2.8, Fig. 2.9, Fig. 2.10, Fig. 2.11, and Fig. 2.12 the frame arrival rate equals to multiplication of the number shown in the horizontal axis and the λ ratio or the

(a) payload size=100B, λ ratio$_k$= 2, 4, 7, 10, No Burst, TXOP$_k = 0$

(b) payload size= 100B, λ ratio$_k$= 2, 4, 7, 10, No Burst, TXOP$_k$ = $11100\mu sec$

(c) payload size= 100B, λ ratio$_k$= 2, 4, 7, 10, No Burst, TXOP$_k$ = $2750, 4900, 8000, 11100\ \mu sec$

(d) payload size= 100B, Mean Burst size= 2, 4, 7, 10, TXOP$_k$ = $2750, 4900, 8000, 11100\ \mu sec$

(e) payload size=100B, equal arrival rates for ACs, No Burst, TXOP$_k = 0$

(f) payload size=500B, equal arrival rates for ACs, No Burst, TXOP$_k = 0$

Figure 2.8: Normalized Throughput in cases of different frame arrival rates and different frame sizes

burst size if applicable. For instance, in Fig. 2.8 (a) the saturation region for the lowest priority class starts when its frame arrival rate is equal to 8=2*4 while the frame arrival rates at the same point for AC$_1$, AC$_2$ and AC$_3$ are equal to 16, 28, and 40 frames per second, respectively.

Fig. 2.8 indicates that the TXOP limit growth extends the non-saturation regions for all the ACs. In addition, increasing the TXOP value helps the medium to be more uti-

(a) payload size=100B, λ ratio$_k$= 2, 4, 7, 10, No Burst, TXOP$_k$ = 0

(b) payload size= 100B, λ ratio$_k$= 2, 4, 7, 10, No Burst, TXOP$_k$ = $11100\mu sec$

(c) payload size= 100B, λ ratio$_k$= 2, 4, 7, 10, No Burst, TXOP$_k$ = $2750, 4900, 8000, 11100$ μsec

(d) payload size= 100B, Mean Burst size= 2, 4, 7, 10, TXOP$_k$ = $2750, 4900, 8000, 11100$ μsec

(e) payload size=100B, equal arrival rates for ACs, No Burst, TXOP$_k$ = 0

(f) payload size=500B, equal arrival rates for ACs, No Burst, TXOP$_k$ = 0

Figure 2.9: Mean Frame Access Delay in cases of different frame arrival rates and different frame sizes

lized which result in higher normalized throughput for all the ACs. Clearly, increasing TXOP value from the sufficient time for transmission of one frame to the sufficient time for transmission of 10 frames improves the total network's normalized throughput from approximately 19% to around 34% under saturation condition. Note that an important reason for the small normalized throughput is the small frame size. In the next section, I will show that the network's normalized throughput is improved when the frame size increases. In

(a) payload size=100B, λ ratio$_k$= 2, 4, 7, 10, No Burst, TXOP$_k = 0$

(b) payload size= 100B, λ ratio$_k$= 2, 4, 7, 10, No Burst, TXOP$_k$ = $11100\mu sec$

(c) payload size= 100B, λ ratio$_k$= 2, 4, 7, 10, No Burst, TXOP$_k$ = $2750, 4900, 8000, 11100 \ \mu sec$

(d) payload size= 100B, Mean Burst size= 2, 4, 7, 10, TXOP$_k$ = $2750, 4900, 8000, 11100 \ \mu sec$

(e) payload size=100B, equal arrival rates for ACs, No Burst, TXOP$_k = 0$

(f) payload size=500B, equal arrival rates for ACs, No Burst, TXOP$_k$ = 0

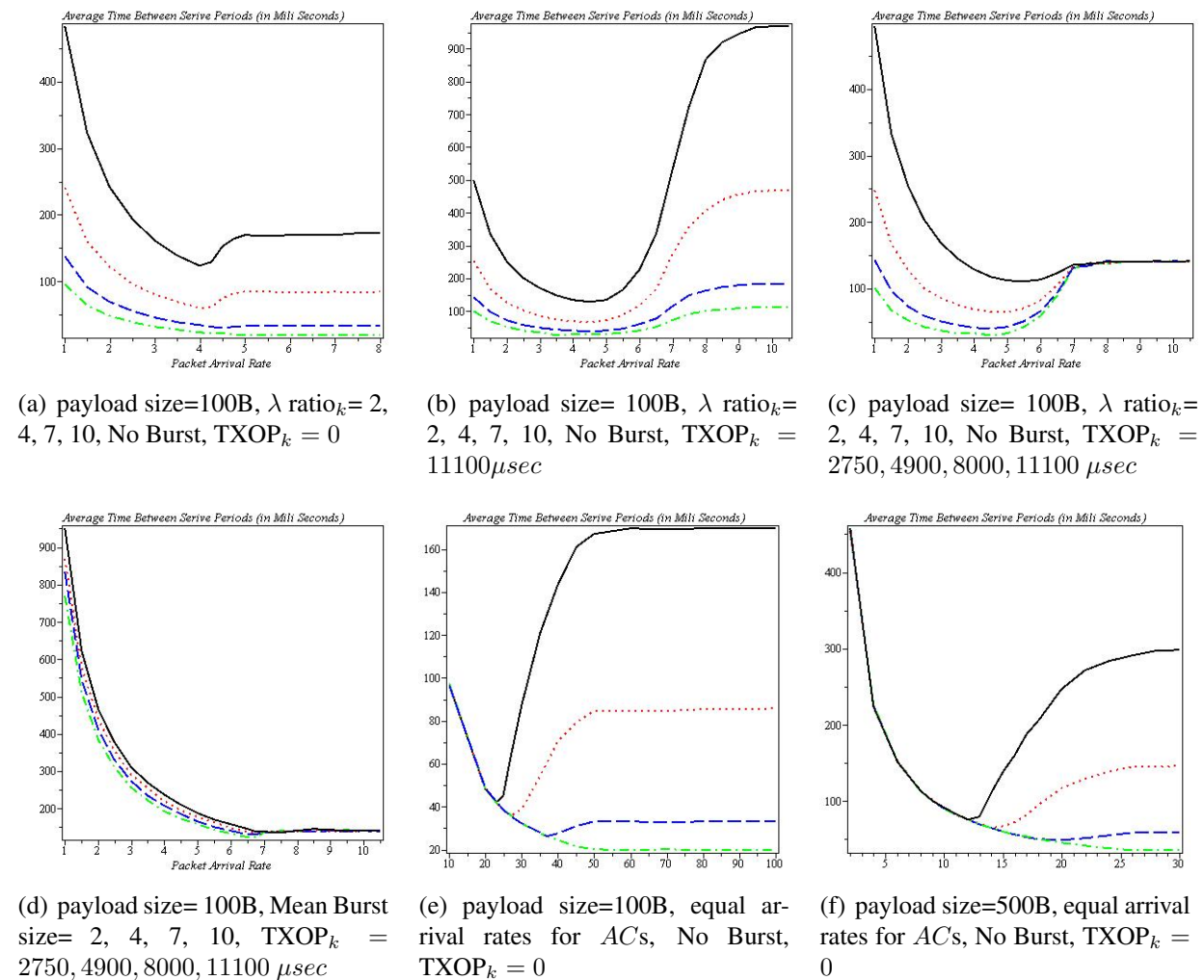Figure 2.10: Average Interval period Between Two Successive TXOP Accesses in cases of different frame arrival rates and different frame sizes

addition, having RTS/CTS mechanism and high traffic in the network are other reasons for the small normalized throughput for the network.

Fig. 2.8 (c) and (d) clearly indicate how different TXOP values play the same role of AIFS$_k$ for differentiating the ACs. In fact, assigning suitable TXOP values to different ACs can significantly improve the network performance. In addition, these plots indicate that in case of having burst arrival with constant burst sizes the network performance is

(a) payload size=100B, λ ratio$_k$= 2, 4, 7, 10, No Burst, TXOP$_k$ = 0

(b) payload size= 100B, λ ratio$_k$= 2, 4, 7, 10, No Burst, TXOP$_k$ = $11100 \mu sec$

(c) payload size= 100B, λ ratio$_k$= 2, 4, 7, 10, No Burst, TXOP$_k$ = $2750, 4900, 8000, 11100 \, \mu sec$

(d) payload size= 100B, Mean Burst size= 2, 4, 7, 10, TXOP$_k$ = $2750, 4900, 8000, 11100 \, \mu sec$

(e) payload size=100B, equal arrival rates for ACs, No Burst, TXOP$_k$ = 0

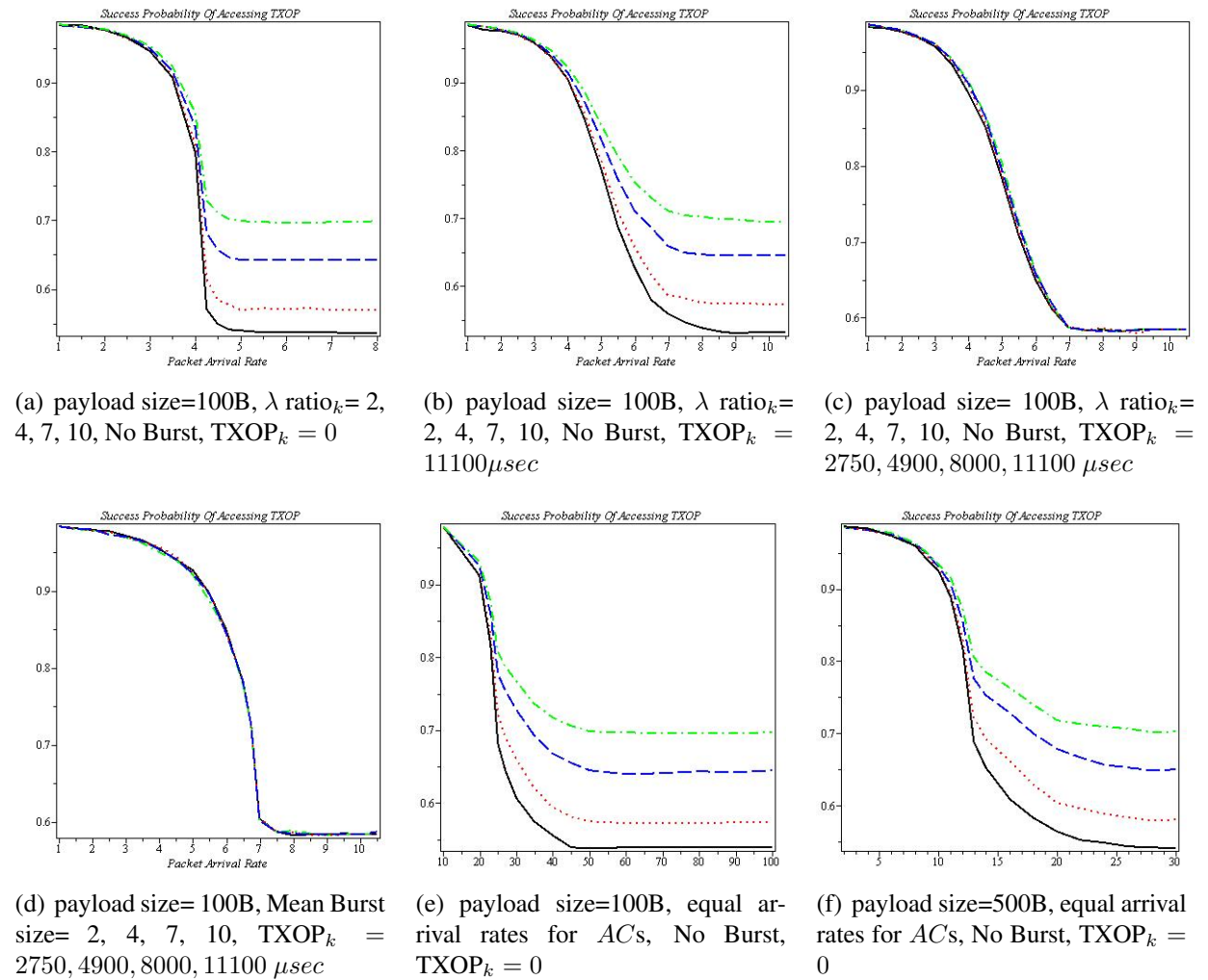(f) payload size=500B, equal arrival rates for ACs, No Burst, TXOP$_k$ = 0

Figure 2.11: Success Probability of Acquiring TXOP in cases of different frame arrival rates and different frame sizes

improved if the TXOP value for ACs are assigned according to the burst size compared to the non-bursty frame arrival.

Fig. 2.9 (a)-(d) show the improvement of packet access delay when the TXOP value increases. It seems that if the frame arrival rates to stations with different ACs are different assigning suitable TXOP values is an efficient tool to improve the network performance without engaging in the other differentiation parameters.

(a) payload size= 100B, λ ratio$_k$= 2, 4, 7, 10, No Burst, TXOP$_k$ = $11100\mu sec$

(b) payload size= 100B, λ ratio$_k$= 2, 4, 7, 10, No Burst, TXOP$_k$ = $2750, 4900, 8000, 11100 \mu sec$

(c) payload size= 100B, Mean Burst size= 2, 4, 7, 10, TXOP$_k$ = $2750, 4900, 8000, 11100 \mu sec$
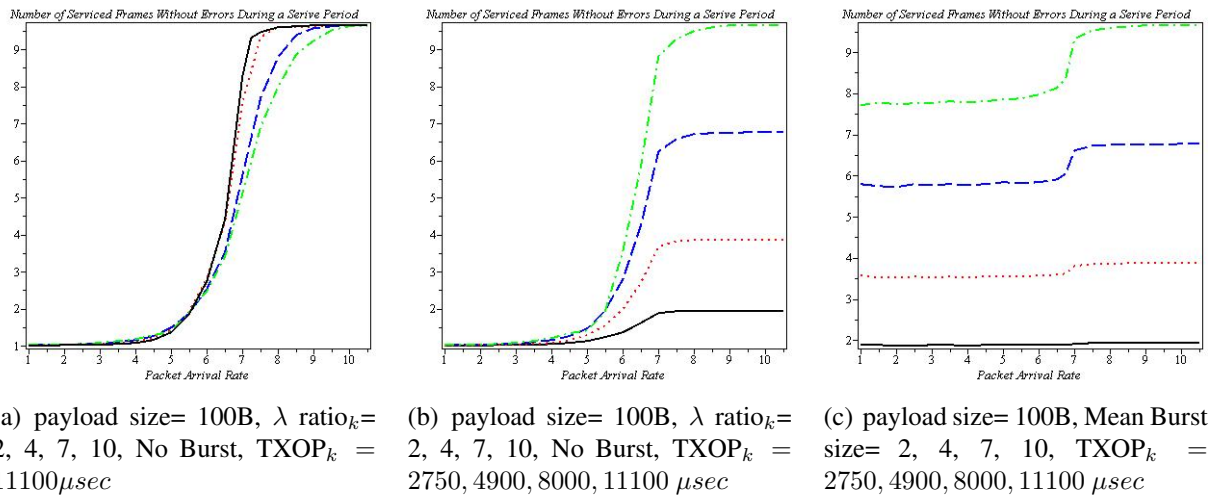
Figure 2.12: Mean Number of Successfully Transmitted Frames during a TXOP period in case of different frame arrival rates

Fig. 2.10 depicts the average service period. When TXOP limit is increased under non-saturation condition the higher priority classes compete less for the medium which improves the network performance. Note that this descriptor is equal for all the ACs when the frames arrive in burst and the sufficient time is assigned to every station to transmits the whole burst in a TXOP period. This helps the stations to improve the frames access delay and lower collision occurs as a result of smaller number of attempts for the medium. A big difference between the first two plots and the next two plots of Fig. 2.10 is the shape of the plots during saturation region. This clearly shows that all the stations in the network have the same probability of winning the medium.

Fig. 2.11 shows how the success probability of access to TXOP period varies for the mentioned scenarios. It is clear how TXOP growth pushes the boundaries between saturation and non-saturation regions. In case of having different values for TXOP for different ACs, the probability of success during the non-saturation region considerably increases

when the frames arrive in burst. The reason is the smaller competition for accessing the medium.

Fig. 2.12 depicts the mean number of successfully transmitted frames during the acquired TXOP period. Fig. 2.12 (a) indicates that because the frames arrive in non-burst mode during non saturation region the TXOP period is underutilized. However, the TXOP utilization significantly increases when the network reaches the saturation boundaries. Note that TXOP value allows the stations to transmit up to 10 frames, but during non-saturation region the actual number of transmitted frames is much lower that forces the stations to compete for the medium as soon as a frame arrives. However, Fig. 2.12 (c) shows that when the frames arrive in burst the TXOP period is much more utilized which decreases the contention on the medium.

2.9 Performance Evaluation of an IEEE 802.11e EDCA-based WLAN under Different Frame Sizes

In this section, I investigate how the data frame sizes affect the performance measures including the network's normalized throughput. Since the channel is noisy frame error rate increases with frame size. For studying the impacts of the frame size, I compare the performance measures for the case when the payload size is 100 B and the case when the size is 500 B. I assume that every station which wins the medium is allowed to transmit just one data frame regardless of the frame size. That is, the TXOP value is set to 0 for all the ACs.

Fig. 2.8 (e) and (f) clearly prove that increasing the frame size significantly improves the total network's normalized throughput and also normalized throughput of all the ACs.

Table 2.2: Frame Size Impacts Experiments

scenario	Frame's Payload Size	TXOP
1	100 Bytes	0
2	500 Bytes	0

In fact, in case of 100 B payload size the network enters into unstable situation at around 24 fps. However, when the payload size is 500 B the network instability occurs when the arrival rate is approximately 13 frames per second. In the first case, under stable condition all the stations can transmit up to 2400 B per second. However, this value is 6500 B per second when the payload size is 500 B. During stable region the throughput considerably increases for all the ACs.

Fig. 2.9 (e) and (f) indicate how the mean frame access delay is changed when the frame size increases. during saturation region when there are always some frames in the queue waiting to be served, in case of larger payload size the mean access delay for all the access categories is less than half of the delay for the case when the payload size is 100 B. In addition, as expected the average time between two TXOP accesses in order for the case when the payload size is 500 B is larger than that of when the fram payload size is 100 B, as shown in Fig. 2.10 (e) and (f). The reason is that all the stations spend more time for transmission of a single frame during TXOP period.

Finally, Fig. 2.11 (e) and (f) show the success probability of winning the TXOP period. These plots indicate that increasing the packet size decreases the stable region with respect to frame arrival rate. In fact, the network enters into unstable region with respect to the frame arrival rate sooner for larger frame sizes.

2.10 Performance Evaluation of an IEEE 802.11e EDCA-based WLAN under Different Node Populations

In this section, I examine how node populations of different ACs affect the normalized throughput achieved by every AC. The normalized throughput plots clearly show non-saturation regions and in fact non-saturation boundaries for all the ACs. Fig. 2.13 (a)-(c) depict the normalized throughput values for different scenarios. Each plot indicates three different scenarios. Each plot includes the normalized throughput values for all the considered traffic rates of all the ACs given fixed numbers of stations with AC_0, AC_1 and AC_2, fixed TXOP value but different number of stations with AC_3 (2, 5, and 8), as shown in Table 2.3. I assume that TXOP$= 3800\mu sec$ for all the ACs which is the required transmission time for three data frames.

Table 2.3: Node Populations Impacts Experiments

scenario	n_0	n_1	n_2	n_3	TXOP
1	5	5	2	2, 5, 8	3800 μsec
2	5	5	5	2, 5, 8	3800 μsec
3	5	5	8	2, 8, 8	3800 μsec

In the previous sections, I assumed that all the stations recover their errors by continuing the transmission during TXOP period if there is enough time. In this section I suppose that if there is transmission failure during the TXOP period the medium becomes idle and the station stops its transmission. Results indicate that the latter approach degrades the network performance because of lower utilization of TXOP period.

In order to study the impact of node populations on saturation regions of the network, I employ 9 different scenarios. In the all cases, I consider five AC_0 and AC_1 stations. Numbers of AC_2 and AC_3 stations are set to 2, 5, or 8. Like before, in all the plots *solid*, *dotted*,
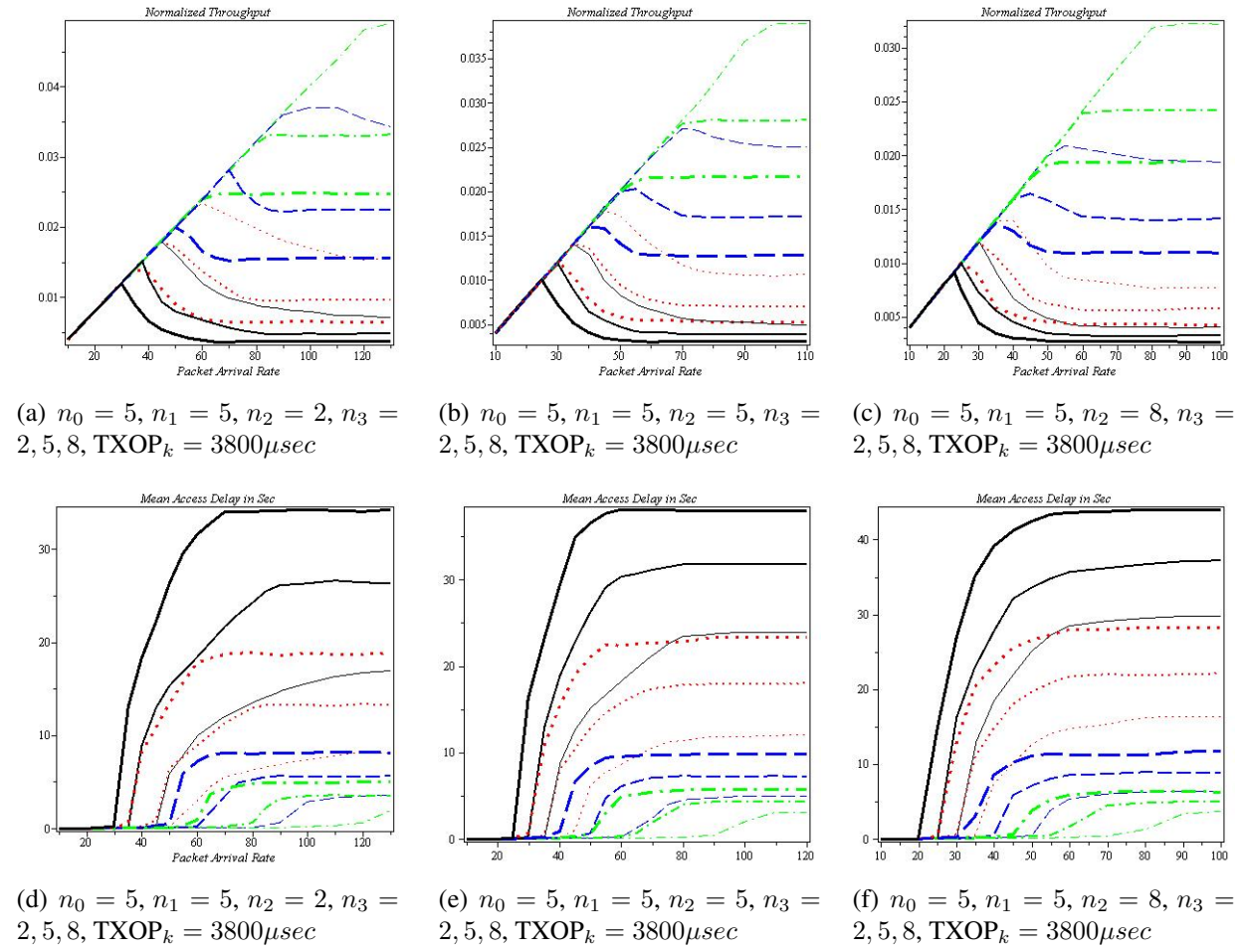
(a) $n_0 = 5$, $n_1 = 5$, $n_2 = 2$, $n_3 = 2, 5, 8$, TXOP$_k = 3800\mu sec$

(b) $n_0 = 5$, $n_1 = 5$, $n_2 = 5$, $n_3 = 2, 5, 8$, TXOP$_k = 3800\mu sec$

(c) $n_0 = 5$, $n_1 = 5$, $n_2 = 8$, $n_3 = 2, 5, 8$, TXOP$_k = 3800\mu sec$

(d) $n_0 = 5$, $n_1 = 5$, $n_2 = 2$, $n_3 = 2, 5, 8$, TXOP$_k = 3800\mu sec$

(e) $n_0 = 5$, $n_1 = 5$, $n_2 = 5$, $n_3 = 2, 5, 8$, TXOP$_k = 3800\mu sec$

(f) $n_0 = 5$, $n_1 = 5$, $n_2 = 8$, $n_3 = 2, 5, 8$, TXOP$_k = 3800\mu sec$

Figure 2.13: Normalized Throughput and Mean Access Delay for Different Node Populations

dashed, and *dash − dotted* lines represent the corresponding values for AC$_0$, AC$_1$, AC$_2$, and AC$_3$, respectively. In addition, the different thickness of the lines indicates different scenarios. Each plot includes the values from three different scenarios that are related to the number of AC$_3$ stations. The thickness of the plots increases when number of AC$_3$ stations changes from 2 to 5 and then 8. In this section, I set $CW_{min} = 31$ and $CW_{max} = 1023$ for all the ACs. That is, number of backoff phases for all the ACs is equal to $m_k = 5$.

I note that, as the traffic increases, the network moves through linear (non-saturation)

regime to saturation regime. In Fig. 2.13(a) numbers of AC_0, AC_1 and AC_2 stations are 5, 5 and 2, respectively. Given 2 AC_3 stations, the lowest priority AC transits from non-saturation regime to saturation one where the arrival rate is about 43 fps. In this case, saturation occurs at loads of 60, 85 and 120 fps for traffic classes 1, 2, and 3, respectively. However, 36 and 30 fps are the transition points from non-saturation to saturation regime when there are 5 and 8 AC_3 stations. Therefore, as plots indicate increasing numbers of stations strongly affect the saturation region. Although at the mentioned point the other ACs except AC_0 are still in their non-saturation regions, the network operates in unstable condition.

In Fig. 2.13(b) number of stations in each of AC_0, AC_1 and AC_2 is 5. The transition points from the non-saturation region to saturation one for AC_0 occur at loads of 36, 30, and 25 fps when number of AC_3 nodes is 2, 5, and 8, respectively. Beyond the rates the network enters into unstable saturated situation, though some ACs may still be in non-saturated situation.

In Fig. 2.13(c), there are 5, 5, and 8 AC_0, AC_1 and AC_2 nodes, respectively. In this case, the network enters into saturation region at loads of 30, 25, and 22 fps when number of AC_3 stations is equal to 2, 5, and 8, respectively.

Fig. 2.13 (d)-(f) depict the mean access delay of frames for all the ACs considering different node populations. The mean access delay plots indicate the non-saturation and saturation regions for all the ACs in different scenarios. For AC_0 the mean packet access delay may be as high as 30 seconds given the mentioned differentiation parameters. These stations may strongly suffer from network traffic congestion. Therefore, the node populations and TXOP limits should be controlled to preserve network stability and provide some

guarantees for throughput and access delay for all the traffic classes.

Fig. 2.14 (a)-(c) represent the average interval period between two successive success-fully acquired TXOP. During the non-saturation region of the station, increase of arrival rate decreases the average service period because the idle period is diminished. When the station enters into the saturation region the service period increases as it is expected. Fig. 2.14 (a)-(c) plots clearly indicate how the low priority AC suffers from saturation condition regarding the service period, inasmuch as the service period may change from around 50 msec to about 330 msec when frame arrival rate increases by about 20 fps.

Fig. 2.14 (d)-(f) present the success probability of accessing TXOP of all the ACs for different node populations. For all the scenarios the success probability of acquiring TXOP degrades when packet arrival rate grows. For instance, based on Fig. 2.14(e) success probability of acquiring TXOP for AC_0 is around 90% when it enters into its saturation region (25, 30, or 36 fps arrival rate) while that probability is approximately 60% when the arrival rate is increased by about 10 fps. Network traffic growth decreases success probability of accessing TXOP with high slopes until all the stations in the network operate under saturation condition. As it is expected increasing network traffic diminishes probability of successfully transmission of RTS and CTS control frames because of the increased contention. Node populations clearly affect the success probability of transmission for contending nodes.

Finally, Fig. 2.14 (g)-(i) represent mean number of transmitted frames during the TXOP period. These plots verify the above discussion about the stability and instability regions of the network and how it is affected by the node populations in the network.

2.11 Summary of the Chapter

In this chapter, I analyzed an IEEE 802.11e EDCA-based single-hop ad-hoc network with bursty traffic and error-prone channel. I developed an accurate analytical model for IEEE 802.11e EDCA which addresses all the differentiation parameters for a network with four access categories. The model consists of three parts; backoff process model, queueing model, and Markov chain model. I solved the analytical model using Maple. I simulated the network by the OPNET simulator to validate the analytical results.

Our results indicate a reasonably good match between analytical and simulation results. I studied how TXOP limit can improve the network performance by considering the burst size. I found out that increasing TXOP limit generally can improve medium utilization. Moreover, if TXOP length is chosen in a way that all the data frames of a burst are transmitted in one access period the network performance is noticeably improved. This helps lower priority classes to have more chance to access TXOP period.

In addition, I investigated the impact of different arrival rates of access categories, frame sizes, node populations of ACs and TXOP limits on performance of the network. The results indicate that in case of having different frame arrival rates for the ACs choosing an appropriate TXOP value can significantly improve the network performance. Based on the results, having larger frame sizes enhances the total normalized throughput of the network. However, the mean access delay of the frames increases due to longer frame transmission time and increased frame error rate. I showed that growth of number of stations, specially higher priority ones, strongly reduces non-saturation regions.

Therefore, TXOP values, frame sizes, and especially the number of nodes in each class are suitable controlling tools for keeping the network in a stable condition when network

load grows. In fact, I came to conclusion that adopting suitable values for TXOP limits improves the QoS provided to all the ACs in the network. The results from this chapter show that admission control can improve the network stability and avoid huge performance drop by controlling the parameters of offered load and the EDCA differentiation parameters.

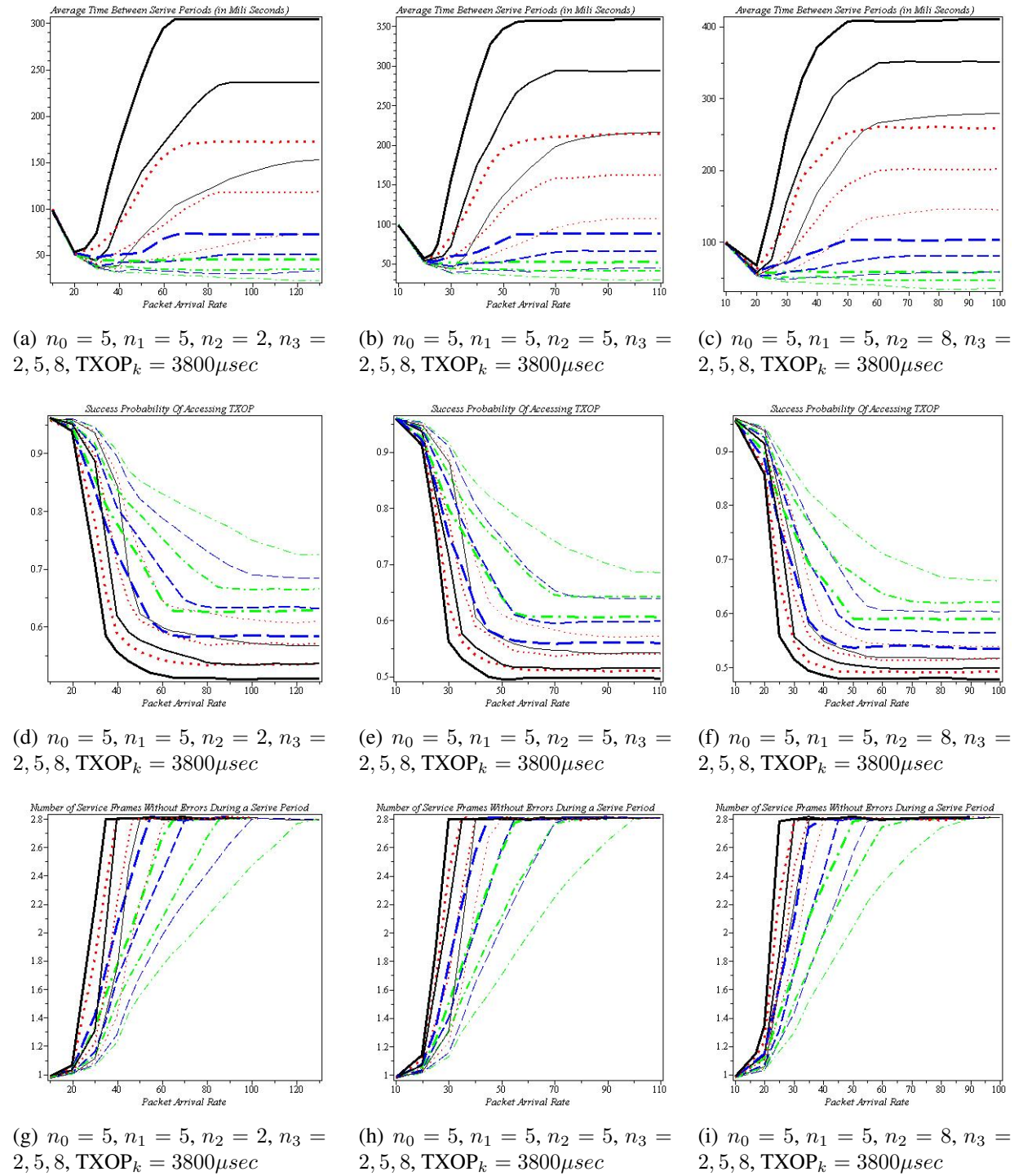The performed research in this chapter is published in [59; 60; 61; 62; 63].

(a) $n_0 = 5$, $n_1 = 5$, $n_2 = 2$, $n_3 = 2, 5, 8$, $\text{TXOP}_k = 3800 \mu sec$

(b) $n_0 = 5$, $n_1 = 5$, $n_2 = 5$, $n_3 = 2, 5, 8$, $\text{TXOP}_k = 3800 \mu sec$

(c) $n_0 = 5$, $n_1 = 5$, $n_2 = 8$, $n_3 = 2, 5, 8$, $\text{TXOP}_k = 3800 \mu sec$

(d) $n_0 = 5$, $n_1 = 5$, $n_2 = 2$, $n_3 = 2, 5, 8$, $\text{TXOP}_k = 3800 \mu sec$

(e) $n_0 = 5$, $n_1 = 5$, $n_2 = 5$, $n_3 = 2, 5, 8$, $\text{TXOP}_k = 3800 \mu sec$

(f) $n_0 = 5$, $n_1 = 5$, $n_2 = 8$, $n_3 = 2, 5, 8$, $\text{TXOP}_k = 3800 \mu sec$

(g) $n_0 = 5$, $n_1 = 5$, $n_2 = 2$, $n_3 = 2, 5, 8$, $\text{TXOP}_k = 3800 \mu sec$

(h) $n_0 = 5$, $n_1 = 5$, $n_2 = 5$, $n_3 = 2, 5, 8$, $\text{TXOP}_k = 3800 \mu sec$

(i) $n_0 = 5$, $n_1 = 5$, $n_2 = 8$, $n_3 = 2, 5, 8$, $\text{TXOP}_k = 3800 \mu sec$

Figure 2.14: Average Time Between Two Successive TXOP Accesses, Success Probability of Acquiring TXOP period, and Mean Number of Successfully Transmitted Frames During TXOP Period for Different Node Populations

Publications

[59] S. Rashwand and J. Misic. IEEE 802.11e EDCA under Bursty Traffic - How Much TXOP Can Improve Performance. *IEEE Transactions on Vehicular Technology (TVT)* , **60**(3):1099-1115, 2011.

[60] J. Misic and S. Rashwand. IEEE Analysis of impact of TXOP allocation on IEEE 802.11e EDCA under variable network load. *IEEE Transimpactactions on Parallel and Distributed Systems (TPDS)* , **23**(5):785-799, 2012.

[61] J. Misic and S. Rashwand and V. B. Misic. Stability Boundaries between non-saturation and saturation regimes for IEEE 802.11e EDCA. *in Proceedings of IEEE International Conference on Communications* (ICC'10), vol. 1, pp. 1-6, May 2010.

[62] S. Rashwand and J. Misic. Stable Operation of IEEE 802.11e EDCA; Interaction Between Offered Load and MAC Parameters. *"Ad Hoc Networks Journal; Special Issue: IEEE 802.11e/p* , **10**(2):162-173, 2012.

[63] S. Rashwand and J. Misic. Impacts of Node Population and TXOP on Stable Operation of IEEE 802.11e EDCA. *in Proceedings of IEEE International Wireless Communications and Mobile Computing Conference* (IWCMC10), vol. 1, pp. 153-157, June 2010.

Chapter 3

Performance Evaluation of IEEE 802.15.6-based WBANs

A WBAN is a novel wireless technology-driven human body monitoring network which aims to predict and diagnose diseases and monitor the body's response to treatments. The network is made of small and intelligent wireless medical sensors which are worn or implanted into the tissue. WBANs must support the combination of QoS, low power, high data rate, and non-interference to address the breath of WBAN applications. The IEEE 802.15 Working Group developed the IEEE 802.15.6 standard which is optimized for low power devices and operation on, in or around the human body [13].

The WBANs have attracted a lot of attention during the last few years. The technology developments have provided small and intelligent medical sensors which can be worn or implanted in the human body. Many researchers have developed wearable materials, wireless sensors, actuators, and other components of a WBAN such as [84; 85]. There are a few studies in the literature which introduce MAC and PHY protocols for WBANs, for instance [56; 57]. Some WBAN projects employ WLAN/WPAN standards such as IEEE 802.11, IEEE 802.15.4, ZigBee, and Bluetooth [86; 87].

In this chapter, I investigate the IEEE 802.15.6-based WBAN performance. I study

how the differentiation parameters (minimum and maximum Contention Window sizes) affect the performance of each user priority. I examine the impact of access phases lengths on medium access of user priorities under both saturation and non-saturation regimes. I analyze how the saturation and non-saturation boundaries change when the lengths of the access phases, node populations, and frame sizes vary. I investigate the IEEE 802.15.6-based WBAN performance under saturation and non-saturation regimes and error-prone channel using both accurate analytical and simulation models. I study important network performance descriptors such as mean frame access delay and normalized throughput of all the user priorities under different conditions.

This chapter is organized as follows: Section 3.1 briefly describes the IEEE 802.15.6 standard. In Section 3.2 I investigate the IEEE 802.15.6-based WBANs performance under saturation conditions by developing analytical and simulation models. Section 3.3 provides the performance evaluation of the IEEE 802.15.6-based WBANs under non-saturation regime through analytical and simulation models. Finally, Section 3.4 concludes the chapter by summarizing the most important findings of the research developed in this chapter.

3.1   IEEE 802.15.6 Standard

IEEE 802.15.6 [13] defines a standard for WBANs which is a short range, low power, and highly reliable wireless communication in the vicinity of, or inside, a human body. The standard is designed to support the advanced medical and entertainment options. It is developed so that medical equipment and consumer electronics manufacturers have small, power efficient, inexpensive solutions for implementation of a wide range of devices. QoS, extremely low power, data rates up to 10 Mbps, and simultaneously complying with strict

non-interference guidelines are the main goals of the standard to achieve. It is designed in a way to consider the effects of portable antennas due to the presence of a person, which varies with male, female, skinny, heavy, etc., radiation pattern shaping to minimize *SAR (Specific Absorption Rate)* into the body, and changes in characteristics as a result of the user motions.

3.1.1   Network Topology

All the nodes and the hubs in the network are organized into logical sets, referred to as Body Area Networks (BANs) and coordinated by their respective hubs for medium access and power management as depicted in Fig. 3.1. In every BAN there is one hub while the number of nodes ranges from zero to 64. The standard supports single-hop and two-hop networks. In a single-hop network all nodes directly communicate with the hub. However, in a two-hop network there can be some nodes which relay the frames between the hub and the nodes.
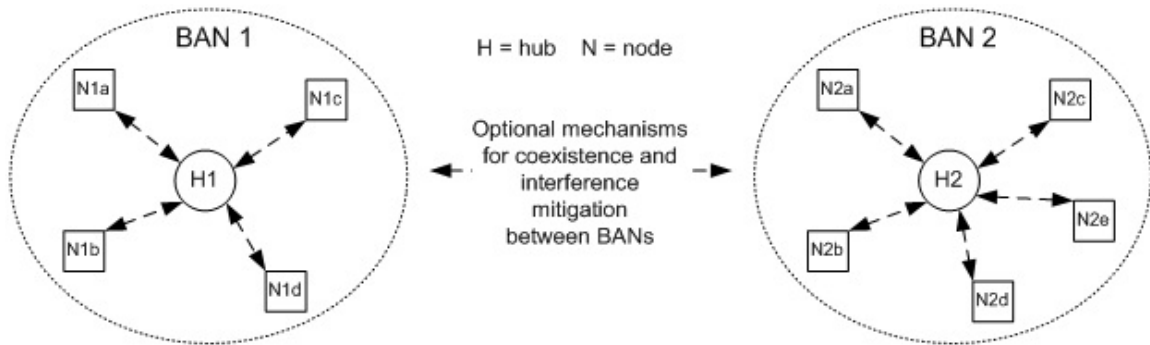
Figure 3.1: BAN Network Topology

3.1.2   Reference Model

All nodes and hubs are internally partitioned into a physical (PHY) layer and a Medium Access Control (MAC) sublayer, in accordance with the ISO/OSI-IEEE 802 reference model, as illustrated in Fig. 3.2. Direct communications between a node and a hub transpires at the PHY layer and the MAC sublayer; the PHY and MAC sublayer of a node or a hub may operate in one channel at any given time. Message security services occur at the MAC sublayer, and security key generations may take place inside and/or outside the MAC sublayer. Note that because our focus in this thesis research is networking, data frame exchange, and network performance evaluation I ignore the security mechanisms specified in the standard. On transmission, the MAC client delivers MAC Service Data Units (MSDUs) to the MAC sublayer through the MAC Service Access Point (SAP). The MAC sublayer passes the MAC frames (known as MAC Protocol Data Units or MPDUs) to the physical layer through the PHY SAP. When the PHY layer receives a data frame it passes the MAC frame to the MAC sublayer. The MAC sublayer passes the MSDUs to the MAC client.

As shown in Fig. 3.2, a BAN device may have a logical entity called *Node Management Entity (NME)* or *Hub Management Entity (HME)* which exchanges network management information with the PHY and MAC as well as other layers. However, implementing the management entities are not mandated and their behaviour is not specified in the standard.

3.1.3   BAN Time Base

The time axis is divided into beacon periods (*superframes*) of equal length and each beacon period consists of allocation slots of equal length, as depicted in Fig. 3.4. An allocation interval may be referenced in terms of the numbered allocation slots and beginning
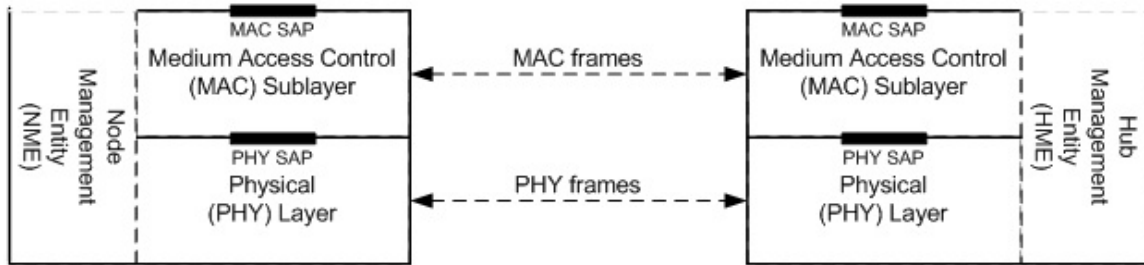
Figure 3.2: BAN Reference Model

allocation slot. A hub may operate in three different modes as described below:

- Beacon mode with beacon period (superframe) boundaries; At the beginning of every superframe a beacon is transmitted on the medium to provide time referenced allocations. Each superframe is divided into Access Phases (APs) as illustrated in Fig. 3.3.

- Non-beacon mode with superframe boundaries in which the hub may have only the type-I/II access phase.

- Non-beacon mode without superframe boundaries in which the hub only provides unscheduled polled allocations.
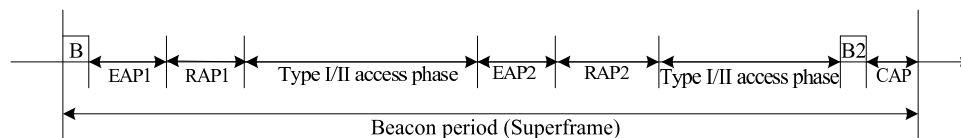
Figure 3.3: Layout of access phases in a beacon period (superframe) for beacon mode

Medium access mechanisms of the IEEE 802.15.6 standard can be divided into four categories; random access (connectionless contention-based access), improvised and unscheduled access (connectionless contention-free access), scheduled access (connection-oriented

contention-free access), and medical implant communications service (MICS) band access. The contention-based access methods for obtaining the allocations are either Carrier Sense Multiple Access/Collision Avoidance (CSMA/CA) if narrowband PHY (Physical Layer) is chosen or Slotted Aloha in case of using Ultra-Wideband (UWB) PHY. In this thesis research, I focus on performance evaluation of the CSMA/CA mechanism of the IEEE 802.15.6 standard.

In our work, I assume that the hub in the wireless BAN operates in beacon mode with superframe boundaries. Hence, all the nodes are synchronized to support the contention-based mechanism of the IEEE 802.15.6. The hub may announce some superframes as inactive beacon periods where it transmits no beacons and provides no access phases, if there are no allocation intervals scheduled in those superframes.

The hub places the access phases - Exclusive Access Phase 1 (EAP1), Random Access Phase 1 (RAP1), type-I/II Access Phase, Exclusive Access Phase 2 (EAP2), Random Access Phase 2 (RAP2), type-I/II Access Phase, and Contention Access Phase (CAP) - in the order stated and shown in Fig. 3.3. The length of any of these access phases may set to zero, but RAP1 must not have a length of shorter than the guaranteed minimum length communicated in Connection Assignment frames sent to nodes that are still connected. The hub transmits a preceding B2 frame to announce a non-zero length CAP.

Type-I/II access phases are utilized by the hub for scheduling uplink allocation intervals, downlink allocation intervals, and bilink allocation intervals which required for the polling mechanisms. However, because in this thesis I do not study the polling mechanisms of IEEE 802.15.6 I assume that the lengths of type-I/II access phases are equal to zero. For more information about the IEEE 802.15.6 polling mechanisms and the way the

allocations in different access phases are allocated the reader may refer to the standard [13].

EAP1, RAP1, EAP2, RAP2, and CAP are contention-based access phases. A hub or nodes may obtain contended allocations in EAP1 and EAP2 if it requires to transmit data frames of UP_7 (i.e. emergency or medical event report). The hub may obtain such a contended allocation SIFS after the start of EAP1 or EAP2 without performing the backoff. Only nodes may obtain contended allocation in RAP1, RAP2, and CAP, to send management or data type frames. SIFS has a period of 50 μsec.

The hub or a node with UP_7 frames may treat the combined EAP1 and RAP1 as a single EAP1, and the combined EAP2 and RAP2 as a single EAP2, to allow continual medium access and improve channel utilization.
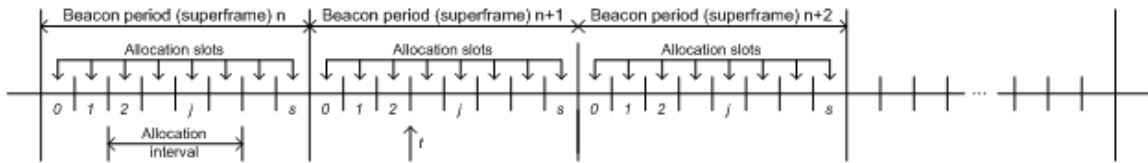
Figure 3.4: BAN Time Reference Base

3.1.4 Priority Mapping

There are 8 different access categories which indicate the User Priorities (UPs) for accessing the medium. UP values are referenced in prioritizing medium access of data and management type frames. The values are determined based on the type of contained payloads in the frame. The UPs are prioritized by the values of the minimum and maximum contention windows. The predefined relationships between Contention Window (CW) bounds, CW_{max} and CW_{min}, and UP for CSMA/CA are depicted in Table 3.1.

Table 3.1: BAN User Priority Mapping

UP	Traffic designation	Frame type	CW_{min}	CW_{max}
0	Background (BK)	Data	16	64
1	Best effort (BE)	Data	16	32
2	Excellent effort (EE)	Data	8	32
3	Controlled load (CL)	Data	8	16
4	Video (VI)	Data	4	16
5	Voice (VO)	Data	4	8
6	Media data or network control	Data or Management	2	8
7	Emergency or medical event report	Data	1	4

3.1.5　IEEE 802.15.6 CSMA/CA mechanism

The IEEE 802.15.6 CSMA/CA mechanism has important differences with the CSMA/CA mechanism of the other wireless communication standards (such as IEEE 802.11e and IEEE 802.15.4):

- The contention window size increments after an unsuccessful medium access and backoff value draw from the window are different than all the other mechanisms.

- Only the UP_7 nodes are allowed to decrease their backoff counter or access the medium during EAP periods, while all nodes can compete for the medium access during RAPs and CAP. Hence, nodes are prioritized by a combination of assigning different medium access contention parameters and medium access time constraints.

- Being in an eligible access phase, a node has to pause its backoff countdown if there is not enough time for completing a data frame transaction.

- There are other differentiation parameters in the other standards such as AIFSs and TXOPs in IEEE 802.11e EDCA [58] which are not present in the IEEE 802.15.6 CSMA/CA mechanism.

These differences necessitate new analytical and simulation models for performance evaluation of the IEEE 802.15.6 CSMA/CA mechanism.

A node maintains a backoff counter and contention window to determine when it obtains a new contended allocation. The node sets its backoff counter to a sample of an integer random variable uniformly distributed over the interval [1,CW]. The node is allowed to transmit one frame of UP over the medium if the backoff counter reaches 0. CW is a contention window chosen as follows:

- If the node did not obtain any contended allocation previously, CW is set to CW_{min}[UP].

- If the node succeeded in transmission, i.e., if the node received an expected acknowledgement to its last frame transmission, in the last contended allocation it had obtained, it sets CW to CW_{min}[UP] as well.

- If the node transmitted a frame requiring no acknowledgement at the end of its last contended allocation, it keeps the CW unchanged.

- If the node failed in frame transmission, i.e., if the node did not receive an expected acknowledgement to its last frame transmission, in the last contended allocation it had obtained,

  - it keeps CW unchanged if this was the *m*-th time the node had consecutively failed, where *m* is an odd number;

  - it doubles CW if this was the *n*-th time the node had consecutively failed, where *n* is an even number.

- If doubling CW would change new CW exceed CW_{max}[UP], the node sets CW to CW_{max}[UP].

The node locks the backoff counter when any of the following events occurs:

- The backoff counter is reset upon decrementing to 0.

- The channel is busy. If the channel is busy because the node detected a frame transmission, the channel remains busy until at least the end of the frame transmission without the node having to re-sense the channel.

- The current time is outside any RAP or CAP if UP does not have the highest value (i.e., not for an emergency or medical event report), or is outside any EAP, RAP, or CAP if UP has the highest value (i.e., for an emergency or medical event report).

- The current time is at the start of a CSMA slot within an EAP, RAP, or CAP, but the time between the end of the slot and the end of the EAP, RAP, or CAP is not long enough for completing a frame transaction and setting aside a nominal guard time mGT-Nominal.

The UP_k node unlocks the backoff counter when both of the following conditions are met:

- The channel has been idle for SIFS within an RAP or CAP for $k = 0..6$, or within an EAP, RAP, or CAP for $k = 7$.

- The time duration between the current time plus a CSMA slot and the end of the EAP, RAP, or CAP is long enough for completing a frame transaction plus a nominal guard time mGT-Nominal.

Table 3.2: Frequency band dependent parameters

Frequency Band (MHz)	402 - 405	420 - 450	863 - 870	902 - 928	950 - 956	2360 - 2400	2400 - 2483.5
Symbol Rate (ksps)	187.5	187.5	250	300	250	600	600
number of channels	10	12	14	48	12	38	79
Channel Bandwidth (MHz)	0.30	0.50	0.40	0.50	0.40	1.00	1.00

Upon unlocking the backoff counter, the node decrements its backoff counter by one for each idle CSMA slot that follows. The node treats a CSMA slot to be idle if it determines that the channel has been idle between the start of the CSMA slot and pCCATime (which has a value of 63 / Symbol Rate, Table 3.2) later. The backoff counter is effectively decremented pCCATime after the start of the CSMA slot. The node will transmit a frame to the transport medium at the end of the CSMA slot in case its backoff counter reaches 0. Every CSMA slot, as depicted in Fig. 3.5, has a fixed duration of pCSMASlotLength (pCCATime + 20 μsec). For instance, considering the operational frequency band of 2400-2483.5 MHz the slot length is equal to 125μsec. Upon having the backoff counter of 0 the node has obtained a contended allocation.
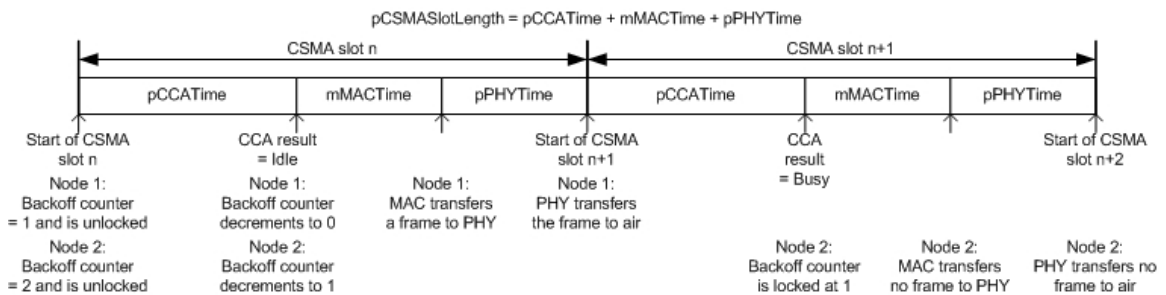

Figure 3.5: CSMA Slot Structure

The data rate dependent parameters for each of the possible operational frequency bands are provided in Table 3.3. In the table, PLCP, PSDU, DBPSK, DQPSK, and D8PSK,

Table 3.3: Data rate dependent parameters

Frequency Band (MHz)	Packet Component	Modulation	Spreading Factor(S)	Information Data Rate (kbps)	Support
402-405	PLCP Header	$\pi/2$-DBPSK	2	57.5	Mandatory
402-405	PSDU	$\pi/2$-DBPSK	2	75.9	Mandatory
402-405	PSDU	$\pi/2$-DBPSK	1	151.8	Mandatory
402-405	PSDU	$\pi/4$-DQPSK	1	303.6	Mandatory
402-405	PSDU	$\pi/8$-D8PSK	1	455.4	Optional
420-450	PLCP Header	GMSK	2	57.5	Mandatory
420-450	PSDU	GMSK	2	75.9	Mandatory
420-450	PSDU	GMSK	1	151.8	Mandatory
420-450	PSDU	GMSK	1	187.5	Optional
863-870	PLCP Header	$\pi/2$-DBPSK	2	76.6	Mandatory
863-870	PSDU	$\pi/2$-DBPSK	2	101.2	Mandatory
863-870	PSDU	$\pi/2$-DBPSK	1	202.4	Mandatory
863-870	PSDU	$\pi/4$-DQPSK	1	404.8	Mandatory
863-870	PSDU	$\pi/8$-D8PSK	1	607.1	Optional
902-928	PLCP Header	$\pi/2$-DBPSK	2	91.9	Mandatory
902-928	PSDU	$\pi/2$-DBPSK	2	121.4	Mandatory
902-928	PSDU	$\pi/2$-DBPSK	1	242.9	Mandatory
902-928	PSDU	$\pi/4$-DQPSK	1	485.7	Mandatory
902-928	PSDU	$\pi/8$-D8PSK	1	728.6	Optional
950-956	PLCP Header	$\pi/2$-DBPSK	2	76.6	Mandatory
950-956	PSDU	$\pi/2$-DBPSK	2	101.2	Mandatory
950-956	PSDU	$\pi/2$-DBPSK	1	202.4	Mandatory
950-956	PSDU	$\pi/4$-DQPSK	1	404.8	Mandatory
950-956	PSDU	$\pi/8$-D8PSK	1	607.1	Optional
2360-2400	PLCP Header	$\pi/2$-DBPSK	4	91.9	Mandatory
2360-2400	PSDU	$\pi/2$-DBPSK	4	121.4	Mandatory
2360-2400	PSDU	$\pi/2$-DBPSK	2	242.9	Mandatory
2360-2400	PSDU	$\pi/2$-DBPSK	1	485.7	Mandatory
2360-2400	PSDU	$\pi/4$-DQPSK	1	971.4	Mandatory
2400-2483.5	PLCP Header	$\pi/2$-DBPSK	4	91.9	Mandatory
2400-2483.5	PSDU	$\pi/2$-DBPSK	4	121.4	Mandatory
2400-2483.5	PSDU	$\pi/2$-DBPSK	2	242.9	Mandatory
2400-2483.5	PSDU	$\pi/2$-DBPSK	1	485.7	Mandatory
2400-2483.5	PSDU	$\pi/4$-DQPSK	1	971.4	Mandatory

GMSK stand for *Physical Layer Convergence Procedure*, *PHY Service Data Unit*, *Differential Binary Phase Shift Keying*, *Differential Quadrature Phase Shift Keying*, *Eight-Ary Differential Phase-Shift Keying*, and *Gaussian Minimum Shift Keying* [88].

For more information regarding the physical layer and the MAC sublayer, such as formats of the data and control frames, security services, transmitter and receiver specifications, and error correction mechanisms the reader may refer to the IEEE 802.15.6 standard [13].

3.2 Performance Evaluation of IEEE 802.15.6-based WBANs Under Saturation Condition

In this section, I develop 3-dimensional Markov chains in order to model the backoff procedure of the CSMA/CA mechanism and the Exclusive and Random Access Phases of IEEE 802.15.6 under saturation condition and error-prone channel. I model all the 8 UPs (UP_k, $k = 0..7$) as specified in the standard so that all the nodes are saturated. That is, at any time at least one data frame in the queue is waiting to be served. I consider a star-topology single-hop network including n_k nodes of UP_k and a hub. The traffic flows between the nodes and the WBAN's hub. Assuming a single-hop network for WBANs is not unrealistic because the WBAN environment is small and the star-topology of the standard allows simply a single-hop network. In addition, the standard supports only up to two-hop networks. In this section, I assume that EAP1, RAP1, first type-I/II access phase, EAP2, RAP2, and second type-I/II access phase may have non-zero lengths while length of CAP is set to 0.

Table 3.4: Important Parameters

Params	Description	Params	Description
k	Index of UP	R	Maximum retransmission limit
δ	Probability that neither RTC nor CTS is corrupted by noise	σ_k	Probability that neither a UP_k data frame nor its ACK is corrupted by noise
n_k	Number of nodes of UP_k	λ_k	Data frame arrival probability during a CSMA slot for a node of UP_k
τ_k	Access probability to medium by a UP_k node	g_k	Probability that medium is idle during backoff countdown for a UP_k node
$L_{k,s}$	Successful data frame transmission time for a UP_k node in slots	$L_{k,so}$	Mean successful data frame transmission time of other nodes for a given UP_k node in slots
$L_{k,c}$	Unsuccessful data frame transmission time for a UP_k node in slots	$L_{k,co}$	Mean unsuccessful data frame transmission time of other nodes for a given UP_k node in slots
η_k	Probability of successful access to the medium for a UP_k node	p_k	Probability that indicates from the current CSMA slot to the end of the RAP1 period for a UP_k node there is not enough time to complete a data frame transaction
$\pi_{k,0}$	Probability of an empty queue after serving a data frame for a UP_k node	$p_{k,Idle}$	Probability of being in the idle state for a UP_k node in a CSMA slot
$p_{so,k}$	Probability of a successful transmission by the other nodes for a given UP_k node	$p_{co,k}$	Probability of an unsuccessful transmission by the other nodes for a given UP_k node
$\Phi_k(z)$	PGF for the duration of backoff process for a UP_k node	$\Pi_k(z)$	PGF of steady state probability distribution of number of frames in the queue after completing a UP_k data frame service
ω_k	Mean waiting time of a UP_k data frame in slots	ζ_k	Mean response time of a UP_k data frame

In our probabilistic approach, I assume that collision probability of a frame transmitted by a node is independent of the number of retransmissions. Using PGFs I compute the average time between two successive successful accesses to the medium and the normalized throughput for all UPs. Our approach also provides the ability to calculate the mean backoff

time in every backoff stage. I validate the analytical results using an accurate simulation model.

In this section, I assume that CAP has a zero length while lengths of the other access phases might be non-zero. Type-I/II access phases which are considered for polling mechanisms may have non-zero lengths. During these access phases the hub may poll traffic from the nodes. However, because the intention of this research is to evaluate the IEEE 802.15.6 CSMA/CA performance, I ignore the polled data frames in our performance investigation. In beacon mode with superframe boundaries all nodes are synchronized with the leading edge of the beacon.

In this section, I evaluate performance of the CSMA/CA mechanism of IEEE 802.15.6 where four contention-based access phases, namely EAP1, RAP1, EAP2, and RAP2, and contention-free type-I/II access phases are taken into account. Our hypothesis is to verify whether addition of EAP2 and RAP2 phases improves the network performance. The type-I/II access phases are used by the hub for contention-free mechanisms. Since our intention is to investigate the CSMA/CA performance, I ignore activities in the contention-free access phases. I develop analytical and simulation models for investigating the IEEE 802.15.6 CSMA/CA-based network performance. I model all 8 UPs according to the standard specifications under saturation condition and an error-prone channel by developing 8 inter-related 3-dimensional Discrete Time Markov Chains (DTMCs). The system of DTMCs are solved to calculate the medium access probabilities of all UPs during RAPs. Afterwards, I develop a single DTMC for the UP_7 nodes which is separately solved for computing the medium access probability of the UP_7 nodes during EAPs. I calculate two important network performance descriptors; normalized throughput and average backoff

time to access the medium, for all UPs. The results acquired by the analytical model are validated by a simulation model.

Since the IEEE 802.15.6 standard was recently released there is not much work in the literature reported, which investigates the IEEE 802.15.6-based network performance. Performance of the CSMA/CA mechanism in IEEE standards has been studied in [89] for IEEE 802.11, [78; 79; 90] for IEEE 802.11e, and [91; 92; 93] for IEEE 802.15.4. The developed models are not appropriate for the IEEE 802.15.6 standard due to the different characteristics of the CSMA mechanisms, as discussed above.

In [94] the authors proposed a simple model to evaluate the theoretical throughput and delay limits of IEEE 802.15.6-based networks. The UPs and the access phases have not been taken into account in their model. They also assumed a collision-free network and an ideal channel. In [95] I studied performance of IEEE 802.15.6 CSMA/CA under saturation condition with respect to EAP1 and RAP1 only. Considering the currently available related work in the literature, I need to investigate performance of the CSMA/CA mechanism of IEEE 802.15.6 where EAP1, RAP1, EAP2, RAP2, and type-I/II access phases are taken into account. The developed analytical and simulation models in this work are much more complex than the models in [95]. Existence of more access phase changes within a super-frame and different values for the phases complicate the model because the lengths affect the backoff durations of the UPs during different phases.

3.2.1   Analytical Model

I first introduce the parameters which are used in our analytical model. I consider all 8 user priorities, $\text{UP}_k \ k = 0..7$, in which the lowest and the highest UPs have indexes 0 and

7, respectively. A UP_k node has a single UP_k queue. The lengths in slots are shown by $eap1$, $rap1$, $typeAC1$, $eap2$, $rap2$, and $typeAC2$.

RTS/CTS mechanism is deployed by the nodes for accessing the medium. rts, cts, l_d, and ack represent the lengths of RTS, CTS, data frames, and ACK in slots while rts_b, cts_b, l_b, cts_b indicate the lengths of RTS, CTS, data frames, and ACK in bits. The relation between the lengths in bits and slots depends on the physical characteristics of the channel and frame transmission rate. The channel is considered noisy having the Bit Error Rate (BER) equal to ber for all user priorities. Hence, the probability that neither RTS nor CTS is corrupted by noise is equal to $\delta = (1 - ber)^{rts_b + cts_b}$ while the probability that neither the data frame nor its ACK is corrupted by noise is equal to $\sigma = (1 - ber)^{l_b + ack_b}$.

For i-th backoff phase the backoff value for a UP_k node is uniformly drawn over the interval $[1, CW_k]$, where $CW_k = W_{k,i}$, $i = 0..R$ in which R is the transmission retry limit. CW_k has the minimum value of $CW_{k,min} = W_{k,0}$ and the maximum value of $CW_{k,max} = W_{k,m_k}$. The contention window size during the i-th backoff phase $i = 0..R$ for a UP_k node, $k = 0..7$, $CW_k = W_{k,i}$, is calculated as follows:

- $W_{k,0} = W_{k,min} = CW_{k,min}$.

- $W_{k,i} = min\{2W_{k,i-1}, CW_{k,max}\}$, for $2 \leq i \leq R$ if i is an even number.

- $W_{k,i} = W_{k,i-1}$ for $1 \leq i \leq R$, if i is an odd number.

I assume that the data frame is dropped if the retransmission count exceeds the retry limit.

3.2.1.1   Performance Descriptors of a UP_k node

In this section, I calculate the performance descriptors of an IEEE 802.15.6 CSMA/CA-based network to investigate the impact of the access phases lengths on the network performance under saturation condition. I study two network performance descriptors, normalized throughput and mean backoff time to access the medium by a UP_k, $k = 0..7$, node. Normalized throughput for a UP_k node is defined as the fraction of time in which the channel is utilized to successfully transmit the payload of frames.

I denote $\tau_{R,k}$, $k = 0..7$, as the transmission probability by a UP_k node during RAP where the medium is not busy, in which R stands for RAP. The medium access probability of a UP_7 node during EAP is defined as $\tau_{E,7}$, in which E stands for EAP. I calculate the performance descriptors for a UP_k node based on the assumption that the medium access probabilities are known, which are calculated in Section 3.2.1.2.

Idle medium probability in a CSMA slot during RAP1 or RAP2, where all user priorities are allowed to access the medium, is equal to

$$f_R = \prod_{k=0}^{7} \left(1 - \tau_{R,k}\right)^{n_k} \tag{3.1}$$

For a UP_k node, I define $f_{R,k}$ as probability that other nodes do not access the medium during an RAP phase:

$$f_{R,k} = \frac{\prod_{i=0}^{7} \left(1 - \tau_{R,i}\right)^{n_i}}{\left(1 - \tau_{R,k}\right)}, \ k = 0..7 \tag{3.2}$$

$f_{R,k}$ is used during the backoff countdown when the node itself does not access the medium. For the nodes without UP_7, I define f_k as follows:

$$f_k = f_{R,k}, \ k = 0..6 \tag{3.3}$$

During EAP1 and EAP2 only the UP_7 nodes are allowed to access the medium while during RAPs all nodes can access the medium. Hence, probability that the medium is idle for the UP_7 nodes during the backoff countdown in an EAP, $f_{E,7}$, is calculated as follows:

$$f_{E,7} = (1 - \tau_{E,7})^{n_7 - 1} \tag{3.4}$$

Due to deploying a probabilistic approach for calculating the performance descriptors it is not known for certain which access phase a CSMA slot belongs to. Thus, I approximate probability that the medium is idle during the backoff countdown for a UP_7 node, either during RAPs or EAPs. I denote this probability as f_7 which is probability that the other nodes in the network transmit on the medium in a CSMA slot, which belongs to one of the contention-based access phases. f_7 is computed as follows:

$$f_7 = \frac{X_1 + X_3}{X} f_{E,7} + \frac{X_2 + X_4}{X} f_{R,7} \tag{3.5}$$

where X_1, X_2, X_3, and X_4 are the mean numbers of slots in EAP1, RAP1, EAP2, and RAP2 access phases, respectively, in which the medium is accessible by the eligible nodes. X_i, $i = 1..4$, values are calculated in Section 3.2.1.2. I denote X as $X = X_1 + X_2 + X_3 + X_4$.

As described before, if the remaining time within the current RAP is not sufficient for completing a frame transaction the node must lock its backoff counter even if the remaining slots are idle. For $k = 0..6$ I define $p_{k,1}$ and $p_{k,2}$ as probabilities that, for a UP_k node, there is not enough time for completing a frame transaction and it has to pause its backoff countdown given that the current phase is RAP1 and RAP2, respectively. However, a UP_7 node must lock its backoff counter if there is not enough time for backoff countdown to 0 and completing a data frame transaction by end of the closest RAP. Probabilities that there

is not enough time for a UP$_7$ node within EAP1-RAP1 and EAP2-RAP2 are denoted by

$p_{7,1}$ and $p_{7,2}$, respectively. The probabilities are calculated as follows:

$$
\begin{aligned}
p_{k,1} &= \frac{1}{rap1 - L_s - C_k} & k &= 0..6 \\
p_{k,2} &= \frac{1}{rap2 - L_s - C_k} & k &= 0..6 \\
p_{7,1} &= \frac{1}{rap1 + eap1 - L_s - C_7} & \\
p_{7,2} &= \frac{1}{rap2 + eap2 - L_s - C_7} & \text{(3.6)}
\end{aligned}
$$

in which $L_s = (rts + cts + l_d + ack + 3sifs)_s$ indicates the successful transmission time in

slots and $C_k = \dfrac{\sum_{v=0}^{\lfloor \frac{R}{2} \rfloor} \frac{2}{2^v CW_{k,min}} \sum_{u=1}^{2^v CW_{k,min}} u}{2(1 + \lfloor \frac{R}{2} \rfloor)}$ approximates the mean initial backoff counter

value, in which $\lfloor \cdot \rfloor$ represents the floor function. The expression $\dfrac{\sum_{u=1}^{2^v CW_{k,min}} u}{2^v CW_{k,min}}$ is the mean

initial backoff counter value for both $2v$-th and $2v + 1$-th backoff phases. This period

indicates the time from the moment when the backoff counter is locked until the beginning

of next RAP, for $k = 0..6$, or EAP, for $k = 7$. $L_c = (rts + cts + sifs)_s$ is the unsuccessful

transmission time in slots in case of failure access to the medium or corrupted frame due to

a noisy channel.

To calculate the performance descriptors for a UP$_k$ node, I develop 4-dimensional

DTMCs. The Markov chain for a UP$_k$ node is depicted in Fig. 3.6 and Fig. 3.7. The

gray boxes in Fig. 3.6 are replaced by the related boxes shown in Fig. 3.7 to compose the 4-

dimensional DTMC. I are separately showing the boxes to improve the understanding of the

Markov chains. Given that the values for the medium access probabilities and X_i, $i = 1..4$,

are known I calculate the PGFs of every backoff phase and total backoff durations before

the medium is successfully accessed for frame transmission. In the developed DTMC the

time interval between two successive Markov points has a length of one slot indicating that
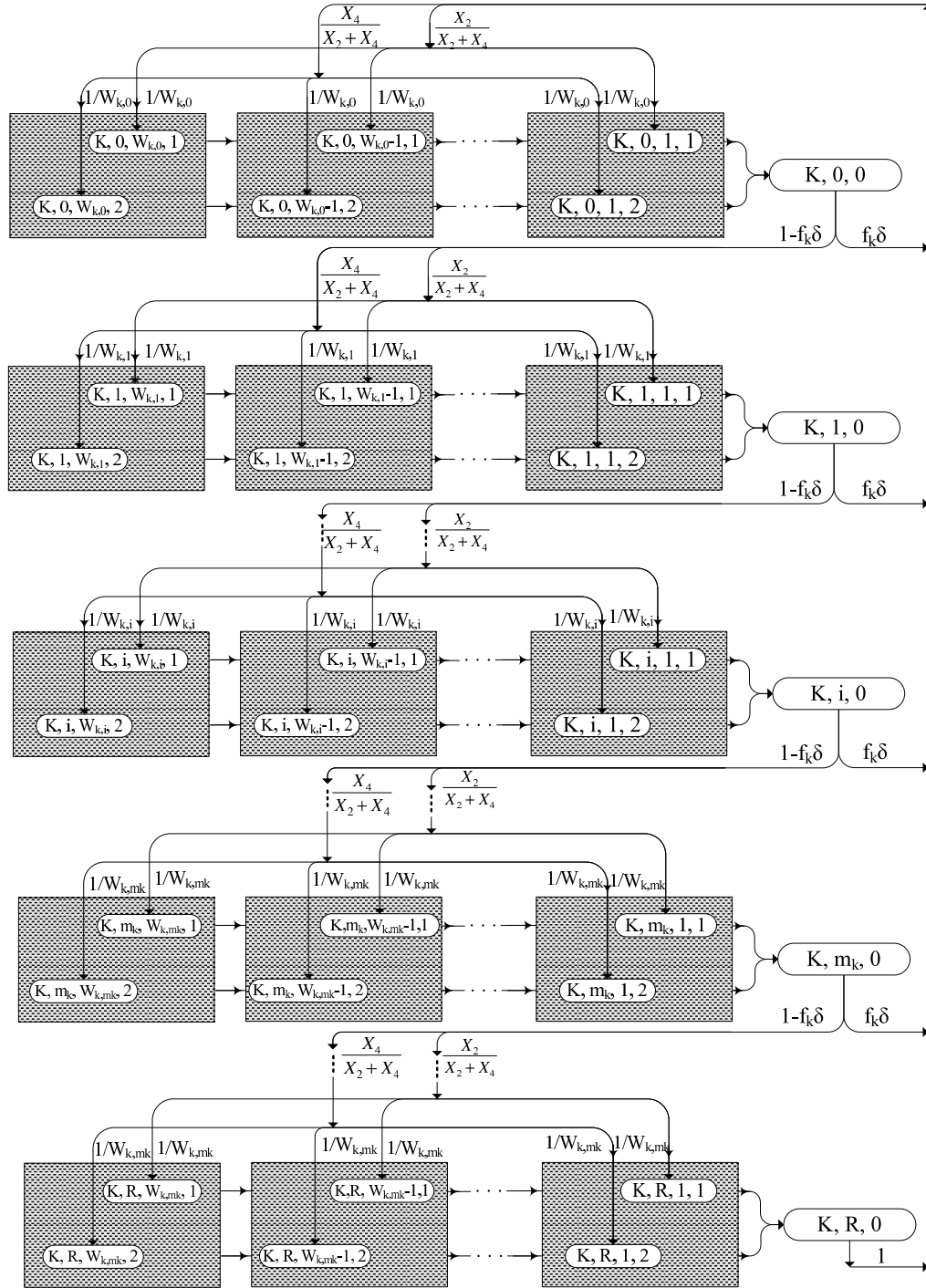
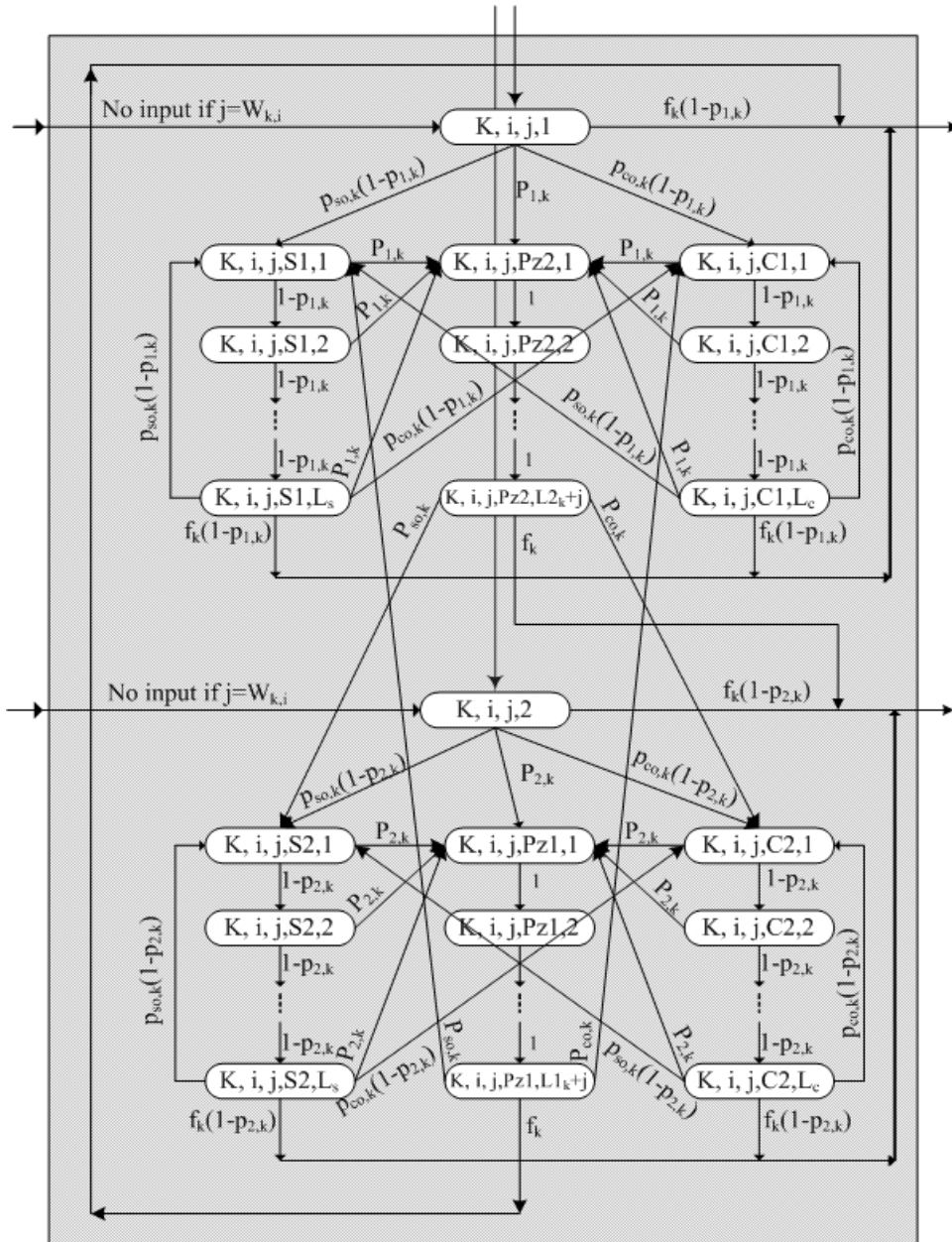Figure 3.6: Markov chain for a UP_k node to calculate performance descriptors of the node

Figure 3.7: Gray box of the Markov chain for a UP$_k$ node

every CSMA slot is a Markov point.

Stationary probabilities $b_{k,i,j,1}$ and $b_{k,i,j,2}$ for $k = 0..7$, $i = 0..R$, $j = 0..W_{k,i}$ represent

state probabilities of Markov chains, shown in Fig. 3.6 and Fig. 3.7, when the current access phase is RAP1 (for $k = 0..6$) or EAP1-RAP1 (for $k = 7$) and RAP2 (for $k = 0..6$) or EAP2-RAP2 (for $k = 7$), respectively. I define $b_{k,i,0}$, $k = 0..7$, $i = 0..R$, as the probability of having the backoff counter equal to zero. At this point the node is able to transmit on the medium.

Stationary distribution of $b_{k,i,j,S1,t}$, $k = 0..7$, $i = 0..R$, $j = 1..W_{k,i}$, $t = 1..L_s$ corresponds to a slot during the time in which a data frame is successfully transmitted by another node (during RAP1 if $k = 0..6$ or EAP1-RAP1 if $k = 7$) while $b_{k,i,j,S2,t}$ represents a slot where the current access phase is RAP2 if $k = 0..6$ or is either EAP2 or RAP2 if $k = 7$. Stationary distributions of $b_{k,i,j,C1,t}$ and $b_{k,i,j,C2,t}$, $k = 0..7$, $i = 0..R$, $j = 1..W_{k,i}$, $t = 1..L_c$ correspond to a slot during the time in which the RTS frame collides or the frame is corrupted by noise during RAP1 if $k = 0..6$ or EAP1-RAP1 if $k = 7$ and during RAP2 if $k = 0..6$ or EAP2-RAP2 if $k = 7$, respectively. Stationary distributions of $b_{k,i,j,Pz1,t}$ and $b_{k,i,j,Pz2,t}$, $k = 0..7$, $i = 0..R$, $j = 1..W_{k,i}$, $t = 1..L_k + j$ correspond to slots during the time in which the node has to lock its backoff counter because there is not enough time for completing a frame transaction or the node is not allowed to access the medium in the current access phase, during RAP1 if $k = 0..6$ or EAP1-RAP1 if $k = 7$ and during RAP2 if $k = 0..6$ or EAP2-RAP2 if $k = 7$, respectively.

I define $L1_k = eap1 + typeAC2 + (rts + cts + 3sifs + l_d + ack)_s$, $k = 0..6$, as the number of CSMA slots in which the backoff counter for a UP_k node must be locked because within the current access phase, RAP2, there is not sufficient time for completing a transmission. Similarly, $L2_k = eap2 + typeAC1 + (rts + cts + 3sifs + l_d + ack)_s$, $k = 0..6$ indicates the numbers of slots in which the backoff counter must be locked because within access phase

RAP1 there is not sufficient time for completing a frame transmission. $L1_7 = typeAC2 + (rts+cts+3sifs+l_d+ack)_s$ and $L2_7 = typeAC1+(rts+cts+3sifs+l_d+ack)_s$ represent the number of slots in which the backoff counter for a UP_7 node must be locked because there is not sufficient time for a frame transmission during EAP2-RAP2 and EAP1-RAP1, respectively. Note that the backoff counter is locked from the slot in which the node comes to know that there is not sufficient time even if the remaining slots within the current access phase are idle and the counter is non-zero. Hence, if the counter is equal to j for a UP_k node it has to lock its counter for $L_k + j$ slots if there is not sufficient time for completing a frame transaction.

Probability that the backoff counter for a UP_k node is locked due to a successful transmission by another node, $p_{so,k}$, is computed as follows:

$$p_{so,k} = \delta \sum_{i=0}^{7} \frac{n_i \tau_i f_k}{1 - \tau_i} - \frac{\delta \tau_k f_k}{1 - \tau_k}, \ k = 0..7 \tag{3.7}$$

in which $\tau_k = \tau_{R,k}$, $k = 0..6$ and $\tau_7 = \frac{X_1+X_3}{X}\tau_{E,7} + \frac{X_2+X_4}{X}\tau_{R,7}$. In the above equation $\frac{\tau_i f_k}{1-\tau_i}, i \neq k$, $i = 0..7$ is the probability that only a UP_i node transmits to the medium while a UP_k node is performing backoff countdown. Thus, $\delta \frac{\tau_i f_k}{1-\tau_i}, i \neq k$, is the successful transmission probability by a UP_i node during the UP_k node's backoff countdown. Since there are n_i nodes with UP_i successful transmission probability by all the nodes is equal to $\delta \sum_{i=0}^{7} \frac{n_i \tau_i f_k}{1-\tau_i}$. However, I have to exclude the probability value for the UP_k node, which results in equation (3.7).

Probability that the backoff counter for a UP_k node is suppressed due to an unsuccessful transmission by the other nodes, $p_{co,k}$, is calculated as follows:

$$p_{co,k} = 1 - f_k - p_{so,k}, \ k = 0..7 \tag{3.8}$$

I now calculate the PGF of the backoff time for all UPs to compute the performance descriptors of the UP_k node. The PGF of successful frame transmission time is defined as $St(z) = z^{rts+cts+l_d+ack+3sifs}$. Failed transmission time due to an RTS collision or a corrupted RTS/CTS transmission as a result of the noisy channel has the PGF of $Ct(z) = z^{rts+cts+sifs}$.

I define $BfS_{1,k,j}(z)$ and $BfS_{2,k,j}(z)$ as the PGFs of times from the moment when the backoff counter is locked due to a successful transmission by another node in the network until the moment when the backoff counter is unlocked, given that the locking occurs in EAP1-RAP1 and in EAP2-RAP2, respectively. $BfC_{1,k,j}(z)$ and $BfC_{2,k,j}(z)$ are defined as the PGFs of the time intervals between the instant when the backoff counter is locked due to an unsuccessful transmission by other nodes, given that the counter is locked in access phases EAP1-RAP1 and EAP2-RAP2, respectively. I introduce $Bfpz_{1,k,j}(z)$ and $Bfpz_{2,k,j}(z)$ as the PGFs of the time interval from the moment when the backoff counter is locked because there is not sufficient time for completing a frame transaction until the moment when the backoff counter is unlocked, given that the counter is locked during EAP1-RAP1 and EAP2-RAP2, respectively. During these time periods the backoff counter is kept locked because either there is not sufficient time for completing a frame transmission or other transmissions may take place on the medium. In the above values $k = 0..7$ represents the UP and $j = 1..W_{k,m_k}$ indicates the backoff counter value when the counter is locked. Based on the developed Markov chains the PGFs are computed as follows:

$$
\begin{aligned}
Bfpz_{1,k,j}(z) &= z^{L1_k+j}\Big(f_k z + p_{so,k} BfS_{1,k,j}(z) + p_{co,k} BfC_{1,k,j}(z)\Big) \\
BfS_{1,k,j}(z) &= p_{k,1} Bfpz_{2,k,j}(z)\frac{1-(1-p_{k,1})^{L_s}z^{L_s}}{1-(1-p_{k,1})z} + (1-p_{k,1})^{L_s}f_k z^{L_s} + (1-p_{k,1})^{L_s}\cdot \\
&\quad \Big(p_{so,k} BfS_{1,k,j}(z) + p_{co,k} BfC_{1,k,j}(z)\Big)
\end{aligned}
$$

$$
\begin{aligned}
BfC_{1,k,j}(z) &= p_{k,1} Bfpz_{2,k,j}(z) \frac{1 - (1 - p_{k,1})^{L_c} z^{L_c}}{1 - (1 - p_{k,1})z} + (1 - p_{k,1})^{L_c} f_k z^{L_c} + (1 - p_{k,1})^{L_c} \cdot \\
&\quad \left(p_{so,k} BfS_{1,k,j}(z) + p_{co,k} BfC_{1,k,j}(z) \right) \\[2mm]
Bfpz_{2,k,j}(z) &= z^{L2_k + j} \left(f_k z + p_{so,k} BfS_{2,k,j}(z) + p_{co,k} BfC_{2,k,j}(z) \right) \\[2mm]
BfS_{2,k,j}(z) &= p_{k,2} Bfpz_{1,k,j}(z) \frac{1 - (1 - p_{k,2})^{L_s} z^{L_s}}{1 - (1 - p_{k,2})z} + (1 - p_{k,2})^{L_s} f_k z^{L_s} + (1 - p_{k,2})^{L_s} \cdot \\
&\quad \left(p_{so,k} BfS_{2,k,j}(z) + p_{co,k} BfC_{2,k,j}(z) \right) \\[2mm]
BfC_{2,k,j}(z) &= p_{k,2} Bfpz_{1,k,j}(z) \frac{1 - (1 - p_{k,2})^{L_c} z^{L_c}}{1 - (1 - p_{k,2})z} + (1 - p_{k,2})^{L_c} f_k z^{L_c} + (1 - p_{k,2})^{L_c} \cdot \\
&\quad \left(p_{so,k} BfS_{2,k,j}(z) + p_{co,k} BfC_{2,k,j}(z) \right)
\end{aligned}
\tag{3.9}
$$

The PGFs in equations (3.9) are computed by following the structure of Fig. 3.7. Equations (3.9) model the pause times during the backoff countdown based on the transition probabilities of Markov sub-chain shown in Fig. 3.7. The Markov sub-chain includes the states in which the backoff counter is locked because either

– A successful transmission or unsuccessful transmission is occurring on the medium

or

– The current CSMA slot is inaccessible due to either it is outside the access phase in which the node is able to transmit or there is not sufficient time for completing a frame transaction.

Based on the transition probabilities the PGFs of time durations, in which the backoff countdown is kept locked, are computed. The PGFs $Bfpz_{1,k,j}(z)$, $Bfpz_{2,k,j}(z)$, $BfS_{1,k,j}(z)$, $BfS_{2,k,j}(z)$, $BfC_{1,k,j}(z)$ and $BfC_{2,k,j}(z)$ can be analytically written based on functions of z and the MAC and traffic parameters. I do not present the formulae here because they are large but they can be derived using the method of substitutions.

Now I are able to calculate the PGF of the time to decrement the backoff counter by one. This time interval is between the moment when the backoff counter of a UP_k node reaches j and the moment when the backoff counter becomes equal to $j-1$. The PGF of this time interval is either equal to $Bf_{1,k,j}(z)$ where the backoff counter reaches j during EAP1-RAP1 or equal to $Bf_{2,k,j}(z)$ where the backoff counter decrements to j during EAP2-RAP2 for $k = 0..7$, $j = 1..W_{k,m_k}$. The PGFs are calculated as follows:

$$Bf_{1,k,j}(z) = p_{k,1}Bfpz_{2,k,j}(z) + (1 - p_{k,1})\Big(f_k z + p_{so,k}BfS_{1,k,j}(z) + p_{co,k}BfC_{1,k,j}(z)\Big)$$

$$Bf_{2,k,j}(z) = p_{k,2}Bfpz_{1,k,j}(z) + (1 - p_{k,2})\Big(f_k z + p_{so,k}BfS_{2,k,j}(z) + p_{co,k}BfC_{2,k,j}(z)\Big)$$

$$(3.10)$$

Due to the probabilistic nature of the Markov chain it is not known for certain if the next backoff state after a backoff counter decrement from state $b_{k,i,j,1}$ is $b_{k,i,j-1,1}$ or $b_{k,i,j-1,2}$. It is also true when the backoff state is $b_{k,i,j,2}$ because the next state after a backoff counter decrement might be $b_{k,i,j-1,1}$ or $b_{k,i,j-1,2}$. Hence, I define $p_{T,k,1}$ as the probability that the next state after a backoff countdown from the backoff state $b_{k,i,j,1}$ is $b_{k,i,j-1,1}$ while the next backoff state is $b_{k,i,j-1,2}$ with the probability $1-p_{T,k,1}$. Similarly, I define $p_{T,k,2}$ and $1-p_{T,k,2}$ as the probabilities that the next state after a backoff countdown from the state $b_{k,i,j,2}$ is $b_{k,i,j-1,2}$ and $b_{k,i,j-1,1}$, respectively. By using the transition probabilities in the extended Markov chains I calculate the above probabilities for $k = 0..7$, $i = 0..R$, $j = 0..W_{k,i}$ as follows:

$$p_{T,k,1} = \frac{f_k(1 - p_{k,1})}{1 - \Big(p_{so,k}(1 - p_{k,1})^{L_s} + p_{co,k}(1 - p_{k,1})^{L_c}\Big)}$$

$$p_{T,k,2} = \frac{f_k(1 - p_{k,2})}{1 - \Big(p_{so,k}(1 - p_{k,2})^{L_s} + p_{co,k}(1 - p_{k,2})^{L_c}\Big)} \qquad (3.11)$$

I define $BfR_{1,k,i,j}(z)$ as the PGF of the backoff time during the i-th backoff phase when

the backoff counter value is drawn within EAP1-RAP1 and equal to j. That is, it indicates

the PGF of the time from the moment when the backoff value is randomly selected until

the instant when the counter reaches 0. Likewise, $BfR_{2,k,i,j}(z)$ represents the PGF of the

backoff time in the i-th backoff phase when the backoff value is drawn within EAP2-RAP2

and equal to j. The PGFs for $k = 0..7$, $i = 0..R$, $j = 2..W_{k,i}$ are calculated as follows:

$$BfR_{1,k,i,1}(z) = Bf_{1,k,1}(z) \tag{3.12}$$

$$BfR_{1,k,i,j}(z) = Bf_{1,k,j}(z)\Big(p_{T,k,1}BfR_{1,k,i,j-1}(z) + (1 - p_{T,k,1})BfR_{2,k,i,j-1}(z)\Big)$$

$$BfR_{2,k,i,1}(z) = Bf_{2,k,1}(z)$$

$$BfR_{2,k,i,j}(z) = Bf_{2,k,j}(z)\Big(p_{T,k,2}BfR_{2,k,i,j-1}(z) + (1 - p_{T,k,2})BfR_{1,k,i,j-1}(z)\Big)$$

By deploying the above probability generating functions I compute the PGF of mean

backoff time during i-th backoff phase where the backoff counter value is uniformly drawn

from the contention window within EAP1-RAP1, $BfR_{1,k,i}(z)$, and where the backoff value

is drawn within EAP2-RAP2, $BfR_{2,k,i}(z)$. For UP$_k$, $k = 0..7$ and $i = 0..R$ I have

$$BfR_{1,k,i}(z) = \frac{1}{W_{k,i}} \sum_{j=1}^{W_{k,i}} BfR_{1,k,i,j}(z)\Big(f_k\delta(L_s p_{k,1} z^{L1_k} + (1 - L_s p_{k,1})) + $$
$$(1 - f_k\delta)(L_c p_{k,1} z^{L1_k} + (1 - L_c p_{k,1}))\Big)$$

$$BfR_{2,k,i}(z) = \frac{1}{W_{k,i}} \sum_{j=1}^{W_{k,i}} BfR_{2,k,i,j}(z)\Big(f_k\delta(L_s p_{k,2} z^{L2_k} + (1 - L_s p_{k,2})) + $$
$$(1 - f_k\delta)(L_c p_{k,2} z^{L2_k} + (1 - L_c p_{k,2}))\Big) \tag{3.13}$$

In equation (3.13) for $BfR_{1,k,i}(z)$, the expression $f_k\delta(L_s p_{k,1} z^{L1_k} + (1 - L_s p_{k,1})) + (1 -$

$f_k\delta)(L_c p_{k,1} z^{L1_k} + (1 - L_c p_{k,1}))$ represents the PGF of distribution of time during which

the backoff counter has to be locked because there is not sufficient time for completing the

frame transaction before the backoff countdown starts within EAP1 for UP$_7$ and RAP1 for other UPs. Likewise, the expression $f_k\delta(L_s p_{k,2} z^{L2_k} + (1 - L_s p_{k,2})) + (1 - f_k\delta)(L_c p_{k,2} z^{L2_k} + (1 - L_c p_{k,2}))$ is the PGF of the time period from the moment when the last transmission attempt is completed until the moment the backoff countdown starts within EAP2 for UP$_7$ and RAP2 for other UPs. I calculate the mean backoff time duirng i-th backoff phase regardless of where the backoff value is drawn for $i = 0..R$ and $k = 0..6$ as follows:

$$
\begin{aligned}
BfR_{k,i}(z) &= \frac{X_2}{X_2 + X_4} BfR_{1,k,i}(z) + \frac{X_4}{X_2 + X_4} BfR_{2,k,i}(z) \\
BfR_{7,i}(z) &= \frac{X_1 + X_2}{X} BfR_{1,7,i}(z) + \frac{X_3 + X_4}{X} BfR_{2,7,i}(z)
\end{aligned}
\tag{3.14}
$$

Finally, the PGF for the total time spent during backoff procedure for a successful access to the medium or before the data frame is dropped for user priority $k, k = 0..7$, is computed as follows:

$$
\begin{aligned}
BfT_k(z) = {}& \sum_{i=0}^{m_k} \Big(\prod_{u=0}^{i} BfR_{k,u}(z) \Big)(1 - f_k\delta)^i (z^{L_c})^i f_k\delta + \\
& \sum_{i=m_k+1}^{R} \Big(\prod_{u=0}^{m_k} BfR_{k,u}(z) \Big) BfR_{k,m_k}(z)^{i-m_k}(1 - f_k\delta)^i (z^{L_c})^i f_k\delta + \\
& \Big(\prod_{u=0}^{m_k} BfR_{k,u}(z) \Big) BfR_{k,m_k}(z)^{R-m_k}(1 - f_k\delta)^{R+1}(z^{L_c})^{R+1}
\end{aligned}
\tag{3.15}
$$

The mean backoff time before the medium is successfully accessed or the data frame is dropped due to the retry limit exceed for UP$_k$, $k = 0..7$ is calculated as follows:

$$
B_k = \frac{d}{dz} BfT_k(z) \Big|_{z=1} \omega
\tag{3.16}
$$

where ω represent the length of one CSMA slot.

I compute the normalized throughput of a node of UP$_k$, $\tau_{N,k}$, $k = 0..7$, as follows:

$$
\tau_{N,k} = \frac{\sigma(l_p)_s h_k \omega}{B_k}
\tag{3.17}
$$

where $(l_p)_s$ is the payload size of a data frame (the data frame excluding the headers) in slots and h_k represents the probability that a data frame is successfully transmitted on the medium which is calculated as follows:

$$h_k = \sigma\Big(1 - (1 - f_k\delta)^R\Big) \tag{3.18}$$

3.2.1.2   Discrete Time Markov Chains (DTMCs)

In this section, I develop 8 dependent DTMCs, as depicted in Fig. 3.8, for 8 UPs which are solved to calculate the medium access probabilities of all UPs during RAPs. A single DTMC is also developed to calculate the medium access probability of the UP$_7$ nodes during EAPs. By solving the set of 8 inter-related DTMCs and the single DTMC I will find out the required parameters for calculating the network performance descriptors. Note that the developed DTMCs in this section are different than the ones in Section 3.2.1.1 inasmuch as the DTMCs in Fig. 3.8 do not consider the CSMA slots in which the backoff countdown is paused. The backoff countdown might be paused due to busy medium or being in an ineligible access phase. The Markov points of the developed DTMCs are beginning of the CSMA slots in which the medium is not set to busy when the slots start. In fact, lengths of interval periods between two successive Markov points are different as there might be backoff countdown pauses. This improves the accuracy of calculated access probabilities and performance descriptors compared to the case where all CSMA slots are considered. In latter case, when the medium is busy the nodes do not compete for the medium and their medium access probabilities in those slots are equal to zero.

I use an iterative approach as shown in Fig. 3.9 to solve the set of DTMCs for calculating the medium access probabilities of all UPs. The iterative approach helps us to decrease the
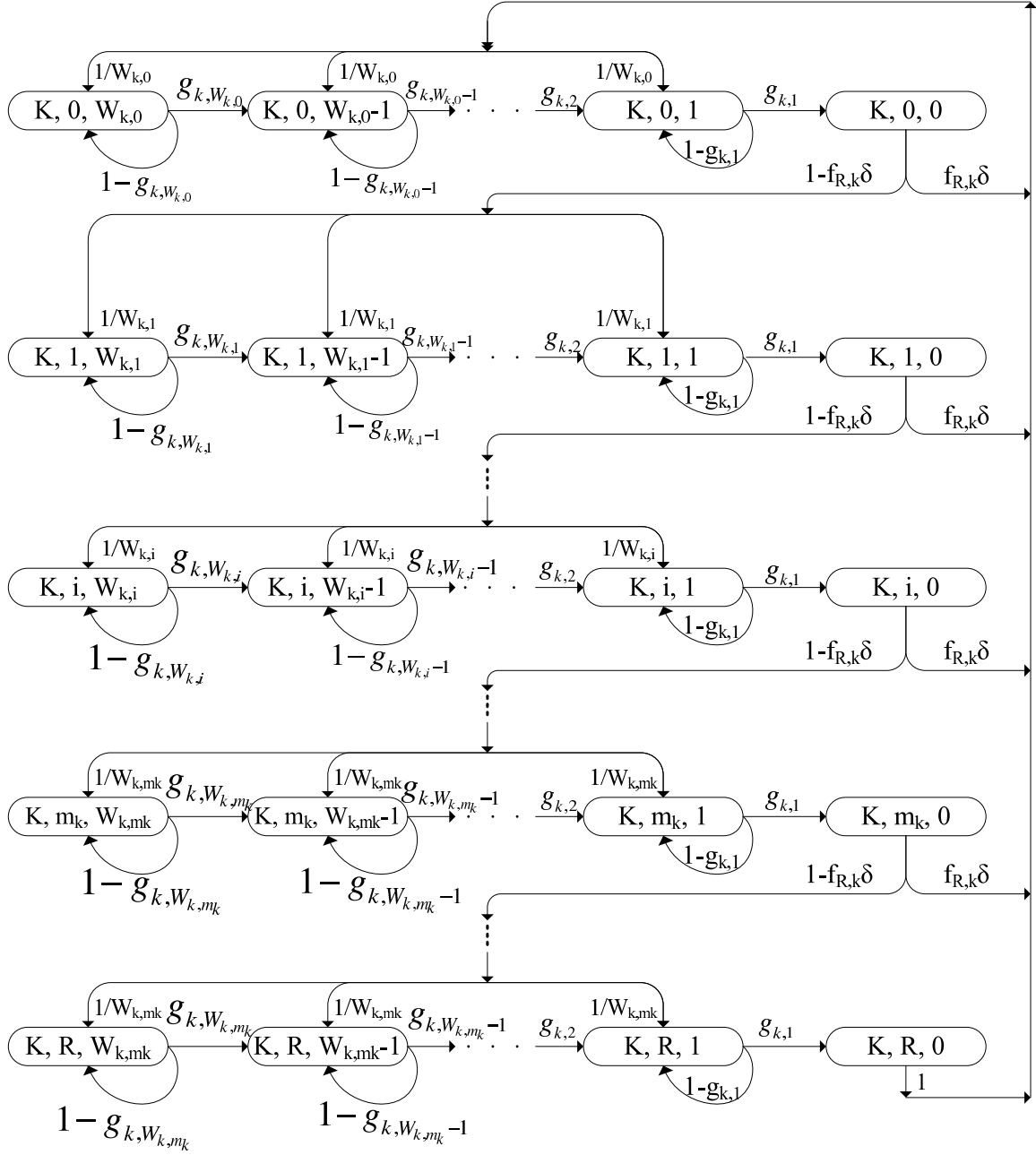
Figure 3.8: Markov chain for UP$_k$, $k = 0..7$

complexity of the model and improve the solution accuracy. X_1, X_2, X_3, and X_4 are

the mean numbers of slots in EAP1, RAP1, EAP2, and RAP2, respectively, which are

---

Compute expressions (1-15) with initial values X$_1$=*eap1*, X$_2$=*rap1*, X$_3$=*eap2*, X$_4$=*rap2*
Solve the set of 8 DTMCs
Compute the values for X$_1$, X$_2$, X$_3$, and X$_4$ using expression (5)
While (|new X$_i$ − previous X$_i$| > 0.1 for any i=1,2,3,4) do
    Re-compute the equations of the DTMCs using new X values
    Solve the set of 8 DTMCs
    Compute the values for X$_1$, X$_2$, X$_3$, and X$_4$ using expression (5)
End
Solve the single DTMC for UP$_7$ based on expression (16)
Calculate performance descriptors of the network using expressions (17-28) employing computed access probabilities

---

Figure 3.9: An iterative approach for solving Markov chains and computing the performance descriptors

considered in the DTMCs. I set their initial values to $X_1 = eap1$, $X_2 = rap1$, $X3 = eap2$, and $X4 = rap2$. The next values are calculated as follows:

$$X_1 = \frac{eap1}{D_1}, \ X_2 = \frac{rap1}{D_2}, \ X_3 = \frac{eap2}{D_1}, \ X_4 = \frac{rap2}{D_2} \tag{3.19}$$

where

$$D_1 = (1 - \tau_{E,7})^{n_7} + n_7\tau_{E,7}f_{E,7}\delta L_s + \left(1 - (1 - \tau_{E,7})^{n_7} - n_7\tau_{E,7}f_{E,7}\delta\right)L_c$$

$$D_2 = f_R + \sum_{t=0}^{7} n_t\tau_{R,t}f_{R,t}\delta L_s + \left(1 - f_R - \sum_{t=0}^{7} n_t\tau_{R,t}f_{R,t}\delta\right)L_c$$

I denote X as the mean number of slots considered in the Markov chain in a superframe which is computed as $X = X_1 + X_2 + X_3 + X_4$.

I define $g_{k,j}, \ k = 0..7, \ j = 1..W_{k,m_k}$ as probability that the backoff counter of a UP$_k$ node is decremented by one when the backoff counter is equal to j, which is calculated as follows:

$$g_{k,j} = f_{R,k}\left(1 - (\frac{X_2}{X_2 + X_4}p_{k,1} + \frac{X_4}{X_2 + X_4}p_{k,2})\frac{1 - f_{R,k}^j}{1 - f_{R,k}}\right)$$

$$g_{7,j} = f_{R,7}\left(1 - (\frac{X_1 + X_2}{X}p_{7,1} + \frac{X_3 + X_4}{X}p_{7,2})\frac{1 - f_{R,7}^j}{1 - f_{R,7}}\right) \tag{3.20}$$

Fig. 3.8 depicts the Markov chain for a UP_k node, during RAPs. The Markov chain represents a random process with stationary distribution $b_{k,i,j}$, where $k = 0..7$ indicates the user priority of the node, $i = 0..m_k..R$ denotes the backoff phase invoked by the node, and $j = 0..W_{k,i}$ indicates the backoff counter value. By solving the set of 8 dependent Markov chains the access probabilities of all UPs, $\tau_{R,k}$, during RAPs are calculated. Medium access probability of a UP_k node is given by

$$\tau_{R,k} = \sum_{i=0}^{R} b_{k,i,0} \tag{3.21}$$

I define Y_k, $k = 0..7$, as the input probability to the zero-th backoff phase which is calculated as follows:

$$Y_k = \tau_{R,k} f_{R,k}\delta + b_{k,R,0}(1 - f_{R,k}\delta) \tag{3.22}$$

Following the Markov chain I can show that for $k = 0..7$ and $j = 1..W_{k,0}$ I have

$$b_{k,0,j} = \frac{(W_{k,0} - j + 1)Y_k}{W_{k,0}\ g_{k,1}} \tag{3.23}$$

Thus, I have

$$b_{k,0,0} = g_{k,1}b_{k,0,1} = Y_k \tag{3.24}$$

It can be shown that for $k = 0..7$, $i = 1..R$, and $j = 1..W_{k,i}$ I have

$$b_{k,i,j} = \frac{(1 - f_{R,k}\delta)^i Y_k (W_{k,i} - j + 1)}{g_{k,j}W_{k,i}} \tag{3.25}$$

$$b_{k,i,0} = (1 - f_{R,k}\delta)^i Y_k \tag{3.26}$$

Using the equations (3.27) and (3.26) I calculate the value of Y_k as follows:

$$Y_k = \frac{f_{R,k}\delta\tau_k}{1 - (1 - f_{R,k}\delta)^{R+1}}, \quad k = 0..7 \tag{3.27}$$

Deploying the equations (3.23) - (3.27) I compute the summation of all stationary probabilities $b_{k,i,j}$ as follows:

$$\sum_{i=0}^{R}\sum_{j=0}^{W_{k,i}} b_{k,i,j} = Y_k \sum_{i=0}^{R} (1 - f_{R,k}\delta)^i \Big(1 + \frac{1}{W_{k,i}} \sum_{j=1}^{W_{k,i}} \frac{W_{k,i} - j + 1}{g_{k,j}}\Big) \quad k = 0..7 \qquad (3.28)$$

The normalization condition of the Markov chain indicates that expression (3.28) must be equal to 1 for $k = 0..7$.

$$Y_k \sum_{i=0}^{R} (1 - f_{R,k}\delta)^i \Big(1 + \frac{1}{W_{k,i}} \sum_{j=1}^{W_{k,i}} \frac{W_{k,i} - j + 1}{g_{k,j}}\Big) = 1 \qquad (3.29)$$

The normalization condition (3.29) provides 8 equations for $k = 0..7$. By using these 8 equations I are able to solve the Markov chains to calculate the medium access probabilities, $\tau_{R,k}$, $k = 0..7$, during RAPs. Deploying the iterative approach I solve the Markov chains with the new values for X_i, $i = 1..4$.

Now, I calculate the medium access probability of the UP$_7$ nodes during EAPs, $\tau_{E,7}$, using a similar DTMC shown in Fig. 3.8 having a few parameters replaced. I replace $g_{7,j}$, $f_{R,7}$, $\tau_{R,7}$ with $f_{E,7}$, $f_{E,7}$, and $\tau_{E,7}$, respectively. Solving the equation which is acquired from the single Markov chain results in the medium access probability of the UP$_k$ nodes during EAPs.

3.2.2 Performance Evaluation

I have conducted a set of experiments to investigate the impact of lengths of the exclusive and random access phases on the performance of an IEEE 802.15.6 CSMA/CA-based WBANs under saturation condition and an error-prone channel. That is, there is always a data frame in the nodes' buffer to transmit. I solved the analytical model using Maple 13

[82] to calculate the performance descriptors including the mean backoff time and the normalized throughput of all UPs. I developed our own Opnet-based IEEE 802.15.6 simulation model [83] since Opnet does not have a module with implementation of IEEE 802.15.6 standard. The simulation model follows exactly the same assumptions and mechanisms as the analytical model, with respect to differentiation parameters and backoff procedure. I compare the simulation and the analytical results to validate the correctness of both models. In fact, having two different models for the network makes the researchers sure that all details of the standard are considered in both models. It also provides an in-depth understanding of the standard.

In the experiments I consider a WBAN having the following characteristics. The network consists of all 8 UPs, two nodes of each UP and a single hub. It is a single-hop network which operates in 2.4 GHz ISM band with a noisy environment having the bit error rate set to $ber = 2 * 10^{-5}$. The data rate is set to 971.4 kbps (kilo bit per second) while the headers and control frames are transmitted with the rate of 91.9 kbps. I set the modulation parameters and transmission rates according to the IEEE 802.15.6 standard (Table 3.3). The payload size of the data frames (the data frame excluding the headers) is set to 100 B. All nodes in the network deploy CSMA/CA which uses the RTS/CTS mechanism for accessing the medium. The size of all access phases excluding the EAPs and RAPs are set to 0. The differentiation parameters including the minimum and maximum contention window sizes for all UPs are set according to the standard (Table 3.1). Retry limit is set to R=7 for all UPs. I assume that every node transmits a single data frame upon a successful medium access.

In all plots in this section, lines indicate the simulation results and points indicate the

analytical results. The lines with the line-styles *thin solid* (black), *dot* (red), *dash* (blue), *dash-dot* (green), *long-dash* (gold), *space-dot* (khaki), *space-dash* (magenta), and *thick solid* (coral) represent user priorities, 0, 1, 2, 3, 4, 5, 6, and 7, respectively. However, symbols which represent analytical results for user priorities 0, 1, 2, 3, 4, 5, 6, and 7 are *asterisk* (black), *circle* (red), *cross* (blue), *diamond* (green), *solid-circle* (gold), *solid-diamond* (khaki), *diagonal-cross* (magenta), *solid-box* (coral), respectively.

In this section, I study the network performance under three different scenarios; First, the network performance is evaluated when the length of EAP1 or RAP1 varies while the lengths of the other access phases are constant. Second, I evaluate the performance when the lengths of both EAPs or RAPs vary while the lengths of the other access phases are constant. Third, the performance evaluation is performed when the lengths of all four access phases vary. Though our models support non-zero lengths for the type-I/II access phases, in order to focus on the contention-based access phases I set the lengths of the type-I/II APs to zero in all experiments.

In the first scenario, I study the network performance where either length of EAP1 or length of RAP1 varies while lengths of the other access phases are constant. I investigate how varying the lengths of the two different access phases may affect the network performance descriptors, mean backoff time and normalized throughput. EAP1 and EAP2 as well as RAP1 and RAP2 have different lengths.

In the first experiment, I set the access phases lengths as $rap1 = 0.2sec$, $eap2 = 0.1sec$, and $rap2 = 0.3sec$ while the length of EAP1 varies from $0.025sec$ to $0.2sec$. The results, shown in Fig. 3.10, indicate a reasonably good match between the analytical and the simulation results. The mean backoff time plot in Fig. 3.10 (a) indicates that increasing
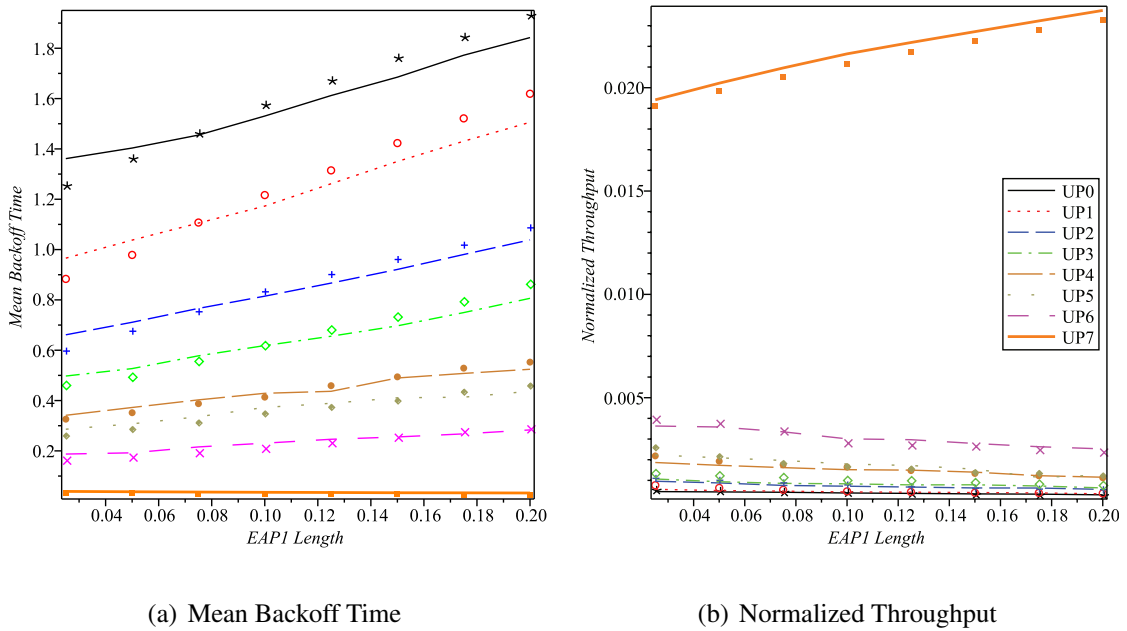
(a) Mean Backoff Time

(b) Normalized Throughput

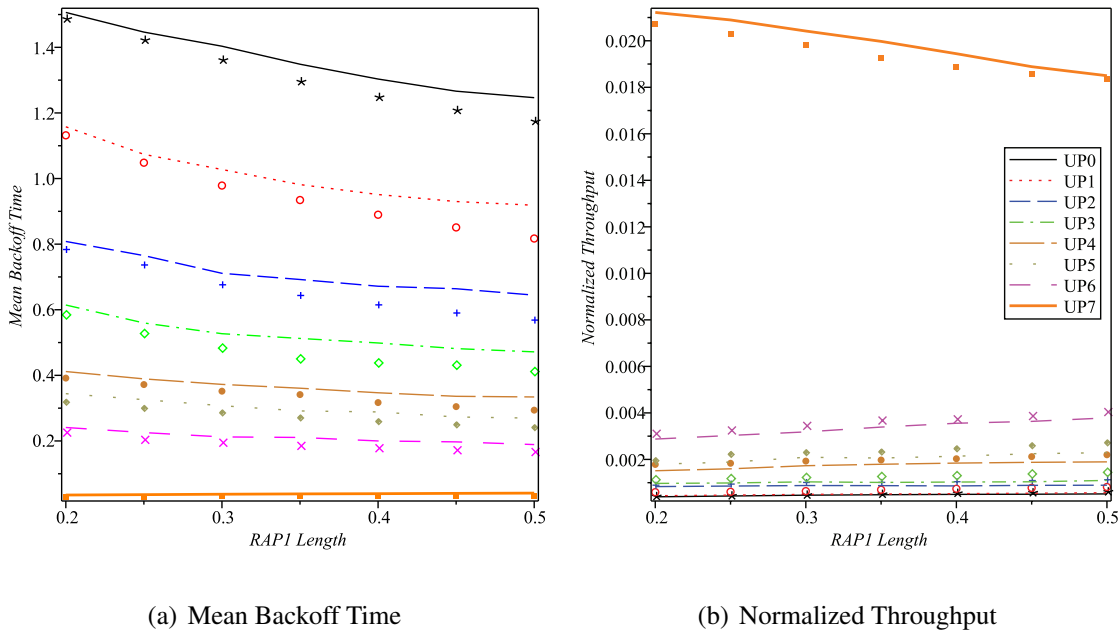Figure 3.10: Mean backoff time and normalized throughput when length of EAP1 varies while $rap1 = 0.2sec$, $eap2 = 0.1sec$, and $rap2 = 0.3sec$

the EAP length generally increases the backoff time of all UPs except UP_7.

Fig. 3.10 (b) shows the normalized throughput of all UPs when length of EAP1 grows while lengths of other access phases are constant. The plot indicates that the UP_7 nodes have almost 2%, as normalized throughput, while the other nodes are starving. The results show that UP_7 is assigned an aggressive prioritization over the other UPs. The UP_7 nodes acquire an unfair access to the medium inasmuch as a UP_7 node accesses to the medium more than all nodes of the other UPs (14 nodes). Increasing the lengths of EAPs while lengths of RAPs are constant worsens the other UPs' starvation.

In the second experiment, I investigate how varying length of an RAP phase affects the network performance. I set the lengths of EAP1, EAP2, and RAP2 to $eap1 = 0.1sec$, $eap2 = 0.05sec$, and $rap2 = 0.2sec$, respectively, while length of RAP1 varies between

(a) Mean Backoff Time

(b) Normalized Throughput

Figure 3.11: Mean backoff time and normalized throughput when length of RAP1 varies while $eap1 = 0.1sec$, $eap2 = 0.05sec$, and $rap2 = 0.2sec$

$0.2sec$ and $0.5sec$. The analytical and the simulation results are shown in Fig. 3.11. Increasing length of an RAP phase improves the mean backoff time of all nodes without UP_7 because they have relatively more chances to compete for the medium. However, it slightly increases the backoff time of the UP_7 nodes as could be seen in Fig. 3.11 (a). As a result, upon RAP1 length growth, from $0.2sec$ to $0.5sec$, the normalized throughputs of the nodes without UP_7 are enhanced though they are still under starvation as shown in Fig. 3.11 (b). The normalized throughputs for the UP_7 nodes decrease which confirms the fact that there is a reverse relation between normalized throughput and mean backoff time.

In the rest of figures in this chapter I only show the simulation results to help the figures to be clearer for the reader. In all the experiments the simulation and analytical results show good match.
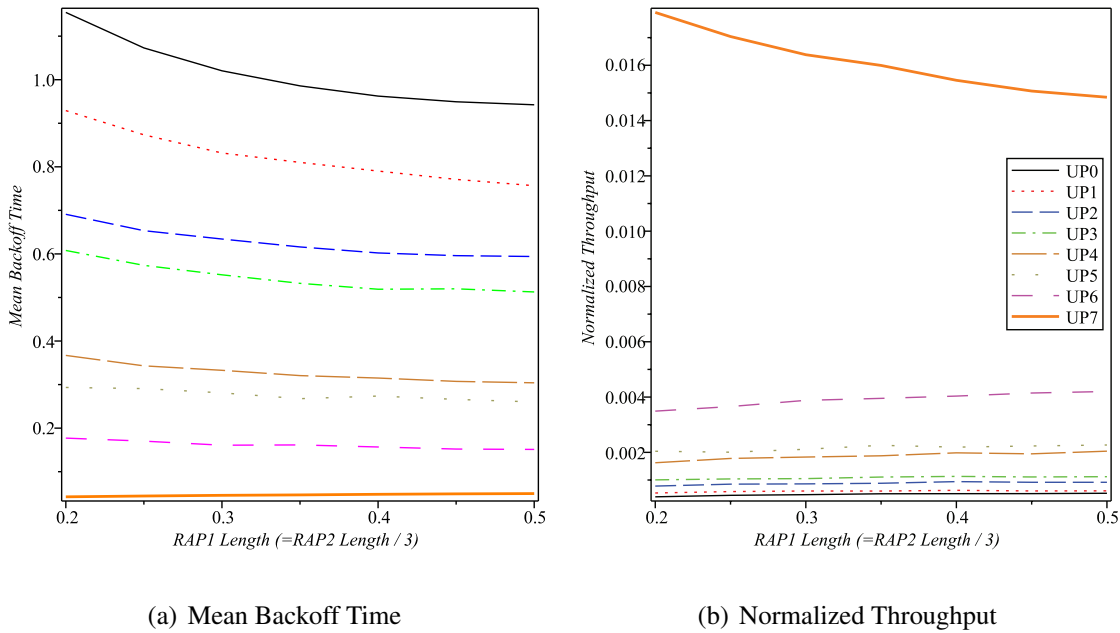
(a) Mean Backoff Time

(b) Normalized Throughput
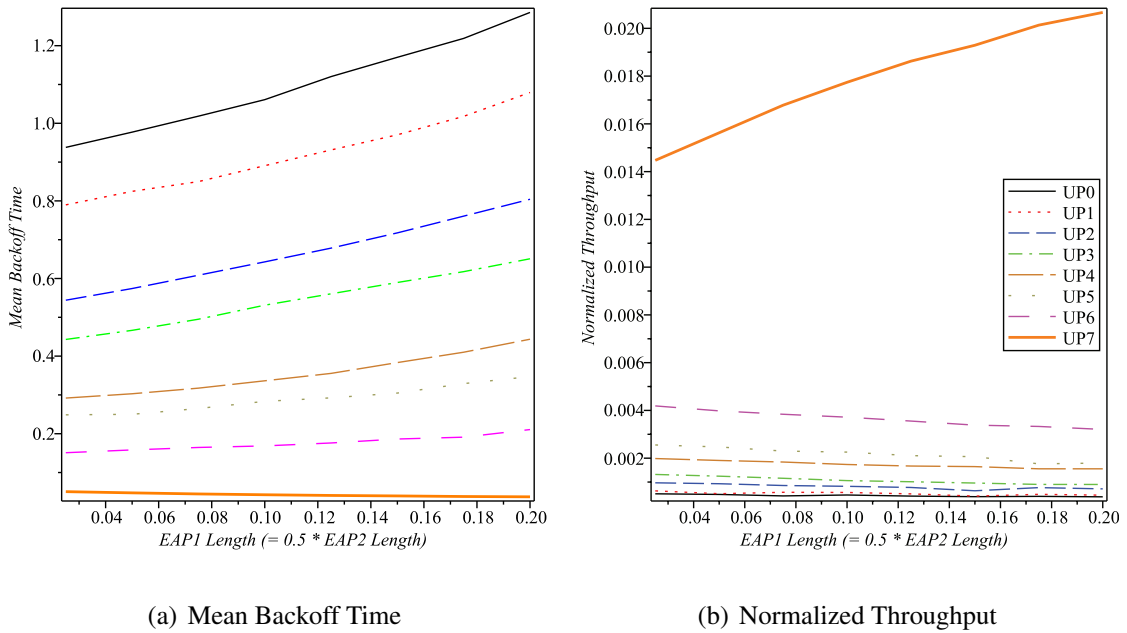
Figure 3.12: Mean backoff time and normalized throughput when lengths of EAP1 and EAP2 vary while $rap1 = 0.5sec$ and $rap2 = 1sec$. In these plots, length of EAP2 is equal to twice of length of EAP1.

In the second scenario, I investigate the network performance when the lengths of both EAPs or both RAPs vary while the lengths of the other two access phases are constant. In the third experiment, I set the lengths of RAP1 and RAP2 to $rap1 = 0.5sec$ and $rap2 = 1sec$. The length of EAP2 is always set to twice of the length of EAP1 where it varies from $0.025sec$ to $0.2sec$. Fig. 3.12 depicts the simulation results of the experiment. Comparing Fig. 3.10 and Fig. 3.12 indicates that varying lengths of both EAPs strongly speeds up the mean backoff time growth and normalized throughput decrease for the nodes without UP_7.

In the forth experiment, the network performance is evaluated when the lengths of RAPs vary while the lengths of EAPs are constant. I set the length of RAP2 to three times of the RAP2 length. The lengths of EAP1 and EAP2 are set to $eap1 = 0.05sec$ and $rap2 = 0.1sec$. The simulation results of the experiment are shown in Fig. 3.13.

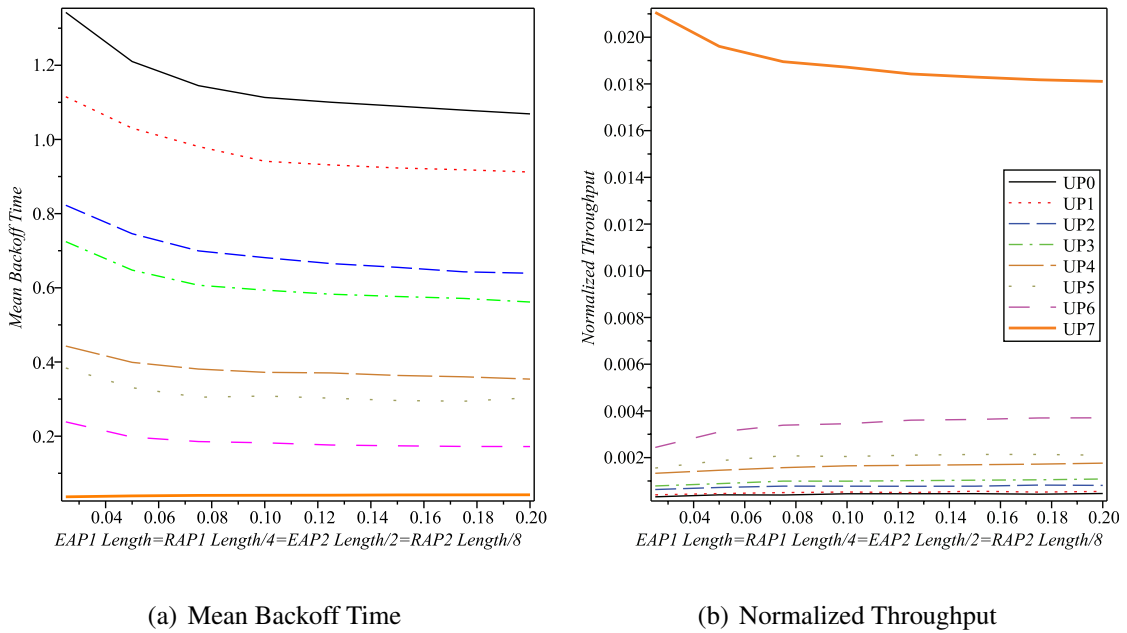(a) Mean Backoff Time   (b) Normalized Throughput

Figure 3.13: Mean backoff time and normalized throughput when lengths of RAP1 and RAP2 vary while $eap1 = 0.05sec$ and $eap2 = 0.1sec$. In these plots, length RAP2 is equal to three times of the length of RAP1.

The interesting finding in this experiment is that when the lengths of RAPs increase the performance descriptors of the nodes without UP_7 are not sharply improved. When the length of RAP1 becomes larger than $0.4sec$ the node's performance descriptors converge to constant values.

Finally, I study the network performance where the lengths of all access phases vary with constant coefficients. In the last scenario, the lengths of RAP1, EAP2, and RAP2 are set to 4 times, 2 times, and 8 times of EAP1 length where it varies from $0.025sec$ to $0.2sec$. The simulation results for this experiment are shown in Fig. 3.14. The results indicate that increasing the access phases lengths generally improves the network performance descriptors in terms of mean backoff time and normalized throughput for all UPs. One reason for the improvement is that during every superframe there are some time slots in which the

(a) Mean Backoff Time

(b) Normalized Throughput

Figure 3.14: Mean backoff time and normalized throughput when lengths of all access phases of EAP1, RAP1, EAP2, and RAP2 vary. Lengths of the access phases in these plots are computed as EAP1 length = RAP1 length/4 = EAP2 length/2 = RAP2 length/8.

nodes are not able to access the medium because there is not sufficient time to complete a frame transaction. Having longer access phases relatively decreases the number of inaccessible time slots for all UPs. Another reason for the improvement is that increasing the access phases lengths decreases the total number of CSMA slots immediately after an EAP period. There is a very high collision probability at the beginning of RAP periods because many nodes had paused their backoff counters during EAPs periods. Hence, shorter access phases imply higher collision probability at the time slots in the superframes. However, the performance descriptors converge to constant values when the access phases are large enough to be highly affected by the high collision probability after the EAP phases.

In this experiment, by incrementing the lengths of EAP1, RAP1, EAP2 and RAP2 with constant ratios, their lengths differences increase. Fig. 3.14 indicates that increasing

the lengths of EAP2 and RAP2 compared to the lengths of EAP1 and RAP2 does not considerably affect the UPs' performance, apart from the fact that increasing the access phases' lengths improves their performance. The reason is that I assume a single traffic type in this work which does not require different values for lengths of EAP1/EAP2 and RAP1/RAP2. In addition, at the beginning of every superframe the WBAN hub is able to change the lengths of access phases. By varying the lengths of EAP1 and RAP1 the feature of different values for EAP1/EAP2 and RAP1/RAP2 could be achieved. Hence, deploying EAP2 and RAP2 for the WBAN is not necessary unless the network contains multiple traffic types.

According to the results of this research, I can comprehend how increasing lengths of the EAPs and RAPs can affect the network performance. The findings of this work could be listed as follows:

- The results quantify how increasing RAPs lengths (while keeping lengths of the other access phases constant) improves the UP_k, $k = 0..6$, nodes performance. Increasing RAPs lengths gives these nodes more opportunities to compete for the medium which improves their performance, in terms of normalized throughput and medium access delay. However, EAPs lengths growth enhances the performance of the UP_7 nodes while it worsens starvation of the other nodes. Increasing length of an EAP phase gives more chances to the UP_7 nodes to have proprietary access period without any interference by the lower priority nodes.

- Longer EAP and RAP phases improve the total network performance. Existence of inaccessible CSMA/CA slots at the end of RAPs and the high collision probability at the beginning of RAPs are the main reasons for the performance deterioration in

case of having shorter EAPs and RAPs.

- EAPs are unnecessary for prioritizing the UP_7 nodes. Even in the absence of EAPs, UP_7 is strongly prioritized over the other UPs because it has very small contention window sizes. Though this work investigates the IEEE 802.15.6-based WBAN performance under saturation condition, according to the results it is expected that EAP periods are not essentially needed for providing QoS for UP_7 nodes under non-saturation condition. Under low to medium traffic, the small contention window sizes enable UP_7 to win the medium access competition within RAP periods. However, if the traffic rate for UP_7 is large and existence of EAPs is a must, lengths of EAPs and RAPs (especially RAPs) should be long to improve the performance of all UPs. In this case, contention-free mechanisms, as another option, could be deployed for transmission of the UP_7 nodes' data frames.

- For a contention-based WBAN, deploying EAP2 and RAP2 phases is not required unless the WBAN contains multiple traffic types to justify different lengths for EAPs and RAPs. Note that in this work I assume that there is a single traffic type in the network.

- Under high traffic loads, the IEEE 802.15.6 CSMA/CA mechanism utilizes the wireless medium poorly. As seen in the plots under saturation condition the UP_7 nodes have plenty of access to the medium while all other nodes are under starvation. The main reason for that is the very small contention window sizes for all UPs. The small contention window sizes cause high collision probabilities in the contention-based access phases. The results indicate that if the network should be in the linear opera-

tion region it has to avoid the saturation condition by performing admission control mechanisms.

3.3 Performance Evaluation of IEEE 802.15.6-based WBANs Under Non-Saturation Condition

I showed that under saturation condition all UPs, except UP_7, starve and the medium is poorly utilized. A node in saturation condition always has a frame in its buffer which means that the node is unstable from the aspect of queuing theory. A WBAN must operate under non-saturation regime in order to prevent large buffer overflows. However, a non-saturation analytical model is more complex than saturation one since it involves queuing analysis of the node together with the access model. A non-saturation model must calculate the duration of the idle period for each node when its queue is empty.

The work on performance evaluation of the IEEE 802.15.6-based WBANs is in an early phase. IEEE 802.15.6 MAC is different from the carrier sense multiple access with collision avoidance (CSMA/CA) in EDCA due to interleaving with the dedicated EAP and RAP phases. In [94] the authors developed a simple model to evaluate the theoretical throughput and delay limits of IEEE 802.15.6-based networks. The developed model does not consider user priorities and access phases of the standard. It also assumes a collision-free network and an ideal channel. CSMA performance under non-saturation regime in IEEE standards has been investigated in [96; 89] for IEEE 802.11, [78; 79; 90] for IEEE 802.11e, and [91] for IEEE 802.15.4. The developed models are not appropriate for the IEEE 802.15.6 standard due to different characteristics of the standards and the CSMA mechanisms. However, there is not currently any work in the literature which evaluates performance of the CSMA mechanism of IEEE 802.15.6 under non-saturation regime considering the UPs and the access phases.

In this section, I study the IEEE 802.15.6 MAC performance under non-saturation regime and an error prone channel. Due to random distribution of time between observation points I model the system as semi Markov process. I develop an analytical model which is composed of three inter-related sub-models; Markov chain, backoff duration, and queuing sub-models. In the Markov chain sub-model, following the backoff procedure of the CSMA mechanism I develop eight dependent 3-dimensional discrete time Markov chains (DTMCs) to compute the medium access probabilities of all UPs. In the backoff duration sub-model, I extend the DTMCs to 4-dimensional DTMCs to calculate the backoff durations of all UPs. In the queuing sub-model, I formulate the probability that the queue is empty after a data frame service completion. The major contributions of this section are summarized as follows:

- The developed analytical and simulation models address all the eight UPs (UP$_k$, $k = 0, ..., 7$) and the first exclusive and random access phases (EAP1 and RAP1) under finite load and an error prone channel. To our best knowledge, this is the first developed analytical model in the literature which investigates the performance of the CSMA mechanism of the IEEE 802.15.6 standard for all UPs under non-saturation regime.

- I develop a Geo/G/1 queuing sub-model of node's buffer in addition to Markov chain and backoff duration sub-models for investigating the performance of the network under non-saturation regime.

- By solving all priority models simultaneously I compute the mean data frame waiting time for all UPs where the lengths of EAP1 and RAP1 vary. I investigate how

increasing the length of the exclusive (random) access phase where the length of the random (exclusive) access phase is constant affects the performance of the network.

- Our analytical model covers the case where the RTS/CTS mechanism is deployed and the case where the nodes immediately transmit a data frame upon decrementing the backoff counter to zero. I study how performing the contention avoidance mechanism for an IEEE 802.15.6-based WBAN impacts the performance of the network.

3.3.1 Analytical Model

In this section, the analytical model for investigating the IEEE 802.15.6-based WBAN performance under non-saturation condition is developed. I assume that a UP_k, $k = 0..7$ node has a single UP_k queue. The network, operating in 2.4 GHz ISM band or 2360-2400 MHz frequency band, is assumed to be single-hop including a hub as the coordinator and n_k, $k = 0..7$ UP_k nodes and therefore I ignore the hidden terminal problem. I assume that there is only uplink traffic from the nodes to the hub. I define λ_k, $k = 0..7$, as the data frame arrival probability during a CSMA slot for a UP_k node. I assume that during a slot at most one data frame arrives to the queue which is not an unrealistic assumption due to the small length of a CSMA slot. It is clear that the inter-arrival time I_k is geometrically distributed with the mean of $\frac{1}{\lambda_k}$ slots. The lengths of EAP1 and RAP1 are indicated by eap and rap in slots, respectively. I assume superframes with boundaries which begin by broadcasting a beacon frame by the hub. Because the size of the beacon is small I ignore it in our analytical model. The assumption will not considerably affect the performance descriptors of the network.

The sizes of RTS and CTS are represented by rts and cts in slots and rts_b and cts_b

in bits, respectively. The control frames and headers are transmitted at 91.9 kbps while I assume the payload of the data frames is transmitted at 971.4 kbps. The size of the data frames for a UP_k node is denoted by l_k in slots and $l_{k,b}$ in bits and ack and ack_b indicate the sizes of an ACK frame in slots and in bits, respectively.

I assume an error-prone channel having BER of ber. The probability that neither RTS nor CTS is corrupted due to the channel noise is defined as $\delta = (1 - ber)^{rts_b + cts_b}$. I define $\sigma_k = (1 - ber)^{l_{k,b} + ack_b}$ as the probability that the data frame and the corresponding acknowledgement are transmitted without getting corrupted by the noise.

The analytical model consists of three inter-related sub-models; Markov chain sub-model, probabilistic sub-model of backoff durations, and queuing sub-model, as described below:

- **Markov chain sub-model**: In the analytical model, I observe the system at moments of beginning of EAPs and RAPs, backoff decrements, and packet departures. In these points the random process under study has a Markov property. These points are called Markov points. The time between two successive Markov points is a random variable which affects the steady state probabilities. Therefore, the process under consideration is a semi Markov process [81]. For evaluating the semi Markov process I need DTMCs and the time distributions between the Markov points. The Markov chain sub-model is composed of a set of eight 3-dimensional DTMCs to compute the access probabilities of the UPs. The DTMCs are developed based on the backoff procedure of the IEEE 802.15.6 CSMA mechanism. This sub-model also needs the probability that the queue is empty after a data frame service completion, which is formulated in the queuing sub-model.

- **Probabilistic sub-model of backoff durations**: The probability distributions of all the backoff phases and the total backoff duration before a successful access to the medium or a data frame drop for all UPs are formulated by the backoff duration sub-model. The probability generating functions (PGFs) of the backoff durations are computed based on the access probabilities of the UPs which are introduced in the Markov chain sub-model. The computed time distributions are used in the queueing and the Markov sub-models to calculate the transition probabilities in the semi Markov chains.

- **Queuing sub-model**: To calculate durations of idle periods and access probabilities of all UPs I need to know the queuing status of every UP in every CSMA slot. The backoff probability distributions of all UPs, acquired by the backoff duration sub-model, are deployed to formulate the empty queue probability, duration of an idle period, and the queue size of every UP.

Since the three sub-models are inter-related they form one monolithic analytical model which can not be partially verified either formally or numerically. Instead, whole model is presented as a set of equations which are solved numerically. Due to large complexity the solution is obtained in an iterative way.

3.3.1.1 Markov Chain Sub-model

In the Markov chain sub-model I introduce eight dependent 3-dimensional DTMCs for the eight UPs to formulate the medium access probabilities of the UPs. The access probability of a UP_k node, τ_k ($k = 0..7$), is calculated by solving the set of DTMCs considering the CSMA slots in which the medium is not set to be busy due to either a transmission
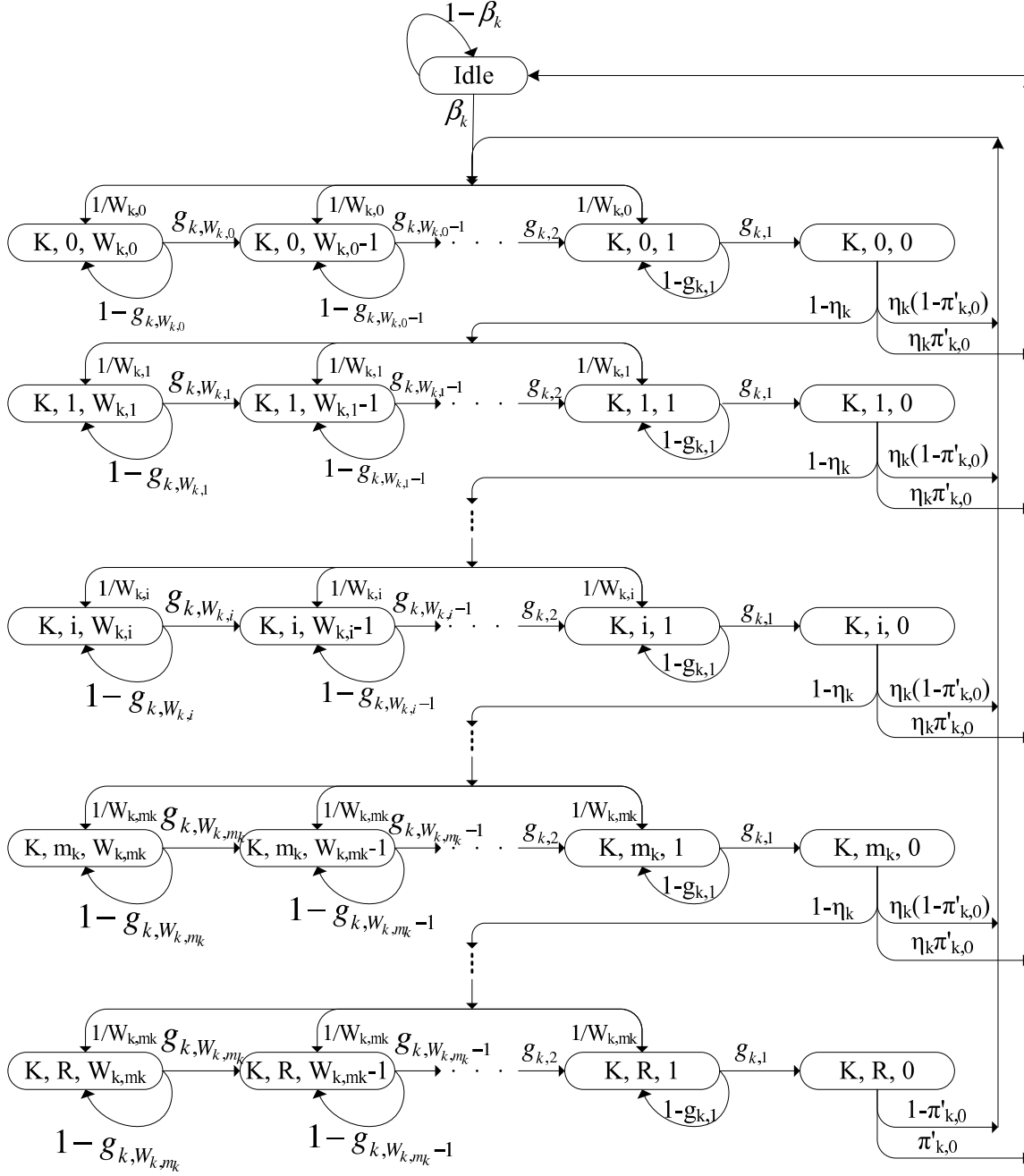
Figure 3.15: 3-dimensional DTMC for UP$_k$

on the medium or being in an inaccessible access phase. The access probabilities vary in different time periods. I calculate the access probabilities in the CSMA slots in which the medium is accessible by the nodes. The DTMC for a UP_k node is depicted in Fig. 3.15. The depicted DTMC in Fig. 3.15 is the extension of depicted DTMC in Fig. 3.8 for non-saturation condition. Fig. 3.15 includes the idle state in which the nodes for data frames from the upper layer to arrive. The transition probabilities between states might also be different in the DTMCs. The Markov points are beginning of the CSMA slots in which the UP_k node is allowed to transmit. Hence, the intervals between two successive Markov points in a DTMC may have different lengths. The Markov chain represents a random process with stationary distribution $b_{k,i,j}$, where $k = 0..7$ indicates the user priority that the node belongs to, $i = 0..m_k..R$ denotes the backoff phase in the backoff procedure invoked by the node, and $j = 0..W_{k,i}$ indicates the value of the backoff counter.

I define f as the probability that a CSMA slot is remained unused by any UP during an RAP period which is given by

$$f = \prod_{i=0}^{7} (1 - \tau_i)^{n_i} \tag{3.30}$$

For a UP_k node the probability that the medium remains idle during its backoff countdown is given by

$$f_k = \frac{\prod_{i=0}^{7} (1 - \tau_i)^{n_i}}{(1 - \tau_k)}, \quad k = 0..7 \tag{3.31}$$

Because only the UP_7 nodes are allowed to transmit during EAP1 while all UPs can access the medium during RAP1, the probabilities that the medium remains idle in a CSMA slot during EAP1 and RAP1 are different. I approximate the probability for a UP_7 node during its backoff countdown as follows:

$$f_7 = \frac{X_R \prod_{i=0}^{7} (1 - \tau_i)^{n_i}}{(X_E + X_R)(1 - \tau_7)} + \frac{X_E(1 - \tau_7)^{n_7 - 1}}{X_E + X_R} \tag{3.32}$$

where X_E and X_R are the mean numbers of CSMA slots in EAP1 and RAP1, respectively, which are the Markov points. In our iterative approach I set the initial values of the numbers to $X_E = eap$ and $X_R = rap$. The values of X_E and X_R for the next iterations are calculated as follows:

$$X_R = \frac{rap - L_{7,s}}{f + \sum_{t=0}^{7} n_t \tau_t \eta_t L_{t,s} + (1 - f - \sum_{t=0}^{7} n_t \tau_t \eta_t) L_{t,c}}$$

$$X_E = \begin{cases} \frac{eap}{\chi + n_7 \tau_7 \psi \delta L_{7,s} + (1 - \chi - n_7 \tau_7 \psi \delta) L_{7,c}}, & \text{if RTS/CTS is deployed} \\[2ex] \frac{eap}{\chi + n_7 \tau_7 \psi \sigma_7 L_{7,s} + (1 - \chi - n_7 \tau_7 \psi \sigma_7) L_{7,c}}, & \text{otherwise} \end{cases} \tag{3.33}$$

where $\chi = (1 - \tau_7)^{n_7}$, $\psi = (1 - \tau_7)^{n_7 - 1}$. In the above formulae, $L_{k,s}$, $k = 0..7$, indicates the successful transmission time for a UP_k data frame in slots which is equal to $L_{k,s} = rts + cts + l_k + ack + 3sifs$ where RTS/CTS mechanism is deployed and $L_{k,s} = l_k + ack + sifs$ where RTS/CTS mechanism is not used. $L_{k,c}$, $k = 0..7$, is the unsuccessful transmission time of a UP_k data frame in slots in case of failure access to the medium, which is equal to $L_{k,c} = rts + cts + sifs$ and $L_{k,c} = l_k + ack + sifs$ in case of deploying RTS/CTS mechanism and withholding the RTS/CTS mechanism, respectively.

In addition to the above transmission times, I define the mean successful and unsuccessful transmission times of other nodes in the network for a given UP_k node. I refer to $L_{k,so}$, $k = 0..7$, as the mean successful transmission time of other nodes in the network for a given UP_k node. Similarly, I refer to $L_{k,co}$, $k = 0..7$, as the mean unsuccessful transmission time of data frames of other nodes in the network for a given UP_k node. For the case where the RTS/CTS mechanism is deployed I compute the durations as $L_{k,so} = rts + cts + l_{k,o} + ack + 3sifs$ and $L_{k,co} = rts + cts + sifs$. However, when the

RTS/CTS is not deployed I have $L_{k,so} = L_{k,co} = l_{k,o} + ack + sifs$. I define $l_{k,o}$, $k = 0..7$ as the average size (in slots) of a data frame transmitted by other nodes in the network for a given UP_k node. The subscript 'o' indicates the word "others". The initial values for $l_{k,o}$ are defined as follows:

$$l_{k,o} = \frac{\sum_{u=0}^{7} n_u l_u - l_k}{\sum_{u=0}^{7} n_u - 1}, \quad k = 0..7 \tag{3.34}$$

I update the values of $l_{k,o}$ for the next iterations as follows:

$$l_{k,o} = \frac{\sum_{u=0}^{7} n_u \tau_u l_u - \tau_k l_k}{\sum_{u=0}^{7} n_u \tau_u - \tau_k}, \quad k = 0..7 \tag{3.35}$$

In the Markov chain (Fig. 3.15) η_k, $k = 0..7$, represents the probability of successful access to the medium for a UP_k node when its backoff counter reaches zero. The probability η_k is computed as follows:

$$\eta_k = \begin{cases} f_k \delta, & \text{if RTS/CTS is deployed} \\ f_k \sigma_k, & \text{otherwise} \end{cases} \tag{3.36}$$

If the remaining time during the current access phase (EAP1 and RAP1 for a UP_7 node and RAP1 otherwise) is not long enough to complete a data frame transaction (RTS-CTS-Data Frame-ACK in case of deploying RTS/CTS mechanism or Data Frame-ACK otherwise) the backoff counter is locked. For a node without UP_7 the counter must be kept locked during EAP1 as well. I introduce p_k to address the probability that in a given CSMA slot the node notices that there is not enough time during the current access period to complete a frame transaction. The backoff counter remains locked until the moment when the node is allowed to transmit (RAP1 for UP_k, $k = 0, ..., 6$ or EAP1 for UP_7). p_k is computed as

follows:

$$p_k = \frac{1}{(rap - L_{k,s} - C_k)}, \quad k = 0, ..., 6$$

$$p_7 = \frac{1}{(rap + eap - L_{k,s} - C_7)} \tag{3.37}$$

where $C_k = \frac{CW_{k,min} + CW_{k,max}}{4}$, $k = 0, ..., 7$ approximates the mean backoff value. Since the denominator indicates the number of CSMA slots during a superframe in which the node is able to access the medium, the p_k value represents the probability that in a given CSMA slot an inaccessible medium access period begins. Number of accessible CSMA slots in a superframe for a UP depends on the length of accessible access phases, frame transmission time, and the backoff counter at which the counter is paused. I approximate the p_k value deploying the approximated mean backoff values for different UPs.

I define $g_{k,j}$, $k = 0, ..., 7$, $j = 1, ..., W_{k,m_k}$ as the probability that the backoff counter of a UP_k node is decremented when the counter is equal to j. $g_{k,j}$ considers the slots in which the backoff counter is locked but the slots should be considered as the Markov points to calculate the access probability.

$$g_{k,j} = f_k(1 - p_k \frac{1 - f_k^j}{1 - f_k}) \tag{3.38}$$

The medium access probability of a UP_k node is equal to $\tau_k = \sum_{i=0}^{R} b_{k,i,0}$.

By solving the Markov chain the following equation is acquired for $k = 0..7$, $i = 0..R$, and $j = 1..W_{k,i}$.

$$b_{k,i,j} = \frac{(1 - \eta_k)^i Y_k (W_{k,i} - j + 1)}{W_{k,i} g_{k,j}}$$

$$b_{k,i,0} = (1 - \eta_k)^i Y_k \tag{3.39}$$

where Y_k, $k = 0..7$, is the input probability to the zero-th backoff phase which is computed as follows:

$$Y_k = \frac{\tau_k \eta_k (1 - \pi'_{k,0}) + p_{k,Idle} \beta_k}{1 - (1 - \eta_k)^{R+1}(1 - \pi'_{k,0})}, \quad k = 0..7 \tag{3.40}$$

where $p_{k,Idle}$ represents the probability of being in "Idle" state and $\pi'_{k,0}$ is computed as follows:

$$\pi'_{k,0} = \begin{cases} \pi_{k,0}\sigma_k, & \text{if RTS/CTS is deployed} \\ \pi_{k,0}, & \text{otherwise} \end{cases} \tag{3.41}$$

in which $\pi_{k,0}$ indicates the probability that the queue of the UP_k node is empty when a data frame is either successfully transmitted or dropped due to an exceeded retry limit. $\pi_{k,0}$ will be formulated in the queuing sub-model while $p_{k,Idle}$ is calculated as follows:

$$p_{k,Idle} = \frac{\tau_k \eta_k \pi'_{k,0}}{\beta_k (1 - (1 - \eta_k)^{R+1})}, \quad k = 0..7 \tag{3.42}$$

where β_k is given by

$$\begin{aligned} \beta_k &= f_k p_k (1 - (1 - \lambda_k)^{L_k}) + f_k(1 - p_k)\lambda_k + (1 - f_k) \cdot \tag{3.43} \\ &+ \left(p_k \sum_{u=0}^{L_{k,so}-1} (1 - p_k)^u (1 - (1 - \lambda_k)^{L_k + u + 1})(1 - p_k)^{L_{k,so}}(1 - (1 - \lambda_k)^{L_{k,so}}) \right) + \frac{1}{x_k} \end{aligned}$$

where $x_k = X_R$, $k = 0..6$ and $x_7 = X_R + X_E$. β_k represents the probability that a data frame arrives to the queue during the time interval between two successive Markov points. The first component corresponds to the case where at the first CSMA slot of the interval no node transmits on the medium but there is not enough time to complete a data frame transaction. In this case, the length of the interval is equal to L_k slots. I define L_k, $k = 0..7$, as the number of slots in which the backoff counter of a UP_k node must be kept locked because there is not enough time to complete a data frame transaction. During EAP1 just the UP_7 nodes are allowed to transmit or decrease their backoff counters. During RAP1 all

the nodes in the network have to lock their backoff counter where there is not enough time for completing a transmission. I have $L_k = eap + rts + cts + 3sifs + l_k + ack, \ k = 0..6$, in case of deploying RTS/CTS mechanism and $L_k = eap + sifs + l_k + ack, \ k = 0..6$, otherwise. A UP$_7$ node does not need to lock its backoff counter during EAP1 unless the medium is busy, resulting in $L_7 = rts + cts + 3sifs + l_k + ack$ when RTS/CTS mechanism is deployed and $L_7 = sifs + l_k + ack$, otherwise. In case of having the backoff counter equal to j, a node has to keep it's counter locked for $L_k + j$ slots if the node notices that there is not enough time to complete a data frame transaction. The second component represents the case where the first CSMA slot remains idle and there is enough time to complete a data frame transaction. This results in the interval length of one slot. The third component corresponds to the case where any node(s) starts transmitting on the medium. $\frac{1}{x_k}$ represents the probability that the first CSMA slot belongs to inaccessible access phases.

I compute the summation of all the stationary distribution $b_{k,i,j}$ as follows:

$$\sum_{i=0}^{R} \sum_{j=0}^{W_{k,i}} b_{k,i,j} = Y_k \sum_{i=0}^{R} (1 - \eta_k)^i \Big(1 + \sum_{j=1}^{W_{k,i}} \frac{W_{k,i} - j + 1}{W_{k,i} g_{k,j}}\Big) \tag{3.44}$$

Based on the normalization condition of DTMCs, summation of all the probabilities is equal to 1 which results in the following set of eight equations for $k = 0..7$:

$$1 = p_{k,Idle} + Y_k \sum_{i=0}^{R} (1 - \eta_k)^i \Big(1 + \sum_{j=1}^{W_{k,i}} \frac{W_{k,i} - j + 1}{W_{k,i} g_{k,j}}\Big) \tag{3.45}$$

Hence, the Markov chain sub-model results in a set of eight equations while there are 16 unknown variables of $\tau_k, \ k = 0..7$, and $\pi_{k,0}, \ k = 0..7$. π values are formulated in the queuing sub-model.

3.3.1.2   Probabilistic Sub-model of Backoff Duration

In this section, I calculate the average durations of every backoff phase and the total backoff period before successfully accessing the medium or dropping the data frame using PGFs.
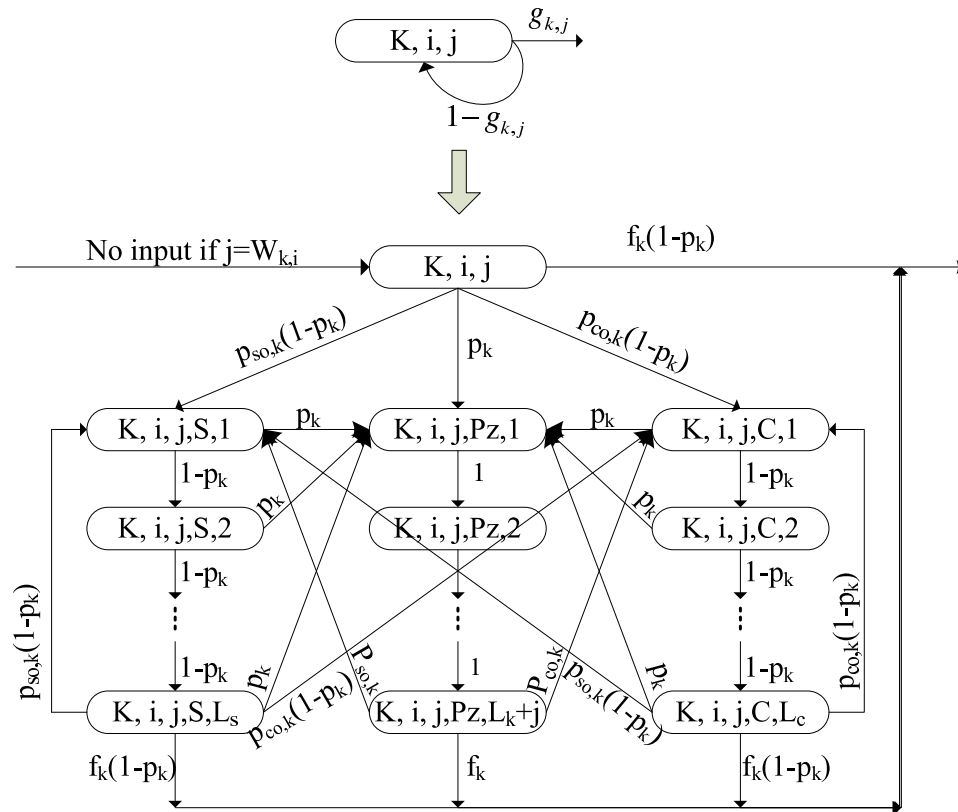

Figure 3.16: Markov chain state extension for UP_k

To calculate the length of backoff durations I extend the DTMCs, described in section 3.3.1.1, to ones that beginning of every CSMA slot represents a Markov point. In the extended DTMCs the distance between every two Markov points is one slot. To compose the extended 4-dimensional DTMCs I replace the component shown on top of Fig.

3.16 with the component shown below that in the 3-dimensional DTMCs (Fig. 3.15) for $k = 0..7$, $i = 0..R$, and $j = 1..W_{k,i}$.

Stationary distributions of $b_{k,i,j,S,t}$, $t = 1..L_{k,so}$, and $b_{k,i,j,C,t}$, $t = 1..L_{k,co}$, correspond to the slots during the time periods in which the data frame is successfully transmitted and the first transmitted frame collides (RTS if RTS/CTS mechanism is deployed and data frame, otherwise), respectively. Stationary distribution of $b_{k,i,j,Pz,t}$ for $t = 1..L_k + j$ corresponds to a slot during the time period in which the node's backoff counter is locked because there is not enough time to complete a data frame transaction.

I refer to $p_{so,k}$, $k = 0..7$, and $p_{co,k}$, $k = 0..7$, as the probabilities that the medium becomes busy due to a successful transmission by another node and unsuccessful accesses by the other nodes in the network, respectively, which are computed as follows:

$$
\begin{aligned}
p_{so,k} &= \sum_{i=0}^{7} \frac{n_i \tau_i \eta_k}{1 - \tau_i} - \frac{\tau_k \eta_k}{1 - \tau_k} \\
p_{co,k} &= 1 - f_k - p_{so,k}
\end{aligned}
\tag{3.46}
$$

$\frac{\tau_i \eta_k}{1 - \tau_i}$ represents the probability of successful transmission by a UP_i, $i = 0..7$ node. Excluding the UP_k node, the other n_i, $i \neq k$ and $n_k - 1$ nodes are counted in the above summation. $p_{so,k} + p_{co,k} = 1 - f_k$ which is the probability that the medium is busy due to a transmission on the medium.

I indicate the PGFs of durations of a data frame transaction and a failed transmission due to an RTS collision by $St_k(z) = z^{rts+cts+l_k+ack+3sifs}$ and $Ct_k(z) = z^{rts+cts+sifs}$, respectively, where the RTS/CTS mechanism is deployed. However, when the nodes do not deploy the RTS/CTS mechanism I have $St_k(z) = Ct_k(z) = z^{l_k+ack+sifs}$. Every backoff period is composed of up to R backoff phases. The backoff phases are made of the time periods in which the backoff counter is decremented by one until the counter reaches zero. I

define $\mathcal{B}_{S,k,j}(z)$ as the PGF of the time duration from the moment when the backoff counter

is locked due to a successful access by another node until the moment when the backoff

counter is unlocked where the backoff counter is equal to j for a UP_k node. $\mathcal{B}_{C,k,j}(z)$ is

defined as the PGF of the time interval between the instant when the backoff counter is

locked due to an unsuccessful medium access by the other nodes and the instant when the

backoff counter is unlocked. I introduce $\mathcal{B}_{P,k,j}(z)$ as the PGF of the time duration from the

moment when the backoff counter is locked because there is not enough time to complete

a frame transaction until the moment when the backoff counter is unlocked. The PGFs are

computed using the extended DTMCs as follows:

$$
\begin{aligned}
\mathcal{B}_{P,k,j}(z) &= z^{L_k+j}(f_k z + \Theta_{k,j}(z)) \\
\mathcal{B}_{S,k,j}(z) &= p_k \mathcal{B}_{P,k,j}(z) \frac{1 - (1-p_k)^{L_{k,so}} z^{L_{k,so}}}{1 - (1-p_k)z} + (1-p_k)^{L_{k,so}} f_k z^{L_{k,so}} \\
&+ (1-p_k)^{L_{k,so}} \Theta_{k,j}(z) \\
\mathcal{B}_{C,k,j}(z) &= p_k \mathcal{B}_{P,k,j}(z) \frac{1 - (1-p_k)^{L_{k,co}} z^{L_{k,co}}}{1 - (1-p_k)z} + (1-p_k)^{L_{k,co}} f_k z^{L_{k,co}} \\
&+ (1-p_k)^{L_{k,co}} \Theta_{k,j}(z) \quad\quad\quad (3.47)
\end{aligned}
$$

where $\Theta_{k,j}(z) = p_{so,k} \mathcal{B}_{S,k,j}(z) + p_{co,k} \mathcal{B}_{C,k,j}(z)$ is PGF of the mean duration of backoff

counter lock due to a transmission on the medium, either successful or unsuccessful. Full

derivations of $\mathcal{B}_{S,k,j}(z)$, $\mathcal{B}_{C,k,j}(z)$, and $\mathcal{B}_{P,k,j}(z)$ are straightforward using the substitution

method of solving system of equations. I now calculate the PGF of the time interval be-

tween the moment when the backoff counter of a node of UP_k becomes equal to j and the

moment when the backoff counter becomes equal to $j-1$ at the i-th backoff phase. The

PGF of the time to decrease the backoff counter by one, where the counter is equal to j for

$k = 0..7$, $j = 1..W_{k,i}$, $i = 0..R$, is given by

$$\Phi_{k,i,j}(z) = p_k \mathcal{B}_{P,k,j}(z) + (1 - p_k)(f_k z + \Theta_{k,j}(z)) \tag{3.48}$$

Having the above PGFs I am able to write the PGF of i-th backoff phase duration as follows:

$$\Phi_{k,i}(z) = \sum_{j=1}^{W_{k,i}} \prod_{t=1}^{j} \Phi_{k,i,t}(z) \Big(\eta_k (L_{k,s} p_k z^{L_k} + 1 - L_{k,s} p_k) + (1 - \eta_k)(L_{k,c} p_k z^{L_k} + 1 - L_{k,c} p_k) \Big) / W_{k,i} \tag{3.49}$$

The PGF for the duration of backoff process for a UP$_k$ node is equal to:

$$
\begin{aligned}
\Phi_k(z) &= \sum_{i=0}^{m_k} (\prod_{u=0}^{i} \Phi_{k,u}(z))(1 - \eta_k)^i (z^{L_{k,c}})^i \eta_k + \\
&\quad \sum_{i=m_k+1}^{R} (\prod_{u=0}^{m_k} \Phi_{k,u}(z)) \Phi_{k,m_k}^{i-m_k}(z)(1 - \eta_k)^i (z^{L_{k,c}})^i \eta_k + \\
&\quad (\prod_{u=0}^{m_k} \Phi_{k,u}(z)) \Phi_{k,m_k}^{R-m_k}(z)(1 - \eta_k)^{R+1} (z^{L_{k,c}})^{R+1} \tag{3.50}
\end{aligned}
$$

Using the equation (3.50), I calculate the mean backoff time before the medium is successfully accessed or the data frame is dropped for a UP$_k$ node as: $\phi_k = \frac{d}{dz} \Phi_k(z) \Big|_{z=1}$

3.3.1.3   Queuing Sub-model

I model the queue of each node in the WBAN using a pure limited Geo/G/1 system with vacations [97]. The Geo/G/1 queue is a single-server discrete time system with a Bernoulli arrival process and generally distributed service times. The inter-arrival time to the queue for all UPs is geometrically distributed with mean of $\frac{1}{\lambda_k}$ slots. A data frame is served when it is successfully transmitted or dropped due to an exceeded retry limit. The time interval in which the node performs the backoff process or is idle because of an empty queue is called a vacation. I assume that upon a successful access to the medium each node transmits a

single data frame. I denote by $B_k(z)$, $k = 0..7$, the PGF of service time (in slots) of a data frame for a UP_k node, which includes a backoff process and successful transmission time, which is given by

$$B_k(z) = \begin{cases} \frac{\sigma_k \Phi_k(z) St_k(z)}{1-(1-\sigma_k)\Phi_k(z) St_k(z)}, & \text{if RTS/CTS is deployed} \\ \Phi_k(z) St_k(z), & \text{otherwise} \end{cases} \quad (3.51)$$

If the RTS/CTS mechanism is not deployed the service time of a data frame consists of the backoff duration to successfully access the medium and the data frame transmission time, which results in $B_k(z) = \Phi_k(z) St_k(z)$. However, in case of deploying the RTS/CTS mechanism a new backoff is started after every unsuccessful data frame transmission while an unsuccessful RTS transmission causes a new backoff phase. Hence, the PGF of the service time is a geometric series with the common ratio of $E_k(z) = (1 - \sigma_k)\Phi_k(z) St_k(z)$ as $B_k(z) = \sigma_k \Phi_k(z) St_k(z) \sum_{u=0}^{\infty} E_k^u(z)$. The mean service time for a UP_k data frame is given by $b_k = B_k'(1)$.

The offered load or traffic intensity of the queue is given by $\rho_k = \lambda_k b_k$. For stability condition the offered load must be less than unity. If the condition is satisfied, the offered load is equivalent to the carried load or the server utilization in the Geo/G/1 system.

I consider a Markov chain $\{D_{k,n}; n = 0, 1, 2, 3, ...\}$, where $D_{k,n}$ is the number of data frames present in the system for a UP_k node immediately after the service completion of the n-th data frame. I refer to $A_{k,n}$ as the number of data frames that arrive during the service of the n-th data frame of a UP_k node. If the number of data frames of UP_k that arrive during an idle period is also denoted by α_k, I have

$$D_{k,n+1} = \begin{cases} \alpha_k + A_{k,n+1} - 1, & \text{if } D_{k,n} = 0 \\ D_{k,n} + A_{k,n+1} - 1, & \text{otherwise} \end{cases} \quad (3.52)$$

The PGF $A_k(z)$ for $A_{k,n}$ is equal to $A_k(z) = B_k[\Lambda_k(z)]$ where $\Lambda_k(z) = 1 - \lambda_k + \lambda_k z$ is the PGF of the number of UP$_k$ data frames that arrive during a single CSMA slot. I refer to $\alpha_k(z)$ as the PGF of α_k which is equal to $\alpha_k(z) = \mathcal{I}_k(\Lambda_k(z))$ where $\mathcal{I}_k(z)$ indicates the PGF of the idle period duration in slots. The idle period duration is the difference between the inter-arrival time and the frame service time. Since the UP$_k$ data frame arrival rate in a CSMA slot is equal to λ_k, the number of idle slots before an arrival follows a geometric distribution with the PGF of $\frac{\lambda_k z}{1-(1-\lambda_k)z}$. However, the service time of the last served data frame must be deducted from the inter-arrival time which results in the following equation:

$$\mathcal{I}_k(z) = \frac{\lambda_k z}{B_k(z)\big(1 - (1 - \lambda_k)z\big)}, \quad k = 0..7 \tag{3.53}$$

I define $\pi_{k,u}$, $k = 0..7$, $u = 0, 1, 2, ...$, as the steady state probability of having u frames in the UP$_k$ queue after its data frame service completion. Based on the above definitions, I have

$$\pi_{k,u} = \pi_{k,0} \sum_{j=1}^{u+1} \alpha_{k,j} a_{k,u-j+1} + \sum_{j=1}^{u+1} \pi_{k,j} a_{k,u-j+1}, \ k = 0..7, \ u = 0, 1, 2, ... \tag{3.54}$$

where $A_k(z) = \sum\limits_{u=0}^{\infty} a_{k,u} z^u$ and $\alpha_k(z) = \sum\limits_{u=0}^{\infty} \alpha_{k,u} z^u$. The PGF of the steady state probability distribution $\{\pi_{k,u}; u = 0, 1, 2, ...\}$ for the queue of a UP$_k$ node is given by

$$
\begin{aligned}
\Pi_k(z) &= \sum_{u=0}^{\infty} \pi_{k,u} z^u \\
&= \sum_{u=0}^{\infty} \pi_{k,0} \sum_{j=1}^{u+1} \alpha_{k,j} a_{k,u-j+1} z^u + \sum_{u=0}^{\infty} z^u \sum_{j=1}^{u+1} \pi_{k,j} a_{k,u-j+1} \\
&= \pi_{k,0} \sum_{j=1}^{\infty} \alpha_{k,j} z^j \sum_{u=j-1}^{\infty} a_{k,u-j+1} z^{u-j+1} + \sum_{j=1}^{\infty} \pi_{k,j} z^{j-1} \sum_{k=j-1}^{\infty} a_{k,u-j+1} z^{u-j+1} \\
&= \frac{\pi_{k,0} \alpha_k(z) A_k(z)}{z} + \frac{(\Pi_k(z) - \pi_{k,0}) A_k(z)}{z}, \ k = 0..7 \tag{3.55}
\end{aligned}
$$

solving equation (3.55) for $\Pi_k(z)$, I get

$$\Pi_k(z) = \frac{\pi_{k,0}(1 - \alpha_k(z))B_k(\Lambda_k(z))}{B_k(\Lambda_k(z)) - z} = \frac{\pi_{k,0}(1 - \mathcal{I}_k(\Lambda_k(z)))B_k(\Lambda_k(z))}{B_k(\Lambda_k(z)) - z}, \ k = 0..7 \quad (3.56)$$

The unknown probability that buffer is empty after a data frame's service completion, $\pi_{k,0}$, is determined from the normalization condition or $\Pi_k(1) = 1$. From 3.56, with a single use of $l'H\hat{o}pital's$ rule, I obtain:

$$\pi_{k,0} = \frac{1 - \rho_k}{E[\alpha_k]} = \frac{1 - \rho_k}{\lambda_k E[\mathcal{I}_k(z)]}, \ k = 0..7 \quad (3.57)$$

The probability $\pi_{k,0}$ indicates the probability that the queue of a UP$_k$ node is empty after a successful data frame transmission or a data frame drop due to an exceeded retry limit. $\pi_{k,0}$ depends on the duration between two successive successful transmissions/data frame drops, which depends on the background traffic, the contention among the nodes, and the data frame arrival rates. The backoff duration of a node is a function of the backoff durations and frame arrival rates of other nodes in the network which might be at different backoff phases at different time slots. Hence, $\pi_{k,0}$ represents an average probability.

From (3.45) and (3.57) I obtain a set of 16 equations which enables us to calculate the 16 unknown variables of τ_k and $\pi_{k,0}$ for $k = 0..7$. To be able to analytically solve the model I employ an iterative approach. I first solve the model based on the initial values for X_E, X_R, and f_7. Iteration $t + 1$, $t \leq 0$ is computed based on the outputs of iteration t and the computed values in equations (3.32) and (3.33). The iterations are repeated until the value difference between two successive X_R values is less than 0.1 up to a maximum of 6 iterations.

Then, I are able to calculate the PGF of waiting time for a UP$_k$ data frame. Waiting time of a data frame is duration of the time interval from the moment when the frame arrives to

the queue until the moment when its successful transmission begins. The PGF of waiting time for a UP$_k$ data frame, $\Omega_k(z)$, is calculated as follows:

$$
\Omega_k(z) = \begin{cases}
\frac{(1-\rho_k)(1-\mathcal{I}_k(z))(1-\Lambda_k[B_k(z)])}{E[\mathcal{I}_k(z)]\lambda_k[1-B_k(z)](\Lambda_k[B_k(z)]-z)} \cdot \left(\frac{eap^2 z}{2(eap+rap)} + 1 - \frac{eap^2}{2(eap+rap)}\right) \cdot \\
\Phi_k(z) \cdot (\theta z + 1 - \theta), & \text{if k=0..6} \\
\frac{(1-\rho_k)(1-\mathcal{I}_k(z))(1-\Lambda_k[B_k(z)])}{E[\mathcal{I}_k(z)]\lambda_k[1-B_k(z)](\Lambda_k[B_k(z)]-z)} \cdot \Phi_k(z) \cdot (\theta z + 1 - \theta), & \text{if k=7}
\end{cases}
$$

where $\theta = rts + 2sifs + cts$ if RTS/CTS mechanism is deployed and $\theta = 0$, otherwise. In the above formula, the first component represents the PGF of the waiting time of the UP$_k$ data frame until it reaches the top of the queue [97]. $\frac{eap^2 z}{2(eap+rap)} + 1 - \frac{eap^2}{2(eap+rap)}$ corresponds to the PGF of the waiting time from the moment when the data frame reaches to the top of the queue until the moment when its transmission backoff process begins. Meanwhile the node keeps its backoff counter locked because the current time is outside the access phase in which the node is allowed to transmit. $\Phi_k(z)$ is the PGF of the backoff duration of the data frame. Finally, $\theta z + 1 - \theta$ is PGF of the RTS/CTS transmission duration, if the collision avoidance mechanism is deployed.

By solving the set of sub-models for all UPs, I are able to compute the mean waiting time of a UP$_k$ data frame, $\omega_k = \frac{d}{dz}\Omega_k(z)\big|_{z=1}$, as follows:

$$
\omega_k = \begin{cases}
\frac{\lambda_k b_k^{(2)} - \lambda_k b_k}{2(1-\rho_k)} + \frac{E[\mathcal{I}_k(z)(\mathcal{I}_k(z)-1)]}{2E[\mathcal{I}_k(z)]} + \frac{eap^2}{2(eap+rap)} + \phi_k + \theta, & \text{if k=0..6} \\
\frac{\lambda_k b_k^{(2)} - \lambda_k b_k}{2(1-\rho_k)} + \frac{E[\mathcal{I}_k(z)(\mathcal{I}_k(z)-1)]}{2E[\mathcal{I}_k(z)]} + \phi_k + \theta, & \text{if k=7}
\end{cases} \tag{3.58}
$$

where $b_k^{(2)} = b_k + \frac{d^2}{dz^2}B_k(z)\big|_{z=1}$. Based on the mean waiting time of a UP$_k$ data frame I are able to calculate the mean response time of the frame which is said to be the most important performance measure for a queuing system [80]. The frame response time is defined as the time interval from its arrival time to the time when it leaves the system. The mean response time of a UP$_k$ data frame is computed as $\zeta_k = \omega_k + (l_k + sifs + ack)$.

3.3.2   Performance Evaluation

I used Maple 13 [82] for solving the analytical model to calculate the performance descriptors of the network. I validate the analytical results by a simulation model. The simulation model was developed using Opnet simulator [83]. The analytical and the simulation models are based on the same assumptions. The simulation model follows the CSMA mechanism of IEEE 802.15.6 as specified in the standard. The exogenous parameters in the experiments are set according to the standard. I set the differentiation parameters of $CW_{k,min}$ and $CW_{k,max}$ for all the nodes according to the standard (Table 3.1). The retry limit is set to $R = 7$ for all the UPs.

The wireless healthcare network which is used for performance evaluation of the IEEE 802.15.6 standard under non-saturation regime consists of a hub and 28 nodes. The nodes include ten channels for *Electroencephalogram (EEG)*, eight channels for *Electrocardiogram (ECG)*, one blood pressure sensor, one glucose monitoring node, one blood oxygen saturation monitoring sensor (pulse oximeter), four physical activity monitoring sensors, one channel for *Electromyogram (EMG)*, one body temperature sensor, and one respiration rate monitoring node. The WBAN is designed in a way to monitor the vital health information of the body. It is an example for investigating the performance of the standard and I do not accurately match a real WBAN, which might have different numbers of nodes or monitor different vital body signals.

I spread the nodes into 8 UPs as shown in Table 3.5. The table shows number of nodes (NN) in all the UPs, their traffic loads (TL) in packets/sec, payload size (PS) of each packet in bytes (B), sampling frequency rates (FR) in hertz (Hz), and sample sizes (SS) in bits (b) [98]. In this work, I assume that all the nodes in the same UP have equal traffic loads and

Table 3.5: Healthcare nodes are spread into 8 UPs (NN: number of nodes, TL: traffic load per packet, PS: payload size, FR: frequency rate, and SS: sample size)

UP	Node	NN	TL	PS	FR	SS
7	ECG	1	2 p/s	150 B	200 Hz	12 b
	EEG	1	2 p/s	150 B	200 Hz	12 b
6	ECG	2	2 p/s	150 B	200 Hz	12 b
5	EEG	1	2 p/s	150 B	200 Hz	12 b
	Blood Pressure	1	2 p/s	150 B	200 Hz	12 b
4	Glucose	1	1 p/s	50 B	50 Hz	16 b
	Oxygen Saturation	1	1 p/s	50 B	50 Hz	16 b
	Temperature	1	0.25 p/s	20 B	5 Hz	8 b
	Respiration Rate	1	0.25 p/s	20 B	5 Hz	8 b
3	Physical Activity	4	1 p/s	50 B	50 Hz	16 b
2	EMG	1	4 p/s	500 B	1 KHz	16 b
1	ECG	5	0.8 p/s	375 B	200 Hz	12 b
0	EEG	8	0.5 p/s	600 B	200 Hz	12 b

payload sizes. Based on this assumption, in our simulation and analytical models I set the temperature and respiration traffic loads to 1 p/s and the payload size of 50 B.

In all plots in this section, the lines with the line-styles *thin solid* (black), *dot* (red), *dash* (blue), *dash-dot* (green), *long-dash* (gold), *space-dot* (khaki), *space-dash* (magenta), and *thick solid* (coral) represent user priorities, 0, 1, 2, 3, 4, 5, 6, and 7, respectively.

The network performance is investigated in two cases. In the first case, the length of RAP1 varies from 0.2 sec to 0.8 sec while the length of EAP1 is set to 0.05 sec. In the second case, the length of EAP1 changes from 0.05 sec to 0.12 sec while the length of RAP1 is set to 0.3 sec. This section includes two sub-sections; First, I investigate the network performance where all the nodes deploy the RTS/CTS mechanism for accessing the medium. Second, I study the performance of the network for the case where the nodes do not deploy the RTS/CTS mechanism. In the latter case, the nodes immediately send their data frames upon having the backoff counter of zero.

3.3.2.1   Medium access using RTS/CTS mechanism

The simulation and analytical results for the mean waiting time of data frames for all user priorities where the RAP1 length varies while the length of EAP1 is constant are shown in Fig. 3.17. The results indicate that increasing the length of RAP1 where the EAP1 length is constant improves the frame delay for all UPs under non-saturation condition. An important reason is that having longer RAP periods compared to EAP periods decreases the collision probability after an EAP period. In addition, having short EAP-RAP periods increases the number of CSMA slots in which the medium cannot be accessed by the nodes because there is not enough time to complete a data frame transaction during the current access phase. The depicted results in Fig. 3.17 indicate reasonably good match between the simulation and analytical results for the case where all the nodes deploy RTS/CTS mechanism. I have plotted the simulation and analytical results in a single plot in Fig. 3.17 (c).

The difference between the simulation and analytical results takes place under unstable condition where the nodes are saturated. In unstable conditions the waiting times have large variations. In addition, the difference between the simulation and analytical results partly originates from the fact that in the analytical model the slot boundaries are synchronized for all the nodes. However, in the simulation model, during the frame transmissions under low to moderate loads slot boundaries might not be synchronized for all the nodes. This triggers higher collision probability in the simulation model since the collision may happen during two successive CSMA slots since the transmission begins.

In the second case, the length of EAP1 varies from 0.05 second to 0.12 second while the length of RAP1 is set to 0.3 second. I only show the analytical results of this case in
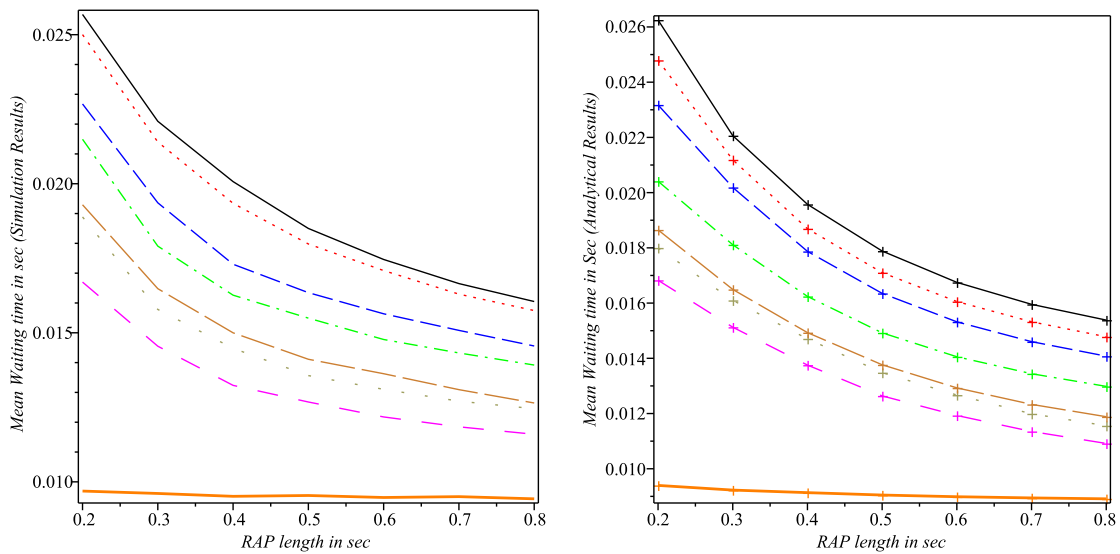
(a) Simulation Results

(b) Analytical Results
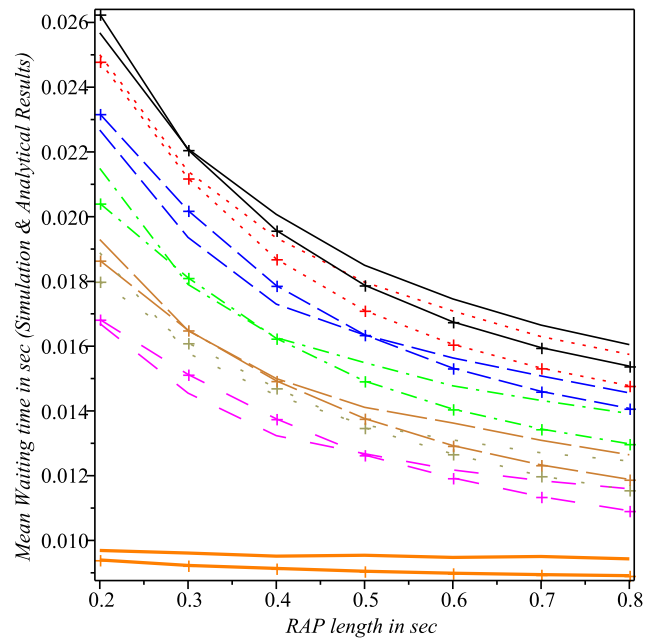
(c) Simulation and Analytical Results in a plot

Figure 3.17: Mean waiting time of data frames when length of RAP1 varies in case of deploying RTS/CTS mechanism (length of EAP1 = 0.05 sec)

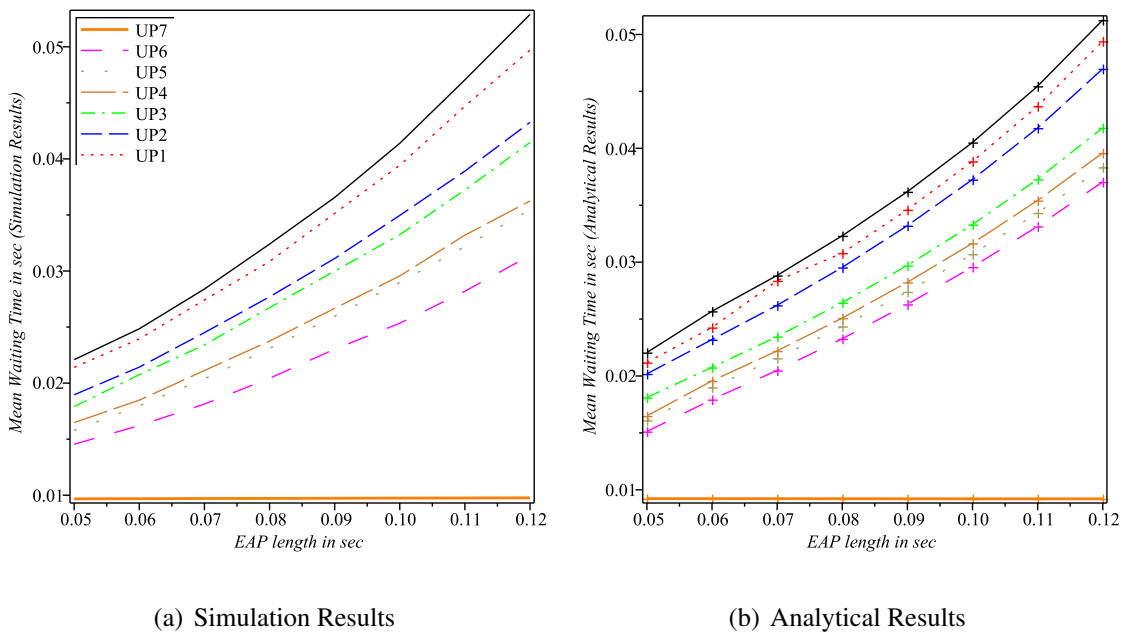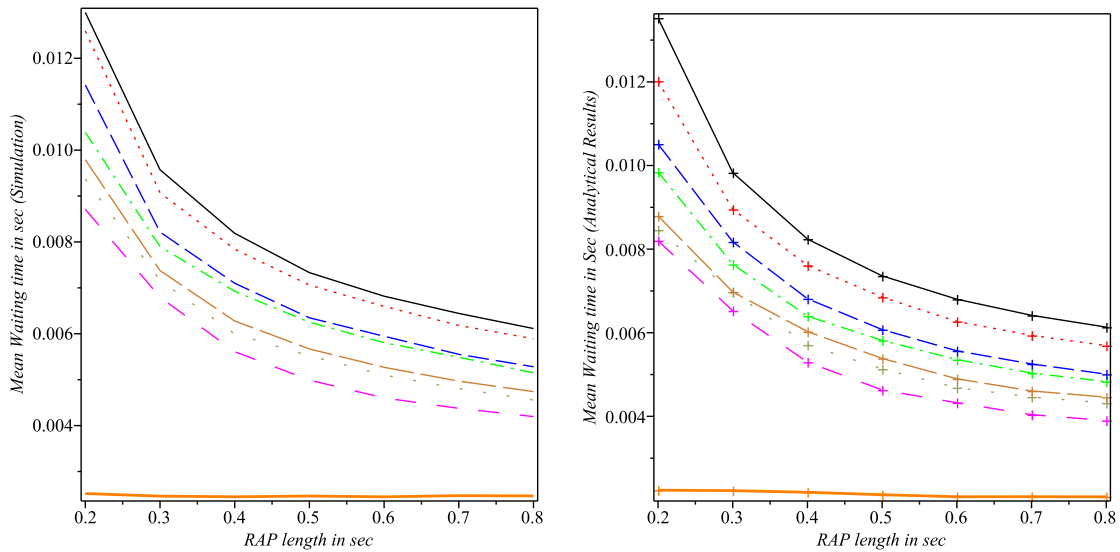(a) Simulation Results   (b) Analytical Results

Figure 3.18: Mean waiting time of data frames when length of EAP1 varies in case of deploying RTS/CTS mechanism (length of RAP1 = 0.3 sec)

Fig. 3.18. The simulation results match the analytical results reasonably good for this case too. The results show how the mean waiting time of data frames for all UPs increases when the length of EAP1 increases. The main reason is that having a long EAP period wastes the network resources during the exclusive access phases because the traffic load of the UP_7 nodes is low. However, during the RAP periods the traffic congestion increases because other nodes have shorter time periods for transmission. Therefore, adopting appropriate RAP and EAP periods according to the traffic loads of the UPs noticeably improves the performance of an IEEE 802.15.6-based WBAN.

The depicted results in Fig. 3.17 and Fig. 3.18 indicate reasonably good match between the simulation and analytical results for the case where all the nodes deploy RTS/CTS mechanism.

(a) Simulation Results

(b) Analytical Results
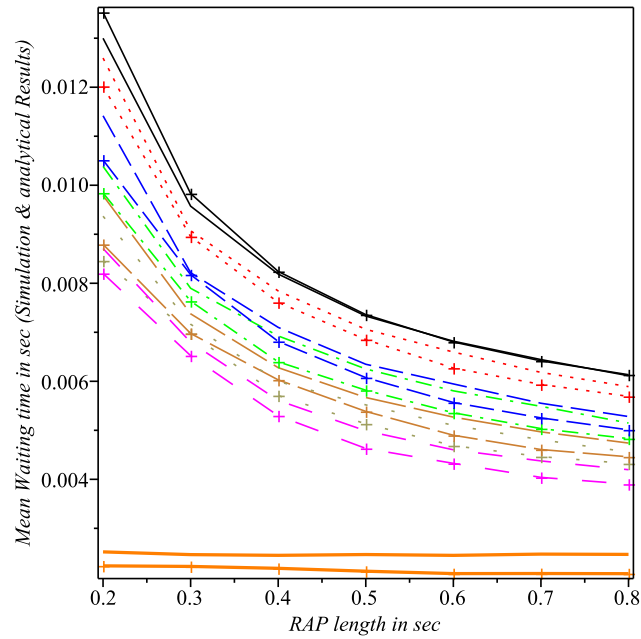
(c) Simulation and Analytical Results in a plot

Figure 3.19: Mean waiting time of data frames when length of RAP1 varies without deploying RTS/CTS mechanism (length of EAP1 = 0.05 sec)
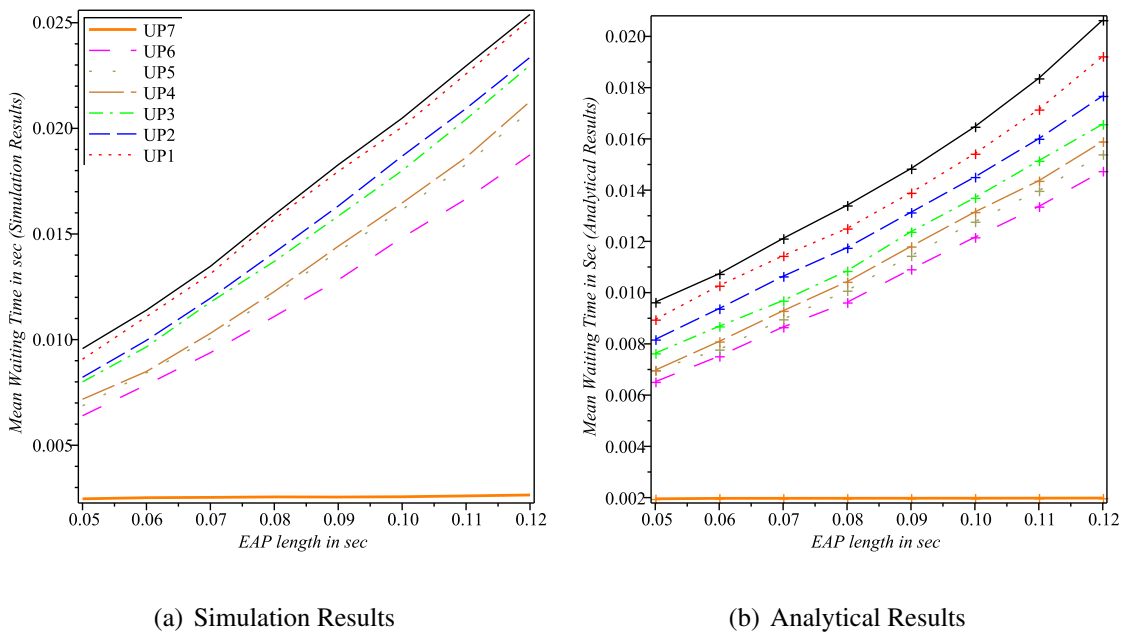
(a) Simulation Results

(b) Analytical Results

Figure 3.20: Mean waiting time of data frames when length of EAP1 varies without deploying RTS/CTS mechanism (length of RAP1 = 0.3 sec)

3.3.2.2 Medium access without deploying RTS/CTS mechanism

In this sub-section, I investigate how the network performance is affected if the nodes do not deploy the RTS/CTS mechanism, compared to the case where the RTS/CTS mechanism is used for accessing the medium. Fig. 3.19 depicts the simulation and analytical results for the case where the RAP1 length varies while the EAP1 length is constant. I have plotted the simulation and analytical results in a single plot in Fig. 3.19 (c) for comparison purposes. Comparing the graphs in Fig. 3.17 and Fig. 3.19 indicates that the performance of the WBAN is dramatically improved when the RTS/CTS mechanism is not deployed. Our study covers small to moderate data frame sizes having the maximum payload size of 600 B. Therefore, for a typical WBAN deploying the RTS/CTS mechanism is counterproductive resulting in deterioration of the network performance.

However, for an IEEE 802.15.6-based network with large frame sizes where either the collision probability or the frame error rate is high deploying the RTS/CTS mechanism improves the performance of the network. The performance is enhanced because the RTS/CTS transmission time is considerably smaller than the transmission time of the data frames. The data frame sizes in WBANs are not large enough to justify the deployment of the RTS/CTS mechanism. The mean waiting times of the data frames for all the UPs are noticeably smaller where the RTS/CTS mechanism is not deployed. Hence, the results indicate that deploying RTS/CTS mechanism is often inappropriate for healthcare systems.

In Fig. 3.20 only the analytical results for the mean waiting time of data frames where the length of EAP1 varies from 0.05 second to 0.12 second while the length of RAP1 is set to 0.3 second are shown. The simulation results are omitted due to lack of space though the simulation and analytical results have a good match. The results confirm that increasing the length of EAP1, under non-saturation condition, increases the mean waiting time of the data frames, specifically the data frames which do not have UP_7.

3.4   Summary of the Chapter

In the first part of the chapter, I evaluated the interaction of RAP1, EAP1, RAP2, EAP2, and contention-free access phases in a single-hop IEEE 802.15.6 CSMA/CA-based WBAN. For that purpose, I developed analytical and simulation models for investigating the network performance considering EAP1, RAP1, EAP2, RAP2, and type-I/II access phases under saturation condition and an error-prone channel. I studied the impact of the lengths of different contention-based access phases on the performance descriptors of all UPs. I came to the conclusion that having short EAP and RAP phases leads to inefficient

use of bandwidth. I showed that existence of EAP phases for a typical WBAN is unnecessary. Unless there are multiple different traffic types in the network, deploying EAP2 and RAP2 access phases is not required. I also showed that the IEEE 802.15.6 CSMA/CA mechanism utilizes the medium poorly under high traffic loads. Our results show that traffic controlling and admission control mechanisms are necessary to keep the network in linear operation regime.

In the second part of the chapter, I developed an analytical model for performance evaluation of IEEE 802.15.6-based WBANs under non-saturation regime. The developed model covers the cases of having and not having the RTS/CTS mechanism deployed. I validated the analytical results by our Opnet-based simulation model. An important finding of this work is that for an unsaturated WBAN with a small to moderate data frame sizes deploying the RTS/CTS mechanism degrades the network performance compared to the case where the nodes immediately transmit their data frames upon having the backoff counter of zero. In addition, the results indicate that setting the EAP and RAP lengths according to the traffic loads of the UPs noticeably improves the performance of the network. It was shown that having short EAP-RAP periods wastes the network resources since number of inaccessible CSMA slots during RAP1 increases. It also increases the collision probability after an EAP1 period. The performed research in this chapter is published in [95; 99; 100; 101; 102].

Publications

[95] S. Rashwand and J. Misic and H. Khazaei. IEEE 802.15.6 Under Saturation: Some Problems To Be Expected. *Journal of Communications and Networks* , **13**(2):142-149, 2011.

[99] S. Rashwand and J. Misic and H. Khazaei. Performance Analysis of IEEE 802.15.6 Under Saturation Condition and Error-Prone Channel. *in Proceedings of IEEE Wireless Communications and Networking Conference* (WCNC'11), vol. 1, pp. 475-480, March 2011.

[100] S. Rashwand and J. Misic. Performance Evaluation of IEEE 802.15.6 Under Non-Saturation Condition. *in Proceedings of IEEE Global Telecommunications Conference* (Globecom11), vol. 1, pp. 1-6, December 2011.

[101] J. Misic and S. Rashwand. Effects of Access Phases Lengths on Performance of IEEE 802.15.6 CSMA/CA Mechanism. *Journal of Computer Networks (COMNET), To appear,2012*.

[102] J. Misic and S. Rashwand. Frame Delay Analysis of CSMA mechanism of IEEE 802.15.6. *IEEE Transactions on Wireless Communications, Under Revision,2012*.

Chapter 4

MAC Performance Modeling of IEEE 802.15.6-based WBANs over Rician-faded channels

The IEEE 802.15.6 standard as the communication standard for WBANs has been optimized for low power devices and operation on, in or around the human body [13]. Since the signal transmission in WBANs takes place around or in the human body, the channel fading significantly affects the error performance of the networks. In this chapter, I investigate the impacts of BER, which is caused by the channel fading, on MAC level performance of IEEE 802.15.6 CSMA-based WBANs. I evaluate MAC performance descriptors of the networks based on the Signal to Noise Ratio (SNR) values for different UPs. I assume Rician-faded channels between the nodes and the hub in the network with unequal Rician factors. I also assume that the WBAN nodes deploy the QPSK modulation scheme to achieve the highest data frame transmission rate in ISM bands. The BER values for differ-

ent nodes are calculated according to the channel quality, diversity level, and SNR values. The obtained BER values for different UPs are used for calculating the data frame error rates of the UPs in the network. Thereafter, I calculate the data frame response times for all UPs are computed.

In addition, because the channel fading in WBANs is quite strong and significantly affects the quality of the received signal, diversity is an important mechanism to improve the error performance of the networks [103]. In this chapter, I also investigate the effects of the diversity level on MAC performance measures of WBANs. To our best knowledge, there is not currently any work in the literature to investigate the effects of fading channels on MAC performance of the IEEE 802.15.6-based WBANs.

The remainder of this chapter is organized as follows: Section 4.1 addresses the related work. In Section 4.2 the analytical model is described. Section 4.3 presents the MAC performance of an IEEE 802.15.6-based WBAN over Rician-faded channels through several experiments. Finally, Section 4.4 concludes the chapter summarizing the findings of the study.

4.1   Channel Modeling for WBANs

In this section, I review the research studies on the channel modeling for WBANs. According to the recent studies, the propagating wave is mostly diffracted around the human body rather than passing through it. Hence, the path loss in WBANs is very high specially when the transmitter and the receiver are shadowed by a part of the body [104]. In the literature, there is a limited research to model the fading channels for WBANs.

In [104; 105] it is shown that Lognormal and Nakagami-m distributions are appropriate

for modeling the WBAN fading channels, respectively. However, it is more accepted that Rician distribution is the best suited scheme for modeling the small-scale fading of WBAN channels [106; 107; 108]. There are other studies indicating that Rician distribution is the best option for WBAN channel modeling [109; 110]. I employ the results in [106] for the fading channel modelling.

To analyse the error performance of a wireless system, for each combination of communication type (modulation/detection) and the channel fading the average BER of the system is calculated. The statistical calculation of BER at the physical layer is utilized to compute the Packet Error Rate (PER) at the higher layers.

There is a large body of work in the literature which models the error performance of wireless channels. However, a few studies consider QPSK as the modulation scheme of the wireless systems. The authors in [111; 112] developed an expression for computing BER of DQPSK over a slow Rician fading channel. By deploying the alternate representations of classic functions, such as Gaussian and Marcum Q-functions, the authors in [113] developed a unified framework for evaluating the error-probability performance of coherent, differentially coherent, and noncoherent communications over generalized fading channels. The average BER is analysed for M-PSK modulation over Rician fading channels considering the linear diversity in [114]. The authors in [115] derived closed-form expressions for calculating the average BER for a class of modulation schemes over Rician fading channels.

The authors in [116] computed BER of linearly modulated signals, including DBPSK, DQPSK, and D8PSK, in Rician, Rayleigh, and Nakagami-m fading channels for coherent receivers with L-th order MRC (Maximal Ratio Combining) diversity. I use the expression

for BER based on SNR derived in [116] to investigate the error performance of the WBAN

channels. The BER of QPSK in Rician fading channels is given as follows [116]:

$$BER = G(0, \frac{\pi}{2}, \overline{\gamma_b}, L, K_R, 1) \tag{4.1}$$

where $\overline{\gamma_b} = \frac{\overline{\gamma_c}}{2}, \overline{\gamma_c} = \frac{1}{2N_0}$ represents the average SNR per channel, N_0 is the power spectral

density of the complex Gaussian random processes for the channels, and K_R is the Rician

factor, and I have

$$G(\theta_1, \theta_2, \overline{\gamma}, L, K_R, d) =$$
$$\frac{e^{-LK_R}}{\pi} \int_{\theta_1}^{\theta_2} \frac{exp(\frac{LK_R}{1+(\overline{\gamma}d^2/(K_R+1)sin^2\theta)})}{[1 + (\overline{\gamma}d^2/(K_R + 1)sin^2\theta)]^L} \, d\theta \tag{4.2}$$

4.2   Analytical Model

In this section, I extend the developed analytical model in Chapter 3, Section 3.3 to

investigate the error performance of an IEEE 802.15.6 CSMA-based WBAN. To avoiding

repeating formulae I only present the model components which are different than Chapter 3,

Section 3.3. The deployed parameters in the model are defined in Table 4.1. I assume that a

UP_k node has a single UP_k queue. The network is considered to be single hop operating in

2.4 GHz ISM band with uplink traffic only. The lengths of EAP1 and RAP1 are indicated

by eap and rap in slots, respectively.

The control frames and headers are transmitted at 91.9 kbps while the payload of the

data frames is transmitted at 971.4 kbps. The size of the data frames for a node of UP_k is

denoted by l_k in slots and $l_{k,b}$ in bits and ack and ack_b indicate the sizes of an ACK frame

Table 4.1: Important Parameters

Parameter	Description
k	Index of UP, $k = 0..7$
n_k	Number of nodes of UP_k
R	Maximum retransmission limit
σ_k	Probability that neither a UP_k data frame nor its ACK is corrupted by noise
λ_k	Data frame arrival probability during a CSMA slot for a node of UP_k
τ_k	Access probability to medium by a UP_k node
g_k	Probability that medium is idle during backoff countdown for a UP_k node
f_k	Probability that medium remains idle in case of medium access for a UP_k node
$L_{k,s}$	Mean successful data frame transmission time for a UP_k node in slots
$L_{k,so}$	Mean successful data frame transmission time of other nodes for a given UP_k node in slots
$L_{k,c}$	Mean unsuccessful data frame transmission time for a UP_k node in slots
$L_{k,co}$	Mean unsuccessful data frame transmission time of other nodes for a given UP_k node in slots
β_k	Probability that a data frame arrives to the queue during the time interval between two successive Markov points
p_k	Probability that indicates from the current CSMA slot to the end of the RAP1 period for a UP_k node there is not enough time to complete a data frame transaction
$\pi_{k,0}$	Probability of an empty queue after serving a data frame for a UP_k node
$p_{k,Idle}$	Probability of being in the idle state for a UP_k node in a CSMA slot
$p_{so,k}$	Probability of a successful transmission by the other nodes for a given UP_k node
$p_{co,k}$	Probability of an unsuccessful transmission by the other nodes for a given UP_k node
$\Phi_k(z)$	PGF for the duration of backoff process for a UP_k node
$\mathcal{I}_k(z)$	PGF of the idle period duration in slots
$\mathcal{B}_{P,k,j}(z)$	PGF of the locked backoff counter because there is not enough time to complete a frame transaction
$\Theta_{k,j}(z)$	PGF of mean duration of locked backoff counter due to a transmission on the medium, either successful or unsuccessful
ζ_k	Mean response time of a UP_k data frame

in slots and in bits, respectively. I assume a Rician fading channel having BER as specified in eq. (5.1). Hence, data frame error rate is equal to $\sigma_k = (1 - BER)^{l_{k,b}+ack_b}$.
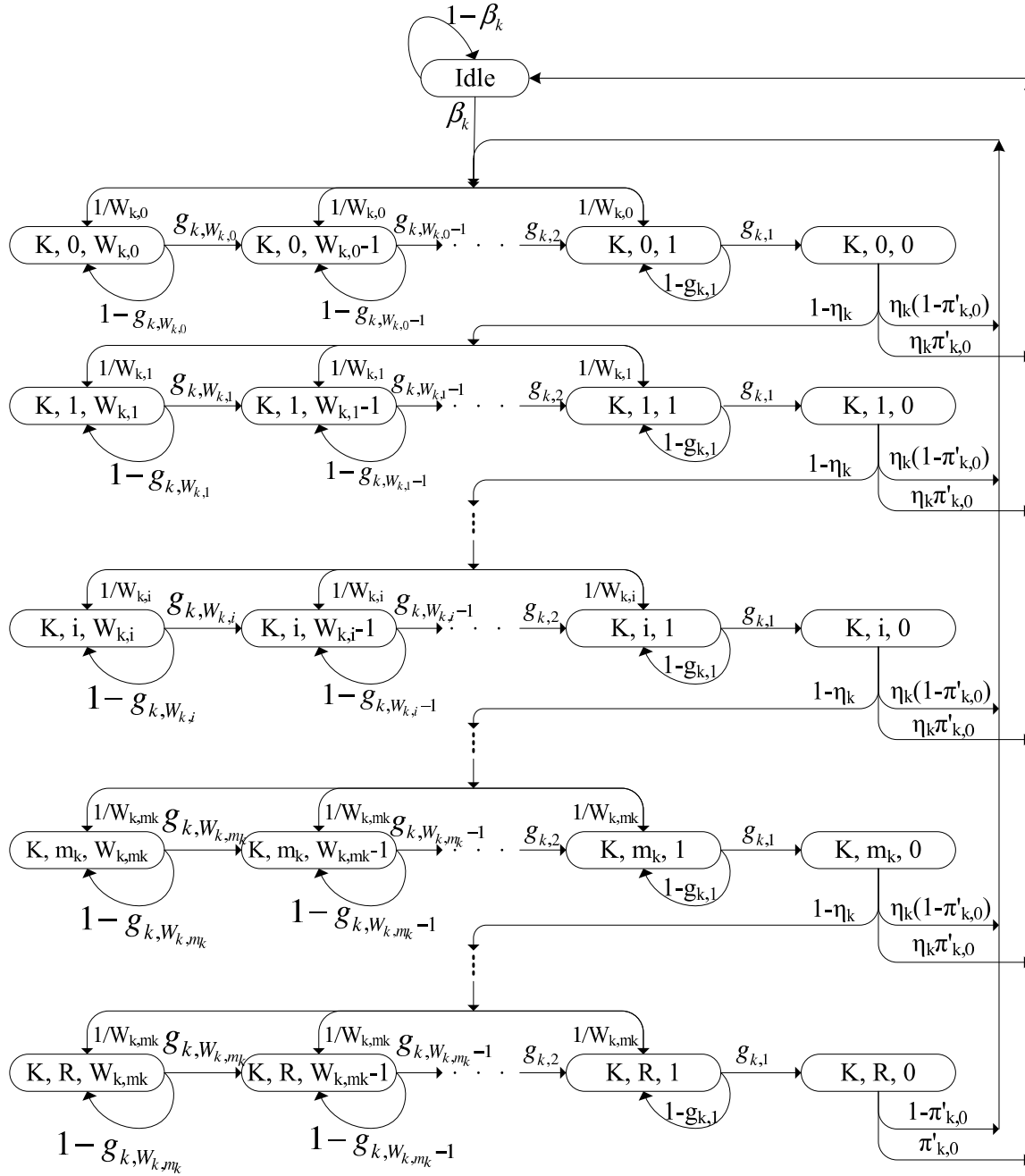
Figure 4.1: 3-dimensional DTMC for UP$_k$

The analytical model is composed of three inter-related sub-models; Markov chain, backoff duration, and queuing models.

4.2.1   Markov Chain Model

In the Markov chain model eight dependent 3-dimensional DTMCs for the eight UPs are introduced to formulate the medium access probabilities of the UPs (Fig. 4.1). The depicted DTMCs in Fig. 4.1 and Fig. 3.15 are identical. I are showing that here to improve the model comprehension in this chapter.

Since the erroneous transmissions affect the mean numbers of considered CSMA slots in EAPs and RAPs in the DTMCs, the values of X_E and X_R are changed as follows:

$$X_R = \frac{rap - L_{7,s}}{f + \sum_{t=0}^{7} n_t \tau_t f_t \sigma_t L_{t,s} + (1 - f - \sum_{t=0}^{7} n_t \tau_t f_t \sigma_t) L_{t,c}}$$

$$X_E = \frac{eap}{\chi + n_7 \tau_7 \psi \sigma_7 L_{7,s} + (1 - \chi - n_7 \tau_7 \psi \sigma_7) L_{7,c}} \qquad (4.3)$$

By solving the DTMCs I obtain 8 equations for $k = 0..7$ as follows:

$$1 = p_{k,Idle} + Y_k \sum_{i=0}^{R} (1 - f_k \sigma_k)^i \Big(1 + \sum_{j=1}^{W_{k,i}} \frac{W_{k,i} - j + 1}{W_{k,i} g_{k,j}} \Big) \qquad (4.4)$$

where Y_k, $k = 0..7$, is the input probability to the zero-th backoff phase which is computed as follows:

$$Y_k = \frac{\tau_k f_k \sigma_k (1 - \pi_{k,0}) + p_{k,Idle} \beta_k}{1 - (1 - f_k \sigma_k)^{R+1} (1 - \pi_{k,0})}, \quad k = 0..7 \qquad (4.5)$$

$p_{k,Idle}$ is calculated as follows:

$$p_{k,Idle} = \frac{\tau_k f_k \sigma_k \pi'_{k,0}}{\beta_k (1 - (1 - f_k \sigma_k)^{R+1})}, \quad k = 0..7 \qquad (4.6)$$

Hence, the Markov chain model results in a set of eight equations while there are 16 unknown variables of τ_k, $k = 0..7$, and $\pi_{k,0}$, $k = 0..7$.

4.2.2   Backoff Duration Model

The average durations of every backoff phase and the total backoff period before successfully accessing the medium or dropping the data frame using PGFs are calculated in this section. In the extended model, the 4-dimensional DTMCs are remained unchanged compared to the presented model in [100].

$p_{so,k}$ and $p_{co,k}$ are computed as follows:

$$
\begin{aligned}
p_{so,k} &= \sum_{i=0}^{7} \frac{n_i \tau_i f_k \sigma_k}{1 - \tau_i} - \frac{\tau_k f_k \sigma_k}{1 - \tau_k} \\
p_{co,k} &= 1 - f_k - p_{so,k}
\end{aligned}
\tag{4.7}
$$

The PGF of the time interval between the moment when the backoff counter of a node of UP_k becomes equal to j and the moment when the backoff counter becomes equal to $j - 1$ at the i-th backoff phase is equal to:

$$
\Phi_{k,i,j}(z) = p_k \mathcal{B}_{P,k,j}(z) + (1 - p_k)(f_k z + \Theta_{k,j}(z))
\tag{4.8}
$$

Due to the fading channel the PGF of i-th backoff phase duration is computed as follows:

$$
\begin{aligned}
\Phi_{k,i}(z) &= \sum_{j=1}^{W_{k,i}} \prod_{t=1}^{j} \Phi_{k,i,t}(z)\Big(f_k \sigma_k (L_{k,s} p_k z^{L_k} + 1 - L_{k,s} p_k) \\
&\quad + (1 - f_k \sigma_k)(L_{k,c} p_k z^{L_k} + 1 - L_{k,c} p_k)\Big)/W_{k,i}
\end{aligned}
\tag{4.9}
$$

The backoff process duration PGF for a UP_k node is given by

$$
\begin{aligned}
\Phi_k(z) &= \sum_{i=0}^{m_k}(\prod_{u=0}^{i} \Phi_{k,u}(z))(1 - f_k \sigma_k)^i (z^{L_{k,c}})^i f_k \sigma_k + \\
&\quad \sum_{i=m_k+1}^{R}(\prod_{u=0}^{m_k} \Phi_{k,u}(z))\Phi_{k,m_k}^{i-m_k}(z)(1 - f_k \sigma_k)^i \cdot \\
&\quad (z^{L_{k,c}})^i f_k \sigma_k + (\prod_{u=0}^{m_k} \Phi_{k,u}(z))\Phi_{k,m_k}^{R-m_k}(z) \cdot \\
&\quad (1 - f_k \sigma_k)^{R+1}(z^{L_{k,c}})^{R+1}
\end{aligned}
\tag{4.10}
$$

4.2.3   Queuing Model

The queueing model is developed to calculate accurate durations of idle periods and access probabilities of all UPs. The value of $\pi_{k,0}$ is calculated as follows:

$$\pi_{k,0} = \frac{1 - \rho_k}{\lambda_k E[\mathcal{I}_k(z)]}, \ k = 0..7 \tag{4.11}$$

where $\rho_k = \lambda_k b_k$ is the traffic intensity of a UP_k node and $b_k = B'_k(1)$ is the mean service time of a UP_k data frame. The PGF of service time (in slots) of a data frame for a UP_k node is computed as $B_k(z) = \Phi_k(z)St_k(z)$.

The 16 unknown variables of τ_k and $\pi_{k,0}$ for $k = 0..7$ are calculated by the set of 16 equations of (4.4) and (4.11).

I are now able to calculate the mean response time of a UP_k data frame for an IEEE 802.15.6 CSMA-based WBAN in a fading channel. The frame response time is defined as the time interval from its arrival time to the time when it leaves the system, which is obtained as follows:

$$
\begin{aligned}
\zeta_k &= \frac{\lambda_k b_k^{(2)} - \lambda_k b_k}{2(1 - \rho_k)} + \frac{E[\mathcal{I}_k(z)(\mathcal{I}_k(z) - 1)]}{2E[\mathcal{I}_k(z)]} + \\
&\quad \theta_k + \phi_k + (l_k + sifs + ack)
\end{aligned}
\tag{4.12}
$$

where $\theta_k = \frac{eap^2}{2(eap+rap)}, \ k = 0..6$ and $\theta_7 = 0$.

4.3   Performance Evaluation

In this section, I study the impacts of fading channel on MAC performance of an IEEE 802.15.6 CSMA-based WBAN under non-saturation regime. At first, I validate the analytical results by simulation results. Then, I investigate the performance of the network
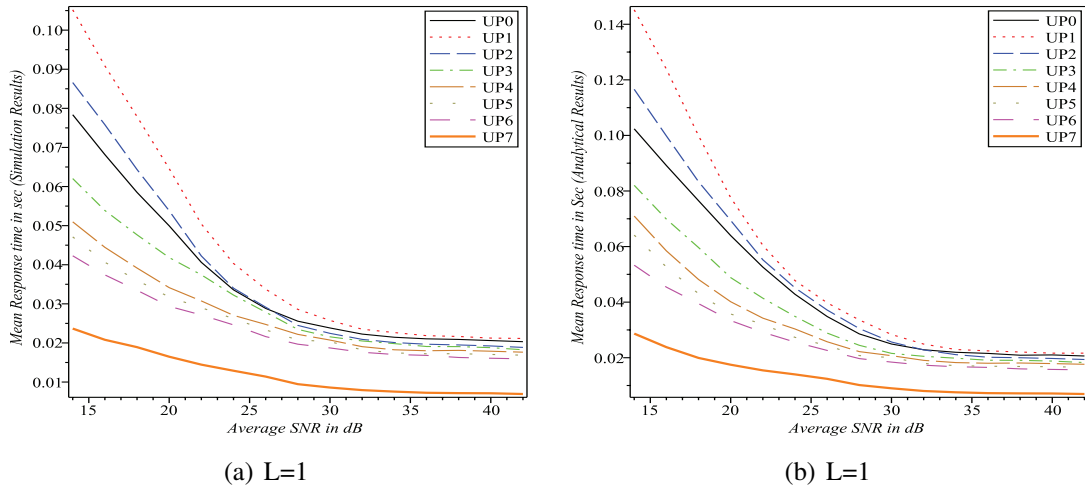
(a) L=1   (b) L=1

Figure 4.2:   Mean response time of data frames; rap=0.5s eap=0.1s, equal
frame sizes (150B), $(K_0, K_1, K_2, K_3, K_4, K_5, K_6, K_7)$ = $(4, 1.5, 3, 3, 2.5, 1.5, 1.5, 4)$,
$(\lambda_0, \lambda_1, \lambda_2, \lambda_3, \lambda_4, \lambda_5, \lambda_6, \lambda_7) = (2, 2, 20/3, 2/3, 1/3, 2, 2, 2)$packets/sec
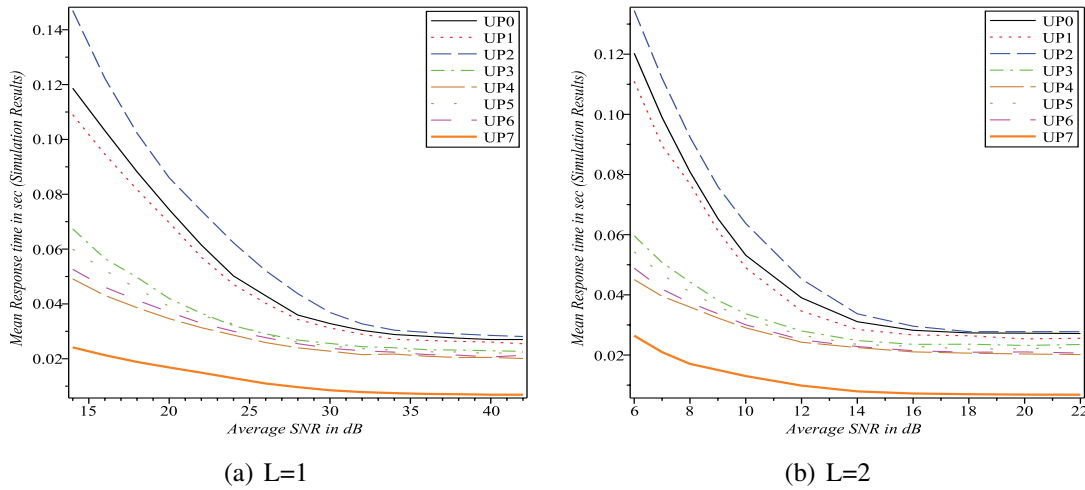

(a) L=1   (b) L=2

Figure 4.3:   Mean response time of data frames; rap=0.3s eap=0.1s, differ-
ent frame sizes $(l_0, l_1, l_2, l_3, l_4, l_5, l_6, l_7)$ = $(300, 150, 500, 50, 50, 150, 150, 150)$B,
$(K_0, K_1, K_2, K_3, K_4, K_5, K_6, K_7)$ = $(4, 1.5, 3, 3, 2.5, 1.5, 1.5, 4)$,
$(\lambda_0, \lambda_1, \lambda_2, \lambda_3, \lambda_4, \lambda_5, \lambda_6, \lambda_7) = (1, 2, 2, 2, 1, 2, 2, 2)$ packets/sec

under different scenarios by presenting the simulation results only due to lack of space. I

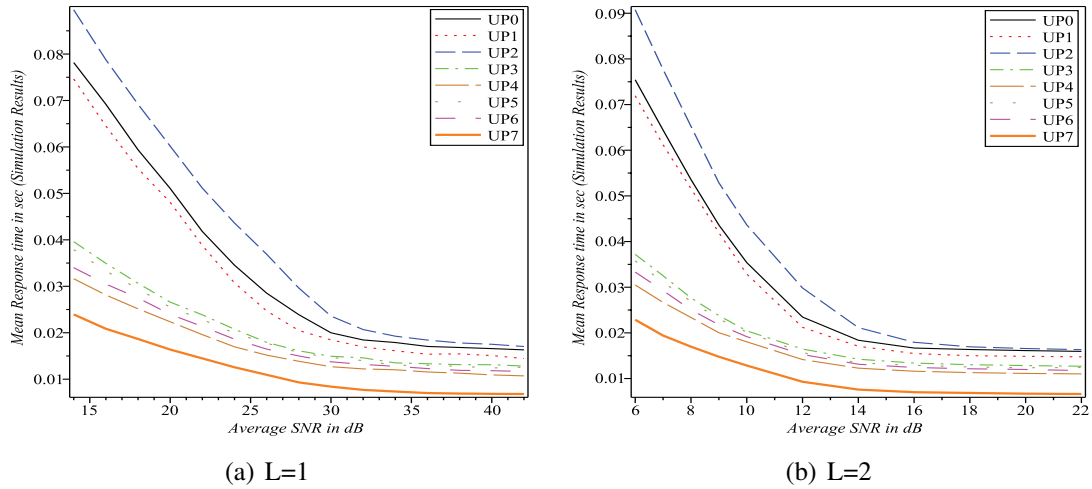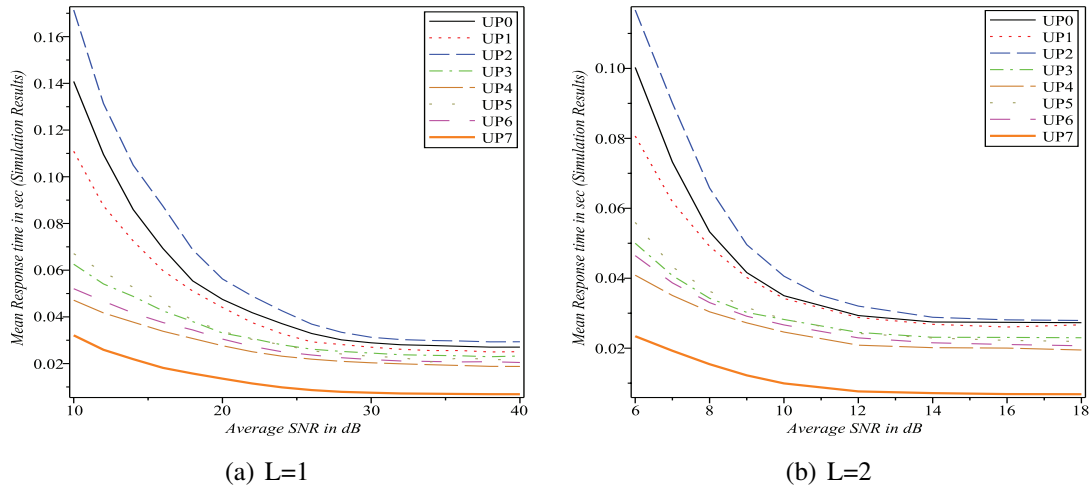develop two performance measures of mean response time of data frames and successful

(a) L=1 (b) L=2

Figure 4.4: Mean response time of data frames; rap=1s eap=0.1s, different frame sizes $(l_0, l_1, l_2, l_3, l_4, l_5, l_6, l_7)$ = $(300, 150, 500, 50, 50, 150, 150, 150)$B, $(K_0, K_1, K_2, K_3, K_4, K_5, K_6, K_7)$ = $(4, 1.5, 3, 3, 2.5, 1.5, 1.5, 4)$, $(\lambda_0, \lambda_1, \lambda_2, \lambda_3, \lambda_4, \lambda_5, \lambda_6, \lambda_7) = (1, 2, 2, 2, 1, 2, 2, 2)$packets/sec

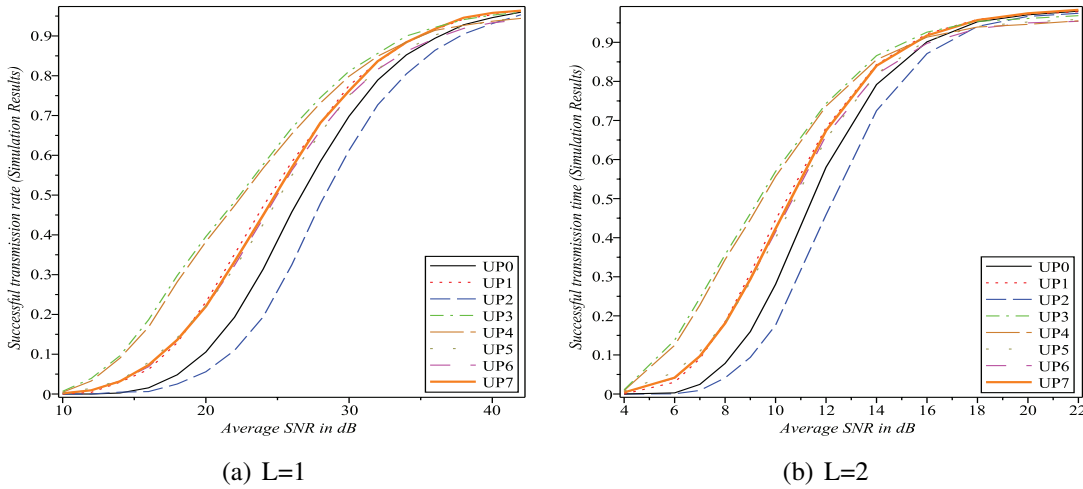(a) L=1 (b) L=2

Figure 4.5: Mean response time of data frames; rap=0.3s eap=0.1s, different frame sizes $(l_0, l_1, l_2, l_3, l_4, l_5, l_6, l_7)$ = $(300, 150, 500, 50, 50, 150, 150, 150)$B, $(K_0, K_1, K_2, K_3, K_4, K_5, K_6, K_7)$ = $(2.2, 4.9, 4.9, 4.9, 4.9, 4.9, 2.2, 4.9)$, $(\lambda_0, \lambda_1, \lambda_2, \lambda_3, \lambda_4, \lambda_5, \lambda_6, \lambda_7) = (1, 2, 2, 2, 1, 2, 2, 2)$packets/sec

(a) L=1   (b) L=2

Figure 4.6: Successful transmission rate; rap=1s eap=0.1s, different frame sizes $(l_0, l_1, l_2, l_3, l_4, l_5, l_6, l_7) = (300, 150, 500, 50, 50, 150, 150, 150)$B, $(K_0, K_1, K_2, K_3, K_4, K_5, K_6, K_7) = (4, 1.5, 3, 3, 2.5, 1.5, 1.5, 4)$, $(\lambda_0, \lambda_1, \lambda_2, \lambda_3, \lambda_4, \lambda_5, \lambda_6, \lambda_7) = (1, 2, 2, 2, 1, 2, 2, 2)$packets/sec

transmission rate of the UPs. I use Maple 13 [82] for solving the analytical model while Opnet simulator [83] is used for simulation modeling. Analytical and simulation models closely follow assumptions and definitions from the IEEE 802.15.6 standard. I set the differentiation parameters of ($CW_{k,min}$, $CW_{k,max}$) for all the UPs according to the standard {(16,64), (16,32), (8,32), (8,16), (4,16), (4,8), (2,8), (1,4) for UP$_0$, UP$_1$, UP$_2$, UP$_3$, UP$_4$, UP$_5$, UP$_6$, UP$_7$, respectively}. The retry limit is set to $R = 7$ for all the UPs.

The wireless healthcare network in this work consists of a hub and 20 nodes of $n_0 = 4$ (EEG - 300B/s per node), $n_1 = 2$ (ECG - 300B/s per node), $n_2 = 2$ (EMG - 1000B/s per node), $n_3 = 2$ (physical activity - 100B/s per node), $n_4 = 4$ (glucose, oxygen saturation, temperature, respiratory - 50B/s per node), $n_5 = 2$ (ECG, blood pressure - 300B/s per node), $n_6 = 2$ (EEG - 300B/s per node), $n_7 = 2$ (ECG - 300B/s per node). I follow two different scenarios for investigating the error performance of the network. In the first

scenario, I assume that the data frame sizes of all UPs are equal to 150B. Through this scenario I evaluate the impacts of different Rician factors of channels between nodes and the hub on performance of the network by varying the SNR values. In the second scenario different UPs may have different channel qualities (different Rician factors) and different frame sizes. The data frame sizes of different UPs are set based on the data rate and the data frame delay sensitivity of the UPs.

In all plots in this section, the lines with the line-styles *thin solid* (black), *dot* (red), *dash* (blue), *dash-dot* (green), *long-dash* (gold), *space-dot* (khaki), *space-dash* (magenta), and *thick solid* (coral) represent user priorities, 0, 1, 2, 3, 4, 5, 6, and 7, respectively.

The mean response times of the UPs for the first scenario are depicted in Fig. 4.2. The Rician factors for the channels between the hub and the nodes of UP_k, $k = 0..7$ are set to 4, 1.5, 3, 3, 2.5, 1.5, 1.5, and 4, respectively. The arrivals rates of the nodes are set to 2, 2, 20/3, 2/3, 1/3, 2, 2, and 2 packets/sec for UP_k, $k = 0..7$, respectively. In addition, the lengths of RAP1 and EAP1 are set to $rap1 = 0.5s$ and $eap1 = 0.1s$. Fig. 4.2(a) shows the simulation results when the diversity order is set to 1 while Fig. 4.2(b) depicts the analytical results in case of diversity order of 1. The results indicate that the channel quality strongly affects the response time of data frames since though the UP_1 nodes have higher priority than UP_0 nodes the data frames of former nodes obtain longer response time. As Fig. 4.2 indicates the simulation and the analytical results acceptably match.

In the second scenario, the data frame sizes of different UPs are set to 300B, 150B, 500B, 50B, 50B, 150B, 150B, and 150B for $\text{UP}k$, $k = 0..7$. I study the error performance of the WBAN through 3 different experiments. In the first two experiments the Rician factors are set as $K_0 = 1.5, K_1 = 4, K_2 = 3, K_3 = 3, K_4 = 2.5, K_5 = 1.5, K_6 =$

1.5, $K_7 = 4$. The only difference between the first and the second experiments is the lengths of RAP1, which are respectively set to $rap = 0.3s$ and $rap = 1s$ while the EAP1 length is equal to $eap = 0.1s$. The arrival rates of the nodes for both experiments are set to $\lambda_0 = 1p/s, \lambda_1 = 2p/s, \lambda_2 = 2p/s, \lambda_3 = 2p/s, \lambda_4 = 1p/s, \lambda_5 = 2p/s, \lambda_6 = 2p/s, \lambda_7 = 2p/s$. The results for the first experiment are shown in Fig. 4.3 for the cases where the diversity order is set to L=1 and L=2. Fig. 4.6 depicts the mean response times of data frames for all UPs for the second experiment where the diversity order is equal to 1 and 2. Comparing the results of the experiments show that increasing the ratio of RAP1 length and EAP1 length generally improves the performance of all UPs in the WBAN since the channel is more efficiently utilized. The third experiment belongs to the case where the Rician factors are changed compared to the all other experiments in this work. I set the Rician factors in this experiment as $K_0 = 2.2, K_1 = 4.9, K_2 = 4.9, K_3 = 4.9, K_4 = 4.9, K_5 = 4.9, K_6 = 2.2, K_7 = 4.9$. The data frame sizes are set to the same values of the first two experiments in this scenario. Arrival rates of this experiment are also kept unchanged. The length of RAP1 and EAP1 are set to $rap = 0.3s$ and $eap = 0.1s$, respectively. The main finding of the second scenario (all three experiments) is that the data frame size is the most effective parameter on error performance of an IEEE 802.15.6 CSMA-based WBAN. In all three experiments the UP_2 nodes have the largest data frame response times since they have the largest frame size (500B).

Fig. 4.6 depicts the successful transmission rate of all UPs in the WBAN where $rap = 1s, eap = 0.1s, K_0 = 1.5, K_1 = 4, K_2 = 3, K_3 = 3, K_4 = 2.5, K_5 = 1.5, K_6 = 1.5, K_7 = 4$, and $\lambda_0 = 1p/s, \lambda_1 = 2p/s, \lambda_2 = 2p/s, \lambda_3 = 2p/s, \lambda_4 = 1p/s, \lambda_5 = 2p/s, \lambda_6 = 2p/s, \lambda_7 = 2p/s$. The results indicate that the data frame size causes the largest

successful transmission rate degradation. However, under non-saturation condition, the Channel Rician factor is not as effective as the data frame size on successful transmission rate of the UPs. Though the Rician factors for UPs of 1, 3, 6, and 7 are different (4, 3, 1.5, and 4, respectively) they almost achieve equal successful transmission rates. The UP_2 and UP_0 nodes obtain the lowest successful transmission rates due to their large data frame sizes.

According to the results of this section, I can set the transmission powers of the nodes having different UPs to the lowest values to fulfil the maximum error tolerance of the nodes. The transmission powers should be chosen based on the channel quality and data frame sizes, as the most effective parameters on the error performance of the WBANs. Appropriate transmission powers and study of the error performance of WBAN are important and necessary since different nodes have different performance due to their transmission medium quality, which is caused by their location on or in the body.

4.4 Summary of the Chapter

In this Chapter, I studied the impacts of channel quality, data frame size, diversity order, data frame arrival rate, access phase lengths, and UPs on error performance of an IEEE 802.15.6 CSMA-based WBAN. I showed how varying SNR values for different scenarios affects the MAC performance descriptors of the network. The results indicate that increasing the diversity order and transmission power generally improves the MAC performance as well. I found that the data frame sizes and the channel quality between nods and the hub are the most effective parameters on the WBAN error performance. The performed research in this chapter is published in [117; 118].

Publications

[117] S. Rashwand and J. Misic and V. B. Misic. MAC Performance Modeling of IEEE 802.15.6-based WBANs Over Rician-faded Channels. *in Proceedings of IEEE International Conference on Communications* (ICC11), vol. 1, pp. 1-6, June 2012.

[118] S. Rashwand and J. Misic. IEEE Survey on Error Modelling of WBANs . *Under Preparation*.

Chapter 5

Bridging IEEE 802.15.6-based WBANs and IEEE 802.11e EDCA-based WLAN for Wireless Healthcare Networks

The medical data collected by the hub in the WBAN might be partly processed, including data aggregation, compression, encryption, etc. The processed data needs to be transmitted to a destination out of the WBAN. The destination could be a medical server to store and maintain all the medical records. The data is further processed by the server to extract the vital health information.

In order to provide an unobtrusive healthcare system for the patients the WBAN hub must communicate with an external source by a wireless connection. WLAN can be employed for transferring the data between a WBAN hub and the medical information system. Reliability, high transmission rate, and cost-effectiveness are a few features of the WLANs which make them appropriate to be used as a building block of the healthcare information system.

The main focus in this chapter is to investigate the performance of interconnection of patient's WBAN and the (e.g., hospital room or ward) WLAN. WBANs must support the combination of reliability, Quality of Service (QoS), low power, high data rate and non-
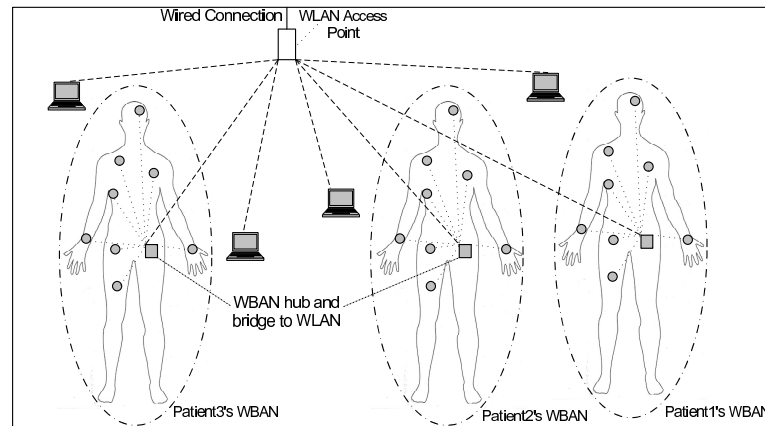
Figure 5.1: Networking structure of two hop healthcare wireless network

interference to address the breadth of WBAN applications. I adopt the IEEE 802.15.6 standard for the patient's body network (WBAN) [13]. Since IEEE 802.15.6 has strict QoS and priorities to transfer the medical data to the server a QoS-enabled WLAN for the next hop is needed to preserve the end-to-end QoS. I adopt IEEE 802.11e standard since the IEEE 802.11e EDCA provides QoS which can match requirements of IEEE 802.15.6 QoS [58].

The WLAN includes the WBAN/WLAN bridges and regular WLAN nodes. The bridge device would be the hub of the WBAN and a station in the WLAN. The bridge communicates with the sensors and actuators inside the WBAN and conveys the data in the WLAN to the server. In Fig. 5.1 networking structure of a healthcare system including the WBANs, bridges, and the WLAN is depicted.

I develop a prioritized bridging mechanism between the IEEE 802.15.6-based WBANs and the IEEE 802.11e EDCA-based WLAN to convey the medical data to the medical center. Although I have developed analytical models for single-hop IEEE 802.15.6-based and IEEE 802.11e EDCA-based networks, in this chapter I use simulations in order to

avoid large computation complexity of analytical models. The frame arrival process in the bridges follows a general distribution due to the characteristics of output process from sensing nodes. This would lead to a G/G/1 queuing model in the bridges which significantly complicates the analytical modelling [119]. Therefore, in this work I deploy simulation modelling for the WBAN/WLAN bridged network.

Bridging WBANs and WLAN imposes lots of challenges which must be considered for designing efficient and seamless communications in the healthcare network. Setting the MAC parameters of the IEEE 802.15.6 and IEEE 802.11e EDCA standards affects the network performance. The WBAN differentiation parameters, CW_{min} and CW_{max}, are constant according to IEEE 802.15.6. However, all four differentiation parameters of IEEE 802.11e EDCA (CW_{min}, CW_{max}, AIFS, and TXOP) are configurable. I map the 8 User Priorities (UPs) in the WBAN into the 4 Access Categories (ACs) in the WLAN to provide the required quality of service and prioritization for the WBAN nodes.

At first, by assignment of WBAN UPs with default MAC parameters to 8 different medical data streams and under the presence of ordinary nodes, I investigate the impact of WLAN AC differentiation by Arbitrary Inter-Frame Space (AIFS) and Contention Window (CW) on performance of medical and regular nodes' data streams. According to the results of the study, I will differentiate WLAN ACs to improve the network performance. Then, I investigate the impacts of a variety of network parameters on performance of interconnection between IEEE 802.15.6 and IEEE 802.11e. I deploy a simulation model for investigating the performance of the interconnected WBAN-WLAN network. I study how the number of patients in the healthcare network, the number of the regular WLAN nodes, channel quality, WBAN and WLAN prioritizing MAC parameters affect the performance

of the patient's healthcare network.

Performance of IEEE 802.15.6 has been investigated through simulation and analytical models so far only in [94; 120; 100]. Models for EDCA are more mature as presented in [79; 73; 121; 59; 122]. The authors in [123] studied performance of a healthcare system which bridges IEEE 802.15.4-based WBANs and IEEE 802.11-based WLAN, but the authors did not address user priorities neither in the WBANs nor the WLAN. To the best of our knowledge there is no work in the literature which evaluates bridging the IEEE 802.15.6 and IEEE 802.11e standards for building a wireless healthcare network.

The remainder of this chapter is organized as follows: Section 5.1 describes the WBANs/WLAN bridging challenges. Section 5.2 discusses the simulation model and the parameters setup in the model. In Section 5.3 I investigate the impacts of WLAN priority differentiation on the performance of the bridged WBANs/WLAN healthcare networks. Section 5.4 evaluates the wireless healthcare network performance by using the simulation models. Finally, Section 5.5 concludes the chapter summarizing the findings of the study.

5.1 Challenges in QoS-Enabled Bridging Between WBAN and WLAN

I discuss the challenges for bridging the IEEE 802.15.6 and the IEEE 802.11e standards and I develop our solution to bridge the WBANs and WLAN for the healthcare network.

5.1.1 WBAN-WLAN bridging challenges

Bridging the WBAN and the WLAN imposes lots of challenges which must be considered for designing efficient and seamless communications in the healthcare network. In

Table 5.1: Frequency band dependent parameters in IEEE 802.15.6

Frequency Band (MHz)	402 - 405	420 - 450	863 - 870	902 - 928	950 - 956	2360 - 2400	2400 - 2483.5
Symbol Rate (ksps)	187.5	187.5	250	300	250	600	600
number of channels	10	12	14	48	12	38	79
Channel Bandwidth (MHz)	0.30	0.50	0.40	0.50	0.40	1.00	1.00
Header Transmission Rate (kbps)	57.5	57.5	76.6	91.9	76.6	91.9	91.9
Maximum Payload Transmission Rate (kbps)	455.4	187.5	607.1	728.6	607.1	971.4	971.4

the following, I discuss the issues which are important in the design of bridges in wireless healthcare systems.

- Deploying one or two network interfaces in the WBAN-WLAN bridges is a challenging issue in the design of the wireless healthcare networks. If the bridge has a single network interface, the interface has to operate in both WBAN and WLAN. Though having only one interface decreases the bridge's cost, it imposes a lot of design and implementation challenges. In order to be able to operate in both networks (working based on different standards) serious re-configurations of PHY and MAC parameters are required. In addition, due to the different characteristics of the WBAN and WLAN environments and the standards the operating antennas for the networks should also be different. To be able to operate in both networks, the interface has to perform the time sharing between the WBAN and the WLAN which degrades the bridge performance in both networks. By deploying two network interfaces, the bridge is able to support simultaneous communications in the networks. Bridges with two network interfaces have the potential to support higher data rates compared with single interface ones. Since the interfaces are inexpensive these days,

I assume that the bridges (hubs) are equipped with two network interfaces.

- An important challenge is related to the frequency bands in which the WBAN nodes and the WLAN stations operate. The WLAN stations operate in 2.4GHz ISM band with 11 channels in North America for high data rate transmission of 5.5 Mbps and 11 Mbps. The WBAN nodes can operate in more extensive frequency ranges as shown in Table 5.1. Choosing an appropriate frequency band for WBANs affects the healthcare network performance. Operating on the license-free 2.4GHz frequency band leads to low network performance for WBANs since the band is overcrowded by many network technologies like IEEE 802.15.1 and IEEE 802.15.4. To improve the WBANs performance and decrease their interference with the other wireless networks, it is reasonable that the WBAN nodes operate on non-ISM frequency bands. In this work, I assume that the WBAN nodes operate on the frequency range of 2360 - 2400 MHz to avoid the contention on the 2.4GHz ISM band and achieve the highest possible data frame transmission rate, 971 kbps. Moreover, the lower the channel frequency is, the higher PHY raw transmission rate can be achieved. Therefore, the WBAN nodes and the WLAN stations do not interfere during their transmissions since they operate on different frequency bands.

- Another concern in the design of the wireless healthcare networks is that if the neighbouring WBANs in an area should perform Frequency-Division Multiple Access (FDMA) or Time-Division Multiple Access (TDMA). Since performing TDMA requires tight synchronization among all the nodes of the WBANs and due to the availability of a plenty of channels for WBANs, it is reasonable to perform FDMA for the WBANs. In this work, I assume that the WBANs in an area operate in different

Table 5.2: WBAN User Priority Mapping into WLAN Access Categories

WBAN				WLAN				
UP	Traffic designation	CW_m	CW_M	AC	Traffic designation	AIFS	CW_m	CW_M
0	Background	16	64	0	Background	7	31	1023
1	Best effort	16	32					
2	Excellent effort	8	32	1	Best effort	5	31	1023
3	Controlled load	8	16					
4	Video	4	16	2	Video	3	31	1023
5	Voice	4	8					
6	Media data or network control	2	8	3	Voice	2	31	1023
7	Emergency	1	4					

frequency channels to avoid mutual interference.

- Setting the MAC parameters of the IEEE 802.15.6 and IEEE 802.11e EDCA standards also affects the network performance. The WBAN differentiation parameters, CW_{min} and CW_{max}, are constant according to IEEE 802.15.6. However, all four differentiation parameters of IEEE 802.11e EDCA (CW_{min}, CW_{max}, AIFS, and TXOP) are configurable. Though AC differentiation can be done by CW_{min} and CW_{max} I don't differentiate the ACs in the WLAN by the contention window sizes since it leads to an aggressive differentiation. Small contention window sizes increase the collision probability for the contending nodes and trigger transition to early saturation for the CSMA/CA-based wireless networks, as indicated in [95; 65]. The results of our study in [95] show that the IEEE 802.15.6 is very sensitive to the network traffic load because of the small contention window sizes. Applying priority differentiation in EDCA-based WLAN using contention window sizes would cause excessive frame collisions in the second hop and results in large end-to-end frame access delays. Therefore, in order to provide moderate differentiation of traffic classes

in the second hop I differentiate the ACs in the IEEE 802.11e EDCA-based WLAN by AIFS values. AIFS values provide the opportunity for higher priority ACs to have higher successful transmission rates by allocating dedicated CSMA slots, as shown in Fig. 2.1. AIFS differentiation decreases the overall collision probability in the network by providing more transmission chances for higher priority ACs. Differentiation through AIFS outperforms the differentiation through the contention window sizes in terms of collision probability. The MAC differentiation parameters set for WBAN and WLAN hops are shown in Table. 5.2. TXOP value is equal for all ACs in the WLAN, though through the experiments I vary it's value to study its impact on the network performance.

- Mapping the WBAN UPs into WLAN ACs is another important challenge for bridging the WBANs and the WLAN. The data frames arriving to the bridges/hubs from the WBAN nodes belong to a specific UP. There is a large number of options to transfer the collected medical data to the WLAN access point. As an option, every received WBAN data frame can be individually transmitted to the WLAN access point. Another option is frame aggregation before transmission over the WLAN. Compressing the WBAN data frames by the hub undoubtedly improves the wireless healthcare network performance. However, data compression in the hubs needs higher processing and storage capabilities. Therefore, in this work I assume that the hubs do not perform any data compression. In case of aggregating the WBAN data frames into a single WLAN data frame, the number of aggregated frames, the UP of the data frames, and the size of the aggregated WLAN data frames must be considered. Making decision on all these issues not only depends on the network traffic

Table 5.3: Healthcare nodes are spread into 8 UPs (NN: number of nodes, TL: traffic load per packet, PS: payload size, AC: mapped into Access Category)

UP	Node	NN	TL	PS	AC
7	ECG	1	2 p/s	150 B	3
	EEG	1	2 p/s	150 B	
6	EEG	2	2 p/s	150 B	3
5	EEG	1	2 p/s	150 B	2
	Blood Pressure	1	2 p/s	150 B	
4	Glucose	1	1 p/s	50 B	2
	Oxygen Saturation	1	1 p/s	50 B	
	Temperature	1	1 p/s	50 B	
	Respiration Rate	1	1 p/s	50 B	
3	Physical Activity	2	2 p/s	50 B	1
2	EMG	2	2 p/s	500 B	1
1	ECG	2	2 p/s	150 B	0
0	EEG	4	1 p/s	300 B	0

rates but also on the network performance. In this work, I examine two cases; in the first one, every four data frames with specific UPs are aggregated into a single WLAN data frame. In the second one, every WBAN data frame is converted to a single WLAN data frame for transmission in the WLAN. I map the WBAN UPs into WLAN ACs based on the priorities of the WBAN data frames and traffic rates of all UPs, as shown in Table 5.2.

- Deploying RTS/CTS mechanism in the networks is another challenge which should be considered. I do not use RTS/CTS mechanism for accessing the medium in WBANs since according to our study in [102] deploying RTS/CTS mechanism is mostly counter productive. However, I deploy RTS/CTS mechanism for accessing the medium in the WLAN since aggregated frames are large. In the all experiments, the TXOP periods are large enough to include transmission of any data frame.

5.2   Simulation setup

I investigate the performance of wireless communications in a healthcare network which consists of WBANs and a WLAN. I developed a simulation model for bridging the IEEE 802.15.6-based WBANs and the IEEE 802.11e EDCA-based WLAN. The simulation model considers all the details from both the IEEE 802.15.6 and IEEE 802.11e standards. Opnet does not have any bridging model implemented. The WBANs consist of 20 healthcare sensors (8 EEG sensors, 3 ECG sensors, 2 Physical Activity sensors, 2 EMG sensors, 1 Blood Pressure sensor, 1 Glucose sensor, 1 Oxygen Saturation sensor, 1 Temperature sensor, and 1 Respiration Rate sensor). The way the sensors are spread into 8 UPs, their traffic rates, and their frames payload sizes are shown in Table 5.3. I set the retransmission limit to 7 for all UPs. Except RAP1, the lengths of the other APs could be set to zero. The results of our study in [100] indicate that short EAP and RAP lengths generally degrade the network performance. Unless explicitly specified, I set the EAP1 length to 0.1 sec while RAP1 length is set to different values (varying between 0.5 sec and 1.2 sec), but identical for all WBANs.

I assume that the hub operates in the beacon mode with superframe boundaries. All nodes are synchronized to support the contention-based mechanism of IEEE 802.15.6. I do not use RTS/CTS mechanism for accessing the medium in WBANs since according to our study in [102] deploying RTS/CTS mechanism is mostly counter productive. The control frames and headers are transmitted at 91.9 kbps while I assume that the payload is transmitted at 971.4 kbps. I assume an error-prone channel having the constant Bit Error Rate (BER).

The payloads of WLAN data frames are transmitted with the transmission rate of 5.5

Mbps while the headers are transmitted with the transmission rate of 1 Mbps. The retransmission limit in the WLAN is set to 7 for all ACs. I deploy RTS/CTS mechanism for accessing to the medium in the WLAN. I evaluate the network performance for the cases where all WLAN ACs operate with TXOP=0 and TXOP= $5000\mu sec$.

In the WLAN, there are two types of nodes; WBAN/WLAN bridges (WBAN hubs) and regular WLAN nodes. The WBAN/WLAN bridges, simply called bridges hereafter, communicate with the central medical server (wireless access point as the first destination) while the regular WLAN nodes may communicate with another server or any other nodes. The hub in a WBAN (bridge) collects the data frames from all the healthcare nodes in its BAN.

I investigate four network performance descriptors including:

– Mean data frame response time (WBAN/WLAN)

– Successful medium access probability (WLAN)

– Mean number of successfully transmitted frames during a TXOP access (WLAN)

– Successful transmission probability during a TXOP access (WLAN)

The performance descriptors are computed for two sets of nodes in the network; the bridges and the regular WLAN nodes.

The medical data frames arrive to the WBAN nodes according to the Poisson distribution with the mean arrival rates shown in Table 5.3. Though the inter-arrival times of the data frames to the WBAN nodes are exponentially distributed, their arrivals to the hubs, which is a function of output process, do not follow the Poisson distribution. Data frame inter-arrival times for regular WLAN nodes are also exponential distributed.

I assume that the WBAN nodes operate over a Rician-faded channel between the nodes and the hub, in which the BER is a function of channel quality, diversity order, and Signal to Noise Ratio (SNR) values for all UPs. In addition, I assume that the WBAN nodes deploy the QPSK modulation scheme to achieve the highest data frame transmission rate. The resulting data frame error rates due to the fading channel affect the mean data frame response time in the WBAN.

Since the signal transmission in WBANs takes place around or in the human body, the channel fading significantly affects the error performance of the the WBANs. I assume that the WBAN nodes operate over a Rician-faded channel between the nodes and the hub, in which the BER is a function of channel quality, diversity order, and Signal to Noise Ratio (SNR) values for all UPs. In addition, I assume that the WBAN nodes deploy the QPSK modulation scheme to achieve the highest data frame transmission rate. The resulting data frame error rates due to the fading channel affect the mean data frame response time in the WBAN.

I calculate the BER of QPSK in Rician fading channels as follows [117]:

$$BER = G(0, \frac{\pi}{2}, \overline{\gamma_b}, L, K_R, 1) \tag{5.1}$$

where $\overline{\gamma_b} = \frac{\overline{\gamma_c}}{2}, \overline{\gamma_c} = \frac{1}{2N_0}$ represents the average SNR per channel, N_0 is the power spectral density of the complex Gaussian random processes for the channels, and K_R is the Rician factor, and I have

$$G(\theta_1, \theta_2, \overline{\gamma}, L, K_R, d) = \frac{e^{-LK_R}}{\pi} \int_{\theta_1}^{\theta_2} \frac{exp(\frac{LK_R}{1+(\overline{\gamma}d^2/(K_R+1)sin^2\theta)})}{[1+(\overline{\gamma}d^2/(K_R+1)sin^2\theta)]^L} \, d\theta \tag{5.2}$$

Based on the positions and types of healthcare nodes I set the Rician factors for different UPs as:

$$(K_0, K_1, K_2, K_3, K_4, K_5, K_6, K_7) = (1.5, 4, 3, 3, 2.5, 1.5, 1.5, 4) \tag{5.3}$$

The diversity order, L, is set to 1 for all UPs. By deploying the above formula and the

parameters I obtain the average BERs for all UPs as shown in Table 5.4.

Table 5.4: BER values for UPs in WBANs

BER_0, BER_5, BER_6	BER_1, BER_7	BER_2, BER_3	BER_4
$13.95866 * 10^{-5}$	$2.31524 * 10^{-5}$	$5.0085 * 10^{-5}$	$7.21 * 10^{-5}$

Opnet simulator [83] is used for simulation modeling of the healthcare network, includ-

ing the WBANs and the WLAN. The simulation model follows assumptions and definitions

from the IEEE 802.15.6 and IEEE 802.11e standards.

5.3   Comparison of AIFS and CW as Priority Differentiation Parameters

Fig. 5.2 shows the data frame mean response time in the WBAN. The plot depicts the

time as the duration between the moment when the sensor generates the data frame until the

moment when the data frame is successfully transmitted to the hub. The results indicate

that increasing the RAP length, while the EAP length is constant, slightly improves the

response time for all UPs. Since the data frame sizes and the data frame error rates are

different for different UPs the priority is not the only factor affecting the data frame access

delay.

As a result of considering results from Fig. 5.2, throughout this work, I set the default

length of RAP1 to 0.5 sec and the length of EAP1 to 0.1 sec, unless explicitly indicated.

I evaluate cases where the WLAN contains 10 bridges and 3 or 10 regular WLAN

nodes. All regular nodes generate data frames of all ACs with the payload size of 100B.

Frame inter-arrival times of regular nodes are exponentially distributed with the mean val-

ues as indicated in the plots, unless explicitly specified. BER in the WLAN is set to a constant value of $2 * 10^{-5}$ due to the homogeneity of WLAN transmission medium.

I avoid displaying the results when any network node is unstable (i.e. saturated [59]). A network node is unstable when an AC is in saturation regime, i.e. when the node's buffer is never empty. Saturation in the WLAN results in buffer overflow in the WBAN/WLAN bridges. The data loss in the bridges severely damages the efficiency of the wireless healthcare network. Fig. 5.3 includes 8 plots for the mean response time of bridges' data frames in the WLAN, in which the number of regular WLAN nodes (3 and 10), the TXOP value (0 and 5000 μsec), and the type of AC differentiation (AIFS differentiation and CW differentiation) vary. The mean response time of the bridges' frames indicates the time duration between the moment when the frame, composed of four WBAN data frames, is created until the moment when the data frame is successfully transmitted to the WLAN access point. The plots in Fig. 5.3 show that when there are 3 regular WLAN nodes in the network, differentiation by CW or AIFS does not considerably affect the response time of the bridges' data frames. However, when there are 10 regular WLAN nodes in the network (larger number of contending nodes), yet under low to moderate traffic loads, the differentiation through AIFS outperforms the differentiation through CW. Small contention window sizes increase the collision probability for the contending nodes and trigger transition to early saturation for the CSMA/CA-based wireless networks. The plots indicate that the non-zero TXOP values can slightly help to avoid the early saturation when AC differentiation is performed through CW sizes. When TXOP=0 (a single data frame can be transmitted upon a successful medium access) and there are 10 regular WLAN nodes the lowest AC data frames response times exceed 0.04 sec when the regular WLAN nodes generate ap-

proximately 10 fps (frames per second) and 8 fps, for the cases where the differentiation is performed through AIFS and CW, respectively. In case of TXOP=5000 μsec and 10 regular WLAN nodes, when AC differentiation is done through AIFS and CW the mean response times of data frames exceed 0.25 sec at approximately 14 fps and 12 fps, respectively.

Fig. 5.4 shows the mean response time of data frames generated by regular WLAN nodes in the WLAN when there are 10 WBAN/WLAN bridges and

- There are 3 or 10 regular WLAN nodes

- TXOP=0 or TXOP=5000 μsec

- AC differentiation is done through AIFS or CW

The data frame mean response time indicates the duration between the moment when the frame is created until the moment when it is successfully transmitted. The results confirm that the IEEE 802.11e EDCA mechanism is very sensitive to the network traffic load because of the small contention window sizes, which causes larger data frame access delay when there are larger number of contending nodes in the network. AC differentiation through AIFS improves the data frame response time for the bridges and regular WBAN nodes since it provides moderate differentiation. The results also indicate that it is necessary to set TXOP values to non-zero values.

Fig. 5.5 and Fig. 5.6 show the successful medium access probability of bridges and regular nodes in the WLAN, respectively, where the number of regular WLAN nodes, TXOP values, and differentiation method vary. The plots indicate that applying priority differentiation in an EDCA-based WLAN using contention window sizes would cause excessive frame collisions in the second hop and would result in large end-to-end frame access de-

lays. The results show that if the CW is used for AC differentiation the higher priority ACs experience larger collision probability while they access the medium more often because of small contention window sizes. The successful medium access probability also depends on the data frame sizes. The AC_1 has the largest aggregated WBAN data frames on average (900 B for AC_0, 1100 B for AC_1, 400 B for AC_2, and 600 B for AC_3). Larger data frames cause higher number of retransmissions due to the error-prone channel. The results also show that larger number of regular WLAN nodes and smaller TXOP values considerably decrease the successful medium access probability of bridges to transmit their data frames to the access point.

Figs. 5.5(a), 5.5(c), 5.5(e), and 5.5(g) show the successful medium access probability for the bridges when AIFS is deployed for AC differentiation. In this case, higher priority aids an AC to have larger successful medium access probability, except for AC_1 and AC_2 under low load. The reason is the larger number of AC_2 nodes compared to that of AC_1 nodes, which causes higher collision probability. Figs. 5.6(a), 5.6(c), 5.6(e), and 5.6(g) represent the successful medium access probability for regular WLAN nodes which have identical numbers of nodes, data frame sizes, and data frame arrival rates. In this case, it is clear that higher priority ACs enjoy higher successful transmission rate. Thus, applying AIFS differentiation parameter for prioritization aids higher priority ACs to more efficiently use the medium. On the contrary, Figs. 5.5(b), 5.5(d), 5.5(f), and 5.5(g) and Figs. 5.6(b), 5.6(d), 5.6(f), and 5.6(g) indicate that if CW is used for AC differentiation the higher ACs experience smaller successful medium access probability because of smaller contention windows. However, since larger numbers of bridges belong to AC_0 and AC_2, compared to AC_1 and AC_3 respectively, according to Figs. 5.5(b), 5.5(d), 5.5(f), and 5.5(g),

AC_0 and AC_2 have smaller medium access probability compared to AC_1 and AC_2, respectively.

Fig. 5.7 represents the mean number of successfully transmitted data frames during a TXOP access for bridges in the WLAN. Figs. 5.7(a), 5.7(b), 5.7(c), and 5.7(d) show the successful transmission rate during the TXOP access since TXOP=0. The frame would be corrupted only because of the error-prone channel since there is no contention when the TXOP period is successfully obtained. AC_2 (encapsulating WBAN UP_4 and UP_5 data frames) and AC_1 (including WBAN UP_2 and UP_3 data frames) have the highest and lowest successful transmission rates since their data frames on average are smallest (400 B) and largest (1100 B), respectively. In addition, when TXOP=0 the number of regular nodes does not affect the mean number of successfully transmitted frames during the TXOP period. However, when TXOP=5000 μsec larger number of regular WLAN nodes causes larger number of data frame transmissions within TXOP periods for bridges. According to Figs. 5.7(e) and 5.7(f), when there are smaller number of regular WLAN nodes in the network, under low to moderate traffic loads, AC differentiation by CW causes smaller number of transmissions during the TXOP periods compared to the case when AIFS is used for differentiation. However, when there is larger number of regular WLAN nodes (10 nodes) the AC differentiation by CW causes larger number of data frame transmissions during the TXOP periods due to higher contention on the medium.

Fig. 5.8 shows the mean number of successfully transmitted data frames for regular WLAN nodes. When TXOP=0, the mean number of successfully transmitted data frames represents the successful data frame transmission rate during the TXOP period where there is no contention. Figs. 5.8(a), 5.8(b), 5.8(c), and 5.8(d) indicate that the successful data

frame transmission rate for all ACs does not depend on number of nodes or the AC differentiation approach. The probabilities are identical for all ACs since they all have equal BERs. Figs. 5.8(e), 5.8(f), 5.8(g), and 5.8(h) confirm that for smaller number of regular WLAN nodes, under low to moderate traffic loads, the differentiation through CW causes smaller number of data frame transmissions during the TXOP period since the nodes access the medium more often, compared to the case where AIFS is deployed for AC differentiation. In case of 10 regular WLAN nodes when AIFS is used for AC differentiation and all regular WLAN nodes generate 14 fps for each AC, AC_0, AC_1, AC_2, and AC_3 successfully transmit on average 2.6, 1.8, 1.4, and 1.3 frames in the TXOP period, respectively. However, for the same condition when CW is deployed for AC differentiation AC_0, AC_1, AC_2, and AC_3 successfully transmit on average 5.2, 3.5, 2.2, and 1.5 frames in the TXOP period, respectively. The reason is higher collision probability for all ACs when CW is deployed for AC differentiation.

Though AC differentiation can be done by CW_{min} and CW_{max} the results of this work indicate that it leads to an aggressive differentiation resulting in lower network performance. Small contention window sizes increase the collision probability for the contending nodes and trigger transition to early saturation in the WLAN. This would cause higher contention in the second hop and results in large end-to-end frame delays. In addition, the saturation in the WLAN causes buffer overflow in the bridges (WBAN hubs) resulting in the medical data loss which is undesirable. Therefore, in order to have moderate differentiation and lower frame collision probability, this work confirms that AIFS is more appropriate for differentiating the WLAN ACs.

5.4 Performance Evaluation of interconnected WBAN-WLAN Subject to Other Parameters

According to the results of the previous section I select AIFS for differentiating the ACs in the WLAN. In the rest of this chapter the CW sizes are set to constant values.

Based on how the bridge forwards the medical data to the access point I design two scenarios. In the first scenario, every four frames destined to a specific AC are aggregated (encapsulated) into a single WLAN data frame, without performing any data compression, and transmitted to the server. Data frames can have different sizes. In the second scenario, I investigate the network performance where the data frames received from the sensors are individually transmitted to the server.

I study the impacts of a variety of WBAN/WLAN parameters on the overall network performance. I study the impacts of the number of patients in the healthcare network, the number of the regular WLAN nodes, channel quality, WBAN and WLAN prioritizing MAC parameters on the performance of the patient's healthcare network.

I deploy four performance descriptors for investigating the performance of the network, including WBAN/WLAN mean data frame response time, WBAN/WLAN successful medium access probability, mean number of successfully transmitted frames during a TXOP access, and successful transmission probability during a TXOP access. The performance descriptors are computed for two sets of nodes in the network; the bridges and the regular WLAN nodes.

In all plots in this section, the lines with the line-styles *thin solid* (black), *dot* (red), *dash* (blue), *dash-dot* (green), *long-dash* (gold), *space-dot* (khaki), *space-dash* (magenta),

and *thick solid* (coral) represent user priorities, 0, 1, 2, 3, 4, 5, 6, and 7, respectively.
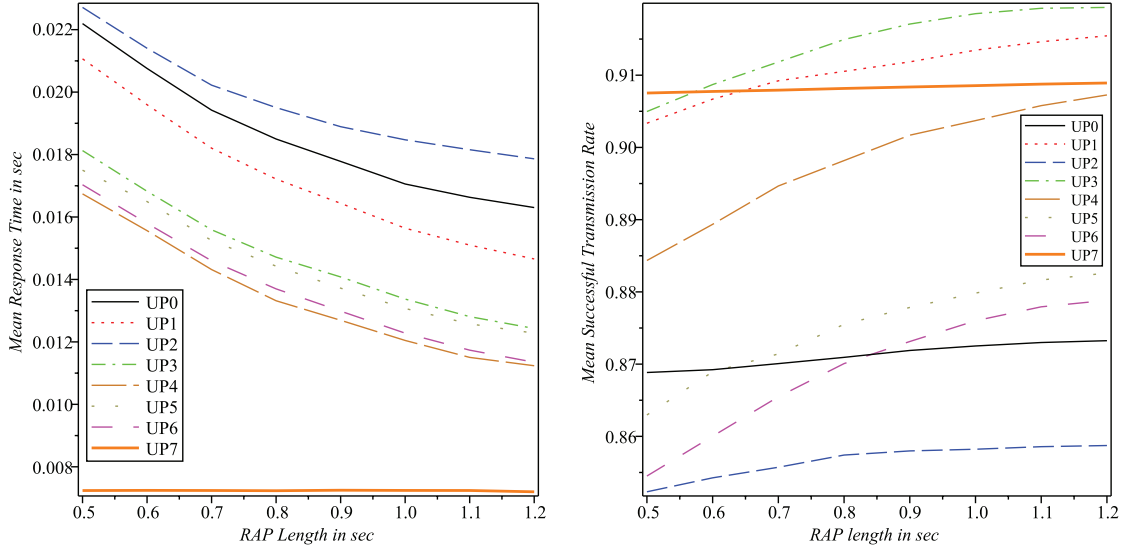
(a) Mean Data Frame Response Time in WBAN   (b) Mean Successful Transmission Rate in WBAN

Figure 5.2: Mean data frame response time and average successful transmission rate in a WBAN when RAP1 length varies (length of EAP1 = 0.1 sec)

In Fig. 5.2 (a) the mean response time of data frames in the WBAN is depicted. The mean data frame response time in WBAN is defined as the time duration between the moment when the sensor generates the data frame until the moment when the data frame is successfully transmitted to the hub. The results indicate that increasing the RAP length, while the EAP length is constant, improves the response time for all UPs. Since the data frame sizes and the data frame error rates are different for different UPs the priority is not the only factor affecting the data frames access delay. In addition, Fig. 5.2 (a) indicates that increasing the RAP lengths does not considerably decrease the delay. Fig. 5.2 (b) shows the successful transmission rates for all UPs. The rate indicates the percentage of times in which the node successfully transmit the data frame. The plot shows how increasing the

RAP length improves the successful transmission rates.

As a result of considering results from Fig. 5.2, throughout this work, I set the default length of RAP1 to 0.5 sec and the length of EAP1 to 0.1 sec, unless explicitly indicated.

5.4.1   Aggregating WBAN data frames to be transmitted to the server

In the first scenario, the bridge aggregates four WBAN data frames into a WLAN data frame. Since the aggregated data frames may include the data frames from different UPs, the data frames vary in size based on the including WBAN frames. I investigate the network performance under the impacts of different MAC and network parameters, including the number of regular WLAN nodes, the traffic rates of the regular nodes, data frame error rate, TXOP lengths and WBAN access phases lengths. Default number of bridges in the WLAN is set to 10 unless explicitly specified.

Impact of number of regular WLAN nodes on network performance

In the first experiment, I consider two cases; where the number of WLAN regular nodes is equal to 3 and 10, respectively. All regular nodes generate data frames of all ACs with the payload size of 100B. Frame inter-arrival time of regular nodes are exponentially distributed with the mean values as indicated in the plots, unless explicitly specified. The BER for both cases are set to a constant value of $2 * 10^{-5}$.

The mean response time of the aggregated WBAN data frames in WLAN indicates the time duration between the moment since the frame, composed of four WBAN data frames,

is created until the moment when the data frame is successfully transmitted to the WLAN access point. In Fig. 5.3 I show the mean response time of the aggregated data frames in the WLAN for the cases where TXOP is equal to 0 and 5000 μsec. When TXOP = 0 the nodes are able to transmit a single data frame upon a successful medium access. When the nodes are able to transmit more than one data frame during TXOP period the performance is enhanced for all ACs. I only show the WLAN's results where the WLAN data frame response time is tolerable for both bridges and regular WLAN nodes. I avoid displaying the results when the network is unstable (i.e. saturated [59]). The network is unstable when an AC is in saturation regime. Let us assume that 0.04 sec is the tolerance threshold for the bridges' data frame response time in the WLAN. According to Fig. 5.3, in case of TXOP=0, the response time of AC_0 data frames exceeds the threshold when the regular nodes' data frame arrival rate rises above 35 fps and 10 fps, when there are 3 and 10 regular WLAN nodes in the network, respectively. In case of TXOP=5000 μsec, Fig. 5.3 (c) and (d) indicate that the response time tolerance threshold is exceeded when the regular WLAN nodes' arrival rate passes 46 fps and 11 fps where 3 and 10 WLAN regular nodes are active, respectively. The results show the the large impact of the number of regular nodes in the WLAN on the bridges' performance. The AC_1 has the largest aggregated WBAN data frames on average (900 B for AC_0, 1100 B for AC_1, 400 B for AC_2, and 600 B for AC_3). However, larger data frames cause higher number of retransmissions due to the error-prone channel. The remaining time in the TXOP period after finishing the data frames in the queue is return by the node for the use of other nodes in the network.

Fig. 5.4 shows the mean response time of data frames generated by regular WLAN nodes in the WLAN. The time indicates the duration between the moment when the frame

(a) 3 regular nodes, TXOP=0

(b) 10 regular nodes, TXOP=0

(c) 3 regular nodes, TXOP=5000 μsec
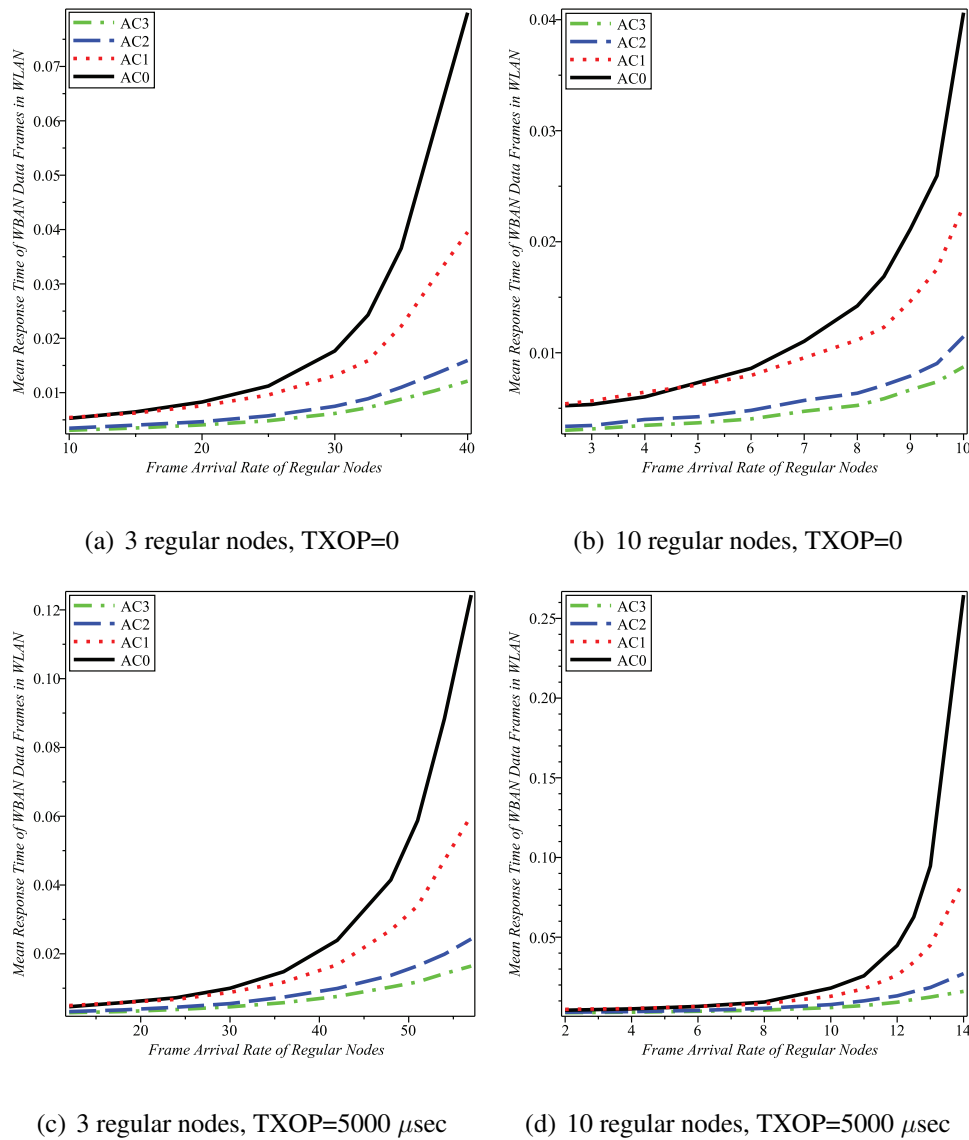
(d) 10 regular nodes, TXOP=5000 μsec

Figure 5.3: Mean response time of aggregated WBAN data frames in the WLAN with 3 and 10 regular WLAN nodes which have all four ACs. TXOP = 0 and TXOP =5000 μsec. BER = 0.00002. There are 10 bridges in the WLAN.

is created until the moment when it is successfully transmitted. When TXOP=0, the frame arrival rate varies between 10 fps and 40 for 3 regular nodes, while the frame arrival rate varies between 2 fps and 10 fps for 10 regular WLAN nodes. The results indicate that

larger TXOP value decreases the data frame response time for all ACs, as expected. As indicated in Fig. 5.4, when there are 3 regular WLAN nodes, TXOP=0 triggers to a saturation condition for AC_0 WLAN data frames at 35 fps while this condition occurs at 57 fps when TXOP=5000 μsec, which is approximately 63% improvement. The results indicate that setting non-zero value for TXOP is a must in the network which improves the network performance.

Fig. 5.5 and Fig. 5.6 show the successful medium access probability of bridges and regular WLAN nodes in the WLAN, respectively. The results show that increasing the number of regular nodes in the WLAN considerably decreases the successful medium access probability of bridges to transmit their data frames to the access point. The higher priority ACs in bridges do not always achieve higher successful medium access probability. This originates from their different frame sizes and traffic rates. According to Fig. 5.5, the successful medium access probability values for AC_1 and AC_2 intersect at 31 fps, 8.5 fps, 40 fps, and 11 fps, in Fig. 5.5 (a), (b), (c), and (d), respectively. At the beginning the probability for AC_1 is higher than that of AC_2, but higher priority aids AC_2 to have larger successful medium access probability than AC_1 upon heavier traffic in the network. The reason for slightly lower successful medium access probability for AC_2 nodes is the larger number of nodes which have AC_2 (6 nodes) but there are only 4 AC_1 nodes in the WBANs. When TXOP =0 the network performance is more affected by the noisy channel since it increases the medium contention. However, according to Fig. 5.6, higher AC priority for regular nodes results in higher successful medium access probability. This is because all traffic parameters are homogeneous for the regular WLAN nodes. The frame sizes, the frame arrival rates, and data frame error rates are equal for all ACs in the regular WLAN
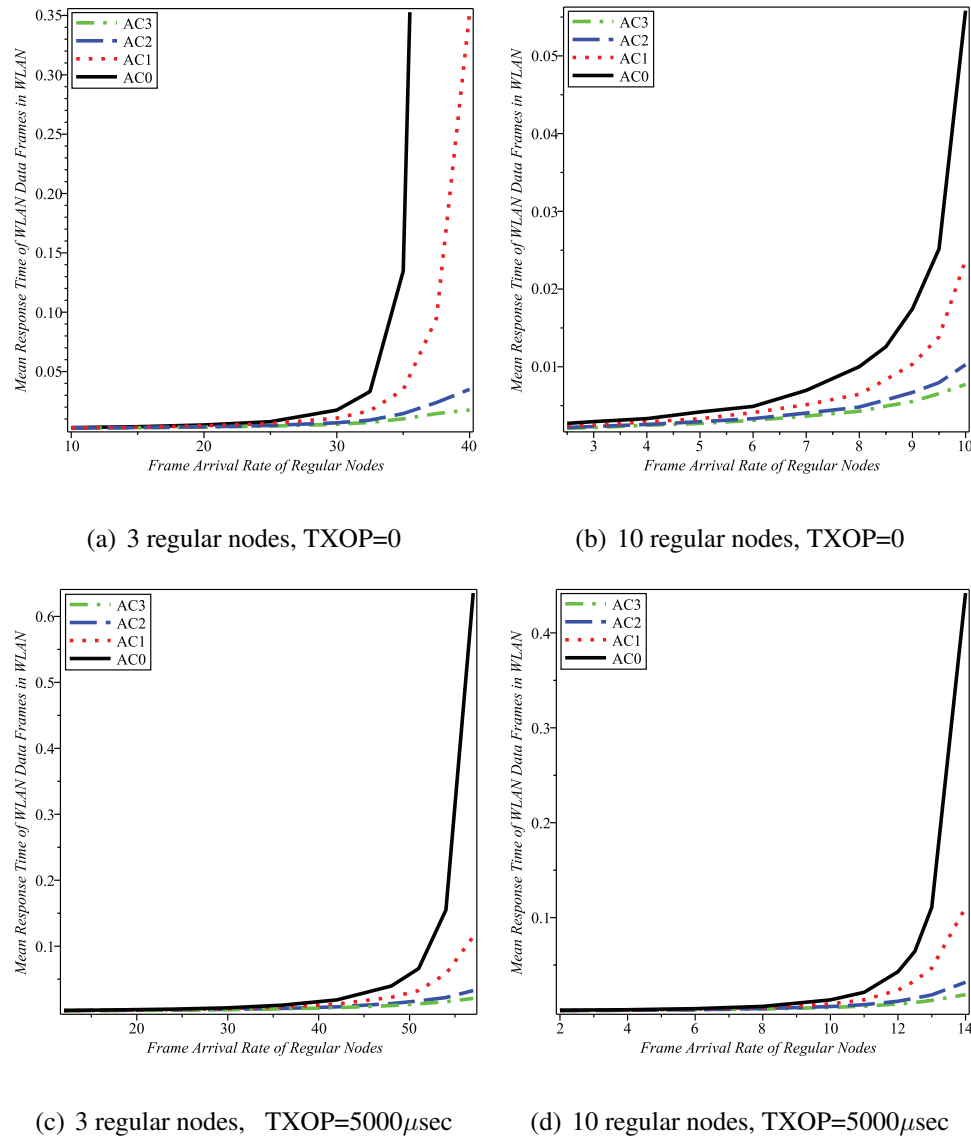
(a) 3 regular nodes, TXOP=0   (b) 10 regular nodes, TXOP=0

(c) 3 regular nodes,   TXOP=5000μsec   (d) 10 regular nodes, TXOP=5000μsec

Figure 5.4: Mean response time of WLAN data frames in the WLAN with 3 and 10 regular WLAN nodes which have all four ACs. TXOP = 0 and TXOP =5000 μsec. BER = 0.00002. There are 10 bridges in the WLAN.

nodes.

Fig. 5.7 represents the mean number of transmitted data frames during a TXOP access for bridges in the WLAN. When TXOP is equal to 0 the graphs show the successful

(a) 3 regular nodes, TXOP=0

(b) 10 regular nodes, TXOP=0

(c) 3 regular nodes, TXOP=5000 μsec

(d) 10 regular nodes, TXOP=5000 μsec
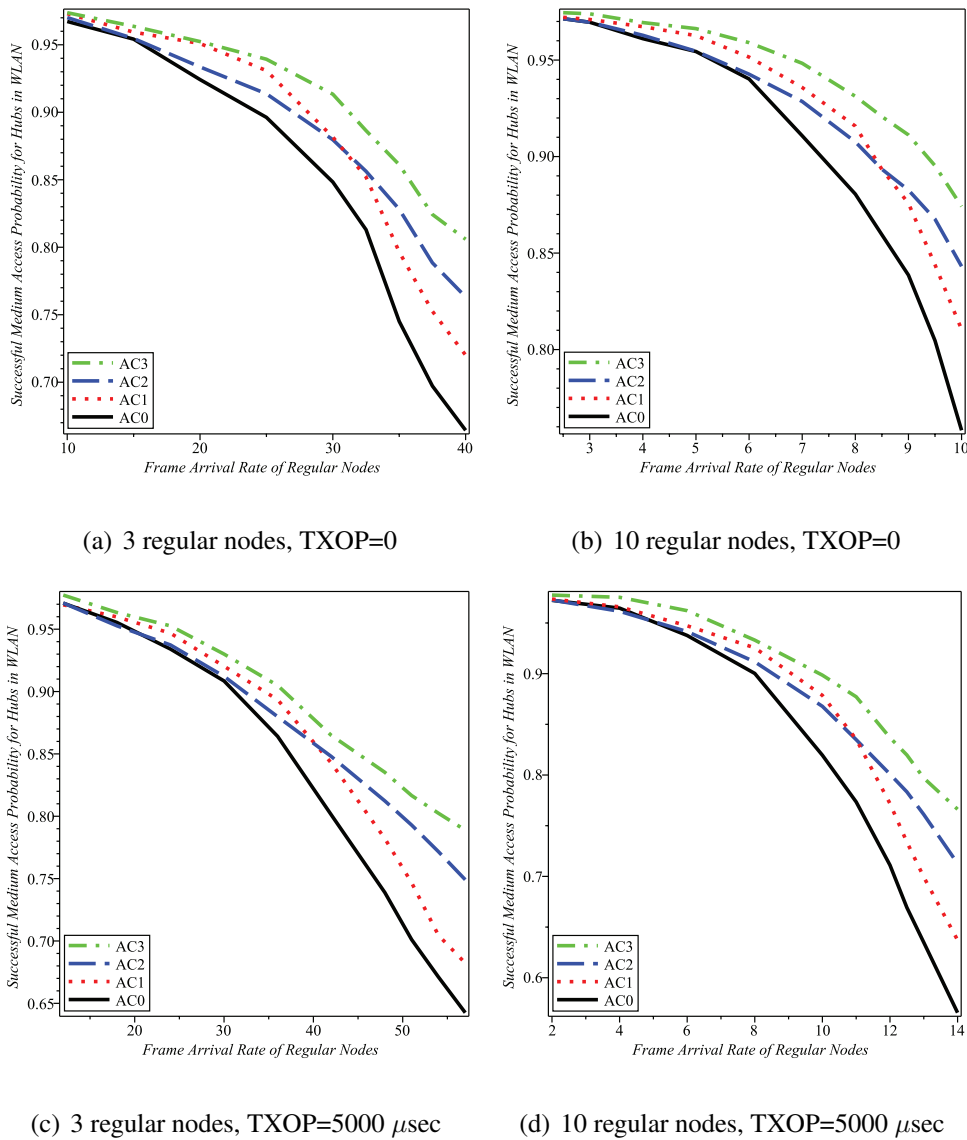
Figure 5.5: Successful medium access probability in the WLAN with 3 and 10 regular WLAN nodes which have all four ACs. TXOP = 0 and TXOP =5000 μsec. BER = 0.00002. There are 10 bridges in the WLAN.

transmission rate during the TXOP access. The frame would be corrupted only because of the error-prone channel since there is no contention when the TXOP period is successfully obtained. AC_2 (encapsulating WBAN UP_4 and UP_5 data frames) and AC_1 (including

(a) 3 regular nodes, TXOP=0

(b) 10 regular nodes, TXOP=0

(c) 3 regular nodes, TXOP=5000 μsec

(d) 10 regular nodes, TXOP=5000 μsec
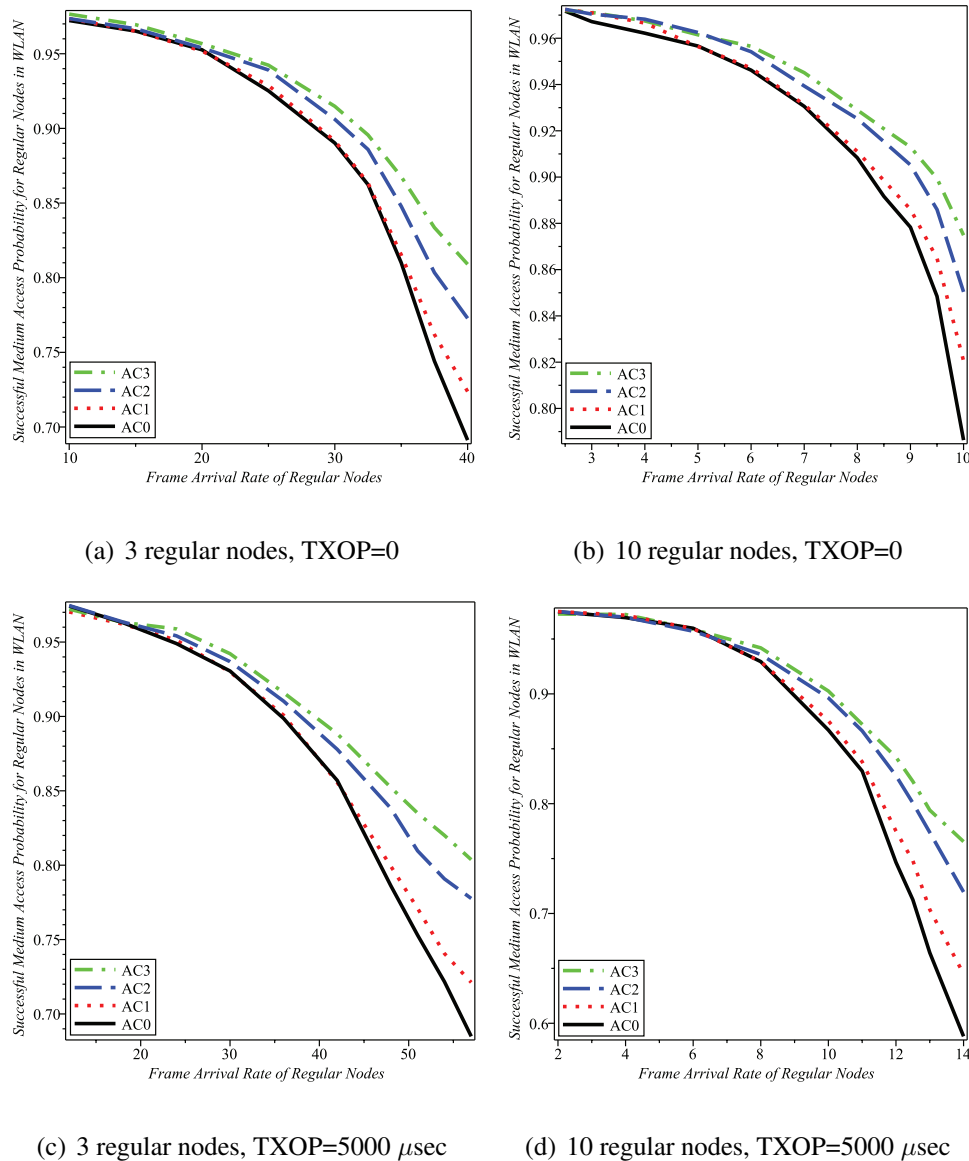
Figure 5.6: Successful medium access probability in the WLAN with 3 and 10 regular WLAN nodes which have all four ACs. TXOP = 0 and TXOP =5000 μsec. BER = 0.00002. There are 10 bridges in the WLAN.

WBAN UP_2 and UP_3 data frames) have the highest and lowest successful transmission rates since their data frames on average are smallest (400 B) and largest (1100 B), respectively. In addition note that when TXOP=0, the number of regular nodes does not affect

the mean number of successfully transmitted frames during the TXOP period. However, when TXOP=5000 μsec larger number of regular WLAN nodes triggers to larger number of transmissions by bridges during TXOP periods.

(a) 3 regular nodes, TXOP=0   (b) 10 regular nodes, TXOP=0

(c) 3 regular nodes, TXOP=5000 μsec   (d) 10 regular nodes, TXOP=5000 μsec
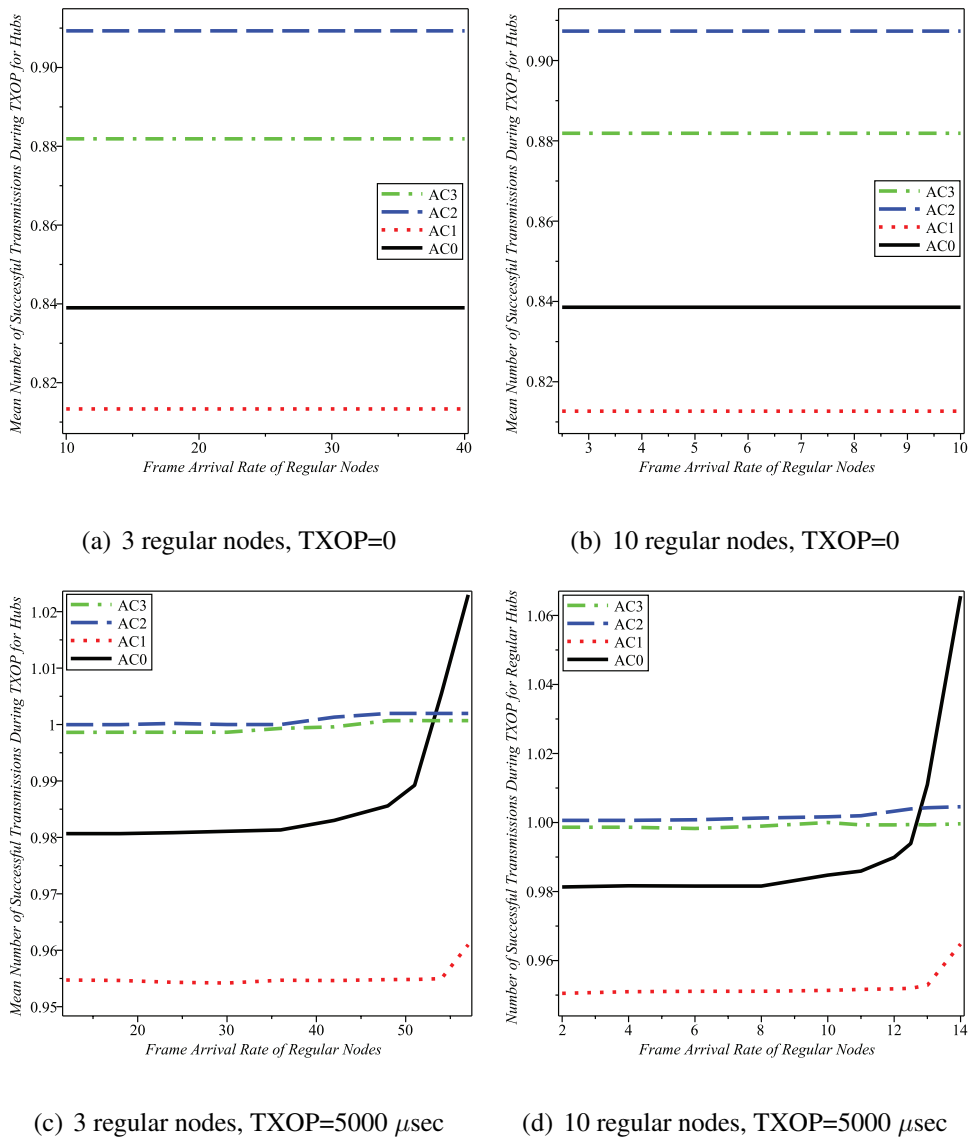
Figure 5.7: Mean number of successfully transmitted frames during a TXOP access for hubs in the WLAN with 3 and 10 regular WLAN nodes which have all four ACs. TXOP = 0 and TXOP =5000 μsec. BER = 0.00002. There are 10 bridges in the WLAN.

Fig. 5.8 shows the mean number of successfully transmitted data frames of regular WLAN nodes. As Fig. 5.8 (a) and (b) indicate the mean successful transmission rates for all ACs in the regular nodes are equal since the data frame sizes and BERs are equal for all the ACs. Fig. 5.8 (c) and (d) depict that when there are 3 regular WLAN nodes in the network with 51 fps as their arrival rates the AC_0, AC_1, AC_2, and AC_3 successfully transmit approximately 2.6, 2, 1.7, and 1.5 frames in the TXOP period, respectively. However, when there are 10 regular WLAN nodes generating 14 fps for each AC, AC_0, AC_1, AC_2, and AC_3 successfully transmit on average 2.6, 1.8, 1.4, and 1.3 frames in the TXOP period, respectively.

Impact of BER on the network performance

In the second set of experiments, I vary the channel quality by changing the BER value. I consider two cases of $BER = 0.00002$ and $BER = 0.00005$ with 5 regular WLAN nodes in the network. I evaluate the network performance when the TXOP value is set to 0 and 5000 μsec. The performance descriptors in this section indicate that BER noticeably affects the network performance. Fig. 5.9 and Fig. 5.10 show the data frame mean response times for bridges and regular WLAN nodes in the WLAN, respectively. Based on Fig. 5.9 (a) and (b) when TXOP=0, the assumed data frame response time tolerance threshold for the bridges' AC_0 (0.04 sec) is exceeded where the regular WLAN nodes generate 20 fps and 16 fps for BER=0.00002 and BER=0.00005, respectively. The same thing happens when TXOP=5000 μ sec, as indicated by Fig. 5.9 (c) and (d), increasing BER from 0.00002 to 0.00005 causes the decrease of approximately 5 fps (from 26 fps to 21 fps) to exceed the tolerance threshold (0.04 sec). BER growth increases the mean data frame response time

(a) 3 regular nodes, TXOP=0

(b) 10 regular nodes, TXOP=0

(c) 3 regular nodes, TXOP=5000 μsec

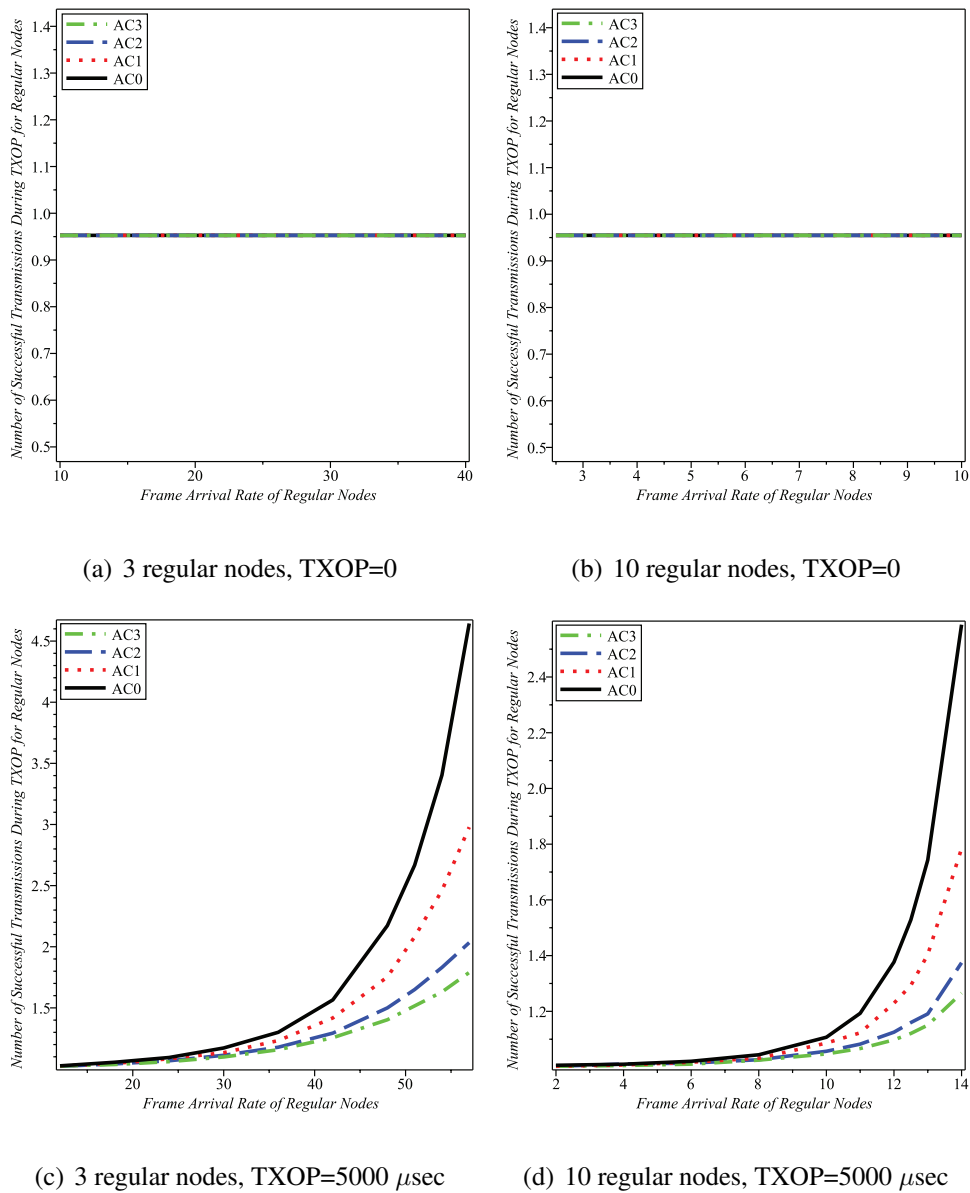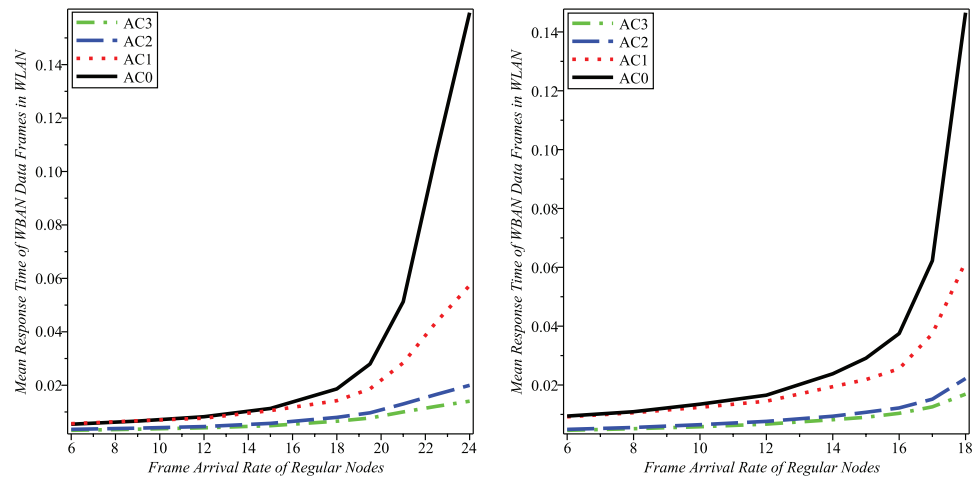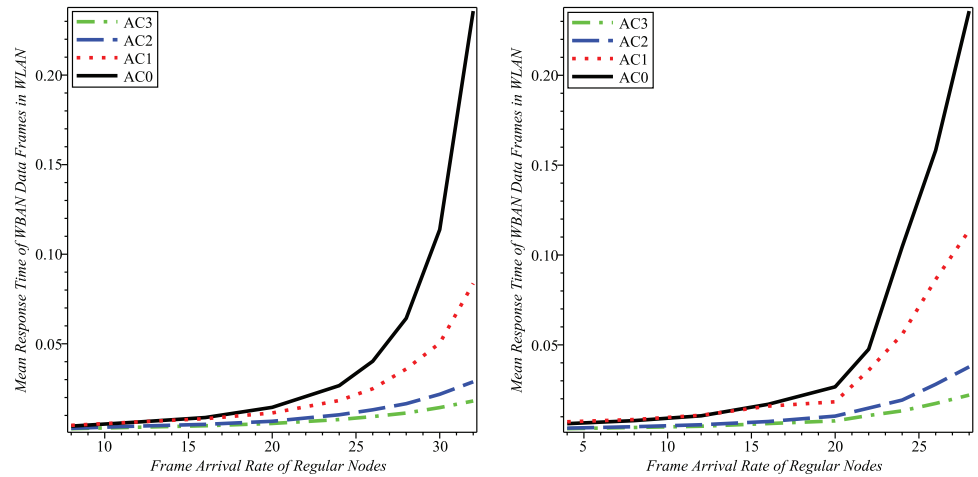(d) 10 regular nodes, TXOP=5000 μsec

Figure 5.8: Mean number of successfully transmitted frames during a TXOP access for regular nodes in the WLAN with 3 and 10 regular WLAN nodes which have all four ACs. TXOP = 0 and TXOP =5000 μsec. BER = 0.00002. There are 10 bridges in the WLAN.

for both bridges and regular WLAN nodes since the frames (including the control and data frames) error rate increases. This forces the nodes to attempt more retransmissions. Larger BER causes more retransmissions and results in much higher contention on the medium.

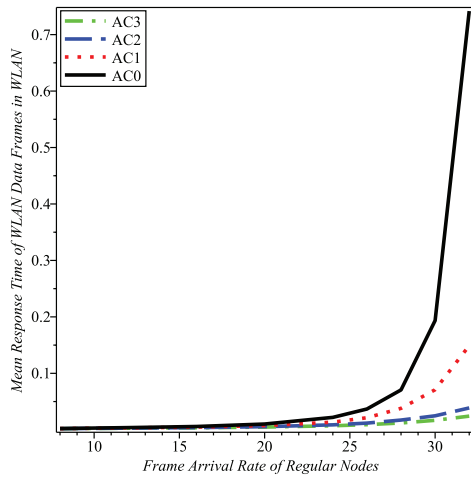(a) 5 regular nodes, TXOP=0, BER=0.00002   (b) 5 regular nodes, TXOP=0, BER=0.00005

(c) 5 regular nodes, TXOP=5000 μsec, (d) 5 regular nodes, TXOP=5000 μsec,

BER=0.00002   BER=0.00005

Figure 5.9: Mean response time of aggregated WBAN data frames in the WLAN with 10 bridges and 5 regular WLAN nodes which have all four ACs, TXOP = 0 and TXOP =5000 μsec, BER = 0.00002 and BER=0.00005.

Fig. 5.11 and Fig. 5.12 depict the successful medium access probability for bridges and regular WLAN nodes, respectively, for the cases when the BER is equal to 0.00002 and 0.00005. The results indicate that BER can have a large impact on the performance of
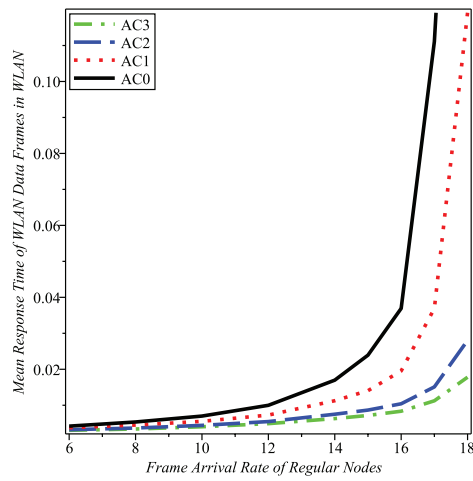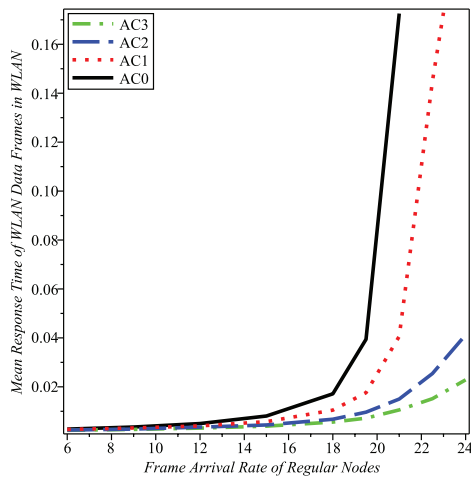
(a) 5 regular nodes, TXOP=0, BER=0.00002   (b) 5 regular nodes, TXOP=0, BER=0.00005
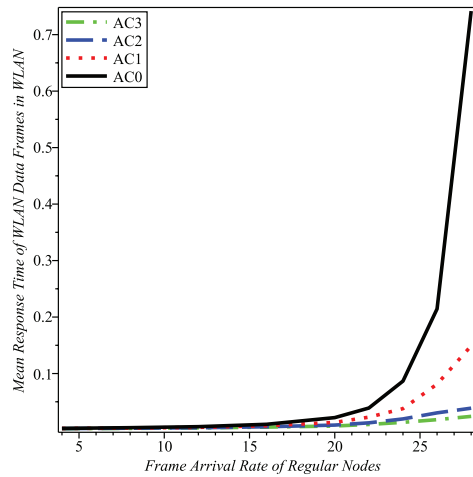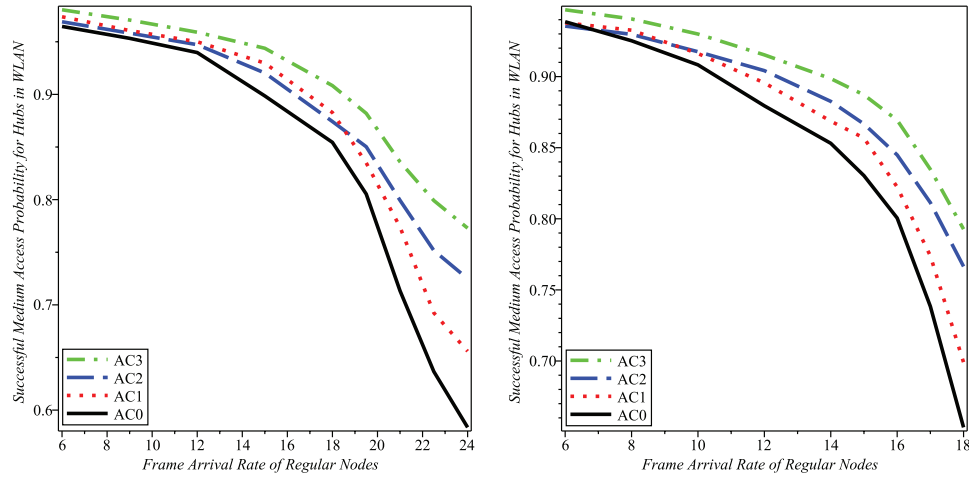
(c) 5 regular nodes, TXOP=5000 μsec, (d) 5 regular nodes, TXOP=5000 μsec,

BER=0.00002   BER=0.00005

Figure 5.10: Mean response time of WLAN data frames in the WLAN with 10 bridges and 5 regular WLAN nodes which have all four ACs, TXOP = 0 and TXOP =5000 μsec, BER = 0.00002 and BER=0.00005.

the bridges. When TXOP=0, the successful medium access probability for AC_0 becomes

equal to 0.65 at 22 fps and 18 fps (as the arrival rate of regular WLAN nodes), in case

of BER=$2*10^{-5}$ and BER=$5*10^{-5}$, respectively. In addition, the plots indicate that

setting larger TXOP values would improve the network performance in case of low channel quality.
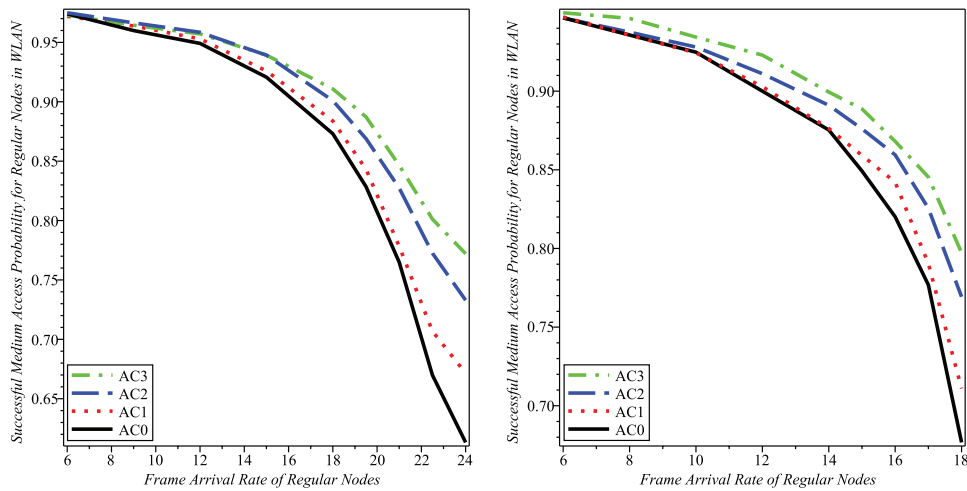

(a) 5 regular nodes, TXOP=0, BER=0.00002
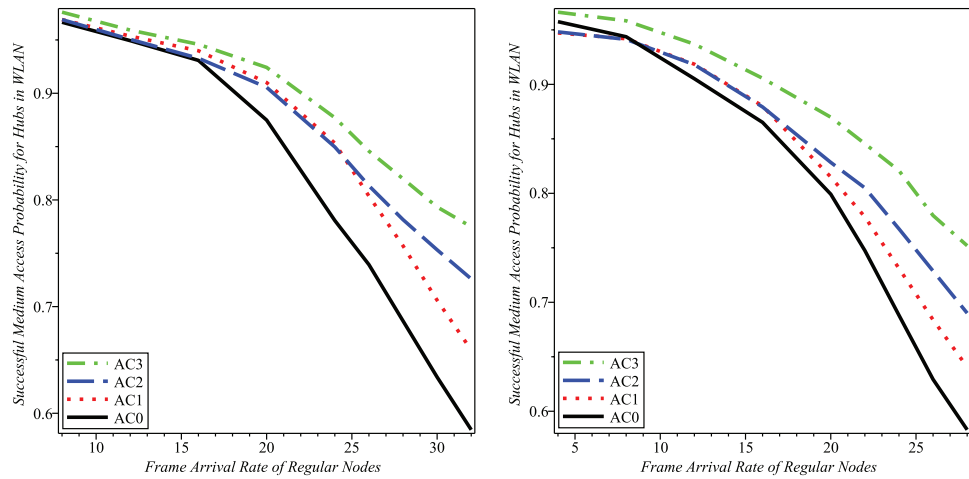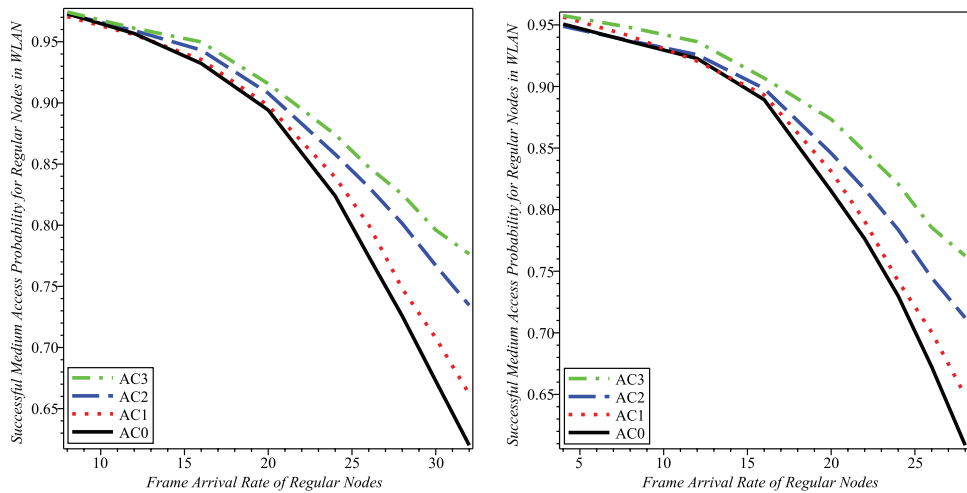
(b) 5 regular nodes, TXOP=0, BER=0.00005

(c) 5 regular nodes, TXOP=5000 μsec, BER=0.00002

(d) 5 regular nodes, TXOP=5000 μsec, BER=0.00005

Figure 5.11: Successful medium access probability for bridges (hubs) in the WLAN with 10 bridges and 5 regular WLAN nodes which have all four ACs, TXOP = 0 and TXOP =5000 μsec, BER = 0.00002 and BER=0.00005.

Fig. 5.13 and Fig. 5.14 show the mean number of successfully transmitted frames dur-

(a) 5 regular nodes, TXOP=0, BER=0.00002

(b) 5 regular nodes, TXOP=0, BER=0.00005

(c) 5 regular nodes, TXOP=5000 μsec, BER=0.00002
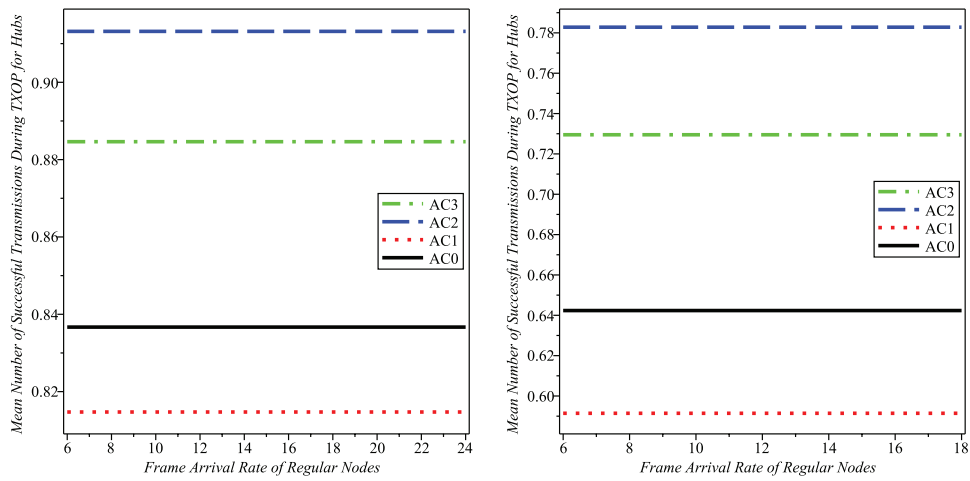

(d) 5 regular nodes, TXOP=5000 μsec, BER=0.00005

Figure 5.12: Successful medium access probability for regular nodes in the WLAN with 10 bridges and 5 regular WLAN nodes which have all four ACs, TXOP = 0 and TXOP =5000 μsec, BER = 0.00002 and BER=0.00005.

ing a TXOP access. The results indicate that the larger the BER is the larger the number of transmitted frames in the access period becomes. I also note the dependency between

the data frame size and successful transmission rate (Fig. 5.13 (a),(b) and Fig. 5.14 (a),(b)). This indicates that if the channel quality is low an effective way to improve the network performance is to decrease the frame sizes. Fig. 5.13 (b) shows when BER=$2 * 10^{-5}$ the transmission success rates of 64%, 59%, 78%, and 73% for AC_0 (900 B on average), AC_1 (1100 B on average), AC_2 (400 B on average), and AC_3 (600 B on average), respectively. Fig. 5.14 (a),(b) show equal values for all ACs since their data frames have eqaul frame sizes of 100 B. Fig. 5.13 (c),(d) show the lower ACs start earlier to transmit more than one frames in a TXOP period. The sharp increase in the mean number of transmitted frames in TXOP periods for AC_0 start at 27 fps and 22 fps when BER=$2 * 10^{-5}$ and BER=$5 * 10^{-5}$, respectively. If the AC_0 nodes were able to transmit only one frame in TXOP periods they would need to compete for accessing to the medium again when the arrival rates for regular WLAN nodes exceed 27 fps and 22 fps for the case when BER=$2*10^{-5}$ and BER=$5*10^{-5}$, respectively. Note that the bridges' performance in the network is extensively affected by the arrival rate of regular WLAN nodes while their own arrival rates do not vary. Fig. 5.14 (c),(d) show that when TXOP=5000 μsec the regular WLAN nodes leave the linear region at 25 fps and 20 fps for the cases when BER=$2 * 10^{-5}$ and BER=$5 * 10^{-5}$, respectively.

5.4.2 Transferring WBAN data frames without aggregation to the WLAN access point

In the second scenario, the bridges transmit individual WBAN data frames to the WLAN access point. Compared to the previous scenario, in which every aggregated data frame encapsulated four WBAN data frames to the same AC, the data frame sizes in the second
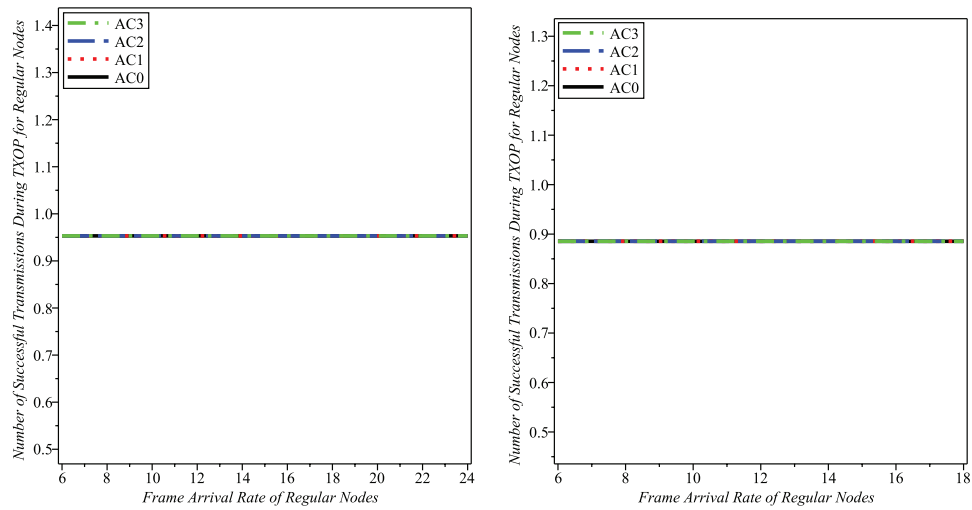
(a) 5 regular nodes, TXOP=0, BER=0.00002   (b) 5 regular nodes, TXOP=0, BER=0.00005
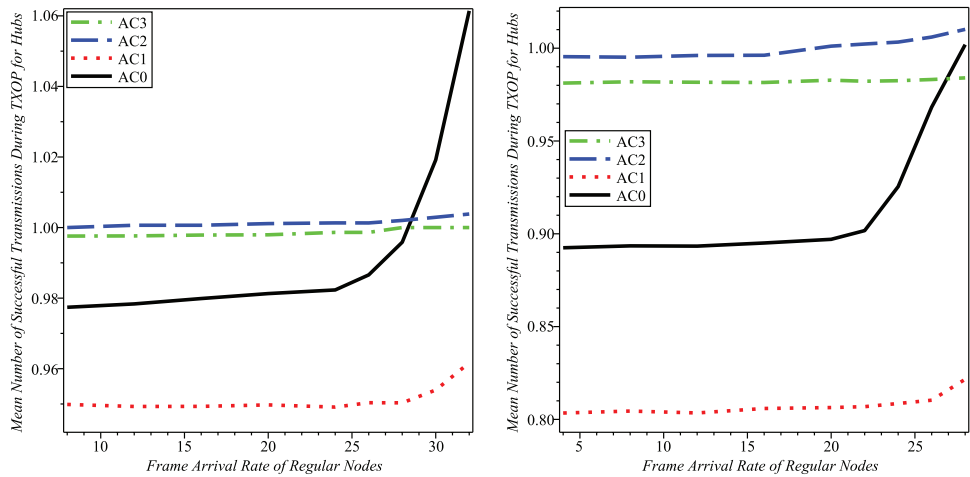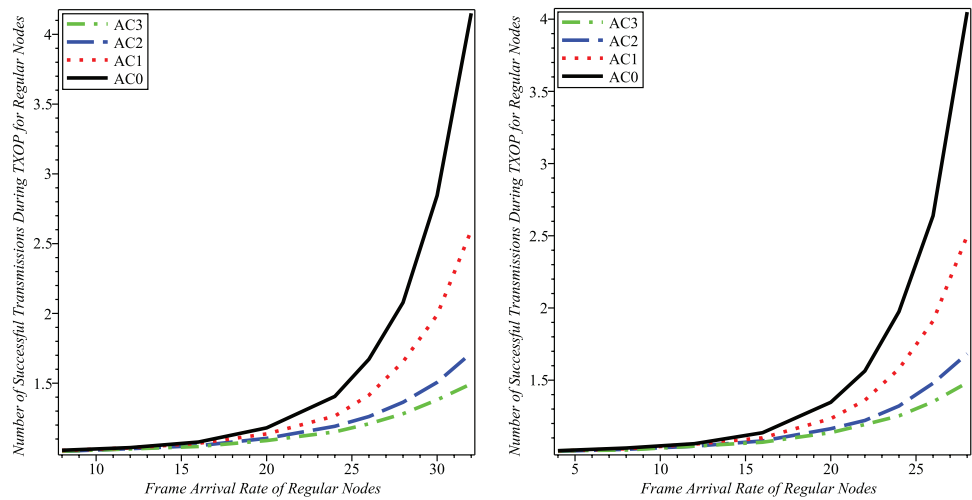

(c) 5 regular nodes, TXOP=5000 μsec, (d) 5 regular nodes, TXOP=5000 μsec,

BER=0.00002   BER=0.00005

Figure 5.13: Mean number of successfully transmitted frames during a TXOP access for bridges (hubs) in the WLAN with 10 bridges and 5 regular WLAN nodes which have all four ACs, TXOP = 0 and TXOP =5000 μsec, BER = 0.00002 and BER=0.00005.

scenare are smaller. However, the bridges in the second scenario have lager numbers of

data frames to transmit to the server. In all experiments in this section, TXOP values are set

to 5000 μsec for all ACs and BER is set to $2 * 10^{-5}$. Frame arrival rates for regular WLAN

(a) 5 regular nodes, TXOP=0, BER=0.00002 (b) 5 regular nodes, TXOP=0, BER=0.00005

(c) 5 regular nodes, TXOP=5000 μsec, (d) 5 regular nodes, TXOP=5000 μsec,

BER=0.00002   BER=0.00005

Figure 5.14: Mean number of successfully transmitted frames during a TXOP access for regular nodes in the WLAN with 10 bridges and 5 regular WLAN nodes which have all four ACs, TXOP = 0 and TXOP =5000 μsec, BER = 0.00002 and BER=0.00005.

nodes are exponentially distributed.

Fig. 5.15 (a),(b) show the mean response time of the data frames generated by the

bridges where the number of the bridges in the network is set to 5 and 10, while there are 3 regular WLAN nodes. Increasing the number of WBANs in an area also considerably affects the network performance as the bridges leave the linear region at 42 fps and 20 fps (as the arrival rate of regular WLAN nodes) where there are 5 and 10 WBANs in the network, respectively. Fig. 5.15 (c),(d) represent the results when there are 10 regular WLAN nodes in the network. The results indicate that for having a stable network and acceptable WBAN data frame response time the number of both WBANs and regular WLAN nodes in the network must be controlled. Admission control mechanisms should be performed to preserve both WBANs and regular WLAN nodes in stable condition. Fig. 5.16 shows the mean response time of data frames for regular WLAN nodes. The results indicate the large impact of the number of WBANs on the performance of the other nodes in the network.

Fig. 5.17 and Fig. 5.18 show the successful medium access probability for the bridges and the regular WLAN nodes, respectively. The results indicate that having 10 hubs and 10 regular nodes in the network, when the bridges do not aggregate the WBAN data frames, causes a high contention on the medium. Arrival rate of only 8 fps for regular WLAN nodes results in successful medium access probability of lower than 60%. Fig. 5.19 and Fig. 5.20 show the mean number of successfully transmitted frames during the TXOP access when every WBAN data frame is individually transmitted. Fig. 5.19 indicates that the plots of AC_1 and AC_2 intersect at some point. At the beginning AC_1 transmits lower number of frames in the TXOP periods while later on AC_2 transmits smaller number of data frames. The reason is the larger number of nodes with AC_2 than the number of nodes with AC_1. However, when the traffic rates of the regular WLAN nodes increase, which results in higher contention on the medium, higher priority aids AC_2 to transmit lower number of

(a) 5 bridges, 3 regular nodes

(b) 10 bridges, 3 regular nodes

(c) 5 bridges, 10 regular nodes

(d) 10 bridges, 10 regular nodes

Figure 5.15: Mean response time of WBAN data frames in the WLAN. 5 and 10 bridges (WBANs), 3 and 10 regular WLAN nodes which have all four ACs, TXOP =5000 μsec, BER = 0.00002.

data frames during the TXOP periods compared to AC_1.

In the last experiment, I investigate the network performance where there are only 10 bridges in the network without any regular WLAN nodes. Fig. 5.21 (a) shows the the mean

(a) 5 bridges, 3 regular nodes

(b) 10 bridges, 3 regular nodes

(c) 5 bridges, 10 regular nodes
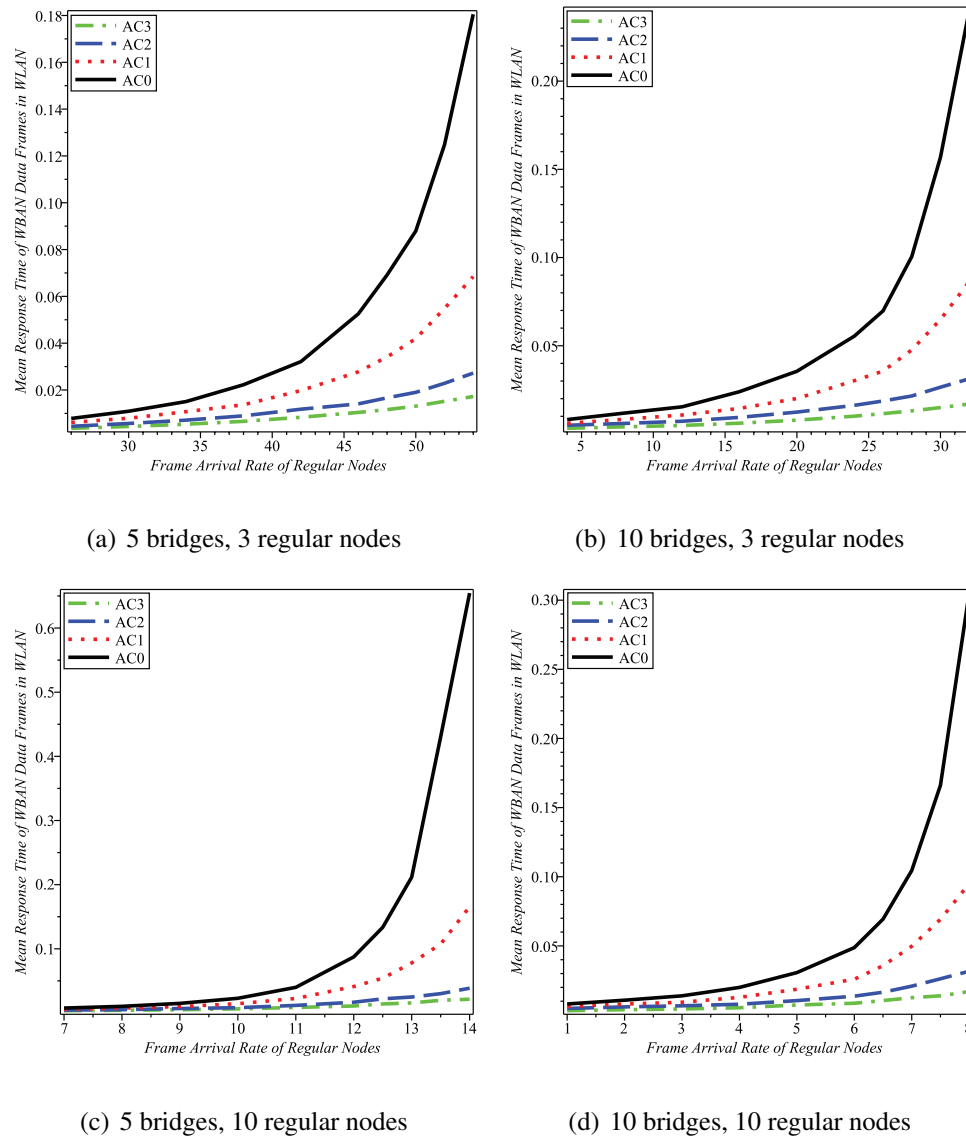
(d) 10 bridges, 10 regular nodes
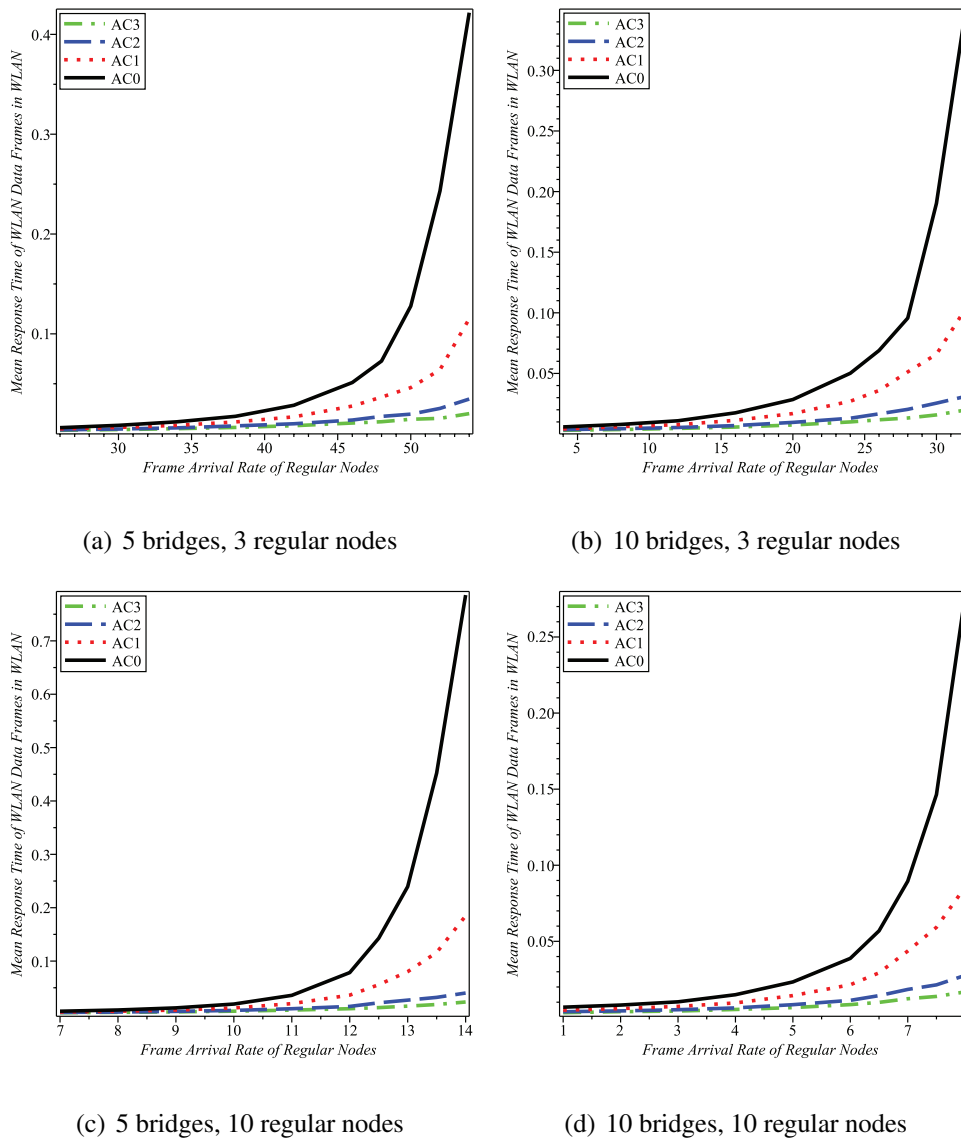
Figure 5.16: Mean response time of WLAN data frames in the WLAN. 5 and 10 bridges (WBANs), 3 and 10 regular WLAN nodes which have all four ACs, TXOP =5000 μsec, BER = 0.00002.

response time of WBAN data frame from the moment they are generated in the bridge until

the moment when they are successfully transmitted. The plot indicates that increasing the

RAP length as a WBAN parameter does not considerably affect the performance of the

(a) 5 bridges, 3 regular nodes

(b) 10 bridges, 3 regular nodes

(c) 5 bridges, 10 regular nodes

(d) 10 bridges, 10 regular nodes

Figure 5.17: Successful medium access probability for bridges in the WLAN. 5 and 10 bridges (WBANs), 3 and 10 regular WLAN nodes which have all four ACs, TXOP =5000 μsec, BER = 0.00002.

hubs in the WLAN. The data frame size is another parameter that affects the data frames response time. Fig. 5.21 (b) depicts the mean successful medium access probability for bridges in the network. The figure indicates when the traffic load is low the successful

(a) 5 bridges, 3 regular nodes

(b) 10 bridges, 3 regular nodes

(c) 5 bridges, 10 regular nodes

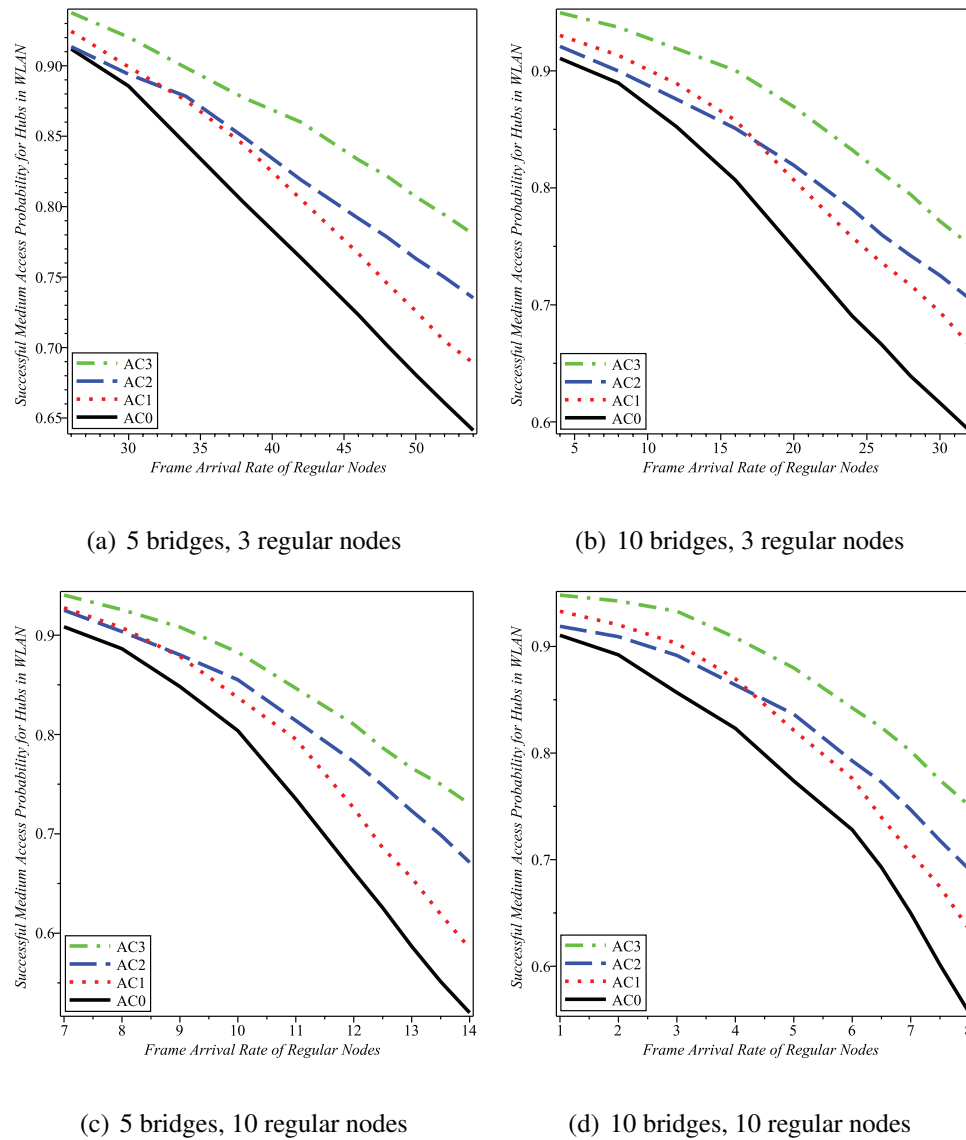(d) 10 bridges, 10 regular nodes
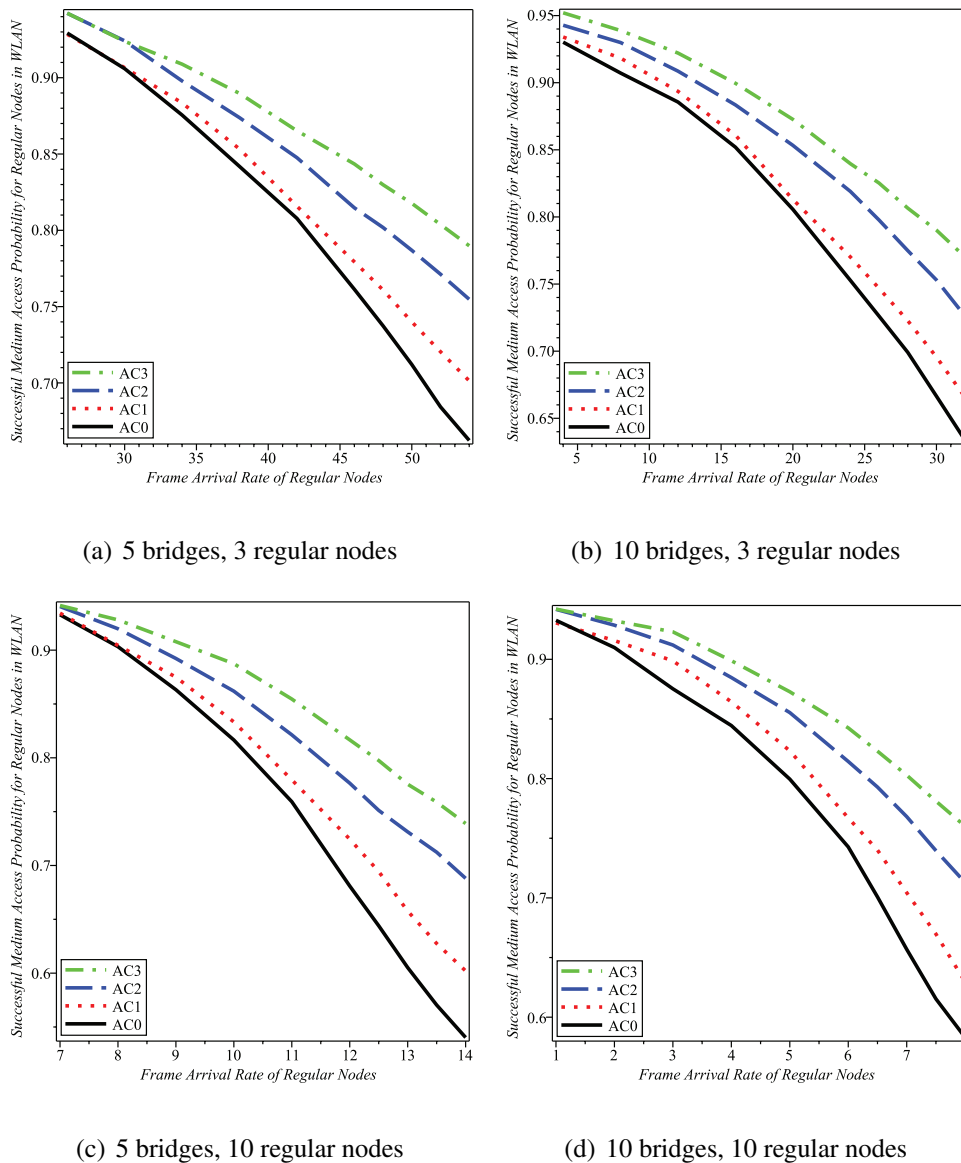
Figure 5.18: Successful medium access probability for regular WLAN nodes in the WLAN.
5 and 10 bridges (WBANs), 3 and 10 regular WLAN nodes which have all four ACs, TXOP
=5000 μsec, BER = 0.00002.

medium access rate is almost equal for all the ACs. Finally, Fig. 5.21 (c) shows the mean

number of successful transmissions during the TXOP periods for bridges. According to the

results, the larger the data frame size is the more transmission attempts are required since

(a) 5 bridges, 3 regular nodes

(b) 10 bridges, 3 regular nodes

(c) 5 bridges, 10 regular nodes

(d) 10 bridges, 10 regular nodes

Figure 5.19: Mean number of successfully transmitted frames during a TXOP access for bridges in the WLAN. 5 and 10 bridges (WBANs), 3 and 10 regular WLAN nodes which have all four ACs, TXOP =5000 μsec, BER = 0.00002.

the frames are more likely corrupted by noise and also lower number of transmissions can be done in the TXOP periods.

(a) 5 bridges, 3 regular nodes

(b) 10 bridges, 3 regular nodes

(c) 5 bridges, 10 regular nodes

(d) 10 bridges, 10 regular nodes

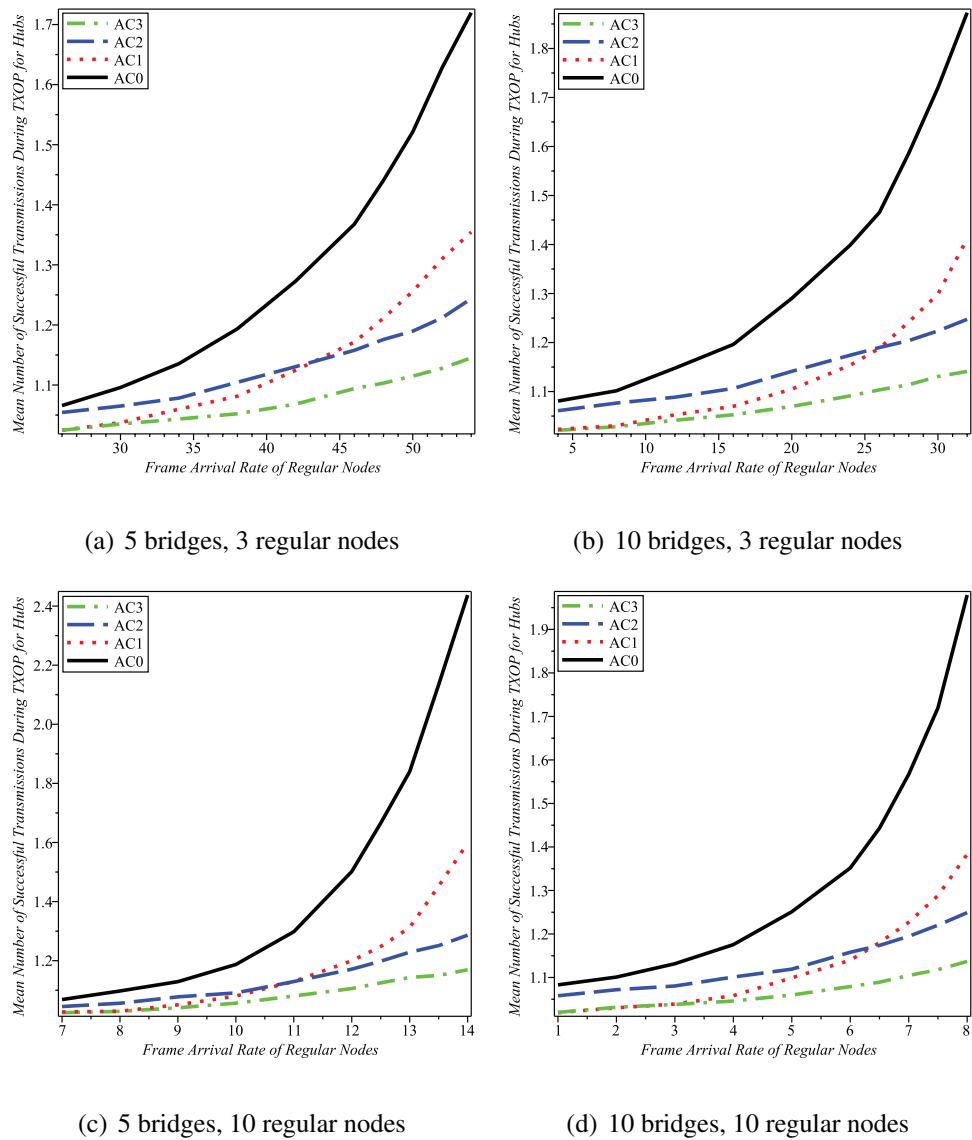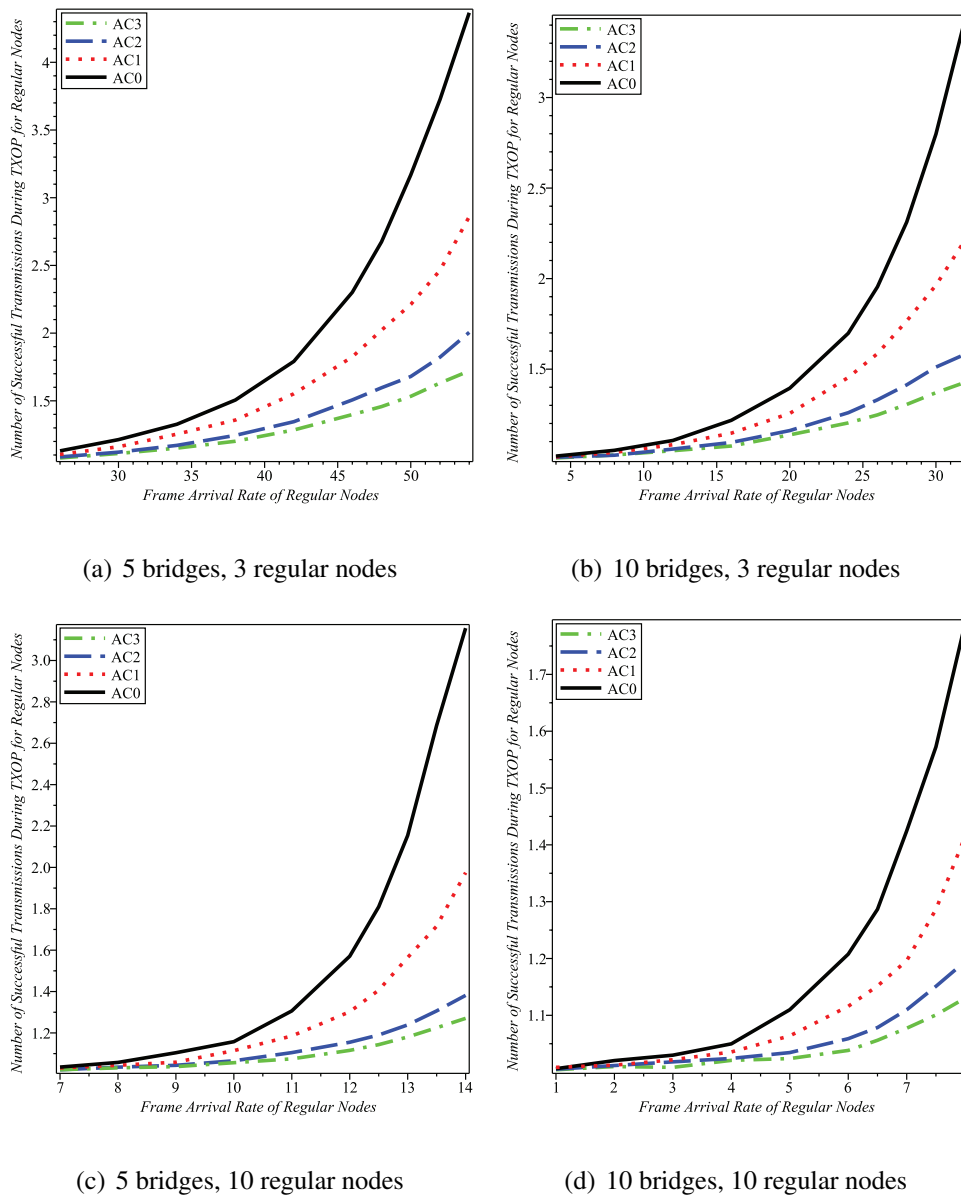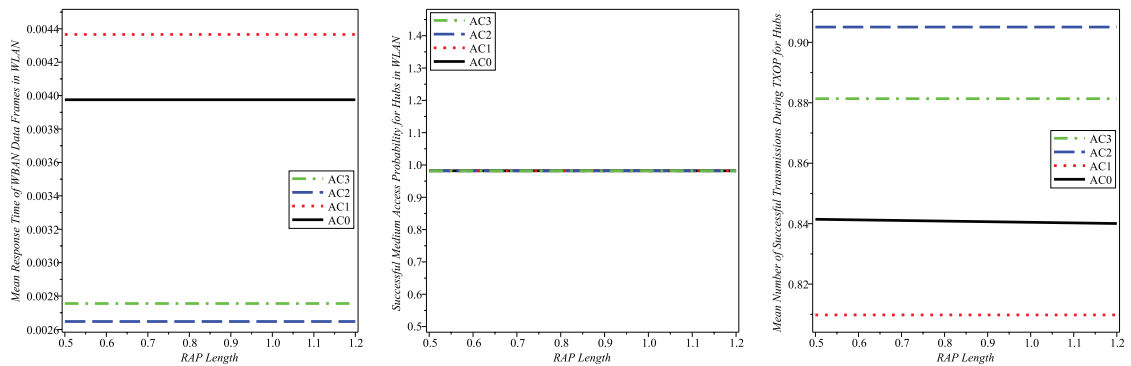Figure 5.20: Mean number of successfully transmitted frames during a TXOP access for regular WLAN nodes in the WLAN. 5 and 10 bridges (WBANs), 3 and 10 regular WLAN nodes which have all four ACs, TXOP =5000 μsec, BER = 0.00002.

(a) Mean Response Time of WBAN Data Frames in WLAN

(b) Successful Medium Access Probability for Bridges in WLAN

(c) Mean Number of Successful Transmissions During TXOP for Bridges

Figure 5.21: Performance descriptors in case there are only bridges in the WLAN. 10 bridges (WBANs), TXOP =0, BER = 0.00002.

5.5 Summary of the Chapter

In this chapter, I investigated the MAC performance of a healthcare network implemented by bridging WBANs and a WLAN. I developed a prioritized bridging mechanism between IEEE 802.15.6-based WBANs and an IEEE 802.11e EDCA-based WLAN considering all 8 UPs in the WBAN and all 4 ACs in the WLAN. In order to have moderate differentiation and lower frame collision probability I deployed AIFS for differentiating the WLAN ACs. I provided an extensive set of simulation experiments to study the impacts of a variety of network and MAC prioritizing parameters on the two-hop network performance. I presented performance descriptors including the mean data frame response time, the successful medium access probability, the mean number of successful transmissions during TXOP accesses and the successful transmission rate. The results of this work indicate that judicious choice of MAC parameters considerably improves the performance of

all WLAN ACs and as the result the network performance. The results also indicate that

not only the number of WBANs but also the number of regular WLAN nodes have a large

impact on the healthcare network performance. Hence, admission control mechanisms for

regular WLAN nodes should be performed to satisfy the required performance bounds of

the healthcare network and the regular nodes. The performed research in this chapter is

published in [62; 124; 125].

Publications

[62] S. Rashwand and J. Misic. Bridging Between IEEE 802.15.6 and IEEE 802.11e for Wireless Healthcare Networks. *Journal of Ad-Hoc Networks, Under Review*.

[124] S. Rashwand and J. Misic. Impact of Priority Differentiation on the Bridged WBAN/WLAN Healthcare Networks. *Journal of Wireless Communications and Mobile Computing (WCMC), Under Review*.

[125] S. Rashwand and J. Misic. Two-Tier WBAN/WLAN Healthcare Networks; Priority Considerations. *in Proceedings of IEEE Global Telecommunications Conference* (Globecom11), Under Review.

Chapter 6

Conclusion and Future Work

In this chapter, I summarize findings of this thesis. In addition, I describe our future work regarding the performance evaluation of a wireless body area network which operates based on the IEEE 802.15.6 standard.

6.1 Research Conclusion and Contributions

The research in this thesis can be generally divided in three parts; performance evaluation of the IEEE 802.11e EDCA-based WLANs under saturation and non-saturation regimes, performance evaluation of IEEE 802.15.6-based WBANs under saturation and non-saturation conditions, and design and performance evaluation of a QoS enabled prioritized bridging between WLAN and WBANs. The most important findings of the research can be summarized as follows:

- I described the applications and the structure of a human body monitoring network. I provided a detailed literature review of the research for developing seamless and

efficient communications in wireless healthcare networks.

- I analyzed IEEE 802.11e EDCA single-hop ad-hoc network under saturation and non-saturation regimes and error-prone channel through analytical and simulation models. I developed an accurate analytical model for IEEE 802.11e EDCA which addresses all the differentiation parameters including TXOP for a network that supports four access categories. The model consists of three parts; backoff process model, queueing model and Markov chain model for an AC_k station. I found out that increasing TXOP limit generally can improve medium utilization. Moreover, if length of TXOP is adopted in a way that all the data frames of a burst are most likely transmitted in one access period the network performance is noticeably improved. I also investigated the effects of different arrival rates of access categories, frame sizes, node populations of ACs and TXOP limits on performance of a single-hop network working based on IEEE 802.11e EDCA. The results indicate that in the case of having different frame arrival rates for the access categories adopting an appropriate TXOP value can significantly improve the network performance. I showed that growth of number of stations, specially higher priority ones, strongly reduces non-saturation regions. I came to the result that TXOP values, frame sizes, and especially the number of nodes in each class are suitable controlling tools for keeping the network in a stable condition when network load grows.

- In addition to the analytical models presented in this thesis, I developed simulation models for the IEEE 802.15.6 standard and the two-tier bridged IEEE 802.15.6-based WBANs and IEEE 802.11e-based WLAN. Opnet simulator does not have any module with implementation of the IEEE 802.15.6 standard and bridging mechanism

between wireless communication standards.

- I evaluated the interaction of RAP1, EAP1, RAP2, EAP2, and contention-free access phases in a single-hop IEEE 802.15.6 CSMA/CA-based WBAN. I developed analytical and simulation models for investigating the network performance considering EAP1, RAP1, EAP2, RAP2, and type-I/II access phases under saturation condition and an error-prone channel. I studied the impact of the lengths of different contention-based access phases on the performance descriptors of all UPs. I came to the conclusion that having short EAP and RAP phases leads to inefficient use of bandwidth. I showed that existence of EAP phases for a typical WBAN is unnecessary. Unless there are multiple different traffic types in the network, deploying EAP2 and RAP2 access phases is not required. I also showed that the IEEE 802.15.6 CSMA/CA mechanism utilizes the medium poorly under high traffic loads. I then developed analytical and simulation models for performance evaluation of IEEE 802.15.6-based WBANs under non-saturation regime. An important finding was that for an unsaturated WBAN with a small to moderate data frame sizes deploying the RTS/CTS mechanism degrades the network performance compared to the case where the nodes immediately transmit their data frames upon having the backoff counter of zero. In addition, the results indicate that setting the EAP and RAP lengths according to the traffic loads of the UPs noticeably improves the performance of the network. It was shown that having short EAP-RAP periods wastes the network resources since number of inaccessible CSMA slots during RAP1 increases. It also increases the collision probability after an EAP1 period.

- I studied the impacts of channel quality, data frame size, diversity order, data frame

arrival rate, access phase lengths, and UPs on error performance of an IEEE 802.15.6 CSMA-based WBAN. I showed how varying SNR values for different scenarios affects the MAC performance descriptors of the network. The results indicate that increasing the diversity order and transmission power generally improves the MAC performance. I found that the data frame sizes and the channel quality between nods and the hub are the most effective parameters on the WBAN error performance.

- I investigated the MAC performance of a healthcare network implemented by bridging WBANs and a WLAN. I developed a prioritized bridging mechanism between IEEE 802.15.6-based WBANs and an IEEE 802.11e EDCA-based WLAN considering all 8 UPs in the WBAN and all 4 ACs in the WLAN. I provided an extensive set of simulation experiments to study the impacts of a variety of network and MAC prioritizing parameters on the two-hop network performance. The results indicates that WLAN AC differentiation by CW leads to an aggressive differentiation resulting in lower network performance. Small contention window sizes increase the collision probability for the contending nodes and trigger transition to early saturation in the WLAN. I came to conclusion that AIFS values are appropriate for WLAN AC differentiation. The results of the research indicated that judicious choice of MAC parameters considerably improves the performance of all WLAN ACs and as the result the network performance. The results also indicated that not only the number of WBANs but also the number of regular WLAN nodes have a large impact on the healthcare network performance.

6.2 Future Work

The future work for this thesis research can have different directions, which are briefly discussed as follows:

- The results of this research indicate that the MAC and network parameters of the IEEE 802.11e and IEEE 802.15.6 standards significantly affect the healthcare network performance. Setting optimal parameters for different conditions is a challenging concern in the WBAN/WLAN bridged healthcare networks. Hence, calculating optimal MAC and network parameters for different circumstances by deploying optimization mechanisms could be an interesting future work to this thesis research.

- The results show that the network traffic, caused by data frames arrival rates for all the nodes and nodes' populations in the WLANs and WBANs, noticeably impact the healthcare network performance. Thus, admission control mechanisms must be deployed in the network to aid the nodes in the network to avoid performance drop and healthcare network performance decrement. Designing efficient and effective admission control for wireless healthcare networks can be considered an attractive future research work.

- Developing medical data aggregation and compression mechanisms to improve the healthcare network performance is another interesting research. These methods would considerably decrease the network traffic which enhances the healthcare network efficiency.

- Design and performance investigation of light-weight and reliable security mechanisms can be considered as an important research direction for the wireless healthcare

networks.

The above mentioned items are a few research directions toward an efficient and effective wireless healthcare network. Other future work can also be considered for reaching to the desirable wireless healthcare network.

Bibliography

[1] W. S. Conner, J. Heidemann, L. Krishnamurthy, X. Wang, and M. Yarvis, *Wireless Sensor Networks: A Systems Perspective*. Artech House, Inc., 2005, ch. Workplace Applications of Sensor Networks, pp. 289–307.

[2] M. A. Labrador and P. M. Wightman, *Topology Control in Wireless Sensor Networks*. Springer Netherlands.

[3] J. A. Stankovic, "Wireless sensor networks," *Journal of Computer*, vol. 41, pp. 92–95, Oct. 2008.

[4] D. Cypher, N. Chevrollier, N. Montavont, and N. Golmie, "Prevailing over wires in healthcare environments: Benefits and challenges," *IEEE Communication Magazine*, vol. 44, pp. 56–63, Apr. 2006.

[5] G.-Z. Yang, *Body Sensor Networks*. London: Springer-Verlag, 2006.

[6] R. S. H. Istepanian, E. Jovanov, and Y. T. Zhang, "Guest editorial introduction to the special section on m-health: Beyond seamless mobility and global wireless healthcare connectivity," *IEEE TRANSACTIONS ON INFORMATION TECHNOLOGY IN BIOMEDICINE*, vol. 8, pp. 405–414, Dec. 2004.

[7] K. V. Dam, S. Pitchers, and M. Barnard, "Body area networks: Towards a wearable future," in *Proc. IEEE WWRF kick off meeting*, Munich, Germany, Mar. 2001.

[8] B. Latre, B. Braem, I. Moerman, C. Blondia, and P. Demeester, "A survey on wireless body area networks," *Accepted for publication in Wireless Networks*.

[9] (2010) Bluetooth technology. [Online]. Available: http://www.bluetooth.com

[10] (2010) Zigbee alliance. [Online]. Available: http://www.zigbee.org/

[11] (2010) General packet radio service (gprs). [Online]. Available: http://www.etsi. org/WebSite/Technologies/gprs.aspx

[12] (2010) Wi-fi alliance. [Online]. Available: http://www.wi-fi.org/

[13] *Wireless Body Area Network Draft Standard*, IEEE Std. 802.15.6, 2010.

[14] (2010) IEEE 802.15 WPAN Task Group 6 (TG6) body area networks. [Online]. Available: http://www.ieee802.org/15/pub/TG6.html

[15] (2010) The world health organization (WHO) website. [Online]. Available: http://www.who.int/mediacentre/factsheets/fs317/en/index.html

[16] A. S. Go, E. M. Hylek, K. A. Phillips, Y. Chang, L. E. Henault, J. V. Selby, and D. E. Singer, "Prevalence of diagnosed atrial fibrillation in adults: national implications for rhythm management and stroke prevention: the anticoagulation and risk factors in atrial fibrillation (atria) study," *The Journal of the American Medical Association*, vol. 285, pp. 2370–2375, May 2001.

[17] J. Malmivuo and R. Plonsey, *Bioelectromagnetism: Principles and Applications of Bioelectric and Biomagnetic Fields*.   New York: Oxford University Press, 1995.

[18] (2010) Heart disease and stroke statistics2010 update: A report from the american heart association. [Online]. Available: http://circ.ahajournals.org/cgi/content/full/121/7/e46

[19] (2010) International diabetes federation. [Online]. Available: http://www.idf.org/about-diabetes

[20] E. Krames, "Implantable devices for pain control: Spinal cord stimulation and intrathecal therapies," *Best Practice and Research Clinical Anaesthesiology*, vol. 16, pp. 619–649, Dec. 2002.

[21] S. Park and S. Jayaraman, "Enhancing the quality of life through wearable technology," *IEEE Engineering in Medicine and Biology Magazine*, vol. 22, pp. 41–48, May 2003.

[22] B. Latre, G. Vermeeren, I. Moerman, L. Martens, and P. Demeester, "Networking and propagation issues in body area networks," in *Proc. 11th Symposium on Communications and Vehicular Technology in the Benelux*, Ghent, Belgium, Nov. 2004.

[23] E. Jovanov, D. Raskovic, A. O. Lords, P. Cox, R. Adhami, and F. Andrasik, "Synchronized physiological monitoring using a distributed wireless intelligent sensor system," in *Proc. IEEE the 25th Annual International Conference of Engineering in Medicine and Biology Society*, vol. 2, Cancun, Mexico, Sep. 2003, pp. 1368–1371.

[24] S. Drude, "Requirements and application scenarios for body area networks," *Mobile and Wireless Communications Summit*, pp. 1–5, Sep. 2007.

[25] R. N. Butler, "Population aging and health," *British Medical Journal*, vol. 315, pp. 1082–1084, Oct. 1997.

[26] W. S. Aronow and C. Ahn, "Elderly nursing home patients with congestive heart failure after myocardial infarction living in new york city have a higher prevalence of mortality in cold weather and warm weather months," *The Journals of gerontology. Series A, Biological sciences and medical sciences*, vol. 59, pp. 146–147, 2004.

[27] A. Arshak, K. Arshak, D. Waldron, D. Morris, O. Korostynska, E. Jafer, and G. Lyons, "Review of the potential of a wireless mems and tft microsystems for the measurement of pressure in the gi tract," *Medical Engineering and Physics*, vol. 27, pp. 347–356, Jun. 2005.

[28] *IEEE Standard for Information Technology - Part 15.4: Wireless Medium Access Control and Physical Layer Specifications for Low Rate Wireless Personal Area Networks*, IEEE Std. 802.15.4, 2003.

[29] P. Johansson, M. Kazantzidis, R. Kapoor, and M. Gerla, "Bluetooth: an enabler for personal area networking," *IEEE Network*, vol. 15, pp. 28–37, Sep. 2001.

[30] E. Jovanov, A. Milenkovic, C. Otto, , and P. C. de Groen, "A wireless body area network of intelligent motion sensors for computer assisted physical rehabilitation," *Journal of NeuroEngineering and Rehabilitation*, vol. 2, pp. 16–23, Mar. 2005.

[31] C. Otto, A. Milenkovic, C. Sanders, and E. Jovanov, "System architecture of a wireless body area sensor network for ubiquitous health monitoring," *Journal of Mobile Multimedia*, vol. 1, pp. 307–326, 2006.

[32] (2010) Sentilla corporation. [Online]. Available: http://www.sentilla.com/

[33] E. Farella, A. Pieracci, L. Benini, L. Rocchi, and A. Acquaviva, "Interfacing human and computer with wireless body area sensor networks: the wimoca solution," *Multimedia Tools and Applications*, vol. 38, pp. 337–363, 2008.

[34] J. Misic and V. B. Misic, *Performance Modeling and Analysis of Bluetooth Networks: Network Formation, Polling, Scheduling, and Traffic Control.*   Boca Raton, FL: CRC Press, 2006.

[35] ——, *Wireless Personal Area Networks: Performance, Interconnection and Security with IEEE 802.15.4.*   Chichester, UK: John Wiley and Sons, 2008.

[36] T. Gao, D. Greenspan, M. Welsh, R. R. Juang, and A. Alm, "Vital signs monitoring and patient tracking over a wireless network," in *Proc. IEEE 27th Annual International Conference of Engineering in Medicine and Biology Society*, Shanghai, China, Apr. 2005, pp. 102–105.

[37] K. Lorincz, D. J. Malan, T. R. F. Fulford-Jones, A. Nawoj, A. Clavel, V. Shnayder, G. Mainland, M. Welsh, and S. Moulton, "Sensor networks for emergency response: Challenges and opportunities," *IEEE Pervasive Computing*, vol. 3, pp. 16–23, 2004.

[38] T. Gao, T. Massey, L. Selavo, D. Crawford, B. rong Chen, K. Lorincz, V. Shnayder, L. Hauenstein, F. Dabiri, J. Jeng, A. Chanmugam, D. White, M. Sarrafzadeh, and

M. Welsh, "The advanced health and disaster aid network: A light-weight wireless medical system for triage," *IEEE TRANSACTIONS ON BIOMEDICAL CIRCUITS AND SYSTEMS*, vol. 1, pp. 203–216, sep 2007.

[39] K. Lorincz, B. rong Chen, G. W. Challen, A. R. Chowdhury, S. Patel, P. Bonato, and M. Welsh, "Mercury: A wearable sensor network platform for high-fidelity motion analysis," in *Proc. ACM 7th Conference on Embedded Networked Sensor Systems*, Berkeley, California, US., Nov. 2009, pp. 183–196.

[40] K. Venkatasubramanian and S. K. Gupta, "Ayushman: a secure, usable pervasive health monitoring system," in *Proc. ACM 2nd International Workshop on Systems and Networking Support for Health Care and Assisted Living Environments*, Breckenridge, Colorado, US., Jun. 2008.

[41] J. Penders, B. Gyselinckx, R. Vullers, O. Rousseaux, M. Berekovic, M. D. Nil, C. V. Hoof, J. Ryckaert, R. F. Yazicioglu, P. Fiorini, and et. al., "Human++: Emerging technology for body area networks," *International Federation for Information Processing (IFIP)*, vol. 249, pp. 377–397, 2008.

[42] V. Jones, A. van Halteren, I. Widya, N. Dokovsky, G. Koprinkov, R. Bults, D. Konstantas, and R. Herzog, *Topics in Biomedical Engineering*.   Springer US, 2006, ch. Mobihealth: Mobile Health Services Based on Body Area Networks.

[43] A. Wood, J. Stankovic, G. Virone, L. Selavo, Z. He, Q. Cao, T. Doan, Y. Wu, L. Fang, and R. Stoleru, "Context-aware wireless sensor networks for assisted-living and residential monitoring," *IEEE Network*, vol. 22, pp. 26–33, aug 2008.

[44] H. Chen, W. Wu, and J. Lee, "A WBAN-based real-time electroencephalogram monitoring system: design and implementation," *Journal of Medical Systems*, vol. 34, pp. 303–311, mar 2009.

[45] N. F. Timmons and W. G. Scanlon, "Analysis of the performance of IEEE 802.15.4 for medical sensor body area networking," in *Proc. First Annual IEEE Communications Society Conference on Sensor and Ad-Hoc Communications and Networks (IEEE SECON)*, Santa Clara, California, US., Oct. 2004, pp. 16–24.

[46] H. Li and J. Tan, "An ultra-low-power medium access control protocol for body sensor network," in *Proc. the IEEE 27th Annual International Conference of the Engineering in Medicine and Biology Society (IEEE-EMBS)*, Shanghai, china, 2005, pp. 2451–2454.

[47] N. Golmie, D. Cypher, , and O. Rebala, "Performance analysis of low rate wireless technologies for medical applications," *Computer Communications*, vol. 28, pp. 1266–1275, jun 2005.

[48] D. Cavalcanti, R. Schmitt, and A. Soomro, "Performance analysis of 802.15.4 and 802.11e for body sensor network applications," in *Proc. 4th International Workshop on Wearable and Implantable Body Sensor Networks (BSN 2007)*, Berlin Heidelberg, Germany, Apr. 2007, pp. 9–14.

[49] R. C. Shah, L. Nachman, and C. yih Wan, "On the performance of bluetooth and IEEE 802.15.4 radios in a body area network," in *Proc. the ICST 3rd international conference on Body area networks*, Tempe, Arizona, US., Mar. 2008.

[50] B. Zhen, H.-B. Li, and R. Kohno, "IEEE body area networks and medical implant communications," in *Proc. the ICST 3rd international conference on Body area networks*, Tempe, Arizona, US., Mar. 2008.

[51] ——, "Networking issues in medical implant communications," *International Journal of Multimedia and Ubiquitous Engineering*, vol. 4, pp. 23–38, jan 2009.

[52] I. E. Lamprinos, A. Prentza, E. Sakka, and D. Koutsouris, "Energy-efficient MAC protocol for patient personal area networks," in *Proc. IEEE 27th Annual International Conference of the Engineering in Medicine and Biology Society (IEEE-EMBS)*, Shanghai, China, Sep. 2005, pp. 3799–3802.

[53] E. Farella, A. Pieracci, L. Benini, and A. Acquaviva, "A wireless body area sensor network for posture detection," in *Proc. IEEE 11th IEEE Symposium on Computers and Communications*, Washington, DC, USA, Sep. 2006, pp. 454–459.

[54] O. C. Omeni, O. Eljamaly, and A. J. Burdett, "Energy efficient medium access protocol for wireless medical body area sensor networks," in *Proc. 4th International Summer School and Symposium on Medical Devices and Biosensors (ISSS-MDBS)*, Cambridge, UK., Aug. 2007, pp. 29–32.

[55] H. Li and J. Tan, "Heartbeat driven medium access control for body sensor networks," in *Proc. 1st ACM SIGMOBILE international workshop on Systems and networking support for healthcare and assisted living environments*, Puerto Rico, US., Jun. 2007, pp. 25–30.

[56] Y.-S. Seo, D.-Y. Kim, J. Cho, and B. Lee, "OCDP: A WBAN MAC protocol for

contention-based medical and CE applications," in *Proc. the 4th International Conference on Ubiquitous Information Management and Communication*, Suwon, Korea, Jan. 2010.

[57] K. S. Kwak, M. A. Ameen, D. Kwak, C. Lee, and H. Lee, "A study on proposed IEEE 802.15 WBAN MAC protocols," in *Proc. the 9th international conference on Communications and information technologies*, Incheon, Korea, Sep. 2009, pp. 834–840.

[58] *Wireless LAN Medium Access Control (MAC) and Physical Layer (PHY) Specification*, IEEE Std. 802.11, 2007.

[59] S. Rashwand and J. Misic, "IEEE 802.11e EDCA under bursty traffic - how much TXOP can improve performance," *IEEE Transactions on Vehicular Technology (TVT)*, vol. 60, pp. 1099–1115, 2011.

[60] J. Misic and S. Rashwand, "Analysis of impact of TXOP allocation on IEEE 802.11e EDCA under variable network load," *IEEE Transactions on Parallel and Distributed Systems (TPDS)*, vol. 23, pp. 785–799, 2012.

[61] J. Misic, S. Rashwand, and V. B. Misic, "Stability boundaries between non-saturation and saturation regimes for IEEE 802.11e EDCA," in *Proc. the 2010 IEEE International Conference on Communications (ICC'10)*, Cape Town, South Africa, May 2010.

[62] S. Rashwand and J. Misic, "Stable operation of IEEE 802.11e EDCA; interaction

between offered load and MAC parameters," *Ad Hoc Networks Journal; Special Issue: IEEE 802.11e/p*, vol. 10, pp. 162–173, 2012.

[63] ——, "Impacts of node population and TXOP on stable operation of IEEE 802.11e EDCA," in *Proc. the IEEE International Wireless Communications and Mobile Computing Conference (IWCMC10)*, Caen, France, Jun. 2010.

[64] Y. Xiao, "An analysis for differentiated services in IEEE 802.11 and IEEE 802.11e wireless LANs," in *Proc. the 24th International Conference on Distributed Computing Systems (ICDCS'04)*, Tokyo, Japan, Mar. 2004, pp. 32–39.

[65] ——, "Performance analysis of priority schemes for IEEE 802.11 and IEEE 802.11e wireless LANs," *IEEE Transactions on Wireless Communications*, vol. 4, pp. 1506–1515, 2005.

[66] J. Hui and M. Devetsikiotis, "A unified model for the performance analysis of IEEE 802.11e wireless LANs," *IEEE Transactions on Communications*, vol. 53, pp. 1498–1510, jan 2005.

[67] Z. Tao and S. Panwar, "Throughput and delay analysis for the IEEE 802.11e enhanced distributed channel access," *IEEE Transactions on Communications*, vol. 54, pp. 596–603, 2006.

[68] Y. Lin and V. W. S. Wong, "Saturation throughput of ieee 802.11e EDCA based on mean value analysis," in *Proc. the IEEE Wireless Communications and Networking Conference (WCNC'06)*, Las Vegas, NV, US., Apr. 2006, pp. 475–480.

[69] Q. Z. H. Wu, X. Wang and X. Shen, "IEEE 802.11e enhanced distributed channel

access (EDCA) throughput analysis," in *Proc. the 2006 IEEE International Conference on Communications (ICC'06)*, Istanbul, Turkey, Jun. 2006, pp. 223–228.

[70] Y. Yan and C. Pan, "An improved analytical model for IEEE 802.11e enhanced distributed channel access," in *Proc. International Symposium on Information Technology Convergence (ISITC'07)*, Jeonju, Korea, Nov. 2007, pp. 135–142.

[71] F. K. I. Inan and E. Ayanoglu, "Saturation throughput analysis of the ieee 802.11e enhanced distributed channel access function," in *Proc. the 2007 IEEE International Conference on Communications (ICC'07)*, Glasgow, Scotland, Jun. 2007, pp. 409–414.

[72] Y. G. D. N.C.Taher and B. ElHassan, "A complete and accurate analytical model for IEEE 802.11e EDCA under saturation conditions," in *Proc. 2009 IEEE/ACS International Conference on Computer Systems and Applications*, Rabat, Morocco, May 2009, pp. 800–807.

[73] J. Y. Lee and H. S. Lee, "A performance analysis model for IEEE 802.11e EDCA under saturation condition," *IEEE Transactions on Communications*, vol. 57, pp. 56–63, 2009.

[74] W. E. Leland, M. S. Taqqu, W. Willinger, and D. V. Wilson, "On the self-similar nature of ethernet traffic (extended version)," *IEEE/ACM Transactions on Networking (TON)*, vol. 2, pp. 1–15, 1994.

[75] P. E. Engelstad and O. Osterbo, "Analysis of the total delay of the IEEE 802.11e

EDCA and 802.11 DCF," in *Proc. the 2006 IEEE International Conference on Communications (ICC'06)*, Istanbul, Turkey, Jun. 2006, pp. 552–559.

[76] ——, "Queueing delay analysis of IEEE 802.11e EDCA," in *Proc. the Wireless On demand Network Systems and Services Conference (WONS'06)*, Les Mnuires, France, Jan. 2006, pp. 123–133.

[77] F. K. I. Inan and E. Ayanoglu, "Modeling the ieee 802.11e enhanced distributed channel access function," in *Proc. the IEEE Global Telecommunications Conference (Globecom07)*, Washington, DC, US., Nov. 2007, pp. 2546–2551.

[78] X. Ling, K. H. Liu, Y. Cheng, X. Shen, and J. W. Mark, "A novel performance model for distributed prioritized MAC protocols," in *Proc. the IEEE Global Telecommunications Conference (Globecom07)*, Washington, DC, US., Nov. 2007, pp. 4692–4696.

[79] O. M. F. Abu-Sharkh and A. H. Tewfik, "Toward accurate modeling of the IEEE 802.11e EDCA under finite load and error-prone channel," *IEEE Transactions on Wireless Communications*, vol. 7, pp. 2560–2570, 2008.

[80] H. Takagi., *Queueing analysis; a foundation of performance evaluation - volume 1: vacation and priority systems*.   NORTH HOLLAND, 1991.

[81] D. P. Heyman and M. J. Sobel, *Stochastic Models in Operations Research, Vol. I: Stochastic Processes and Operating Characteristics*.   New York: Dover Publications, INC., 2005.

[82] (2010) Maple 13, maplesoft. Waterloo, Canada. [Online]. Available: http://www.maplesoft.com

[83] (2010) Opnet modeler, opnet technologies, inc. Bethesda, MD. [Online]. Available: http://www.opnet.com/

[84] M. R. Yuce, "Implementation of wireless body area networks for healthcare systems," *Sensors and Actuators A: Physical*, vol. 162, pp. 116–129, Jul. 2010.

[85] H. Chen, W. Wu, and J. Lee, "A WBAN-based real-time electroencephalogram monitoring system: Design and implementation," *Journal of Medical Systems*, vol. 34, pp. 303–311, 2010.

[86] F. E. H. Tay, D. G. Guoa, L. Xua, M. N. Nyana, and K. L. Yap, "MEMSWear-biomonitoring system for remote vital signs monitoring," *Journal of the Franklin Institute*, vol. 346, pp. 531–542, Aug. 2009.

[87] D. Albu, J. Lukkien, and R. Verhoeven, "On-node processing of ECG signals," in *Proceedings of the 7th IEEE conference on Consumer communications and networking conference*, Las Vegas, Nevada, USA, Jan. 2010, pp. 1165–1169.

[88] E. N. Farag and M. I. Elmasry, *Mixed Signal VLSI Wireless Design Circuits and Systems*. Springer US, 1999, ch. Digital Modulation Schemes.

[89] C.-S. Hwang and J. M. Cioffi, "Opportunistic CSMA/CA for achieving multi-user diversity in wireless LAN," *IEEE Transactions on Wireless Communications*, vol. 8, pp. 2972–2982, 2009.

[90] I. Inan, F. Keceli, and E. Ayanoglu, "Analysis of the 802.11e enhanced distributed channel access function," *IEEE Transactions on Communications*, vol. 57, pp. 1753–1764, 2009.

[91] J. He, Z. Tang, H.-H. Chen, and Q. Zhang, "An accurate and scalable analytical model for IEEE 802.15.4 slotted CSMA/CA networks," *IEEE Transactions on Wireless Communications*, vol. 8, pp. 440–448, 2009.

[92] C. Jung, H. Hwang, D. Sung, and G. Hwang, "Enhanced markov chain model and throughput analysis of the slotted CSMA/CA for IEEE 802.15.4 under unsaturated traffic conditions," *IEEE Transactions on Vehicular Technology*, vol. 58, pp. 473–478, 2009.

[93] F. Shua and T. Sakurai, "A new analytical model for the ieee 802.15.4 CSMA-CA protocol," *Computer Networks, in press*, 2011.

[94] S. Ullah and K. S. Kwak, "Throughput and delay limits of IEEE 802.15.6," in *Proc. IEEE WCNC*, Cancun, Mexico, Mar. 2011.

[95] S. Rashwand, J. Misic, and H. Khazaei, "IEEE 802.15.6 under saturation: Some problems to be expected," *Journal of Communications and Networks*, vol. 13, pp. 142–149, 2011.

[96] F. Daneshgaran, M. Laddomada, F. Mesiti, and M. Mondin, "Unsaturated throughput analysis of IEEE 802.11 in presence of non ideal transmission channel and capture effects," *IEEE Transactions on Wireless Communications*, vol. 7, pp. 1276–1286, 2008.

[97] H. Takagi., *Queueing analysis; a foundation of performance evaluation - volume 3: discrete-time systems*. NORTH HOLLAND, 1991.

[98] J. D. Bronzino, *The Biomedical Engineering Handbook - Third Edition. Volume 2: Biomedical Engineering Fundamentals*. Taylor & Francis Group, LLC, 2006.

[99] S. Rashwand, J. Misic, and H. Khazaei, "Performance analysis of IEEE 802.15.6 under saturation condition and error-prone channel," in *Proc. the IEEE Wireless Communications and Networking Conference (WCNC'11)*, Cancun, Mexico, Mar. 2011, pp. 475–480.

[100] S. Rashwand and J. Misic, "Performance evaluation of IEEE 802.15.6 under non-saturation condition," in *Proc. the IEEE Global Telecommunications Conference (Globecom11)*, Houston, Texas, US., Dec. 2011.

[101] ——, "Effects of access phases lengths on performance of IEEE 802.15.6 CSMA/CA mechanism," *Journal of Computer Networks (COMNET)*, p. Under Review, 2011.

[102] ——, "Frame delay analysis of CSMA mechanism of IEEE 802.15.6," *IEEE Transactions on Wireless Communications*, 2012, Under Revision.

[103] A. F. Molisch, *Wireless Communications*. John Wiley and Sons, 2010.

[104] A. Taparugssanagorn, A. Rabbachin, M. Hmlinen, J. Saloranta, and J. Iinatti, "A review of channel modelling for wireless body area network in wireless medical communications," in *Proc. IEEE WPMC*, Lapland, Finland, 2008.

[105] S. L. Cotton and W. G. Scanlon, "An experimental investigation into the influence of user state and environment on fading characteristics in wireless body area networks at 2.45 GHz," *IEEE Transactions on Wireless Communications*, vol. 8, pp. 6–12, 2009.

[106] Y. I. Nechayev, P. S. Hall, and Z. H. Hu, "Characterisation of narrowband communication channels on the human body at 2.45 GHz," *IEEE Microwaves, Antennas & propagation*, vol. 4, pp. 722–732, 2010.

[107] I. Khan, Y. I. Nechayev, and P. S. Hall, "On-body diversity channel characterization," *IEEE Transactions on Antennas and propagation*, vol. 58, pp. 573–580, 2010.

[108] Z. H. Hu, Y. I. Nechayev, P. S. Hall, C. C. Constantinou, and H. Yang, "Measurements and statistical analysis of on-body channel fading at 2.45 GHz," *IEEE Antennas and Wireless Propagation Letters*, vol. 6, pp. 612–615, 2007.

[109] S. L. Cotton and W. G. Scanlon, "Measurements and statistical analysis of on-body channel fading at 2.45 GHz," *IEEE Antennas Wireless Propagation Letters*, vol. 6, pp. 51–55, 2007.

[110] ——, "A statistical analysis of indoor multipath fading for a narrowband wireless body area network," in *Proc. IEEE PIMRC*, Helsinki, Finland, 2006, pp. 1–5.

[111] T. T. Tjhung, C. Loo, and N. P. Secord, "BER performance of DQPSK in slow rician fading," *IEEE Electronics Letters*, vol. 28, pp. 1763–1765, 1992.

[112] C. Tellambura and V. K. Bhargava, "Unified error analysis of DQPSK in fading channels," *IEEE Electronics Letters*, vol. 30, pp. 2110–2111, 1994.

[113] M. K. Simon and M. S. Alouini, *Digital communications over fading channel.* John Wiley, 2005.

[114] J. Sun and I. S. Reed, "Linear diversity analysis for M-PSK in rician fading channels," *IEEE Transactions on Communications*, vol. 51, pp. 1749–1753, 2003.

[115] J. G. Proakis and M. Salehi, *Digital Communications (5th Ed.).* McGraw-Hill, 2008.

[116] M. G. Shayesteh, "Exact symbol and bit error probabilities of linearly modulated signals with maximum ratio combining diversity in frequency nonselective rician and rayleigh fading channels," *IET Communications*, vol. 5, pp. 12–26, 2011.

[117] S. Rashwand, J. Misic, and V. B. Misic, "MAC performance modeling of IEEE 802.15.6-based WBANs over rician-faded channels," in *Proc. the IEEE International Conference on Communications (ICC'12)*, Ottawa, Canada, Jun. 2012.

[118] S. Rashwand and J. Misic, "Bridging IEEE 802.15.6 and IEEE 802.11e networks for wireless healthcare systems," *Under Preparation*.

[119] L. Kleinrock, *Queuing Systems - Volume1: Theory.* New York: John Wiley & Sons, 1975.

[120] F. Martelli, C. Buratti, and R. Verdone, "On the performance of an IEEE 802.15.6 wireless body area network," in *Proc. IEEE European Wireless Conference*, Vienna, Austria, 2011, pp. 1–6.

[121] T. D. Lagkas, D. G. Stratogiannis, and P. Chatzimisios, "Modeling and performance

analysis of an alternative to IEEE 802.11e hybrid control function," *Telecommunication Systems*, pp. 1–16, Jun. 2011.

[122] R. S. Uppal and S. Puri, "Performance and evaluation of IEEE 802.11e using QUAL-NET," *International Journal on Computer Science and Engineering (IJCSE)*, vol. 3, pp. 1327–1332, 2011.

[123] J. Misic and V. B. Misic, "Bridging between IEEE 802.15.4 and IEEE 802.11b networks for multiparameter healthcare sensing," *IEEE Journal on Selected Areas in Communications*, vol. 27, pp. 435–449, May 2009.

[124] S. Rashwand and J. Misic, "Impact of priority differentiation on the bridged WBAN/WLAN healthcare networks," *Journal of Wireless Communications and Mobile Computing (WCMC), Under Review*.

[125] ——, "Two-tier WBAN/WLAN healthcare networks; priority considerations," in *Proc. the IEEE Global Telecommunications Conference (globecom'11), Under Review*, Anaheim, USA, Dec. 2012.